University of Strathclyde

Department of Pure & Applied Chemistry

Development of DNA Detection Assays Using Functionalised Nanoparticles

By

Natalie Clark

A thesis presented in fulfilment of the requirements for the degree of Doctor of Philosophy.

2013

ACKNOWLEDGEMENTS

I would like to thank my supervisors Prof. Duncan Graham and Dr. Karen Faulds for their advice and support throughout my Ph.D research.

I thank Dr. Joanna Wrzesien for the synthesis of the linker molecule used for the silver nanoparticle conjugates; Dr Iain Larmour for the SEM images; and Andrea MacDonald for her input into the magnetic nanoparticle experiments.

Thank you to Danny and Iain for their entire help problem solving both in and out of the lab. I would like to say a massive thanks to Louise, Leanne and Kirsten for all of their support and advice.

Huge thanks to my family for their words of wisdom and tireless support throughout this entire process.

Most of all, I thank Douglas for always believing in me and being there to keep me going.

ABSTRACT

The ability to detect DNA relating to a specific disease is at the forefront of current research in molecular diagnostics. The detection techniques utilised for such work need to afford excellent selectivity as well as sensitivity. Current methods commonly involve the use of fluorescence; however there has been a heightened interest in the use of SERRS for these purposes in recent years due to the numerous advantages SERRS offers over fluorescence. Nanoparticles are often selected as the SERRS substrate of choice. These nanoparticles can undergo a number of functionalisation steps in order for them to either act as labels for detection or to detect specific target molecules, or perform both tasks simultaneously. This research details the preparation of a number of biofunctionalised SERRS active nanoparticle conjugates and their incorporation into a DNA detection assay. The assay is based on a split-probe principle, with one of the probes becoming attached to a SERRS active particle giving rise to a SERRS signal from the assay, whilst the other probe is tethered to a magnetic bead to allow immobilisation of the completed assay. The nanoparticle conjugates were functionalised with a Raman reporter and stabilised by a polyethylene glycol layer on the surface of the nanoparticles. A biomolecule of choice was then used to functionalise the nanoparticle, allowing it to either bind to an oligonucleotide probe or to the target DNA strand directly. After the assay protocol has been completed the samples were measured by SERRS. The assay systems developed were tested to assess their ability to selectively and sensitively detect DNA with a specific sequence. The assay protocol was optimised in order to improve these aspects of the assay performance with a view to making the assay more suitable for testing of genomic samples. A method was developed for the synthesis of gold-shelled magnetic nanoparticles for incorporation into the assay system. Iron oxide core nanoparticles were synthesised and coated with a metallic gold shell. The shelling protocol was optimised and a method for the assessment of the shelling protocol developed. Using analysis of SEM images, zeta potential measurements and SERRS, the gold-shelling of the magnetic nanoparticles was verified. A proof of concept assay demonstrated the suitability of the resultant magnetic nanoparticles for use in the DNA detection assay.

ABBREVIATIONS

A	Adenine
antiDIG	Anti-digoxigenin
AuMG	Malachite green labelled gold nanoparticles
AuMGPEG	Malachite green labelled, pegylated gold nanoparticles
AuMGPEGAb	Antibody functionalised, malachite green labelled gold nanoparticles
AuMGPEGDNA	DNA functionalised, malachite green labelled gold nanoparticles
BPE	Trans-1,2-bis(4-pyridyl)-ethylene
BMBA	2-Bromo-4-mercaptobenzoic acid
C	Cytosine
DCM	Dichloromethane
DIC	*N,N'*-diisopropylcarbodiimide
DIG	Digoxigenin
DLS	Dynamic Light Scattering
DMAP	4-Dimethylaminopyridine
DNA	Deoxyribonucleic Acid
DSNB	5,5'-Dithiobis(succinimidy-2-nitrobenzoate)
DTDC	3,3'-Diethylthiadicarbocyanine Iodide
DTNB	5,5'-Dithiobis(2-nitrobenzoic acid)
DTT	Dithiothreitol
EDC	Ethyldimethylamino propyl carbodiimide
EDTA	Ethylenediaminetetraacetic Acid
EGFR	Epidermal Growth Factor Receptor
EIA	Enzyme Immunoassay
FAM	5-(and 6)-Carboxyfluorescein
FEI	Field Emission Electron Microscope
FWHM	Full Width Half Maximum
G	Guanine
HIV-1	Human Immunodeficiency Virus Type 1
IgG	Immunoglobin G
LNA	Locked Nucleic Acid

MBA	4-Mercaptobenzoic Acid
MCH	6-Mercaptohexanol
MG	Malachite Green
MGITC	Malachite Green Isothiocyanate
MP	4-Mercaptopyridine
NAATS	Nucleic Acid Amplification Tests
NHS	*N*-hydroxysuccinimide
OGN	Oligonucleotide-Gold Nanoparticle
OSN	Oligonucleotide-Silver Nanoparticle
PBS	Phosphate Buffered Saline
PCR	Polymerase Chain Reaction
PDDA	Poly(diallyldimethylammonium)
PEG	Poly(ethylene)glycol
RRS	Resonance Raman Scattering
RNA	Ribonucleic Acid
SAM	Self Assembled Monolayer
SAMSA fluorescein	5-(2-(and 3)-*S*-(acetylmercapto)succinoyl)amino) fluorescein
SEM	Scanning Electron Microscopy
SERRS	Surface Enhanced Resonance Raman Scattering
SERS	Surface Enhanced Raman Scattering
T	Thymine
TAMRA	5-(and 6)-Carboxytetramethylrhodamine
TEA	Triethylamine
TEM	Transmission Electron Microscopy
TFA	Trifluoroacetic Acid
T_m	Melting Temperature
TRITC	Tetramethylrhodamine-5-isothiocyanate
U	Uracil
UV	Ultra Violet
XRITC	Rhodamine-5-(and 6)-isothiocyanate

TABLE OF CONTENTS

1. INTRODUCTION

The rapidly expanding field of molecular diagnostics is centred on the detection of specific DNA sequences. [1] One of the primary reasons for DNA detection is in the identification and treatment of diseases. The detection of specific DNA sequences has also been successfully introduced to forensic applications for the identification of suspects in legal proceedings. [2]

The majority of detection techniques currently employed use fluorescence spectroscopy alongside DNA amplification techniques, for example in a real time polymerase chain reaction (PCR). [3] There are a number of factors introduced by the use of PCR that will have an impact on the sensitivity of the detection technique. Firstly, due to the intrinsic limit of detection of fluorescence, a number of PCR cycles are required in order to generate adequate target for detection. The efficiency of the PCR cycling has a direct relationship to the number of copies of DNA produced. As a result, inefficient PCR cycling will impede detection since the number of DNA strands available for detection is minimised. Furthermore, background fluorescence associated with some of the quenching techniques employed in popular detection strategies, such as Taqman probes, can also result in a loss of sensitivity. Likewise, the selectivity of these techniques is also affected by the use of PCR. The co-amplification of undesired sequences present in the original sample reduces the selectivity of the system. Finally, owing to the broad nature of the emission spectra associated with fluorescence, multiplexing of this technique can prove problematic due to the potential overlapping of emission profiles.

In the case of disease diagnosis, it is beneficial to improve both the sensitivity and multiplexing capability of the detection method. An alternative to the use of fluorescence is surface enhanced (resonance) Raman scattering (SE(R)RS). Although single molecule detection has been reported by both fluorescence [4-6] and SERS,[7-11] it has been shown that in some cases SERRS detection limits can be as much a four orders of magnitude lower than those obtained by fluorescence. [12] SE(R)RS examines the vibrational output of the molecule, which relates directly to the structure. As such, it can be seen that whilst fluorescence affords a broad emission band, SE(R)RS produces distinctive fingerprint spectra. These sharp, distinctive bands allow for discrimination between mixed analytes. [13] Consequently,

SE(R)RS can offer a substantial advantage over fluorescent techniques in terms of ability to detect multiple species.

1.1 INTRODUCTION TO DNA

DNA contains all the genetic coding needed to control the functions, behaviour and development of all living organisms. Nucleic acids are complex macromolecules, which are used as a long term storage device to store these genetic instructions. There are two types, deoxyribonucleic acid (DNA), which preserves hereditary information and ribonucleic acid (RNA), which transcribes and translates to allow the synthesis of proteins.

1.1.1 PRIMARY STRUCTURE OF DNA

Nucleic acids are long polymeric chains that consist of monomeric sub-units called "nucleotides". These sub-units are composed of: [14]

- A five-carbon monosaccharide;
- A phosphate residue, and
- A weakly basic nitrogen heterocyclic base.

These heterocyclic bases are substituted monocyclic pyrimidines and bicyclic purines. The purine bases are adenine (A) and guanine (G) (Figure 1.1). These are found in both DNA and RNA. The pyrimidine bases are cytosine (C), thymine (T) and uracil (U) (Figure 1.2). Cytosine is found in both DNA and RNA, whilst thymine is found exclusively in DNA, and uracil solely in RNA.

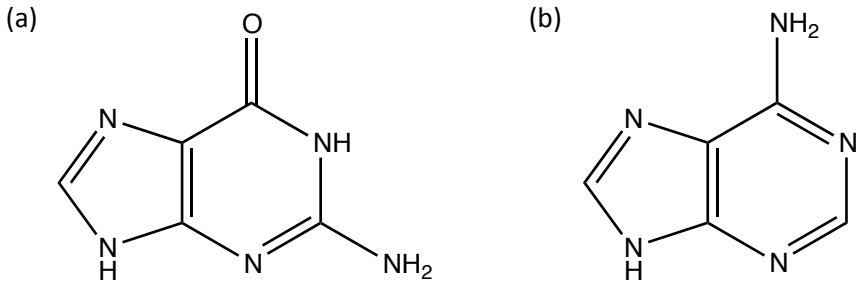

Figure 1.1 - Molecular structure of the purine bases, (a) guanine and (b) adenine.

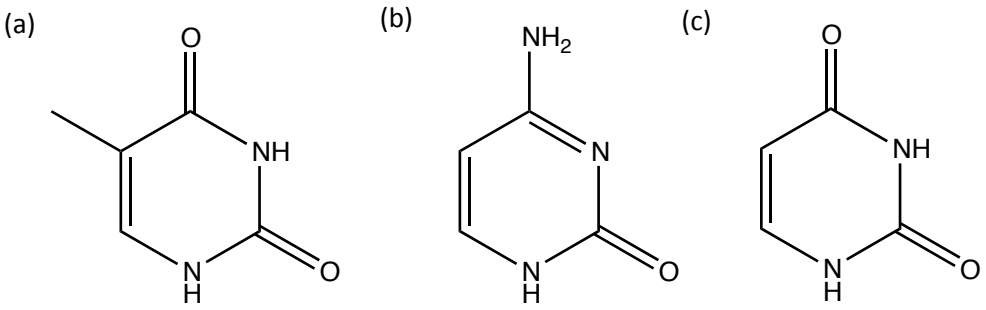

Figure 1.2 - Molecular structure of the pyrimidine bases, (a) thymine, (b) cytosine and (c) uracil.

Both classes of base are unsaturated, containing conjugated double bonds. This feature makes the rings planar, and also accounts for the molecules ability to absorb ultraviolet (UV) light at approximately 260 nm.

There are two main types of pentose sugar present in nucleic acids. The first of which is ribose (*D*-ribofuranose). The nucleotides containing ribose are called ribonucleotides. These are commonly found in RNA. Their structure can be seen in Figure 1.3.

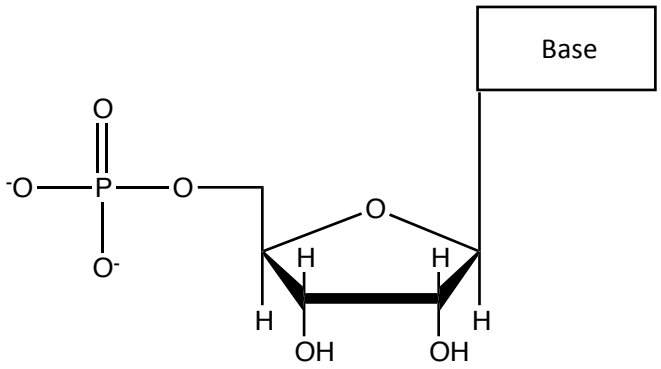

Figure 1.3 - A ribonucleotide consisting of a ribose sugar, phosphate and nitrogenous base.

The second of these sugars is 2-deoxyribose (2-deoxy-*D*-ribofuranose), which is found in DNA. Nucleotides containing deoxyribose are called deoxyribonucleotides. The general structure for these can be seen in Figure 1.4.

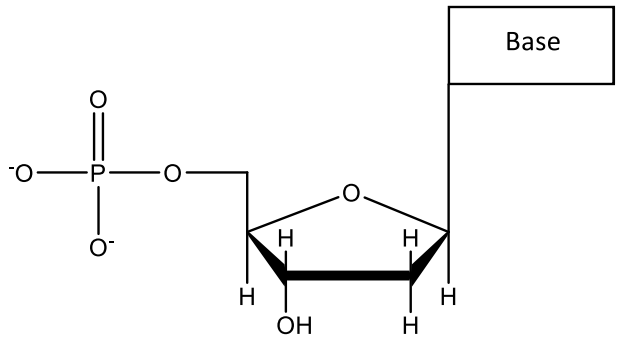

Figure 1.4 - A deoxyribonucleotide, consisting of a deoxyribose sugar, a phosphate and a heterocyclic base.

The pyrimidine or purine *N*-glycosides of these sugars are called nucleosides. A nucleoside consists of a purine or pyrimidine base bonded to a sugar unit. Nucleotides are the phosphate esters of the nucleosides, consisting of a nitrogenous base, a sugar and a phosphate group. Commonly, the nucleotides contain between one and three phosphoryl groups. These nucleotides can be linked by either the 3' or 5' carbon. Indeed, the ability of these groups to link to both the 3' and 5' carbon allows the formation of the phosphodiester linkages between the 3' hydroxyl in one of the nucleotides and the 5' hydroxyl group of the other. This linkage therefore proceeds to form a linear polynucleotide, creating the primary structure of DNA (Figure 1.5).

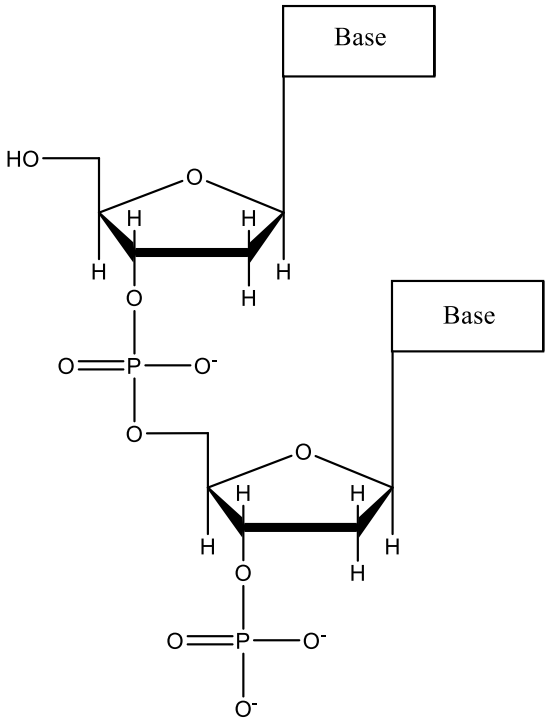

Figure 1.5 - A DNA dimer, consisting of two deoxyribonucleotides joined by a phosphodiester linkage.

1.1.2 SECONDARY STRUCTURE OF DNA

Watson & Crick are the scientists credited with the discovery of the structure of DNA; however for many years several great scientific minds had been puzzling over this "secret of life". Without the work done previously, Watson and Crick may never have made this tremendous discovery, published in their 1953 Nature paper. [15]

In 1947, J. Masson Gulland and D. O. Jordan published a series of papers describing the preparation of a pure sample of DNA, [16] along with the study of its properties in aqueous solution by potentiometric titrations [17] and determination of viscosity and streaming birefringence. [18] During this work, Gulland and Jordan concluded that DNA must be composed of a structure with a substantial amount of hydrogen bonding between the bases of the polynucleotide. They were unsure at the time whether these hydrogen bonds connected bases of the same or different chains, but later were convinced that the data they had collected was due to hydrogen bonding between adjacent chains. However, there was no suggestion that this hydrogen bonding of bases on neighbouring chains resulted in a

double stranded structure, instead it was suggested that aggregates or “micelles” of several chains were the result.

In 1950, Erwin Chargaff began his own investigation into the structure of DNA. He began by using paper chromatography to study the base composition of DNA by separating the products of hydrolysis of DNA, and using ultra violet (UV) spectrometry to measure their relative abundance. [19] The data he produced through this series of experiments proved that each DNA base is not present in equal proportions, as had been thought previously. Instead, there was a 1:1 ratio of adenine with thymine, and guanine with cytosine, however the amount of adenine was not necessarily equal to the amount of guanine.

From this the conclusion was made that the proportion of purine (A+G), is always equal to the proportion of pyrimidines, (C+T). The ratio (G+C)/(A+T) varies from species to species, however different samples from within a single species will always have the same DNA composition.

$$\frac{[\boldsymbol{A}]}{[\boldsymbol{T}]} = \frac{[\boldsymbol{G}]}{[\boldsymbol{C}]} = \mathbf{1}$$

Figure 1.6 - Chargaff’s Rule which states that the amount of guanine is equal to that of cytosine, and the amount of adenine is equal to that of thymine in a DNA molecule.

Later, in 1953, Rosalind Franklin and Maurice Wilkins performed a study using x-ray crystallography in order to investigate the structure of the DNA molecule. [20] Since a molecule of DNA has a high level of regularity, it is possible to crystallise it in fibres that have an extremely high degree of molecular order. This work was carried out by studying this oriented crystal in order to produce a three-dimensional representation of the DNA molecule.

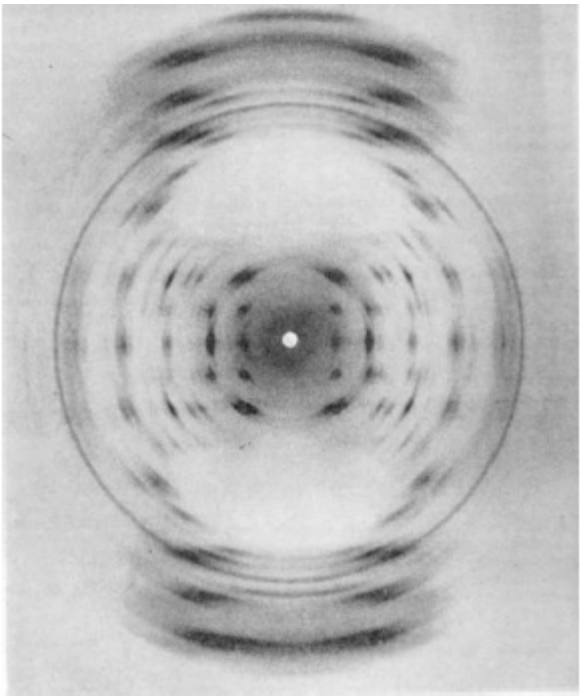

Figure 1.7 - X-ray diffraction pattern of DNA. [20]

Franklin discovered that DNA possessed a helical structure, indicated by the x-shaped pattern, shown in Figure 1.7, with the phosphate groups to the outside of the chain, forming the backbone. The pattern also showed ladder-like rungs held together by two strands at each side.

Watson and Crick built on this information to correctly propose the structure of DNA. [15] Using Chargaff's work, [19] they discovered that each nitrogenous base had a specific pairing partner, i.e. adenine with thymine and guanine with cytosine. This base pairing allows for maximum hydrogen bonding between potential partners. This specific base pairing along the chain remains constant; however the base sequences differ dramatically from one species to another. This specific pairing of the nitrogenous bases became known as Watson-Crick base pairing, where the bases are held together by hydrogen bonding, as demonstrated in Figure 1.8.

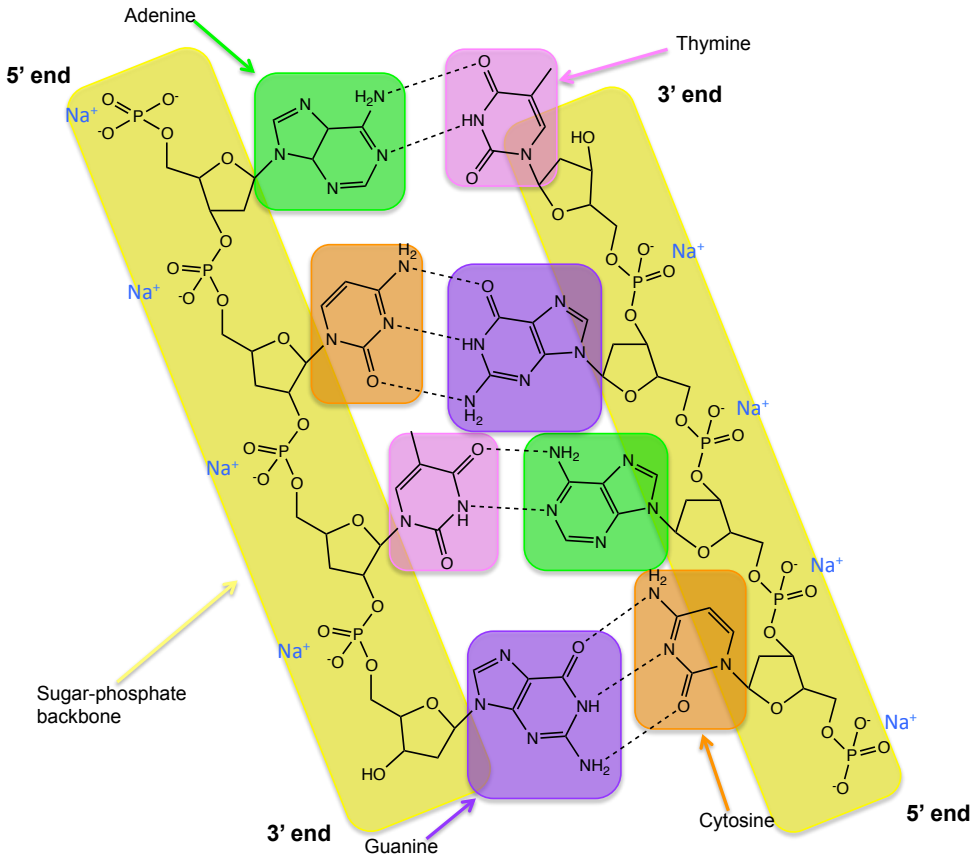

Figure 1.8 - Watson-Crick base pairing in DNA showing A-T and G-C base pairs and the DNA backbone consisting of deoxyribose sugar and phosphate units held together by phosphodiester linkages.

Watson and Crick used the information published by Franklin and Wilkins earlier in 1953 [20] to support their proposal that a molecule of DNA consisted of two right-handed helical chains, coiled around an axis. The complementary base sequences were contained within the outer phosphate-sugar chain, which form the backbone of the structure, 10 Å from the central axis. The bases were found to be approximately perpendicular to their adjacent sugar, occurring with a regularity of 3.4 Å along the polynucleotide chain.

Every 34 Å, or 10 residues the coil repeats itself (Figure 1.9). Consequently, the backbone can be easily accessed by cations and, since the structure is open, a high internal water content is present. This preserves the helical shape of the molecule by preventing the bases from tilting inwards.

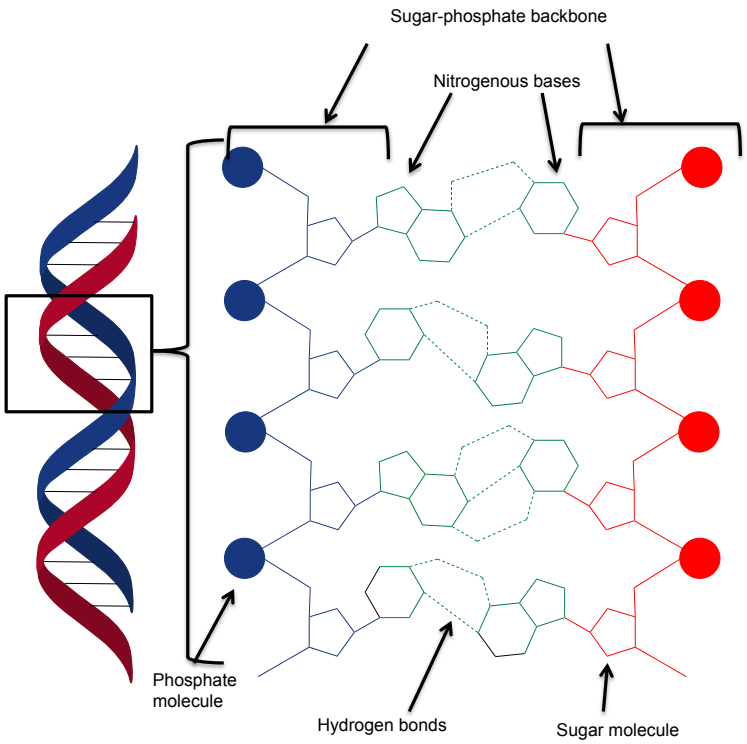

Figure 1.9 - Double helix structure of DNA showing schematic representation of Watson-Crick base pairing between the two DNA strands.

Due to its highly specific nature, DNA has become the focus of many diagnostic assays for the detection of diseases. A number of strategies have been developed for the detection of DNA, many of which utilise fluorescence spectroscopy. However, in the field of diagnostics sensitivity is key, and recently it has been shown that SERRS could provide lower limits of detection in comparison to fluorescence. [12] Consequently, incorporation of this enhanced Raman spectroscopy technique could provide a significant advantage over previously developed methods.

1.2 RAMAN SPECTROSCOPY

Scattering of light was observed by Rayleigh [21] as early as 1871, and Einstein and Compton [22] both studied this process at the beginning of the 20th century, however it was not until 1923 that the inelastic scattering of light was proposed by Smekal. [23] Until this time, all investigations had focused on the elastic scattering of particles, in which the scattered photons are of the same energy and wavelength as the incident photons. This

elastic scattering was termed Rayleigh scattering after its founder. In 1928, Raman and Krishnan first observed experimentally the inelastic scattering of incident light. [24] Since then, this phenomenon has been referred to as Raman Scattering. Inelastic scattering results in the scattered photons having a different energy than that of the incident photons, resulting in a frequency change.

1.2.1 THEORY OF RAMAN SPECTROSCOPY

The technique of Raman spectroscopy utilises a single frequency of radiation to irradiate a sample and the radiation scattered by the molecule is detected. The energy of this scattered radiation will be one vibrational unit of energy less or more than the incident beam. Only one in every 10^6 – 10^8 photons scattered will do so with a change of energy, therefore this can be considered to be a very weak process. As a result of this, a very intense radiation source is required. The most common source used is a laser since it is monochromatic, and will provide adequate energy to produce a discernible effect.

When the incident light comes into contact with a sample, photons from the beam interact with the molecules and exchange energy. The majority of this light undergoes Rayleigh scattering, i.e. has the same energy as the incident photon; however a small number of photons will undergo inelastic scattering, resulting in photons of lower or higher energy than the incident photons being observed. The energy difference observed corresponds with the molecular vibrations of the molecule, thereby providing vibrational information about the molecule. These energy differences are known as Raman Shifts, and there are two types of Raman Scattering that are measured.

The first of these is Stokes scattering which results in photons being scattered with less energy than the incident photons, therefore occurring at a longer wavelength. This is due to the molecule absorbing energy from the incident photons. The second type of inelastic scattering is Anti-Stokes scattering in which photons with higher energy than the incident photons are observed. This results in these photons being observed at shorter wavelengths. This will occur when the molecule loses energy to the scattered photons. This is demonstrated in Figure 1.10.

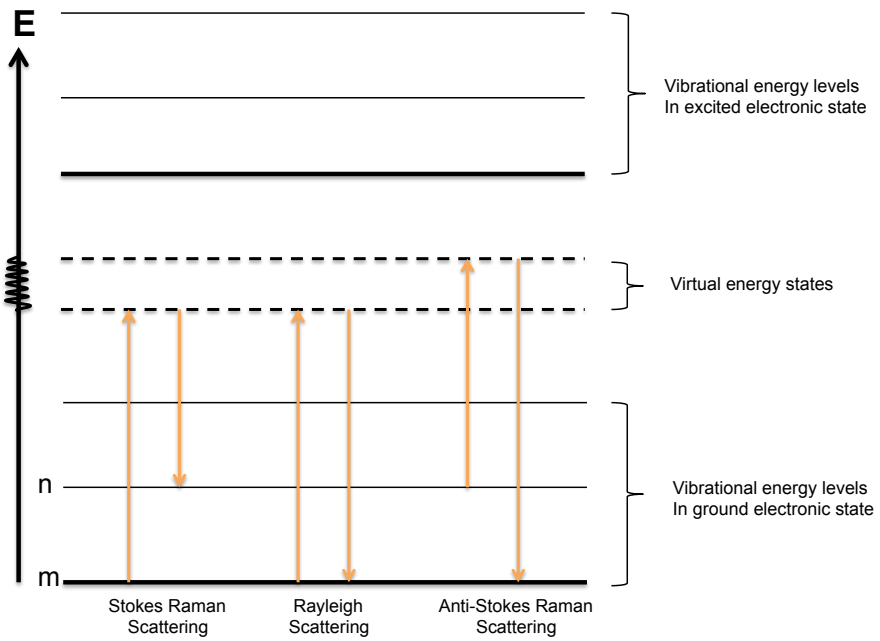

Figure 1.10 - Energy transitions associated with Stokes scattering, Rayleigh scattering & Anti-Stokes scattering.

In order for Anti-Stokes scattering to occur, the molecule has to be in an excited state. A typical cause of this is thermal excitation. However, if we consider the Boltzmann distribution (Equation 1.1), at thermal equilibrium the lower energy states will have more molecules in them, therefore Stokes scattering dominates.

$$N_i = \frac{Ne^{-En/kT}}{q}$$

Where: N_n = number of particles in a sample of N particles that will be found in a state with an energy E_n when it is part of a system in thermal equilibrium at a temperature T

k = Boltzmann's constant = 1.381×10^{-23} J K^{-1}

$$q = \sum_i e^{-E_n/kT}$$

Equation 1.1 - Boltzmann distribution.

Hence, Stokes scattering is much more intense than anti-Stokes scattering at room temperature. Usually, Raman scattering is recorded only on the low-energy side to give Stokes scattering but occasionally anti-Stokes scattering is measured.

Fluorescence and photo-degradation can be problematic when collecting the Raman spectrum of a molecule. Fluorescence produces broad peaks on the Raman spectrum that can obscure Raman scattering signals, and photo-degradation can lead to a decrease in intensity of an already weak signal. The issues of high background fluorescence and photo-degradation [25] have therefore been investigated and suitable solutions have been created to address them. A near infra-red source of excitation can be used to minimise the emission of fluorescence from the system. This is a consequence of few molecules having excited states low enough to give fluorescence.

One way to minimize photodegradation is to use a sampling method in which the sample passes through the laser beam but does not stay in the beam for the entire analysis time. Consequently any one part of the sample is not retained in the beam for any extended period of time. Raman scattering is then obtained from the cumulated spectra from a large area of the sample. [26-29]

1.3 RESONANCE RAMAN SCATTERING (RRS)

The introduction of laser technology into Raman spectroscopy led to the development of resonance Raman. This technique uses a laser with an excitation wavelength close to the absorbance maxima (λ_{max}) of the chromophore being examined. This means that the frequency of the laser beam will correspond with an electronic transition within the molecule, therefore allowing enhancement of these bands, as seen in Figure 1.11. A chromophore is a conjugated molecule that results in the absorbance of UV or visible light, giving the molecule a visible colour. As a consequence of the resonance contribution, scattering enhancements of up to 10^6 have been observed, with an improvement of 10^3 to 10^4 being common place. [30] An advantage of this enhancement is that it allows for analysis of dilute samples. A common problem in the use of RRS is that certain chromophores exhibit a high level of background fluorescence, thereby obscuring the Raman signals. In

order to minimise this effect, chromophores with low background fluorescence are chosen if possible, although this is not always feasible and in this case a dilute sample or pulsed laser can also help to eradicate fluorescence issues.

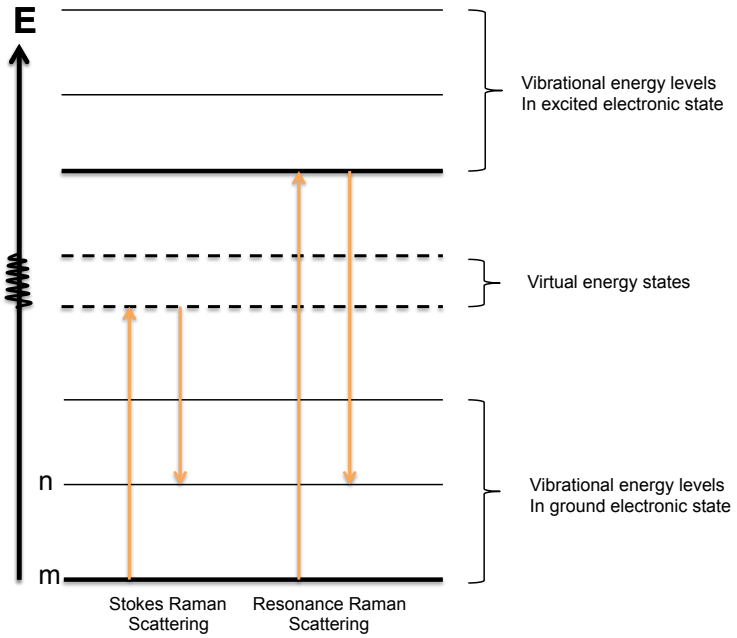

Figure 1.11 - Resonance Raman Spectroscopy associated energy levels.

1.4 SURFACE ENHANCED RAMAN SCATTERING (SERS)

Fleischman *et al*. initially observed SERS in 1974 [31] when examining pyridine in an aqueous solution in the presence of a silver electrode. An increased Raman signal was obtained due to the absorption of the pyridine onto the roughened silver surface of the electrode. It was not known what caused this enhancement effect and later two groups came up with two differing theories. Jeanmaire and Van Duyne proposed an electromagnetic effect, [32] whilst Albrecht and Creighton proposed a charge transfer effect. [33] However, both found that an enhancement was obtained routinely in the order of 10^6 and concluded that the increased scattering was due to the surface plasmon of the roughened silver electrode.

The electromagnetic theory proposes that the enhancement is a result of an increase in the electromagnetic field experienced by a molecule on a roughened metal surface. [34] In order for an enhancement to be observed, it is necessary for the laser to be tuned to the surface plasmon. The surface plasmon can be thought of as being the collective oscillation of

conduction band electrons at the metal surface. This careful tuning of the laser to the frequency of the surface plasmon results in a larger number of scattered photons and consequently, an enhancement effect is observed. The molecule does not need to bind directly to the surface; however it must be in close proximity to experience this effect. [35, 36] The charge transfer theory hypothesises that the enhancement is based upon the formation of new electronic states due to interactions between the substrate and the analyte bonded to it. [37] It is believed that the enhancement relates to a coupling between the analyte and the metal surface. [38, 39] It has been concluded that both mechanisms contribute to the enhancement seen in SERS, however the electromagnetic effect appears to be the dominant contributor. [39, 40]

1.5 SURFACE ENHANCED RESONANCE RAMAN SCATTERING (SERRS)

The combination of RRS and SERS has led to the development of surface enhanced resonance Raman scattering (SERRS). This technique combines the enhancement provided by both scattering systems described previously, resulting in a potential increase in sensitivity by up to 10^{14} over normal Raman. [7, 8, 10] The consequence of this is that less intense lasers are needed, thereby reducing the occurrence of photo-degradation of the sample. [25]

It is believed that the principles behind the enhancement effect seen are the same in SERRS as those in SERS. However; it has been revealed that the contribution proposed in the charge transfer theory is significantly smaller with the laser line in-resonance, i.e. in SERRS, than out of resonance, i.e. in SERS. [41-43]

In SERRS, as in SERS, the molecule being analysed must be adsorbed onto a roughened metal surface, which is commonly in colloidal form. This colloidal suspension contains nanoscale particles of the metal in a solution. The surface enhancement observed upon addition of the analyte to the metal surface is dependent upon the amount of roughening of the surface, and therefore in the case of colloidal metal depends upon the size of the nanoparticles, as well as the metal chosen and the area of the surface. [44] An aggregating agent is often added to the analyte before addition of the nanoparticles in order to gather

the particles together, thereby increasing the surface roughness and plasmon. Consequently, the potential enhancement in SERS and SERRS is maximised.

Like with RRS, for SERRS to occur the analyte must also contain a chromophore. In order for enhancement to occur, the excitation frequency used must be coincident or close to an electronic transition of the chromophore. This enhancement is maximised if the surface plasmon of the metal is also coincident with this frequency.

1.6 SUITABLE SE(R)RS SURFACES

A series of different metals have been used to provide the surface enhancement effect, such as silver, gold and copper, as well as a selection of other transition metals. [45-53] Silver and gold are most commonly used due to their stability and because they have surface plasmons within the visible region, however silver tends to give the largest enhancement factor. [54] The roughened surface can be made available in a variety of forms, most commonly aggregated colloidal suspensions, electrodes and roughened metal films. Colloidal nanoparticles are often selected as the SE(R)RS substrate of choice as they offer a number of advantages over a bulk metal surface.

The use of a suspension of nanoparticles allows for a high number of particles to be interrogated by the laser beam at once, thereby resulting in the signal observed being that of an average of the signal detected from each particle. This makes quantitative analysis possible. Furthermore, different batches of nanoparticles can be mixed to result in a large stock of colloidal SE(R)RS substrate. Subsequently, the signal detected using nanoparticles is often more reproducible and stable. Nanoparticles are subject to Brownian motion, a phenomenon that proves advantageous for SE(R)RS analysis, in comparison to a stationary surface. The continuous motion of the nanoparticles in the solution help to eliminate problems that arise due to sample drying, sample heating and photodecomposition.

1.7 NANOPARTICLES

One area that makes notable use of nanoparticles is in the field of Raman spectroscopy. As a result of the success achieved by their use, colloidal metal suspensions are often used in

enhanced Raman spectroscopy as the roughened metal surface required for enhanced scattering to occur. This therefore allows both SERS and SERRS spectra to be obtained.

Although examples of colloidal gold can be traced as far back as the 5th Century BC, it wasn't until the experiments performed by Michael Faraday in 1857, involving the reduction of an aqueous solution of chloroaurate to form a red solution of colloidal gold nanoparticles, that the properties of nanoparticles became subject to further investigation. [55]

Whilst silver and gold are the principal metals of choice to be used in SE(R)RS analysis, copper can also be utilised in order to provide the roughened surface needed to induce the enhancement effect seen in these spectroscopic methods. This is due to the surface plasmon of these metals being found within the visible region of the electromagnetic spectrum. [46]

Silver nanoparticles have drawn a lot of attention in recent years, becoming a vast research area in the field of enhancement of Raman scattering. Silver colloid is frequently synthesised *via* a method pioneered by Lee and Meisel [48] in which silver nitrate is reduced by citrate. An alternative method of reduction is by using ethylenediaminetetraacetic acid (EDTA), [56] or sodium borohydride [57] in place of the citrate. Both of these methods result in the particles surface having an overall negative charge. [58] This charge induces monodispersion of the colloidal suspension given that the nanoparticles are prevented from aggregating due to the repulsive forces. Typically, the silver nanoparticles produced have a diameter of approximately 35 nm. As a result of the additional long term stability of the citrate and EDTA reduced silver colloids, these are the preferred choice for use in this area of research. Aggregation can occur by the modification of the environment, for example by addition of salt. This aggregation process can however be controlled by modification of the nanoparticle surface, therefore allowing calculated management of the aggregation in the system.

Aggregation is a dynamic process, and as such it requires careful control in order to obtain reproducible results. [59-61] Many compounds have successfully been used as aggregation agents, for example; sodium chloride, spermine tetrachloride [62] and poly-L-lysine. [54, 59, 63]

The aggregating agent can assume two roles within the system, both facilitating adsorption of the analyte onto the metal surface as well as promoting aggregation of the nanoparticles. [60] Greater SE(R)RS enhancement is observed as a result of aggregation since at the junction between particles intense electric field gradients are created, some of which create exceptional intensity ("hot-spots"). [64] Furthermore, the aggregation process results in a large range of units, ranging in size from dimers and trimers to small clusters. These clusters of varying sizes all give different plasmon resonance frequencies, thereby ensuring that the plasmon resonance frequency of at least some of the species will be in resonance with any visible or near infrared excitation. Consequently, aggregation will increase the enhancement through the intense fields created at particle junctions and thus increase both the enhancement of the analyte molecule and extend the wavelength range at which some particles are active. A positive charge can be adopted by the surface by addition of poly-L-lysine and spermine tetrachloride, whereby allowing for adsorption of negatively charged analytes. [65]

The preparation of metallic nanoparticles is simple, whereby a metal salt is reduced in the presence of a stabiliser molecule. The agents most commonly selected to reduce the metal ions include; tri-sodium citrate, [48] sodium borohydride [57] and EDTA. [56] These methods typically afford nanoparticles in the region of 5-40 nm, dependent upon the protocol followed and the metal used. Generally, the optical properties of the colloidal suspension are determined by the nanoparticles size, shape and chemical composition. To get the best SE(R)RS signal, the size of nanoparticles must be carefully selected, alongside the excitation wavelength used to excite the surface plasmon on the nanoparticles. In order for quantitative SE(R)RS analysis to be possible, the nanoparticle suspensions should have a narrow size distribution, as these will result in similar SE(R)RS intensities.

1.8 FUNCTIONALISED NANOPARTICLES

As a consequence of the successful implementation of metallic nanoparticles as SE(R)RS substrates, the field has evolved further to include the functionalisation of nanoparticles for use in SE(R)RS assays, and to act as SE(R)RS tags. Two main types of nanoparticle functionalisation can be performed depending upon the function of the nanoparticle in the

assay. Firstly, if the nanoparticle is to act as a tag that can be easily visualized by the use of SE(R)RS, the nanoparticle surface is encoded with SE(R)RS active small molecules, providing an enhanced signal corresponding to the immobilized molecule. Secondly, if the nanoparticle is to bind to a target biomolecule, the surface can be modified by the immobilization of a molecule that will interact with the target molecule. For instance, the nanoparticle surface could be functionalized with an antibody that interacts with an antigen whose presence indicated the presence of a disease, thereby providing diagnostic information for the sample. [66-69] The immobilization of DNA on the nanoparticle surface is often performed in order to detect the presence of target DNA with a specific DNA sequence. [70, 71] This approach is highly favourable as probes can be designed to give a high level of specificity to the nanoparticle binding process. Single base mismatches in DNA can be detected easily using this approach. [72] Furthermore, the two functionalization approaches can be combined resulting in a SE(R)RS encoded nanoparticle that can bind to a molecule of interest, indicating its presence. This approach is frequently adopted in multiplex assays where a variety of different labeled nanoparticles can be made, each indicating the presence of a different target molecule.

1.9 ENCODED NANOPARTICLES

Due to the distance dependent nature of SE(R)RS enhancement, the proximity of an analyte to the roughened metal surface of choice is of vital importance. As a result of their robust nature, and surface plasmon in the visible region, metallic nanoparticles are often used alongside an analyte as a labelling system in assays involving SE(R)RS analysis. However; steric hindrance can limit the availability of the analyte to the nanoparticle surface, thereby resulting in lowered signal enhancement, and in turn less sensitivity from the assay. [73-77] In recent years, the field of nanoparticle functionalisation has grown rapidly, with researchers working towards the synthesis of SE(R)RS active nanoparticles which can be successfully incorporated as a labelling technique in a number of assay formats. [78]

In 2003, Mulvaney *et al.* published details of the glass encapsulation of analyte tagged nanoparticles. [79] Gold nanoparticles were encoded with trans-1,2-bis(4-pyridyl)-ethylene (BPE) and 4-mercaptopyridine (MP), before glass encapsulation. The spectra observed from both sets of tagged nanoparticles were examined and it was noted this work shows

potential for use in a multiplexed manner due to the distinct spectral peaks observed for both reporters at the same excitation wavelength.

Later that year, Nie *et al.* detailed the synthesis of dye-coded metallic nanoparticles, encapsulated in silica. [80] Gold nanoparticles were embedded with a series of sulphur containing dye molecules; 3,3'-diethylthiadicarbocyanine iodide (DTDC), malachite green isothiocyanate (MGITC), tetramethylrhodamine-5-isothiocyanate (TRITC) and rhodamine -5-(and 6)-isothiocyanate (XRITC). Three of the four dyes used contained the isothiocyanate group, whilst the fourth contained two sulphur atoms as part of the ring structure. Both of these functional groups bind the dye molecule to the gold metal surface. It was shown that the enhancement factors achieved are significantly large enough to potentially allow for single-particle spectroscopy to be carried out.

In 2009, Schlücker and co-workers published details on multiplexing SERS labels immobilised on gold nanoparticles by SAM formation. [81] Firstly, three different nanoparticle reporter conjugates were made, each with a one-component self-assembled monolayer (SAM) of a different Raman label. The labels selected were 5,5'-dithiobis(2-nitrobenzioc acid) (DTNB), 2-bromo-4-mercaptobenzoic acid (BMBA), and 4-mercaptobenzioc acid (MBA). Two-component monolayer Raman tags were then synthesised. Three different combinations of Raman labels were analysed, with each combination showing clearly distinguishable peaks for the two labels present. The particles labelled with the two-component SAM could not be distinguished from a mixture of the two batches of nanoparticles labelled with the one-component SAM containing the same two Raman labels. This was then extended to a three-component SAM containing all three labels. Peaks corresponding to each individual Raman label could be distinguished from the SERS signal obtained. It was also seen that the contribution from each label, to the SERS spectrum collected, could be tuned by altering the ratio of the three components.

A method for the functionalisation of nanoparticles with oligonucleotides, as well as Raman reporter molecules, without the need for formation of a mixed layer on the metal surface, was recently demonstrated by Graham *et al*. [82] A series of linker molecules containing three principal groups were synthesised for the conjugation of biomolecules to metallic nanoparticles. Each linker contained a Raman tag, a surface-complexing group and a

functional group for bioconjugation. The linkers contained a short-chain polyethylene glycol (PEG) to afford stability to the conjugates, and also to prevent non-specific binding of biomolecules to the nanoparticle surface. The surface-complexing group selected was thioctic acid, a cyclic disulphide. The linker molecule was capped with a carboxylic acid group, designed for the bio-conjugation of proteins or amino-functionalised oligonucleotides. A selection of dyes were incorporated into the linker molecules; fluorescein, 6-aminofluorescein and tetramethylrhodamine (TAMRA). Both gold and silver nanoparticles were successfully functionalised with the three linker molecules produced. The successful conjugation of amino-functionalised oligonucleotides was demonstrated.

1.9.1 DNA-NANOPARTICLE CONJUGATES

Gold and silver nanoparticles can be functionalized with a number of different small molecules by their immobilisation onto the nanoparticle surface *via* a thiol group. Sulphur atoms are capable of covalently bonding to the gold or silver surface, providing a robust anchor for molecular labeling.

Oligonucleotide-gold nanoparticles, and oligonucleotide-silver nanoparticles provide highly stable, functional nanoparticle labels. These conjugates are functionalized by oligonucleotides on the nanoparticle surface, usually by means of a thiol-linkage. These nanoparticle conjugates can be used in two different ways. Firstly, the nanoparticles themselves can be used directly as detection labels indicating the presence of target DNA. [83, 84] Additionally, the conjugates can act as a probe which, in the presence of target DNA become aggregated, allowing for the novel optical properties of aggregated nanoparticles in comparison to aggregated nanoparticles to be taken advantage of. [70, 71, 85, 86]

Irudayaraj and co-workers demonstrated in 2007 the possibility of using nanoparticle tags in multiplexed DNA detection assays. [87] The development of a series of nanoparticle tags containing both Raman reporter molecules and probe oligonucleotides allowed the successful detection of eight probes simultaneously.

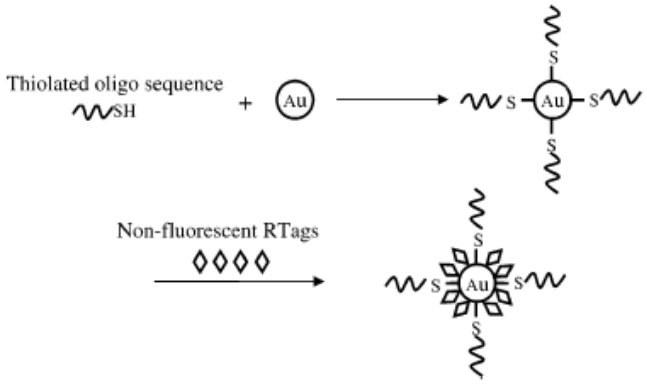

Figure 1.12 - Schematic representation of the synthesis of the nanoparticle tags. Gold nanoparticles are functionalised with thiol-DNA strands to produce DNA-nanoparticle conjugates. Non-fluorescent Raman tags are then introduced to the nanoparticle surface, resulting in a labelled DNA-nanoparticle conjugate. [87]

Eight non-fluorescent Raman tags were selected, all containing either sulphur or nitrogen as an affinity tag to attach the reporter molecule to the gold nanoparticle surface. As shown in Figure 1.12 the nanoparticle tags were co-functionalised with thiol-modified oligonucleotides, allowing for hybridisation of the nanoparticle tag conjugates with a target DNA molecule of choice.

1.10 DNA DETECTION METHODS BASED ON SE(R)RS

The detection of DNA is an exceptionally important field of research for medical diagnostics. Many researchers in recent years have been focussing on the creation of DNA detection systems using SE(R)RS as a detection method. To aid in this detection, metallic nanoparticles are also incorporated into these diagnostic assays. The use of DNA conjugates is becoming more frequent due to the unique properties they can offer these detection systems in terms of both selectivity and sensitivity.

1.10.1 COLLOID BASED DETECTION TECHNIQUES

1.10.1.1 Molecular Sentinels

In 2005, Vo-Dinh *et al.* detailed the use of molecular sentinels for the successful detection of DNA relating to the *gag* gene sequence of the human immunodeficiency virus type 1 (HIV-1). [88] The probes were used to detect PCR amplicons of the HIV gene.

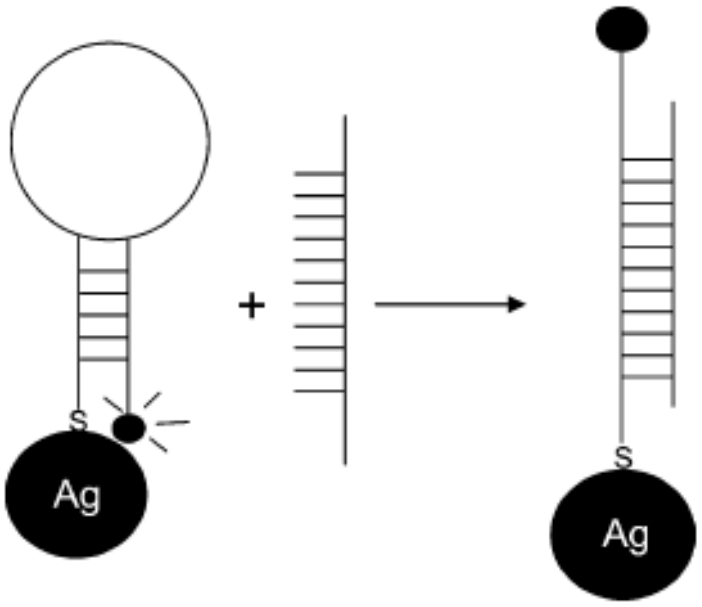

Figure 1.13 - Schematic of molecular sentinel concept. When in the closed hairpin configuration, a SERS signal corresponding to the dye can be seen. When in the open conformation, the signal is reduced. [88]

The molecular sentinel molecule consists of a metallic nanoparticle and a dye-labelled stem-loop DNA strand, as seen in Figure 1.13. The DNA sequence consists of a central section that is complementary to the target DNA sequence, and two flanking complementary sequences, which give rise to the hairpin loop structure. In the absence of target DNA, the stem-loop configuration remains in the "closed" position, with the Raman label held in close proximity to the nanoparticle surface. Consequently, upon interrogation with a laser of suitable wavelength, a strong SERS signal is observed. In the presence of target DNA, the stem-loop configuration is changed, resulting in the Raman reporter being removed from the nanoparticle surface. In this case, the SERS enhancement is dependent upon the distance *d* between the Raman reporter and the nanoparticle surface. Accordingly, the SERS effect is dramatically reduced due to the increase in *d*, resulting in the related reporter signal being reduced.

This group also reported the first proof of concept that the molecular sentinel approach could be multiplexed in a homogeneous solution assay format without the need for separation or washing steps. [89] Two nanoprobes containing different Raman reporter molecules were designed towards targeting two separate genes, *erbB-2* and *ki-67*. The two genes selected are used clinically as diagnostic biomarkers for breast cancer. Multiplex detection was performed in the presence of both corresponding target DNA sequences, as

well as in the presence of individual DNA targets. When both target molecules were present, the SERS signal associated with both reporters was reduced. However, in the presence of one target sequence, only the spectrum associated with the reporter from the corresponding nanoprobe relating to the target present was reduced.

1.10.1.2 SERRS Beacon

In 2005, Faulds *et al.* released details of a new approach to DNA detection by SERRS. [90] A thiolated DNA strand was coupled *via* Michael addition to dye labels, which were specifically designed for attachment to silver surfaces. This resulted in a "SERRS Beacon" being formed that could be used for both fluorescence and SERRS detection.

The assay was based around the concepts used for fluorescence detection of molecular beacons. [91] Molecular beacons are a dual labelled, single strand of DNA, with complementary bases at either end, resulting in the strand being closed over and held in a hairpin conformation. The loop section of the hairpin is the probe sequence, which is complementary to the target DNA sequence being detected. One end of the probe strand is functionalised with a fluorescent dye, whilst the other is typically labelled with a quencher molecule. In the "closed" conformation, the fluorescent dye is held in close proximity to the quencher molecule, resulting in no fluorescence being observed. In the presence of target DNA, however; the hairpin is opened, removing the fluorescent dye from the proximity of the quencher molecule, thereby allowing for fluorescence to be detected.

The SERRS Beacon is a dual-labelled probe with a fluorophore at the 3' end of the oligonucleotide strand, and a second dye at the other. In this case, benzotriazole dye was coupled to the beacon DNA strand at the 5' end. This was carried out in order to facilitate attachment of the oligonucleotide to the surface of a silver nanoparticle *via* complexation of the benzotriazole moiety with the silver surface. 5-(and 6)-carboxyfluorescein (FAM) was selected as the fluorophore label present at the 3' end. The resultant beacon configuration displayed 98% fluorescence quenching when immobilised on the nanoparticle surface.

Whilst in the "closed" conformation, the signal observed by the SERRS Beacon was dominated by FAM. This is a result of FAM giving a more intense signal than the benzotriazole dye by approximately two orders of magnitude. The fluorescence of the

beacon in this arrangement was also recorded, resulting in no signal being detected. This is a direct result of the highly efficient fluorescence quenching from the silver nanoparticle. Upon addition of target DNA, a fluorescence signal could then be detected. Upon analysis by SERRS, the spectrum collected had changed to reflect the distancing of the FAM from the nanoparticle surface.

Further work was carried out using a complementary sequence containing overhanging bases to mimic hybridisation to a target sequence within a longer strand of DNA. Discrimination could clearly be seen between the signal observed in the absence of target DNA, where sharp bands relating to the spectrum of FAM could be seen, and in the presence of target DNA, where a significant fluorescent background can be observed. This fluorescent background was a result of the FAM dye moving further from the nanoparticle surface, and consequently, the fluorescence from the dye being quenched to a lesser degree by the nanoparticle.

1.10.1.3 Assembly Induced Aggregation Based SERRS Assays

In 2008, Graham *et al.* published details of the successful synthesis of oligonucleotide-silver nanoparticles (OSNs), and their subsequent use in a sandwich assay format for the detection of DNA. [85] Oligonucleotide probes were immobilised on the nanoparticle surface *via* a terminal alkyl thiol group situated on either the 3' or 5' end of the strand. The method of synthesis for the silver nanoparticle conjugates is similar to that of their gold counterparts. [70] A spacer group was introduced to the oligonucleotide for two purposes. Firstly; to prevent attachment of the reactive functional groups, present in the oligonucleotide bases, to the nanoparticle surface. Secondly, the spacer group aids the DNA hybridisation process by decreasing steric hindrance caused by other immobilised oligonucleotide strands. It was found that subsequent to OSN synthesis, the conjugates were stable for up to 3 months at room temperature.

Hybridisation of OSN conjugates was performed in a sandwich assay format, with two different OSN conjugates being made. Each set of conjugates was functionalised with a sequence of DNA that was half complementary to the sequence of the desired target being detected. Upon hybridisation of both probes with the target DNA, the nanoparticles were brought into close proximity to one another, resulting in aggregation occurring. This

aggregation process was observed by both scanning electron microscopy (SEM) and UV-vis spectroscopy. The UV-vis spectrum showed a broadening of the surface plasmon peak associated with the silver nanoparticle conjugates, with an absorbance maxima at 540 nm. The ability of the system to detect single base mismatches was also tested in comparison with oligonucleotide-gold nanoparticles (OGNs). Consequently, the OSN conjugates giving a minimum detectable target oligonucleotide concentration 50 x lower than that of their gold counterparts.

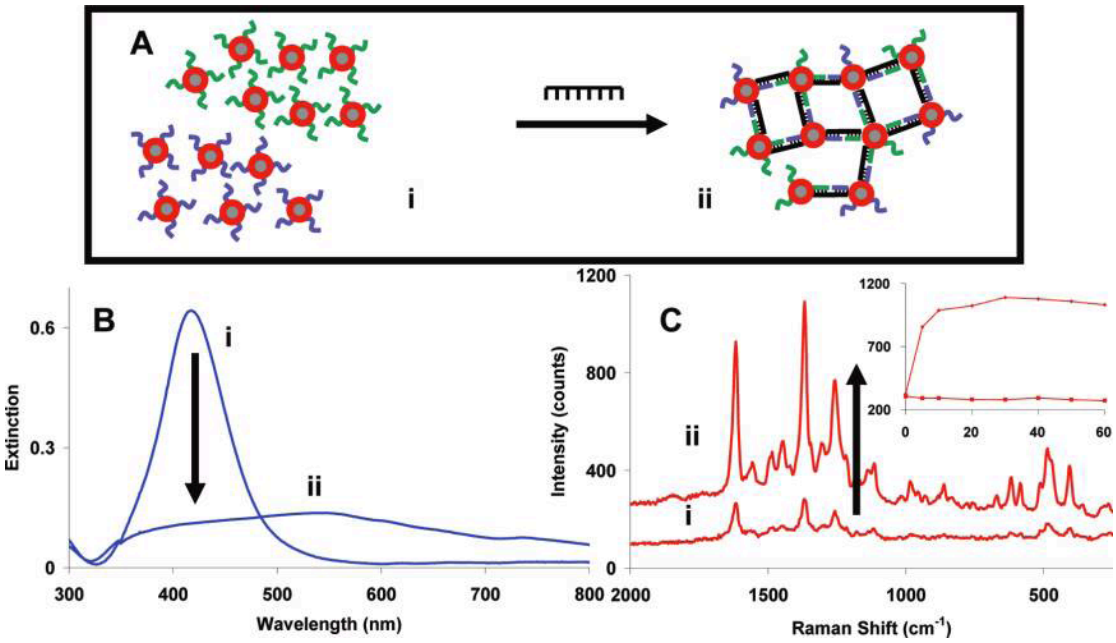

Figure 1.14 -(A) A diagrammatic representation of the controlled aggregation of OSNs; (B) A Uv-vis spectra (i) pre and (ii) post target addition, indicating a red shift in surface plasmon alongside a drop in peak intensity, (C) SERRS spectra before (i) and after (ii) target addition showing the increase in the SERRS intensity. The inset graph shows the increase in SERRS intensity over time. [92]

This initial work was later expanded upon by introducing the use of SERRS for sequence specific DNA detection. [92] A Raman dye was introduced to the surface of the OSN detailed previously, resulting in SERRS active conjugates. The assay concept focuses on the enhancement of SERRS signals when nanoparticles were brought in close proximity to each other, creating "hot spots" in the interstices between particles, as shown in Figure 1.14 (A). Two sets of OSN conjugates were synthesised, each with the same dye but with different probe sequences. The conjugates prepared were stable in 0.3 M sodium chloride and 10 mM phosphate buffer at pH 7 for over 6 months. Upon addition of target DNA with a sequence complementary to that of the two probe sequences, a yellow to green/blue

colour change was observed. As indicated in Figure 1.14 (B), this colour change could also be observed in the extinction spectrum. This change is indicative of aggregation of the nanoparticle conjugates having occurred.

When this assay construction was analysed by monitoring the SERRS spectral intensity of the oligonucleotide conjugates, a dramatic increase in signal was observed upon addition of target DNA as shown in Figure 1.14 (C). It was observed that upon heating the assay sample, the SERRS signal was reduced to a minimal level. This is a direct consequence of the heat inducing the denaturation of the duplex, resulting in the nanoparticles becoming unaggregated. To test the specificity of this approach, three separate batches of nanoparticle conjugates were functionalised with different DNA sequences and dyes. It was shown that in the presence of the three different conjugates; SERRS signals are only observed for the dyes from the probe relating to the targets present. It was later shown that in the presence of a single base mismatch in the target sequence, there was no increase in SERRS intensity. [93]

This work has been expanded to include the use of mixed metal nanoparticle assemblies containing a mixed network of silver and gold nanoparticles. [94] It has also been shown that DNA triplexes containing locked nucleic acid (LNA) bases can be used to successfully direct nanoparticle assembly in this approach. [95]

1.10.1.4 Magnetic Capture Assay

In 2011, Johnson and co-workers published details of the successful detection of DNA corresponding to the genome of the West Nile Virus by SERS. [96] The assay format adopted a split-probe configuration, with two probes for detection of a specific sequence of DNA. An oligonucleotide functionalised-paramagnetic nanoparticle was designed to act as a capture probe, immobilising the target-probe duplex upon successful hybridisation. The second probe utilised within the assay was a gold nanoparticle functionalised with a Raman reporter and a reporter oligonucleotide. In the presence of target DNA, the probes will successfully bind to the target sequence, resulting in a duplex labelled with both a SERS active nanoparticle, and a magnetic nanoparticle. This duplex could then be immobilised by application of a magnetic field, resulting in the hybridised SERS active nanoparticle probes being removed from the solution and compacted into a pellet, before interrogation with a

laser. The Raman reporter molecule selected was 5,5'-dithiobis(succinimidy-2-nitrobenzoate), DSNB.

In the presence of target DNA, the magnetically pulled-down assay gave a large SERS signal, relating to the SERS peaks of DSNB. However, in the absence of target DNA, the nanoparticle conjugates were not immobilised by the magnetic pull down process, thereby resulting in a small SERS response being observed. The specificity of the assay was tested by the introduction of a non-complementary 50 base oligonucleotide, in place of the target DNA strand. The same minimal response was seen in the presence of non-complementary DNA as was observed for the negative control samples. It was shown that the assay in the absence of target DNA (or presence of nonsense of DNA) gave a 200-fold decrease in SERS response when compared with the signal observed in the presence of target DNA. The limit of detection for this assay was found to be 10 pM.

Whilst a vast array of research into the use of DNA conjugates for DNA detection has been done in solution, a number of research groups have had success developing techniques utilising DNA nanoparticle conjugates with a bulk substrate.

1.10.2 SURFACE BASED DETECTION TECHNIQUES

1.10.2.1 Scanometric Detection

In 2000, Mirkin *et al.* detailed the use of DNA-nanoparticle probes in a scanometric array format to successfully detect a specific DNA sequence. [84] The detection utilised the light scattering properties of metallic nanoparticles, in conjunction with a conventional flatbed scanner.

The assay consisted of a three-component sandwich assay immobilised on a glass slide, shown in Figure 1.15**.** Gold nanoparticles were modified with oligonucleotides complementary to a section of the target DNA being detected. A glass microscope slide was functionalised by attachment of 3' thiol-modified capture oligonucleotides to the slide surface. Upon addition of target DNA, the capture probe and nanoparticle probe hybridise to the target sequence, resulting in immobilisation of the gold nanoparticles on the glass surface. A signal amplification process was introduced to allow for detection of lower levels

of DNA. The immobilised gold nanoparticles were subjected to staining with silver *via* reduction of silver ions on the gold surface by hydroquinone. The process increased the scattering intensity by as much as a factor of 10^5.

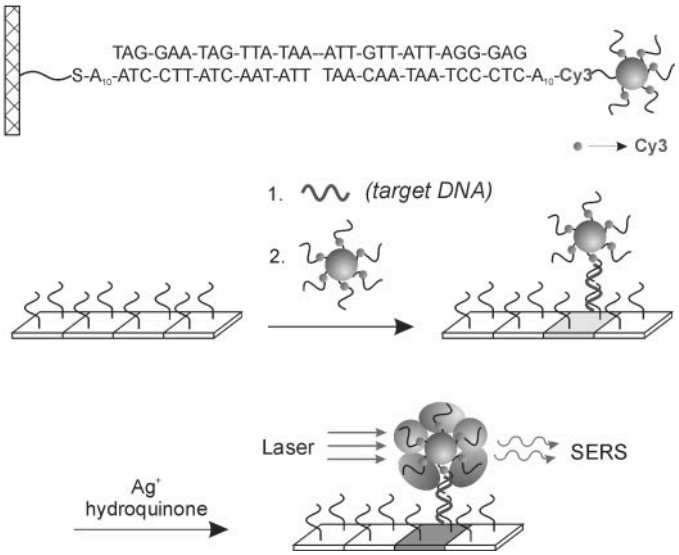

Figure 1.15 - (a) SERS active nanoparticles are immobilised on the surface of the glass slide in the presence of target DNA by formation of a target-probe sandwich, (b) Target DNA is immobilised by the capture oligonucleotides bound to the slide surface, followed by the hybridisation of the dye-labelled nanoparticle probes. The gold nanoparticles are subjected to shelling by silver ions in the presence of hydroquinone, resulting of amplification of the SERS signal. [84]

Further to their publication in 2000, a two colour scanometric assay was developed for the selective detection of two different DNA targets. [83] The assay incorporated two different sizes of gold nanoparticles as the basis for the oligonucleotide nanoparticle probes into the assay system detailed previously. [84] Due to the differing sizes of the nanoparticles, the surface plasmon of each had a different λ_{max} value. This property was exploited, with each nanoparticle probe giving a different colour of scattered light. In the presence of both targets, signals for both respective nanoparticle probes were observed. Selective independent detection of each of the targeted DNA sequences was also performed, resulting in only signal for the nanoparticle probe corresponding to the target present being seen.

Expanding further on the concept of multiplexed DNA detection, Mirkin *et al.* detailed the use of Raman reporters in tandem with DNA-nanoparticle probes. These probes were

designed for the parallel detection of six different nanoparticle probes, each relating to a different target sequence, using SERS as a detection technique. [97] Gold nanoparticles were functionalised with Raman dye-labelled oligonucleotides. Six target DNA sequences were selected, with a Raman dye designated to a complementary probe for each target. Successful detection of all six probes simultaneously was reported, as well as varying combinations of the six probes. Furthermore, it was shown that two targets could be differentiated in a semi quantitative manner by monitoring the ratios of the major peaks from the two dyes relating to the targets present.

1.10.2.2 DNA Detection on Smooth Metal Films

Recently, Braun *et al.* published details of the utilisation of a smooth metal film in conjunction with nanoparticles for the detection of a specific DNA sequence by SERS. [98] The assay was based upon the prediction that the junctions between nanoparticles and smooth metallic surfaces serve as SERS hot spots.

Silver nanoparticles were functionalised with a probe DNA sequence corresponding to the complement of one half of the target DNA being detected. A smooth, non-SERS active silver film was functionalised with a DNA probe corresponding to the complement of the other half of the target DNA strand, illustrated in Figure 1.16. The silver film was then capped with 6-mercaptohexanol (MCH) to prevent non-specific binding and aid the DNA hybridisation. The film was then functionalised with a thiol-modified SERS dye, 5-(2-(and 3)-*S*-(acetylmercapto)succinoyl)amino) fluorescein (SAMSA fluorescein). The functionalised film was incubated with the target DNA strand, followed by the oligonucleotide-nanoparticle probes. As shown in Figure 1.16, the target DNA was captured onto the silver film surface, followed by binding of the silver nanoparticle to the target DNA. This results in the nanoparticles becoming bound, in close proximity, to the surface of the silver film. The surface was washed to remove any nanoparticles that have not been immobilised onto the surface.

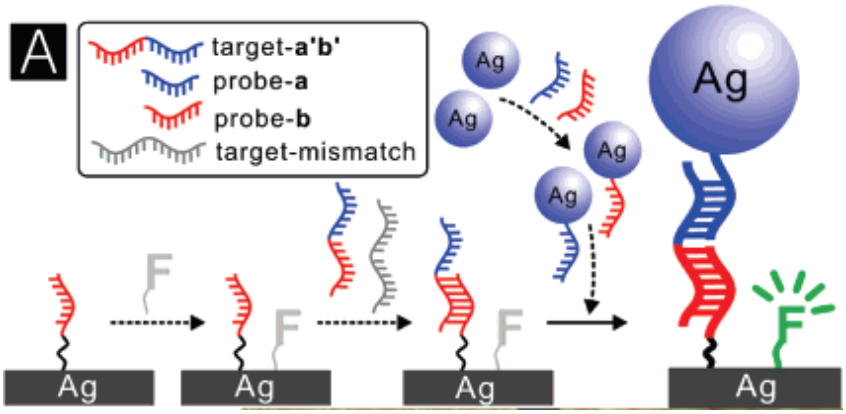

Figure 1.16 - Schematic illustration for the detection of single-stranded DNA by SERS. The target DNA strand (a'b') is immobilised by the capture probe (b) and the nanoparticle probe (a) is in turn hybridised to target strand. This results in the production of SERS hotspots between the nanoparticle and the silver surface. The presence of target DNA is indicated by the collection of SERS spectra corresponding to the surface-bound SERS dye (F). [98]

In the presence of target DNA, a strong SERS signal was observed corresponding to the surface bound SERS dye, indicating the immobilisation of the silver nanoparticles on the silver film. Control experiments demonstrated that in the absence of the functionalised nanoparticles, the captured target DNA does not give any SERS signal when immobilised on the dye-modified silver film. This is due to the surface's lack of roughness, a property required in order for SERS signals to be observed. No observable SERS signal was observed when the functionalised silver film was incubated with the nanoparticle probes in the absence of target DNA, or when non-complementary DNA was used.

It has been demonstrated that there has been a number of developments in recent years, leading to the successful detection of DNA by SERRS. However, there is a requirement for an assay to be developed which could both sensitively and specifically detect DNA relating to a specific disease in clinical samples. Consequently, the work detailed within this thesis was directed towards fulfilling this requirement.

2. DNA DETECTION ASSAY CONTAINING SILVER-TAMRA NANOPARTICLE CONJUGATES

2.1 AIMS & CONCEPT

In this chapter, a new method is proposed which will allow for the detection of target DNA of a specific sequence relating to a disease state. The success of this concept relies on the detection of a measurable signal following sequence specific hybridisation of two split probes, each relating to half of the sequence of the target of interest (Figure 2.1). It is anticipated that this technique will provide the high level of sensitivity and specificity necessary for genomic detection of specific DNA sequences.

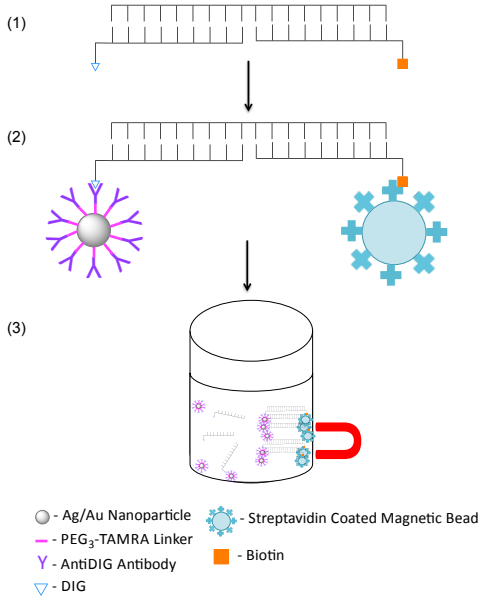

Figure 2.1 - Schematic representation of the fully constructed assay. (1) Target DNA hybridised to digoxigenin and biotin labelled probes. (2) The digoxigenin probe is bound by a hapten-antibody interaction to silver nanoparticles, functionalised with a TAMRA linker coupled to an anti-DIG antibody. The biotin probe is bound by a biotin-streptavidin interaction to a streptavidin coated magnetic bead. (3) Upon introduction of a magnetic field, the magnetic particles with the SERRS-active particles tethered to them are gathered at the side of the sample vial. Any excess assay components present in the sample will remain in the buffer solution. SERRS analysis is then performed on the magnetic particles either in solution, or directly on the immobilised beads.

The principle of the assay is that both probes will hybridise to the target DNA sequence of interest (step 1). The DIG label on the oligonucleotide probe can then interact with the

antiDIG antibody on the nanoparticle conjugates, allowing the duplex formed to become labelled with a SERRS active nanoparticle. This labelled duplex can interact via the biotin label on the capture probe with the streptavidin coated magnetic beads, resulting in the immobilisation of the SERRS active nanoparticle on the magnetic bead (step 2). In the idealised assay this would be performed in a sealed tube with the magnetic particles gathered at the side of the tube for analysis by the introduction of a magnet, and the excess assay components remaining in solution (step 3). However, whilst the assay is being optimised a washing step is introduced whereby upon construction of the assay the magnetic beads are pulled to the side of the tube and the supernatant is removed and the assay resuspended in buffer. This step is repeated to remove any excess assay components and the magnetic beads are resuspended. The SERRS analysis is then performed on the solution containing the magnetic beads.

If full complementarity is not achieved, both probes will not bind to the target strand. This will result in either the loss of the binding of the functionalised nanoparticles or the magnetic bead. If the nanoparticles are no longer bound to the hybridised DNA, when a magnetic field is applied to the sample (thereby separating the assay from the supernatant) no SERRS signal will be seen due to the absence of both the metal surface, and the SERRS dye. Likewise, if the magnetic beads are no longer bound to the hybridised DNA, when separation occurs no SERRS signal will be observed due to the absence of the metal nanoparticles and the SERRS dye. These would have been removed in the supernatant after washing, or in the case of the closed tube assay, these would remain in solution whilst the magnetic beads are analysed as a pellet on the side of the sample tube.

Silver nanoparticles were functionalised with the fluorescent dye TAMRA, which has been previously shown to give a strong SERRS signal. [54, 99] This functionalisation was facilitated by the incorporation of the dye into a PEG (poly ethylene glycol) linker (Figure 2.2). This linker was in turn bound to the surface of a silver nanoparticle *via* interaction of a thioctic acid terminating group on the linker with the metallic surface. This will allow for an intense SERRS signal to be detected, as the TAMRA dye is held closely to the metal surface. An anti-digoxigenin (antiDIG) antibody was then coupled to the linker by a sulfo-NHS/EDC coupling process.

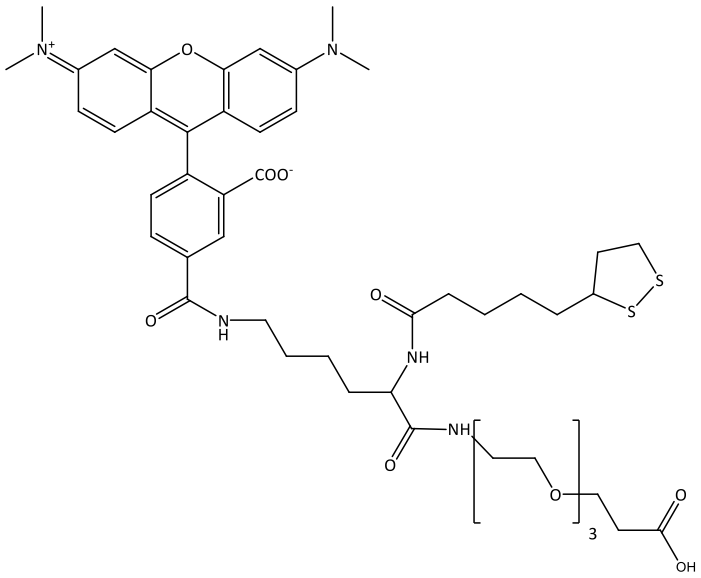

Figure 2.2 - PEG_3-TAMRA linker with thioctic acid terminating group.

Two probes were used in this assay, each of which corresponds to a different half of a specific target sequence, therefore when both are present, a full complementary sequence is available to the target strand of DNA. Both probes are modified in order to afford an interaction between the modification on the oligonucleotide probe and a particle within the system. The first of these probes was 5'-labelled with a digoxigenin molecule. This molecule can thereby interact with the anti-digoxigenin antibody on the silver nanoparticles resulting in a nanoparticle tagged oligonucleotide probe. The second probe is 3'-labelled with a biotin molecule. This molecule can then readily bind with the streptavidin coupled to the surface of a magnetic bead, allowing for magnetic separation of this probe, and all components of the assay that are bound to it. The interactions exploited in the construction of this assay are the streptavidin-biotin interaction and the digoxigenin (DIG)-antiDIG interaction.

Streptavidin is a tetrameric protein capable of binding with 4 biotin molecules through a number of interactions between the two molecules. As a result of these multiple interactions between streptavidin and biotin, streptavidin has a high avidity as well as a high affinity for biotin. The biotin-streptavidin interaction is the strongest known non-covalent biological interaction, with a dissociation constant, $K_d = 4x10^{-14}$ M. [100] The bonds form very rapidly and are stable in a series of differing temperatures and pH. [101] The versatility, accompanied by the strength of this interaction results in its wide-spread use in

biochemistry. It has been extensively used as the affinity pair of choice in molecular, immunological, and cellular assays. [102]

Digoxigenin (DIG) is a hydrophilic steroid found only in the flowers and leaves of the plants *Digitalis purpurea* and *Digitalis lanata*. [103] Digoxigenin can also be described as a hapten. A hapten is a small molecule with high immunogenicity. In general, antibodies raised against haptens have a higher affinity for their targets than those raised against antigens. Haptens will only illicit an immune response once attached to a larger carrier, for example a protein, however this carrier may be one which does not illicit an immune response when free. As a direct result if this, haptens are often conjugated to other biological molecules as immuno-tags.

Digoxigenin is found as a component of cardioactive glycosides, and therefore is of general medical and therapeutic interest. [104-109] Additionally, DIG has become popular as a biochemical reagent for the non-radioactive labelling of proteins and nucleic acids. As a direct consequence of its popularity in this area, a variety of reactive digoxigenin derivatives are available including activated esters, alkylating agents and reagents for oligonucleotide synthesis. [110] Due to its strong binding with the corresponding antibody, the DIG-antiDIG interaction is often used as an alternative when the use of the streptavidin-biotin interaction must be avoided. For instance, streptavidin-biotin and DIG-antiDIG are both commonly used in assays such as ELISA, since both interactions are stable enough to resist dissociation by thermal fluctuations. [111] It can also be seen as advantageous that digoxigenin is not naturally occurring within animals, since when compared to biotin which occurs in almost all natural tissues, the amount of unspecific binding which can occur during *in situ* hybridisations is reduced, thereby improving the sensitivity of the system. [112]

The target DNA sequence used within this assay corresponds to a fragment of the *Chlamydia trachomatis* gene. This target was chosen since *Chlamydia* is the most common bacterial sexually transmitted disease in the UK. [113] Consequently, clinical samples relating to this disease could be obtained with relative ease. Currently in the UK, the detection technique employed in detection of *C. Trachomatis* is nucleic acid amplification tests (NAATS). [114] Presently there are no enzyme immunoassays (EIAs), point of care tests (POCT)

or DNA probe technology that can compete in terms of sensitivity and specificity with the tests currently employed. [114]

Several components of the assay required optimisation to ensure the maximum signal and specificity were obtained. Experimental parameters required investigation to ascertain the best working conditions for the proposed assay. There are two main components of the assay construct that required optimisation.

- The functionalised nanoparticles used as a reporter required to be optimised in order to give a strong SERRS signal whilst remaining stable in the assay buffer. Variables such as the metal used for the nanoparticles, the dye selected, and the wavelength used for analysis all had to be considered.

- The DNA hybridisation process had to be monitored to assess the effect that the buffer selected for the assay construction has on the stability of the duplex formed.

Furthermore, a number of control experiments were required in order to assess the specificity of the assay, including testing its ability to distinguish between target DNA and nonsense DNA.

2.2 SYNTHESIS & CHARACTERISATION OF NANOPARTICLE CONJUGATES

2.2.1 REQUIREMENTS

The nanoparticle conjugates designed for use in this assay must meet a number of requirements. The three main requirements of these nanoparticles are:

- The conjugates must give a relatively intense, distinct SERRS signal in order for them to be successfully detected;
- The nanoparticles must be stable in the buffer in which the assay is performed in order for them to remain intact during construction of the final assay;
- The conjugates must have the ability to be easily biofunctionalised, whilst allowing the biomolecule immobilised on the nanoparticle to retain its functionality.

A number of differing approaches have been developed in order to produce metallic nanoparticles that are stable in a variety of environments. One of the most successful, and most highly utilised methods involves the introduction of a polyethylene glycol (PEG) layer onto the nanoparticle surface. In 2012, Graham *et al*. published details on the synthesis of a number of SERRS active linkers. [82] These linkers contain three key components (Figure 2.3); a surface complexing group (shown in green), a Raman tag (shown in red) and a chemical functionality available for conjugation to a biomolecule of choice (shown in blue). A thioctic acid moiety is introduced as the surface complexing group, responsible for anchoring the linker molecule to the nanoparticle surface. Mattoussi *et al*. published findings in 2009 detailing the increased stability of gold nanoparticles functionalised with thioctic acid modified PEG molecules, in the presence of both DTT and high salt concentrations, when compared with gold nanoparticles functionalised with monothiol modified PEG molecules. [115] The three Raman tags selected for incorporation into the synthesised linker molecules were all fluorescent dyes; fluorescein, 6-aminofluorescein and carboxytetramethylrhodamine (TAMRA). The dyes were incorporated into the linker in a position close enough to the metallic nanoparticle surface to allow for SERRS enhancement to be possible. The metal surface used to provide this enhancement quenched any fluorescence emitted from the dye molecules. [116-119] A terminal carboxylic acid moiety is

introduced in order to allow conjugation between the linker molecule and a biomolecule of interest.

The linker molecule selected for use within this work is the TAMRA labelled counterpart of these linker molecules (Figure 2.3), and was provided by J. Wrzesien. [82]

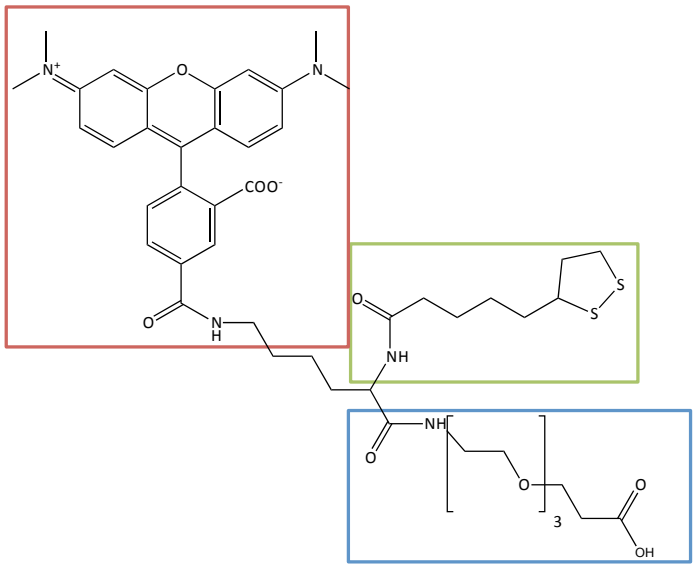

Figure 2.3 - Structure of the PEG_3-TAMRA linker. The linker molecule consists of a thioctic acid group (green) to allow the molecule to be immobilised on the nanoparticle surface, a TAMRA group (red) to provide a chromophore responsible for the SERRS signal, and a PEG chain terminated with a carboxylic acid group (blue). This carboxylic acid moiety provides a means of coupling biomolecules to the linker molecule.

As can be seen in Figure 2.3, the fluorescent TAMRA group is incorporated into the linker molecule in a position that prevents any steric hindrance between this group and the terminal carboxylic acid group. This should ensure that the carboxylic acid functional group remains available for biofunctionalisation.

2.2.2 Buffer Selection

The biotin-streptavidin and the DIG-antiDIG interaction are both strong, robust interactions which can be utilised without the need for any specific buffer conditions. [112, 120-123] As such, the dominant interaction with regard to the selection of the optimal buffer for the assay is the hybridisation of the probes to the target DNA. The hybridisation of single stranded DNA

to form a duplex can be monitored using UV-vis spectroscopy. Unmodified DNA absorbs light at 260 nm, a wavelength corresponding to the electronic transitions within the purine and pyrimidine bases in the oligonucleotide. [124] Single stranded DNA absorbs more light at 260 nm than double stranded DNA, thereby producing a sigmoidal curve upon monitoring the melting of the DNA duplex. The point of inflection on the curve produced is the melting temperature (T_m) and represents the temperature at which half of the DNA in the sample exists in the double helical state. This point can therefore be used to monitor the thermal stability of the duplex produced. The higher the value of the T_m, the more stable the duplex.

In order for a buffer to be selected, it was important to ascertain the concentration of salt required to afford a stable DNA duplex at room temperature. The DNA phosphate backbone is negatively charged, and therefore the backbone of the two complementary strands that make up a duplex will repel each other. The addition of NaCl to the hybridisation mixture results in the negative charge from the phosphate backbone being screened, thereby reducing the repulsive effect exhibited from the negative phosphate groups and resulting in a duplex with greater thermal stability, exhibiting a higher T_m. The higher the salt concentration in the hybridisation solution, the more stable the duplex formed.

Ideally, this assay will be performed and analysed at room temperature. Therefore, it is vital that the DNA duplex produced between the target sequence and the probes is stable at approximately 25 °C. A DNA melting experiment was performed in two different buffers to ascertain whether hybridisation to form a stable duplex at room temperature was possible using 0.3 M phosphate buffered saline (PBS). A control experiment was performed where the hybridisation was conducted in water. The DNA solutions were suspended in water or 0.3 M PBS, and the melting curves shown in Figure 2.4 were collected. As expected, the DNA solution suspended in 0.3 M PBS successfully hybridised to the target strand creating a stable duplex with a T_m of 47 °C. In contrast, the DNA solution suspended in distilled water showed no distinct melting profile indicative of hybridisation. This would suggest that at room temperature the target-probe duplex formed in the 0.3 M PBS buffer would be stable, whilst the duplex formed in water would be completely dissociated. Consequently, it can be concluded that 0.3 M PBS can be successfully utilised as the hybridisation buffer to yield a stable probe-target duplex at room temperature.

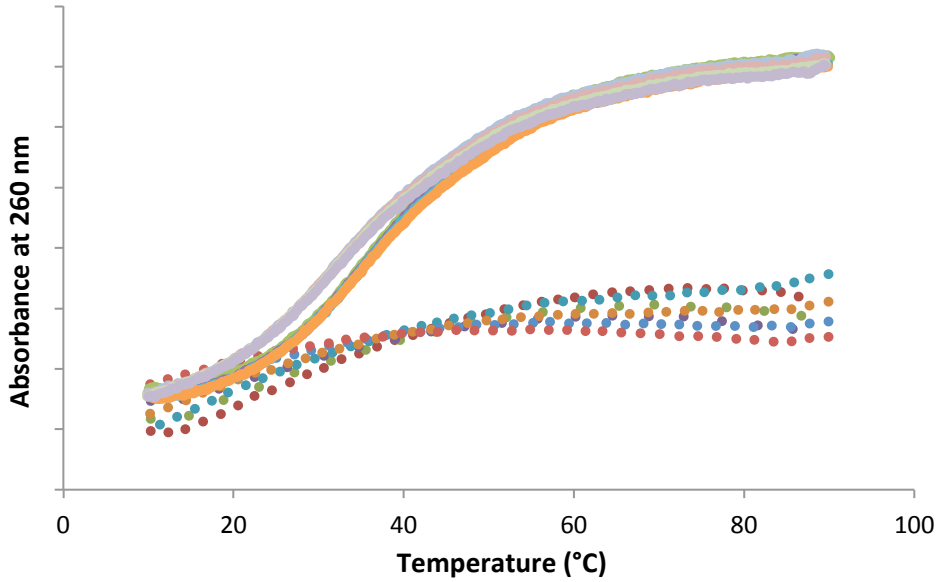

Figure 2.4 - UV melt collected between 10 °C and 90 °C at 260 nm. The sample solution contained the biotin capture probe, the digoxigenin probe and the target DNA. 8 cycles are displayed, 4 showing the heating process and 4 showing the cooling. One DNA solution was suspended in water (dashed lines), the other was suspended in 0.3 M PBS (solid lines).

The addition of salt to the assay buffer was a key point, as nanoparticles are known to be less stable in a salt-containing buffer. [125] It is important that the nanoparticle conjugates used within this assay remain intact and stable, therefore the development of a functionalisation protocol for the production of these conjugates would have to take this into consideration.

2.2.3 NANOPARTICLE SELECTION

It has been discussed previously that it is useful for different types of metallic nanoparticles to be used to give an optimised SERRS response. [54] Figure 2.5 illustrates the absorbance spectra of both silver and gold nanoparticles, as well as TAMRA. It can be seen that the absorbance maximum of TAMRA is approximately 560 nm. As such, the laser excitation frequency selected for use with this linker was 532 nm, represented by the vertical line in Figure 2.5. This wavelength was selected as it overlaps with the absorbance profile of the dye molecule, resulting in excitation at a wavelength close to its absorption maximum (λ_{max}). Although an overlap does occur, the laser wavelength is slightly "off resonance" with the dye. This allows for a resonance Raman effect to be observed, whilst minimising the fluorescent background observed from the dye.

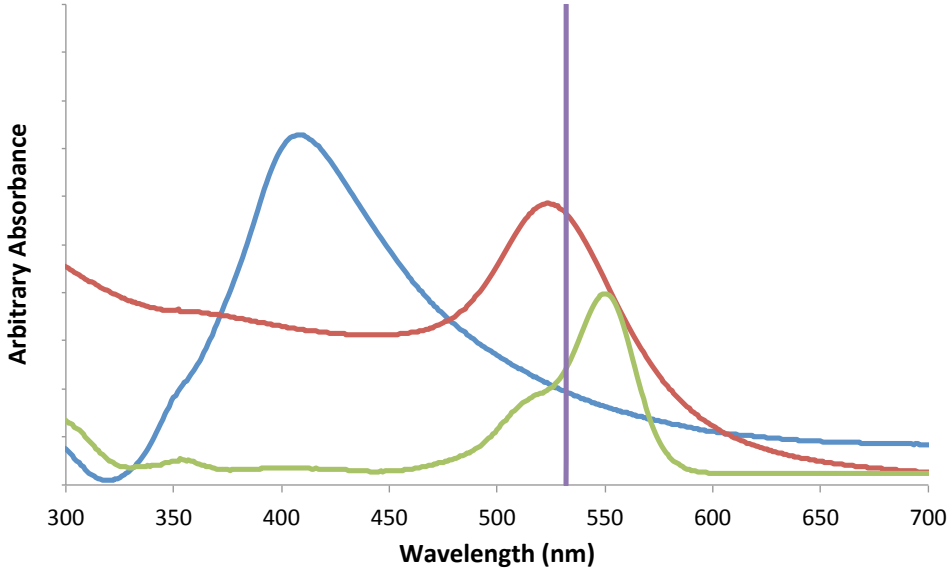

Figure 2.5 - UV-vis spectrum of silver nanoparticles (35 nm) (blue), gold nanoparticles (60 nm) (red) and TAMRA (green). The vertical line (purple) represents the laser excitation wavelength at 532 nm.

As illustrated by Figure 2.5, it could be expected that the SERRS enhancement may be greater with the use of gold nanoparticles, with an extinction maxima at about 520 nm, compared with silver nanoparticles, which have an extinction maxima at 400 nm. The signal observed from both gold and silver conjugates was compared to optimise the metal used in construction of the nanoparticle conjugates.

Gold and silver nanoparticles were prepared *via* citrate reduction of the metal salt. The nanoparticles were functionalised with the PEG_3-TAMRA linker, following the protocol detailed by Graham *et al.* [82] and the particles washed with distilled water. The SERRS signal obtained from each sample at 532 nm was compared, as shown in Figure 2.6. It can be seen that contrary to the expected result when considering the absorbance profile of both types of nanoparticle and TAMRA, the silver functionalised nanoparticles exhibit a higher intensity SERRS response in comparison to that seen from their gold counterparts. It should be noted that although the particles investigated are of different diameters, and consequently have different surface areas, the nanoparticle suspensions used for the functionalisation are also different concentrations. Consequently, the total surface area available for functionalisation with the linker molecule is comparable between the two nanoparticle suspensions.

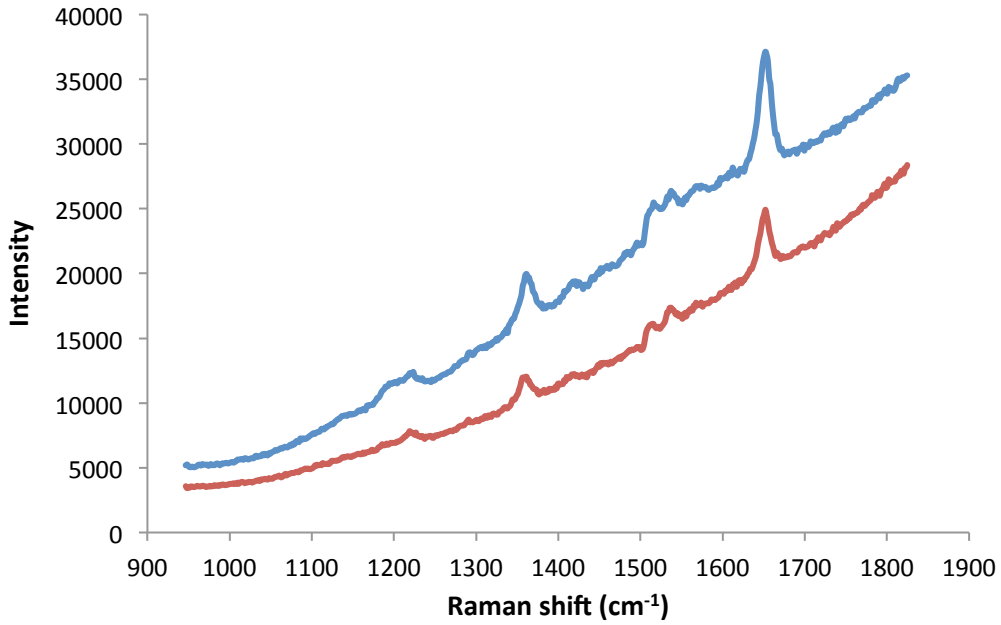

Figure 2.6 - SERRS signal obtained using 532 nm laser excitation, 20 x 1 s accumulation, from 45 nm silver nanoparticles functionalised with PEG_3-TAMRA linker (blue), and 60 nm gold nanoparticles functionalised with PEG_3-TAMRA linker (red), investigating the effect of different metallic nanoparticles on the SERRS response observed. The nanoparticles examined were not deliberately aggregated prior to analysis.

These results correspond well with previous work seen in the literature, which has found that silver has a greater SERRS enhancement factor than gold when used as the enhancing metal surface for the analyte. [54, 126] This is a consequence of the greater scattering to absorbance ratio for silver compared to gold, and the greater polarisability of the silver electrons, [127] resulting in greater overall surface enhancement.

As a result of these findings, silver citrate nanoparticles were selected as the core nanoparticle for functionalisation. It was postulated that in comparison to the use of gold nanoparticles, the silver nanoparticles would give rise to a lower limit of detection for the assay due to their more intense SERRS signals.

2.2.4 Characterisation of Silver Core Nanoparticles

In order for the nanoparticle conjugates prepared to give reproducible signals, with little variation in SERRS signal intensity, it was important that the nanoparticles used as the core for the conjugates were relatively unaggregated and stable.

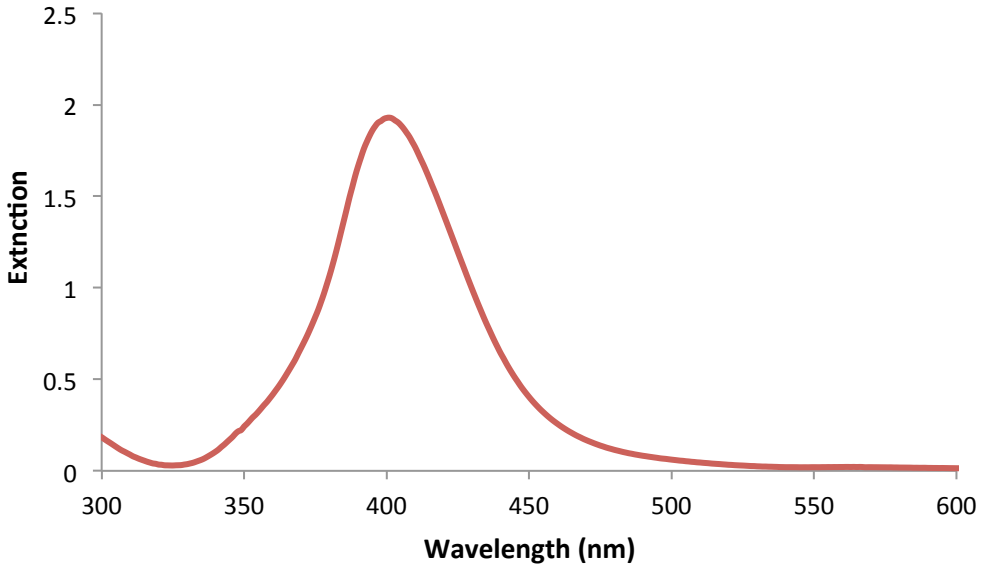

Figure 2.7 - Extinction spectrum of citrate stabilised silver nanoparticles, λ_{max} = 401 nm, FWHM = 50 nm. Dilution factor = 10.

Silver nanoparticles (35 nm) were prepared *via* citrate reduction of silver nitrate. [48] The silver salt was reduced from a +1 to 0 oxidation state, followed by the adsorption of excess citrate anions. [128, 129] The citrate anions afford a negative charge onto the nanoparticle surface, thereby providing the particles with electrostatic protection against irreversible aggregation.

Figure 2.7 shows an extinction spectrum obtained from a batch of citrate stabilised silver nanoparticles prepared for use as nanoparticle cores for the SERRS active nanoparticle conjugates. The absorbance maximum observed is approximately 400 nm, with the absorbance profile having a full width half maximum (FWHM) of approximately 50 nm. As such, the nanoparticles within the solution could be regarded as relatively discrete with a moderately narrow size distribution. This corresponds well with the SEM images obtained for this silver colloid. A representative example of these images is shown in Figure 2.8.

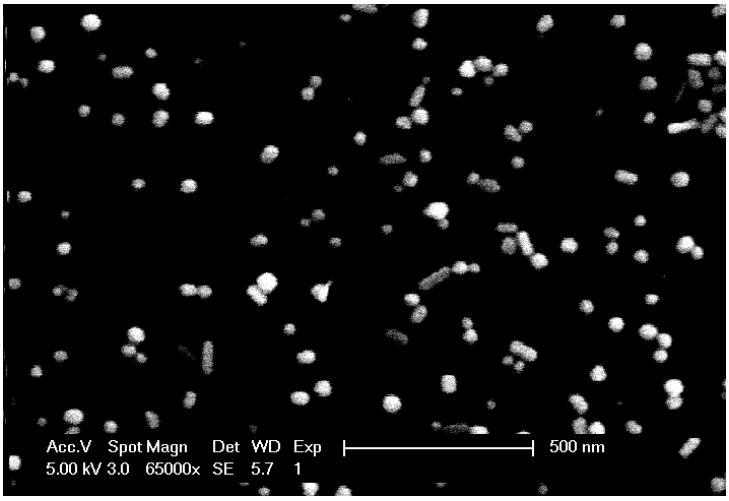

Figure 2.8 - Representative SEM image of silver colloid.

The SEM images obtained show a large number of monomeric silver nanoparticles, alongside a small number of dimers. A few silver nanorods can also be seen which are by-product of the nanoparticle synthesis. It should be noted that SEM images alone cannot be used to identify the aggregation state of the nanoparticles when in solution, however alongside the extinction spectrum, it can be suggested that the nanoparticle suspension consists of relatively discrete particles with an average size of approximately 35 nm.

2.2.5 FUNCTIONALISATION OF CORE NANOPARTICLES

In order for the Raman active nanoparticle conjugates to be incorporated successfully into the proposed assay, the nanoparticles must remain relatively discrete throughout the functionalisation procedure. This is vital since the aggregation of these SERRS active particles will provide "hotspots", an area of intense electromagnetic fields at the junction between aggregated nanoparticles with a heightened level of SERS enhancement. [64] As a result of this increase in enhancement, the nanoparticle suspension would give variable signal intensities, depending on whether the volume of sample being analysed contains aggregates or not, and if so, the degree of aggregation. Furthermore, in the idealised closed tube assay the presence of these aggregates would result in high background signals. Ideally, during the process of pulling the nanoparticles to the side of the sample tube, a degree of physical aggregation will be induced by the magnetic beads being gathered in close proximity to one another. As such, in order for the nanoparticle conjugates prepared

to give reproducible signals, they must remain relatively discrete, with the degree of aggregation kept to a minimal.

As previously stated, during the synthesis of silver citrate nanoparticles, a silver metal salt is reduced by citrate and as a result, unoxidised reducing agent is adsorbed onto the nanoparticle surface, rendering it negatively charged. [48] The charge introduced to the nanoparticle surface induces a repulsive force between particles, thereby preventing aggregation of the particles. Upon the addition of NaCl, the negatively charged citrate layer that stabilises the nanoparticle solution is displaced by the Cl^- ions present in the salt. [130] The repulsion between particles is consequently minimised, thereby resulting in the aggregation of the nanoparticles. This aggregation process can be monitored by extinction spectroscopy due to the change in the optical properties of the metallic nanoparticle upon aggregation. As the particles begin to aggregate, the surface plasmon resonance shifts to lower energies, resulting in a red-shift of the extinction maxima of the nanoparticle suspension. The original plasmon band will also decrease in intensity, and broaden as peaks begin to appear at longer wavelengths. Upon extreme cases where aggregation is complete, the absorbance band corresponding to the nanoparticle solution will flatten out, indicating that the nanoparticles have completely aggregated and been removed from the suspension.

A solution of silver nanoparticles was centrifuged and resuspended in buffer. The buffers investigated were distilled water compared with 0.3 M PBS, Figure 2.9 shows an extinction spectrum collected from these samples.

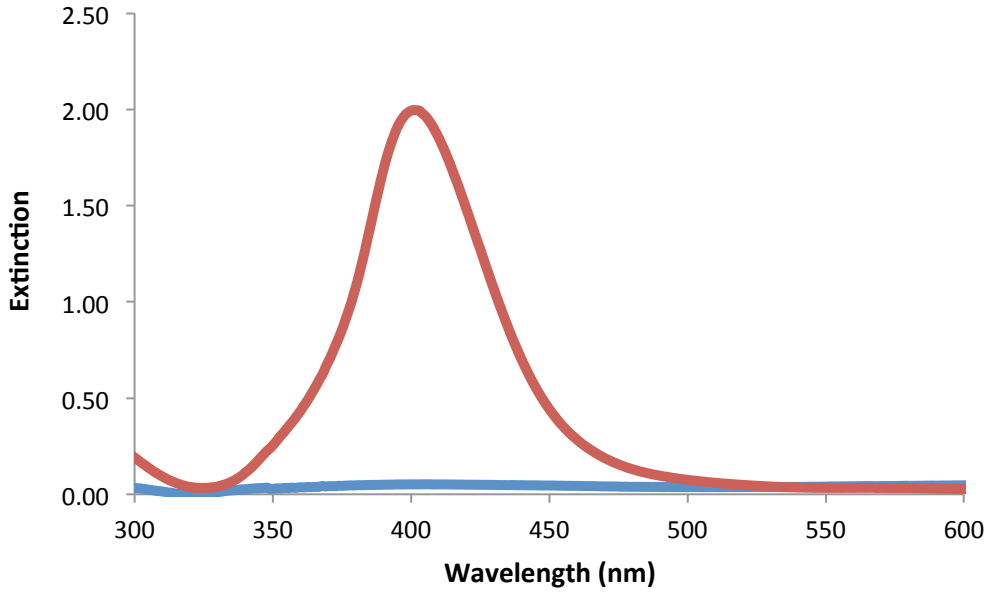

Figure 2.9 - Extinction spectra of silver nanoparticles resuspended in water (red) and 0.3 M PBS (blue). Dilution factor = 10.

This spectrum clearly indicates that upon addition of the NaCl containing buffer to the centrifuged sample, the nanoparticles fail to become resuspended into solution. This is likely due to the destabilisation and aggregation of the particles upon addition of NaCl to the system, resulting in the particles falling out of solution. This was visible when analysing the sample since, upon mixing of the pellet of nanoparticles in the PBS solution, large clusters of particles could be seen falling to the bottom of the sample tube. Subsequently, the plasmon band corresponding to the surface plasmon resonance of the silver nanoparticles is completely depleted upon the addition of the salt. As such, it is clear that unmodified silver nanoparticles are unstable in a buffer containing salt.

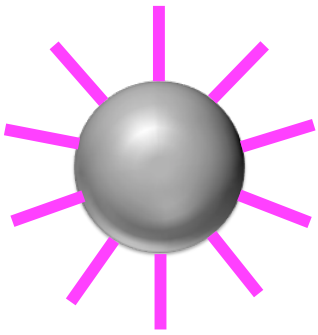

Figure 2.10 - Schematic of silver citrate nanoparticle functionalised with PEG_3-TAMRA linker. The linker molecule is tethered to the nanoparticle surface *via* a thioctic acid group, and contained a carboxylic acid moiety at the terminus free from the particle surface.

The DNA hybridisation is conducted in a salt containing buffer; therefore it was important to ascertain whether the functionalised nanoparticles could withstand these conditions. An aliquot of the PEG_3-TAMRA linker, shown in Figure 2.2, was added to a sample containing silver nanoparticles and incubated for at least 3 hours. The linker was immobilised on the nanoparticle surface *via* the thioctic acid group terminating the linker, resulting in PEG_3-TAMRA functionalised nanoparticles (Figure 2.10). The nanoparticles were then centrifuged and resuspended in a number of different buffers. The buffers investigated were distilled water, phosphate buffer (pH 7.6) and 0.3 M PBS (pH 7). An extinction spectrum was collected for each sample. The results obtained can be seen in Figure 2.11.

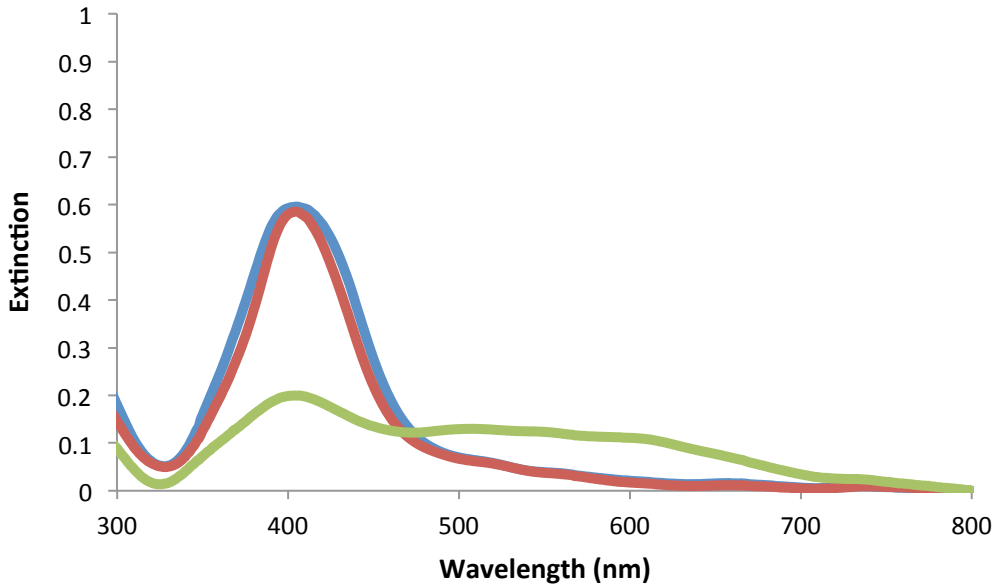

Figure 2.11 - Extinction spectra of silver nanoparticles functionalised with PEG_3-TAMRA linker in water (blue), phosphate buffer (pH 7.6) (red) and 0.3 M PBS (green). Dilution factor = 10.

Little effect is seen by resuspending the nanoparticles in phosphate buffer (pH 7.6) when compared to resuspension in water. A slight narrowing in the surface plasmon band is seen upon resuspension of the pegylated nanoparticles in phosphate buffer, however this could be due to a loss of some polydispersity during centrifugation. The overall extinction observed from the plasmon peak has not diminished however, and there is no appearance of a second peak at higher wavelengths, indicating that the nanoparticles have remained unaggregated. This is substantiated by the fact that the plasmon band at approximately 400 nm, attributed to the silver nanoparticles, has not shifted. This was supported by SEM imaging of the pegylated nanoparticles in phosphate buffer. A representative image is

shown in Figure 2.12, where it can be seen that the majority of the nanoparticles are isolated. When compared with the images obtained from the bare silver nanoparticles, shown in Figure 2.8, there is no significant aggregation visible.

However, when the pegylated nanoparticles were resuspended in 0.3 M PBS, the surface plasmon peak for the silver nanoparticles broadened and the extinction of this peak dramatically decreased. A second peak also appeared at approximately 600 nm. These results are indicative of the nanoparticles aggregating. It could be concluded that whilst the pegylated nanoparticles are stable in both distilled water and phosphate buffer, further functionalisation would have to be performed in order for the conjugates to be stable upon resuspension in 0.3 M PBS.

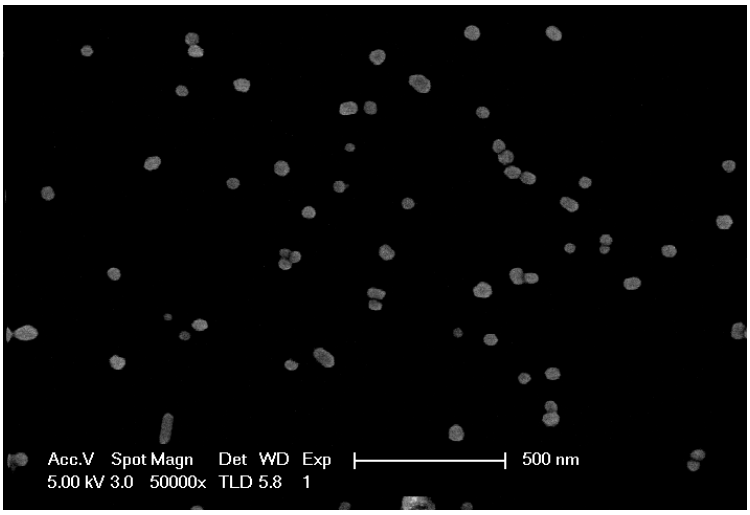

Figure 2.12 - Representative SEM image of silver colloid functionalised with PEG_3-TAMRA linker resuspended in phosphate buffer (pH 7.6).

2.2.6 BIOFUNCTIONALISATION OF PEGYLATED NANOPARTICLES

An aliquot of PEG_3-TAMRA linker solution was added to a sample of silver nanoparticles and incubated at room temperature for a minimum of 3 hours, affording a solution of pegylated nanoparticles. The nanoparticles were then centrifuged and resuspended in phosphate buffer (pH 7.6). AntiDIG antibody was then conjugated to the carboxylic acid group on the end of the linker molecule *via* an sulfo-NHS/EDC coupling mechanism with an amino group present in the antibody (Figure 2.13); the nanoparticles were subsequently washed with

and resuspended in two different buffers. The buffers used were phosphate buffer (pH 7.6) and 0.3 M PBS. An extinction spectrum was collected for each sample (Figure 2.14).

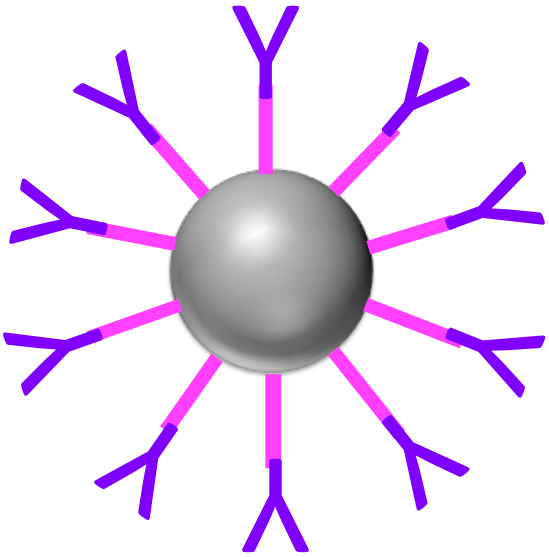

Figure 2.13 - Schematic of silver citrate nanoparticle functionalised with PEG_3-TAMRA linker. The linker molecule is tethered to the nanoparticle surface *via* a thioctic acid group, and contained a carboxylic acid moiety at the terminus free from the particle surface. An antiDIG antibody is then conjugated to the carboxylic acid group *via* an EDC/sulfo-NHS coupling process.

It can be seen that, in this case, resuspension of the functionalised nanoparticles in 0.3 M PBS, compared with phosphate buffer (pH 7.6), has very little effect on the extinction spectra. The peak corresponding to the surface plasmon of the silver nanoparticles at approximately 400 nm appears to have decreased slightly upon introduction of salt into the buffer system, however there is no appearance of a second peak at approximately 600 nm (previously seen in Figure 2.11). This would suggest that slight aggregation may have occurred, however this was not considered to be significant. Therefore, it can be concluded that the addition of the antiDIG antibody to the pegylated nanoparticles aids in the stabilisation of the nanoparticles in an ionic environment. It is likely that the introduction of the antibody to the terminus of the PEG linker shields the nanoparticle surface, making it less accessible to the destabilising chloride ions, and providing additional stabilisation to the surface.

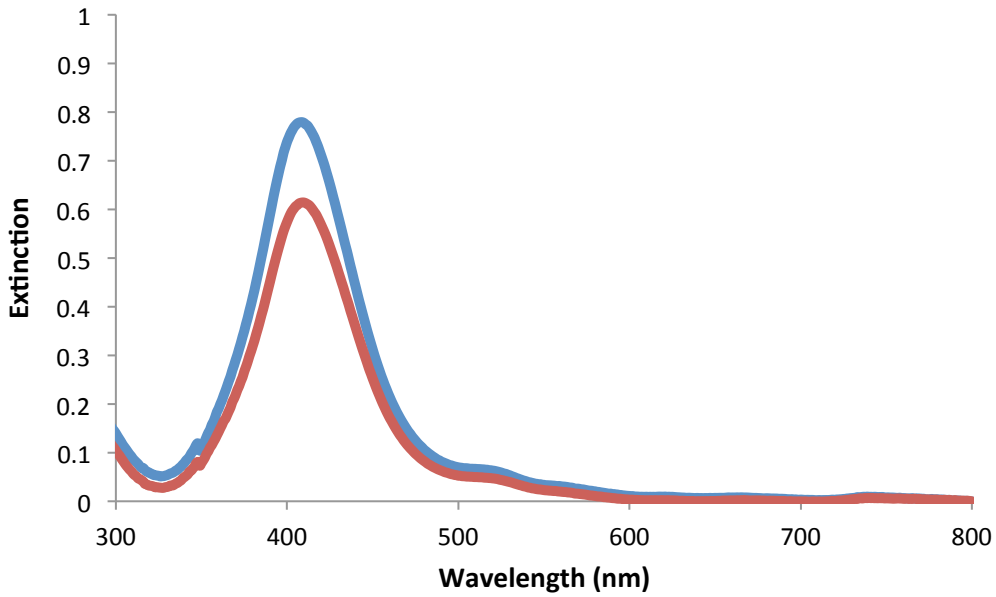

Figure 2.14 - Extinction spectra of silver nanoparticles functionalised with PEG_3-TAMRA and conjugated to anti-DIG antibodies, resuspended in phosphate buffer (pH 7.6) (blue) and 0.3 M PBS (red). Dilution factor = 10.

These findings are supported by the SEM images collected of the functionalised nanoparticles resuspended in 0.3 M PBS. An example of these images can be seen in Figure 2.15. It can be seen here that a number of small clusters, primarily containing up to four nanoparticles, have begun to form. However, there are still a number of isolated nanoparticles, and the aggregation, although visible, is minimal with no large aggregates observed. This corresponds with the lack of a surface plasmon peak at 600 nm, which would be attributed to the formation of larger aggregates.

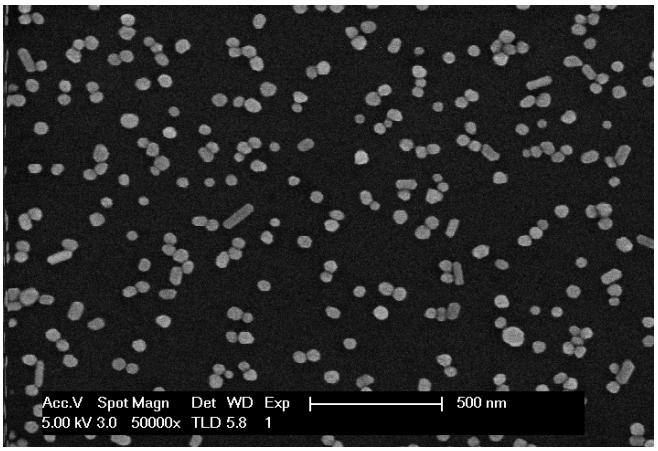

Figure 2.15 - Representative SEM image of silver colloid functionalised with PEG_3-TAMRA linker, and conjugated to antiDIG antibodies.

Consequently, it was concluded that the functionalised nanoparticles could be resuspended in the salt-containing buffer after the addition of the antibody without any detrimental effect to the nanoparticle stability.

2.2.7 QUANTIFICATION OF ANTI-DIG ANTIBODY

In order to gain a full understanding of the construction of the assay, it was vital to ascertain the number of active antibodies on the nanoparticle surface. This is important since the number of antibodies available for binding will directly affect the number of oligonucleotide probes bound to the nanoparticle. Conventional methods to quantify the number bound to the nanoparticles often use fluorescently labelled antibodies however this method poses two problems. The first of these issues arose due to the supplier (Abcam) not offering a labelled version of this antibody, and it could only be purchased in small quantities, making on-site labelling difficult due to cost. An alternative fluorescently labelled antibody could have been selected however the size and properties of the alternative antibody may differ from the antiDIG antibody used in the assay. Consequently, the calculations performed using this antibody were unlikely to be accurate. Secondly, the detection of the fluorescently labelled antibody will merely indicate the number of antibodies immobilised on the nanoparticle surface. Since the antibody in this assay is responsible for tethering the nanoparticle to the DIG-labelled probe, it is vital that it remain functional in order for this interaction with its corresponding hapten to occur. The quantification of a fluorescently labelled antibody will not give any indication about the functionality of the bound antibody; therefore no information can be gained about the number of probes that are successfully bound to each nanoparticle. A method was therefore developed in order to gain an insight into both the number and functionality of the immobilised antibodies. The method developed was based upon the quantification of the number of DIG-labelled probes bound to the nanoparticle. These probes will be bound *via* the DIG-antiDIG interaction and are therefore tethered to the antiDIG antibody present on the nanoparticle surface, as shown in Figure 2.16. Consequently, upon quantification of the number of DNA probes bound to these nanoparticles, an estimation of the number of active antibodies bound to the nanoparticle can be made.

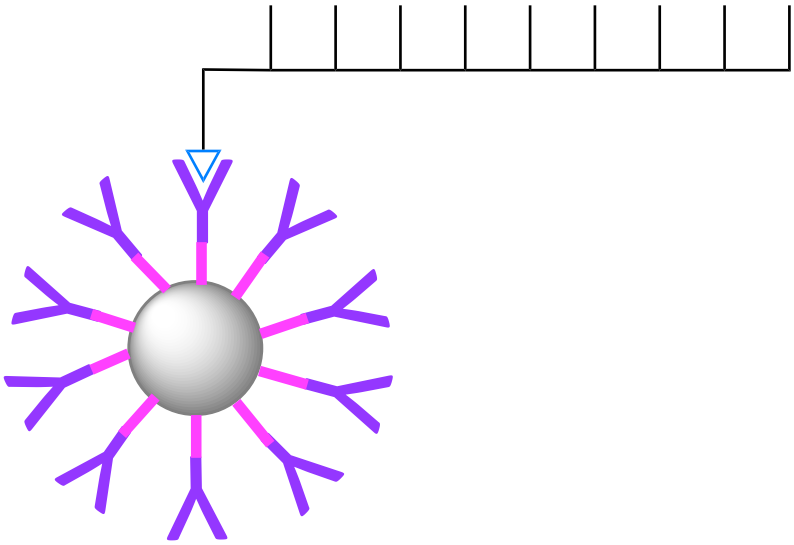

Figure 2.16 - Schematic demonstrating the immobilisation of the DIG-labelled DNA probe to the SERRS-active, antibody functionalised nanoparticle conjugates. Silver citrate nanoparticles are functionalised with PEG_3-TAMRA linker. The linker molecule is tethered to the nanoparticle surface *via* a thioctic acid group, and contained a carboxylic acid moiety at the terminus free from the particle surface. An antiDIG antibody is then conjugated to the carboxylic acid group *via* an EDC/sulfo-NHS coupling process. The oligonucleotide probe functionalised with a DIG molecule then becomes bound to the antibody functionalised nanoparticle *via* the DIG-antiDIG interaction.

The number of active antibodies bound to a single nanoparticle was calculated using Quant-iT OliGreen (Invitrogen, Paisley), a nucleic acid stain that fluoresces upon binding to single stranded DNA. The OliGreen dye used has an excitation wavelength of 480 nm and emits at 520 nm. This means that should any fluorescence be observed from the TAMRA in the linker molecule, it should be easily distinguished from that observed from the OliGreen dye.

A sample of antiDIG antibody functionalised nanoparticles was incubated with a solution of DIG-labelled DNA probe, allowing for the probe DNA to become tethered to the nanoparticles. An aliquot of OliGreen dye was then added to the sample, fluorescently labelling the single stranded DNA. The nanoparticles were centrifuged and washed three times to remove any unbound DNA and OliGreen dye that would emit a fluorescent signal, therefore the only DNA remaining in the sample should be bound to the nanoparticles. It has been shown that metal nanoparticles are able to quench [116-119] or enhance [131, 132] fluorescence; therefore it was necessary to displace the fluorescently labelled

oligonucleotides from the nanoparticle surface prior to analysis. In order to do so, the antibody-hapten interaction tethering the DNA to the nanoparticle was disrupted by denaturation of the antibody. The antiDIG antibody is a monoclonal IgG antibody. It has been previously reported by Vermeer *et al*. that IgG antibodies denature fully at 71 °C. [133] Upon denaturation, the antibody's ability to bind with its corresponding hapten or antigen is markedly diminished. Consequently, upon denaturation of the antiDIG antibody coupled to the PEG linker, the nanoparticle will no longer be bound to the oligonucleotide probe. This denaturation was initiated by heating and holding the sample at 75 °C. The sample was centrifuged to remove the supernatant containing the oligonucleotide probes from the vicinity of the metallic nanoparticles. The supernatant was analysed and the fluorescence recorded. A control sample was also prepared containing the pegylated nanoparticle conjugates prior to the addition of the DIG-labelled probe and the OliGreen dye in order to ensure no signal was observed in the absence of the oligonucleotide probe. The concentration of the OliGreen labelled DNA was determined by correlation with a standard calibration graph prepared from various dilutions of the DIG-labelled oligonucleotide probe incubated with an aliquot of the OliGreen dye (Figure 2.17), which was evaluated against the original nanoparticle concentration.

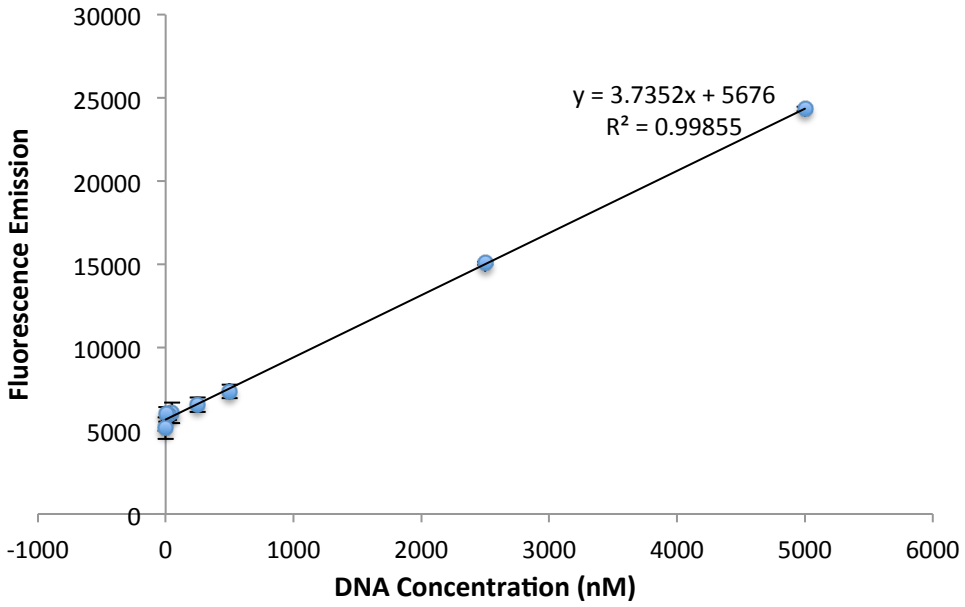

Figure 2.17 - Calibration Graph of DIG probe and OliGreen single strand binder. The error bars represent the standard deviation between replicate samples.

Using this method, the number of fluorescently labelled probe sequences per silver nanoparticle was estimated to be 8407.1 ± 2167.4. It is important to note that this number related to the number of DIG-labelled probes bound to the nanoparticle *via* the DIG-antiDIG interaction, and does not directly quantify the number of antibodies on the nanoparticle. However, each antibody contains two binding sites at most where the DIG label on the oligonucleotide probe could bind to the antiDIG antibody. This therefore can be used to estimate the number of active antibodies bound to the particle. If each antibody on the nanoparticle successfully binds two DIG labels, the number of active antibodies could be estimated to be approximately 4203.5. If each antibody on the nanoparticle only binds to one DIG label, the number of active antibodies could be considered to be approximately 8407.1. In reality it is likely that a combination of these two outcomes is the case and that the number of active antibodies immobilised *per* nanoparticle therefore falls in the region between 4203.5 and 8407.1. It is anticipated that due to the size of the antiDIG antibody it is likely that the number of antibodies bound to the nanoparticle would be significantly less than the number of linker molecules present on the surface. Consequently, this data should be considered alongside the findings published by Graham *et* al. [82] It was previously stated that the number of linker molecules bound to each nanoparticle was 114,000 ± 2080.

Although there is a large difference in the number of linker molecules immobilized on the nanoparticle surface compared with the hypothesized number of active antibodies bound to each nanoparticle there are a number of considerations to make. Firstly, Graham *et al*. covalently coupled amino-modified oligonucleotides to the linker molecule using a protocol akin to the method used to couple the antibody to the nanoparticle conjugates. Their findings suggest that although a large number of linker molecules were bound, only a small number of oligonucleotides were successfully coupled in comparison. Secondly, this protocol is designed to quantify only the number of active antibodies on the nanoparticle surface, not the total number of antibodies. Consequently, it is possible that a higher number of antibodies are in fact bound to the nanoparticles however; they are coupled in such a manner that they are rendered inactive.

However, when comparing the number of antibodies calculated on the surface *per* nanoparticle with the available surface area on each nanoparticle and the estimated

dimensions of the antibody, [134-136] it appears unlikely that this many antibodies could be bound to the nanoparticle. Consequently, the calculated number of antibodies on the nanoparticle surface should be regarded as an estimate until the definitive dimensions of the antiDIG antibody are known and further data analysis can be performed.

2.2.8 NANOPARTICLE FUNCTIONALISATION OVERVIEW

During the preparation of the Raman active nanoparticle conjugates to be used in the DNA detection assay detailed in Figure 2.1, a number of functionalisation steps were performed. This functionalisation process can be followed using a number of techniques to ensure successful functionalisation, and to indicate the aggregation state of the nanoparticle conjugates produced.

Figure 2.18 shows the extinction spectrum collected from the nanoparticle suspension at each stage in the functionalisation process. It can be seen that upon pegylation, a diminishing in the extinction spectrum is observed, however there is no appearance of a second peak at around 600 nm. This indicates that during the introduction of the PEG_3-TAMRA linker to the nanoparticle surface, no significant aggregation has occurred. After biofunctionalisation, the plasmon band has slightly red-shifted but has not decreased significantly. This red-shift is thought to be indicative of the successful conjugation of the antiDIG antibody to the linker molecule immobilised on the silver nanoparticle, as this would result in an increase in the nanoparticle size. There does however appear to be a peak beginning to appear in the red region of the spectrum. This may be suggestive of a small amount of aggregation beginning to occur. This is supported by the formation of small aggregates observed in the SEM images of the sample (Figure 2.15). However, this is not unexpected since, at this stage, the conjugates have been resuspended in 0.3 M PBS, whilst at the previous two stages the nanoparticles were dispersed in aqueous buffers free from salt.

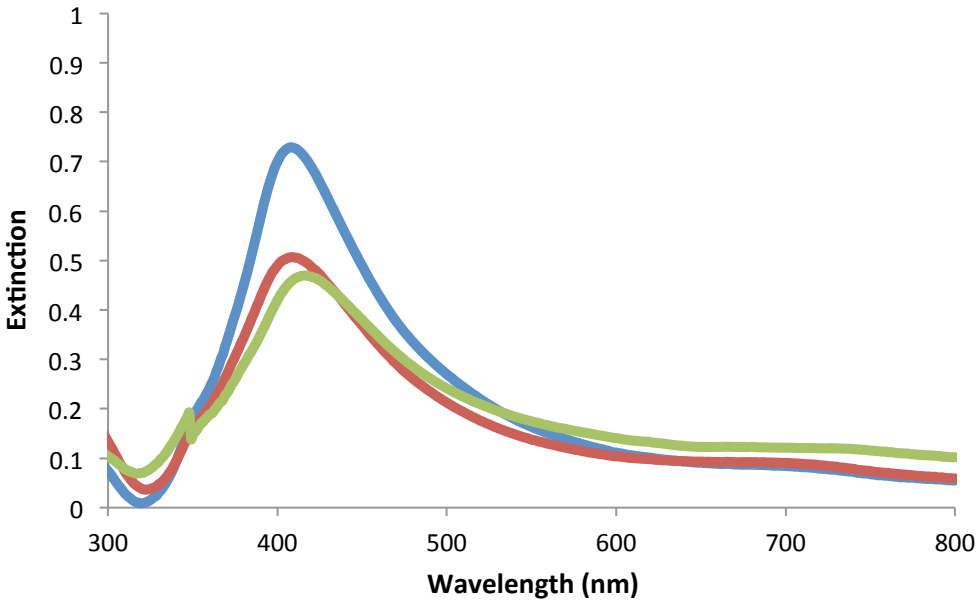

Figure 2.18 – Extinction spectra showing the construction of Raman active silver nanoparticle – antibody conjugates. Silver colloid (blue) is functionalised with PEG_3-TAMRA linker, washed and resuspended in phosphate buffer (pH 7.6) (red). An antiDIG antibody is then coupled to the terminal carboxylic acid group on the linker, and the particles washed and resuspended in 0.3 M PBS (green). Dilution factor = 10

The construction of the nanoparticle conjugates can also be monitored by measuring the particle size at each stage of functionalisation. It would be expected that upon addition of the PEG linker to the silver nanoparticles a minimal change in particle size would be observed due to the small size of the linker molecule, as was seen previously by Graham *et al.* [82] Upon further functionalisation of the pegylated nanoparticle with antiDIG antibodies, it would be anticipated that an increase in particle diameter of at least 28 nm would be observed. Whilst the exact dimensions for the antibody used are unknown, it has previously been published that IgG antibodies measure in the region of 8-10 nm wide and 14 nm high. [134-136]

Table 2.1 shows the dynamic light scattering (DLS) size measurements obtained for bare silver nanoparticles, pegylated nanoparticles and antibody labelled nanoparticle conjugates. The silver nanoparticles were sized at 45.7 nm, whilst the pegylated particles were sized at 47.9 nm. These measurements were in good agreement with the SEM images obtained for the silver nanoparticles (Figure 2.8) and the pegylated silver nanoparticles (Figure 2.12). These measurements agree with the predicted outcome, with the introduction of the PEG linker not resulting in any great difference in size. When the size of

these conjugates is compared to that of the biofunctionalised nanoparticles however, it can be seen that there is a marked increase in particle diameter. This result could be the combination of two differing outcomes. Firstly, the DLS measurements recorded are a measurement of the hydrodynamic diameter of the nanoparticle, not the physical size of the nanoparticle. As such, this increase in size would indicate the successful conjugation of the antiDIG antibody to the nanoparticle surface. Secondly, this increase in particle size could be an artefact of the slight aggregation of the nanoparticles previously proposed. It should be noted however that the particle size measurements recorded for the fully functionalised conjugates are, at most, twice the value obtained for the bare colloid. As such, it can be deduced that if aggregation has occurred, no large clusters have been produced, and the aggregation is only slight. These results are in good agreement with the SEM image shown in Figure 2.15 where an increase in the nanoparticle size and only small clusters of nanoparticles were observed.

Sample	Z-Average Diameter (nm)	Standard Deviation
Ag colloid	45.7	0.916
Ag – PEG_3 TAMRA	47.9	0.119
Ag – PEG_3 TAMRA - Ab	89.6	1.351

Table 2.1 – Zeta particle size measurements of prepared conjugates.

The zeta potential of the conjugates at varying stages of functionalisation was also recorded (Table 2.2) in order to monitor changes to the surface charge of the nanoparticle.

Sample	Zeta Potential (mV)	Standard Deviation
Ag colloid	-44.1	0.763
Ag – PEG_3 TAMRA	-35.5	0.986
Ag – PEG_3 TAMRA - Ab	-25.8	3.997

Table 2.2 - Zeta potential measurements of prepared conjugates.

The magnitude of the zeta potential value is predictive of the stability of the nanoparticles within the suspension. Nanoparticle suspensions with a zeta potential value greater than +25 mV or less than -25 mV typically have high degrees of stability. [137] Upon

functionalisation with the PEG_3-TAMRA the conjugates exhibited an increase in zeta potential. This is a direct consequence of the addition of the positively charged moiety in the dye molecule to the nanoparticle surface. The antiDIG antibody is a monoclonal IgG antibody. It is known that IgG antibodies have an isoelectric point in the region of 6.4 to 9, with the IgG1 antibody subclass having an isoelectric point of approximately 8.6. [138, 139] Consequently, at pH 7 the antiDIG antibody immobilised on the surface of the nanoparticles are likely to be positively charged. The addition of this positive charge therefore accounts for the increase in zeta potential observed upon functionalisation of the nanoparticles with the antibody. Consequently, although higher than the values obtained for unmodified silver citrate nanoparticles, the zeta potential values obtained for the fully functionalised nanoparticles are still lower than -25 mV, indicating that these modified nanoparticles still exhibit high stability. These findings compliment the UV and DLS sizing results discussed previously.

2.3 ASSAY CONSTRUCTION

There are a number of steps involved in the construction of the final assay, as shown in Figure 2.1. First of all the oligonucleotide probes must be hybridised to the target DNA (step 1), followed by introduction of the antibody labelled nanoparticles and the streptavidin coated beads (step 2). The magnetic beads are then washed by introduction of a magnetic field, which allows the beads to be collected at the side of the sample tube (step 3). The supernatant is removed and the beads resuspended in 0.3 M PBS. This wash step is repeated three times in order to remove all unbound DNA and SERRS active nanoparticles. The magnetic beads are then analysed in solution by SERRS at 532 nm. Once the assay has been fully optimised, the final concept for the assay is for it to be performed in a closed tube. In this case, the supernatant would not be removed prior to analysis to allow the magnetic beads to be washed. Instead, the beads would be pulled to the side of the sample tube, and SERRS analysis performed directly on the immobilised pellet. Consequently, any excess assay components would remain in the solution and would not be analysed.

2.3.1 DNA HYBRIDISATION

DNA melting experiments were performed using UV-vis spectroscopy to ensure efficient hybridisation of the probes to the target DNA sequence was occurring and to confirm the specificity of the probes for the target sequence. The successful hybridisation of the oligonucleotide probes was demonstrated previously in Figure 2.4, where a duplex with a T_m of approximately 46 °C is formed. Whilst this confirms that during the hybridisation process a duplex is being formed, it does not give information on whether both of the probes are being hybridised to the target strand. In order to ensure that both of the probes are capable of successfully hybridising to the target sequence the probes were then hybridised to the target independently. Figure 2.19 shows the melting profile obtained from a mixture of DIG-labelled probe and target DNA. It is clear that the probe successfully hybridises to the target DNA, forming a duplex with a T_m of approximately 48 °C.

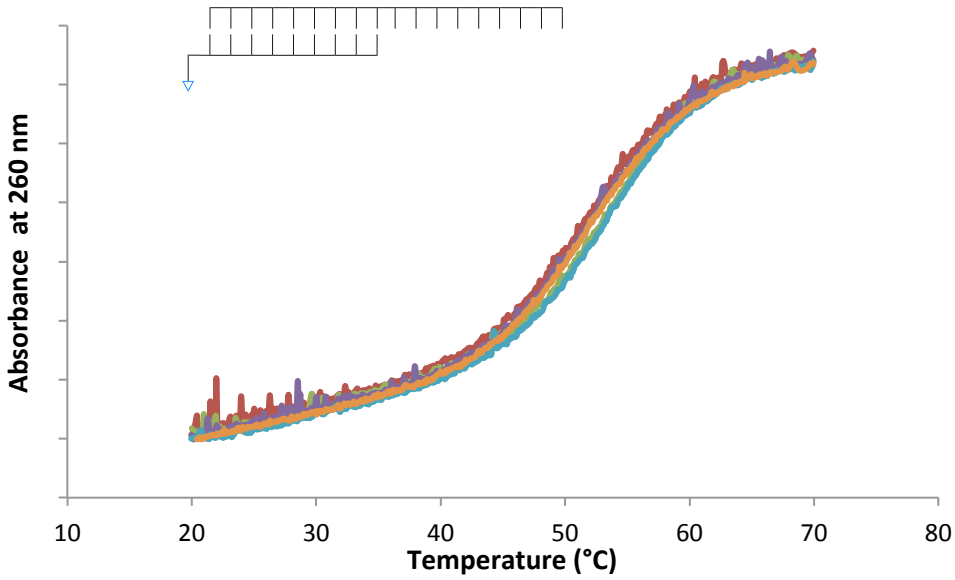

Figure 2.19 - DNA melt using UV-vis spectroscopy collected between 20 °C and 70 °C at 260 nm. The sample solution contained the DIG-labelled probe and the target DNA. 8 cycles are displayed, 4 showing the heating process and 4 showing the cooling.

Figure 2.20 shows the melting profile collected from a solution containing the biotin-labelled capture probe and the target DNA. The distinctive melting curve obtained is indicative of the successful binding of the biotin-labelled probe to the target DNA strand. The duplex which results from this hybridisation process has a T_m of approximately 35 °C.

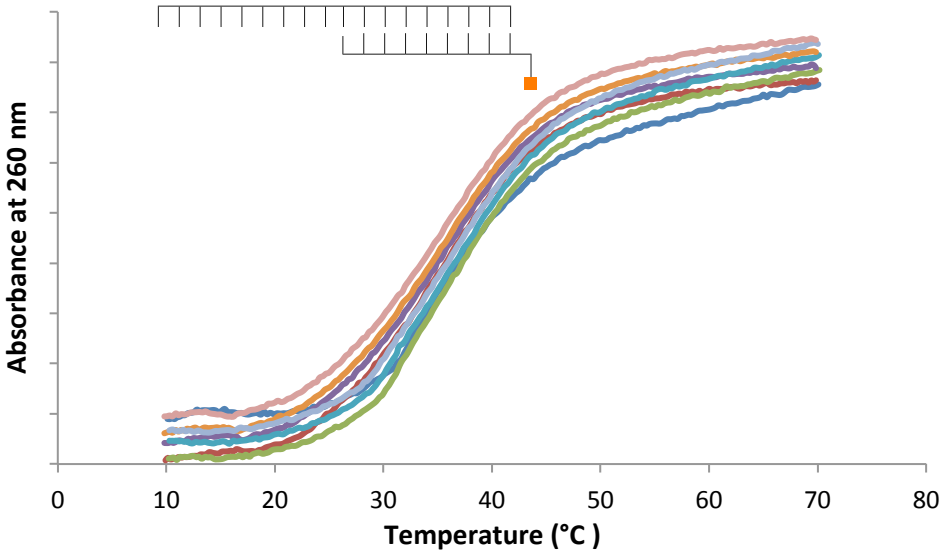

Figure 2.20 - DNA melt using UV-vis spectroscopy collected between 10 °C and 70 °C at 260 nm. The sample solution contained the biotin-labelled capture probe and the target DNA. 8 cycles are displayed, 4 showing the heating process and 4 showing the cooling.

It was important to confirm if the probes designed for use within the assay offered any degree of self-complementarity which could result in them hybridising to each other in the absence of target DNA. This complementarity was assessed by performing a DNA melt using UV-vis spectroscopy of a solution containing the two probes resuspended in 0.3 M PBS (Figure 2.21).

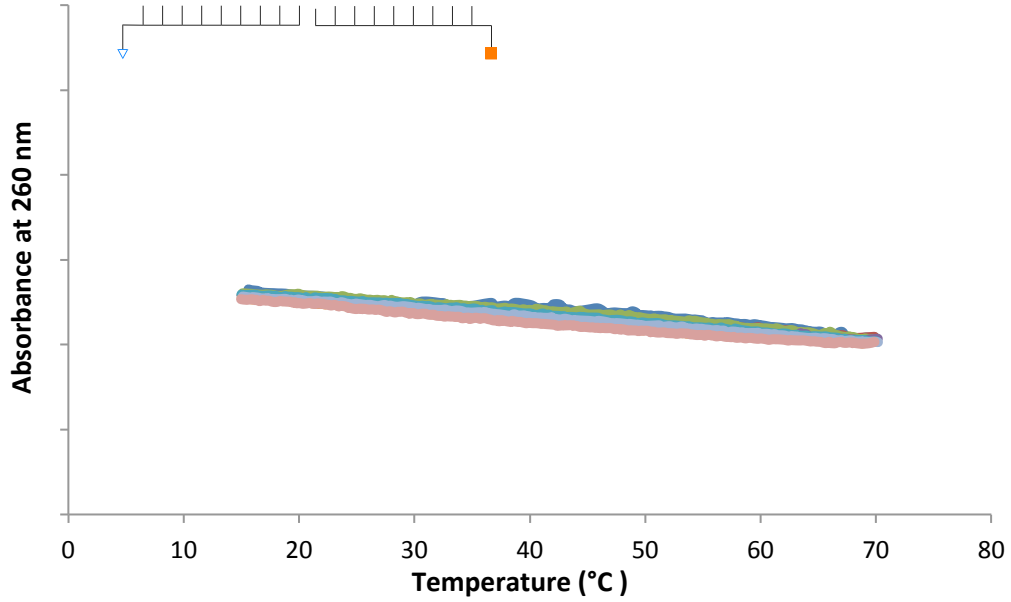

Figure 2.21 - DNA melt using UV-vis spectroscopy collected between 10 °C and 70 °C at 260 nm. The sample solution contained the biotin-labelled capture probe and the DIG-labelled probe. 8 cycles are displayed, 4 showing the heating process and 4 showing the cooling.

It can be observed by comparison of the melting profile of the probes alone with that obtained for the probes in the presence of target DNA (Figure 2.4) that the probes exhibit little, if any, self-complementarity. Under hybridisation conditions, the results obtained would suggest that the probes are present in the single stranded form, with no duplex DNA being formed.

2.3.2 Effect of Magnetic Beads on SERRS Response

The effect that the introduction of streptavidin coated magnetic beads into the assay to capture the biotin-labelled oligonucleotide probe has on the intensity of the SERRS response was investigated. Since the success of this assay depends markedly on it's sensitivity, it was considered that any detrimental effects caused by the beads could make a notable difference to the final detection limit.

To investigate the effect of the magnetic beads on the SERRS response observed from the assay, a sample of silver nanoparticles was functionalised with the PEG_3-TAMRA linker. A SERRS spectrum was collected of this sample using 532 nm laser excitation. An aliquot of streptavidin coated magnetic beads were then added to the sample, and a second spectrum collected. The intensity of the SERRS signal obtained from each of the samples was then compared, as seen in Figure 2.22.

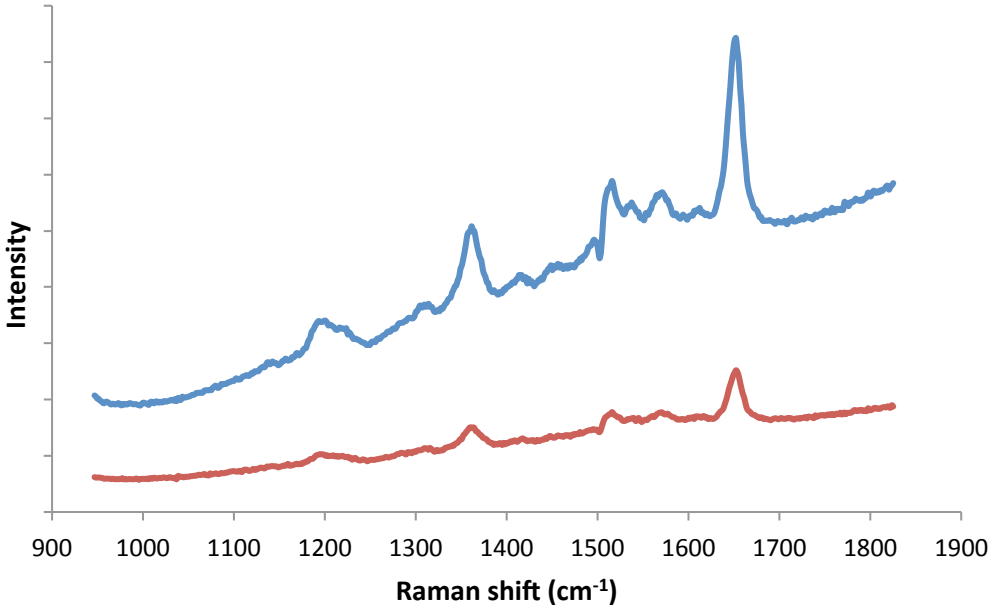

Figure 2.22 - SERRS spectrum obtained using 532 nm laser excitation, before the addition of streptavidin coated magnetic beads (blue), and after the addition of streptavidin coated magnetic beads (red), investigating the effect of addition of magnetic beads on the SERRS response collected.

It can be seen that the addition of the streptavidin coated magnetic beads does indeed have a profound effect on the intensity of the SERRS signal collected. The observed response is drastically reduced upon introduction of these beads, with a slight broadening of the spectral peaks.

SERRS is a spectroscopic technique based upon the inelastic scattering of light due to the interaction of the light with the analyte molecules. The SERRS spectrum obtained is based upon the difference in energy of the light used for excitation compared with the energy of the scattered light. It is therefore postulated that the dampening observed in the presence of the magnetic beads is due to interference from the beads with the scattered light from the sample. These magnetic particles are approximately 1 µm in diameter, significantly

larger than the nanoparticles in solution. Consequently, it is hypothesised that the large beads could be preventing the scattered light from reaching the detector by absorbing the Raman scattered light, thereby reducing the intensity of the SERRS signals collected.

However, whilst a significant dampening is observed due to the presence of the magnetic particles, a clear SERRS signal can still be observed from the SERRS active nanoparticles. Furthermore, during the process of construction of the assay it was postulated that further enhancement of the SERRS signal could be possible due to aggregation of the nanoparticles. First, the nanoparticles are tethered to the magnetic beads *via* the interaction of the biotin-labelled probe with the streptavidin on the surface of the beads. Streptavidin is a tetrameric protein capable of forming 4 bonds with biotin. Furthermore, the surface of the magnetic beads is coated with streptavidin. Consequently, it is likely that a number of nanoparticles are bound to the surface of one of the magnetic beads. Therefore, dependent upon the proximity of the nanoparticles to each other, it is possible that an enhancement of the SERRS signals could occur. Furthermore, in the idealised closed tube system the magnetic particles will be drawn into a pellet on the side of the sample tube by the application of a magnetic field. Consequently, the magnetic particles will be pulled into close proximity with each other. Since the SERRS active nanoparticles are tethered to the surface of the magnetic particles, it is therefore likely that the nanoparticles will be brought close together during this process. Therefore, there is a possibility that a further enhancement of the SERRS signals from the nanoparticle conjugates would be observed. Consequently, since the unaggregated nanoparticle conjugates give rise to an observable signal in the presence of the magnetic beads, and there a number of situations which could result in an enhancement of this signal it was decided to progress with the assay analysis as described.

2.3.3 TARGET VS NO TARGET DISCRIMINATION

In order to test the selectivity of the assay, the assay was carried out in the presence and absence of target DNA, with milliQ water replacing the target strand in the control assay. This was performed to confirm that non-specific binding of the SERRS active nanoparticles to the magnetic beads will not result in false positive results. The oligonucleotide probes

were previously shown to exhibit little self-complementarity (Figure 2.20). This suggests that the control assay i.e. in the absence of target DNA, should give a negative result.

The assay was constructed as detailed in section 2.5.5. The sample was agitated for one hour after the addition of the nanoparticle conjugates and streptavidin coated magnetic beads to allow both biological interactions to occur. The magnetic beads were then separated on a magnetic separation rack, and the supernatant removed. The assay was resuspended, and this wash step repeated three times. The SERRS spectra were recorded for each sample using 532 nm laser excitation. The SERRS analysis of the completed assay is shown in Figure 2.23. A peak was observed at approximately 1100 cm^{-1} in the target sample, however the same peak was also observed in the control sample with a similar intensity, and was concluded to be an artefact of the buffer.

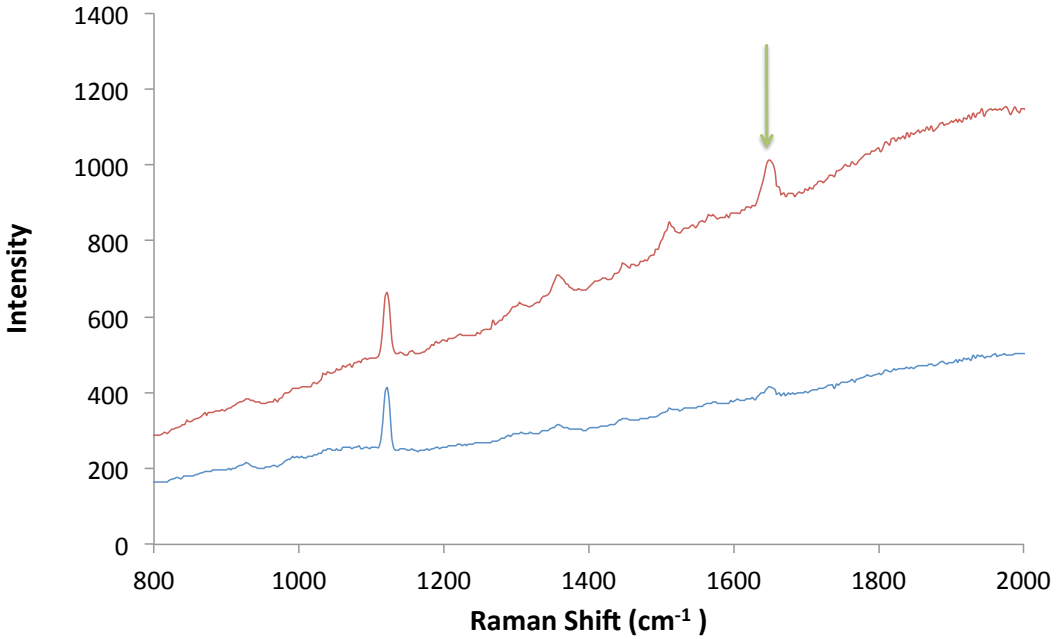

Figure 2.23 - SERRS spectrum obtained of the assay in the presence of target DNA (61.5 nM final concentration) (red), and the assay in the absence of target DNA (blue). The assay was constructed, washed three times with 0.3 M PBS and analysed in solution using 532 nm laser excitation, 15 x 1 s accumulation. The green arrow indicates the peak selected to monitor the peak height from each sample.

It can be seen that although the background fluorescence in the presence of the target DNA is higher, the SERRS signal corresponding to the TAMRA dye incorporated into the linker is clearly visible. In the case where no target DNA is present, there is a minimal SERRS

response observed. The heightened level of fluorescence in the presence of the target DNA is to be expected as the nanoparticles labelled with the fluorescent dye are successfully bound to the magnetic beads. Whilst the close proximity of the fluorescent dye to the nanoparticle surface will result in some quenching of the fluorescence emitted from the dye molecule it is unlikely that the dye will be fully quenched, therefore a background signal due to unquenched fluorescence will be observed. In the absence of the target sequence, the dye labelled nanoparticle would be removed in the washing steps. Consequently, there will be less fluorescent dye present in the system, giving rise to a lower fluorescence background. Due to the varying fluorescent backgrounds obtained from the samples, the peak height of one of the principal peaks from the TAMRA SERRS spectrum was used to monitor the assay. The prominent peak at ~1650 cm^{-1} indicated in Figure 2.23**,** corresponding to the aromatic C-C stretch,[49] was chosen for this purpose.

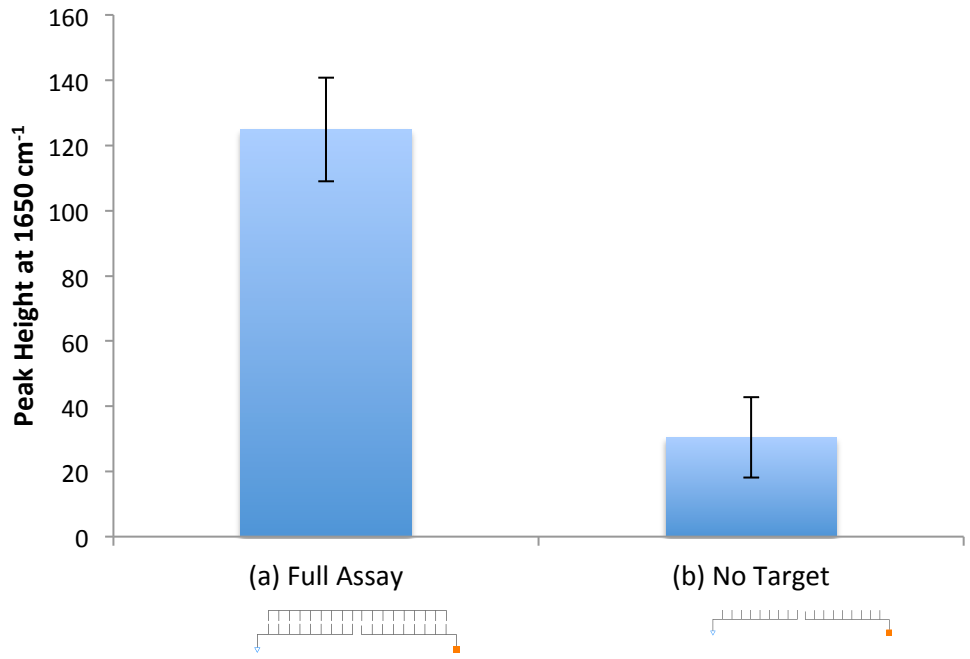

Figure 2.24 - Peak height at 1650 cm^{-1} from assay (a) in the presence of target DNA (61.5 nM final concentration), (b) in the absence of target DNA. The assay was constructed, washed three times with 0.3 M PBS and analysed in solution using 532 nm laser excitation, 15 x 1 s accumulation. The error bars represent the standard deviation from replicate samples.

By comparing the peak height measured from the spectra collected, it can be seen that there is a clear discrimination between the signal observed in the presence of the target sequence in comparison with that measured in the absence of the target strand (Figure

2.24). This corresponds well with the results collected from the UV melting experiments where a clear melting profile was observed in the presence of the target strand in comparison to the lack of distinct melting curve seen when the target is absent (Figure 2.4 & Figure 2.21).

A small signal is observed however in the absence of target DNA. There are a number of reasons that could result in this low background signal. The first of which is that the assay is subject to a small degree of non-specific binding, causing the nanoparticle conjugates to stick to the magnetic beads, giving rise to a SERRS signal, even after washing. An alternative source of this signal could be that the SERRS active nanoparticles are becoming trapped between the magnetic beads when they cluster together during the washing step.

It was postulated that increasing the number of washing steps from three may reduce this signal further, however increasing the number of washing steps performed also introduces a second difficulty. Each time a wash step is performed, the sample tube containing the assay components is placed in a magnetic separation rack allowing the magnetic beads to be pulled to the side. The supernatant is then removed from the sample tube, and the beads are resuspended in 0.3 M PBS. Upon removal of the supernatant, a small number of the magnetic beads are likely to be lost during each washing step. If the number of washing steps is increased, the number of magnetic beads lost is also likely to increase, resulting in a decrease in the SERRS signal collected from the sample. Furthermore, the loss of these magnetic beads cannot be controlled in such a way that the loss remains consistent from one sample to another, resulting in a variation between the signals observed for replicate samples. The larger the number of magnetic beads lost, the larger the sample-to-sample variation is likely to become. Overall, although not ideal, the small signal seen in the absence of target DNA is not an issue as long as it is consistent and a control is always used. The discrimination between the assay in the presence of the target sequence in comparison with its absence is large enough for a clear distinction to be made between the two.

2.3.4 CONTROL EXPERIMENTS

In order to ensure that the signal observed in the presence of target DNA (Figure 2.22) is due to the successful hybridisation of the DIG-labelled probe and the biotin-labelled

capture probe to the target followed by the interaction of the DIG with the antiDIG labelled antibody, and the binding of the biotin with the streptavidin coated magnetic nanoparticle, a series of control experiments were designed. In the following experiments one component of the assay was removed to assess its requirement for a positive signal to be obtained. Four differing versions of the assay were constructed; one containing both probes and the target sequence, one containing the probes alone, one containing the target sequence and the DIG-labelled probe and the final one containing the biotin-labelled capture probe and the target sequence. The assay was constructed using the same protocol as before, and the SERRS signals obtained from each sample was compared (Figure 2.25).

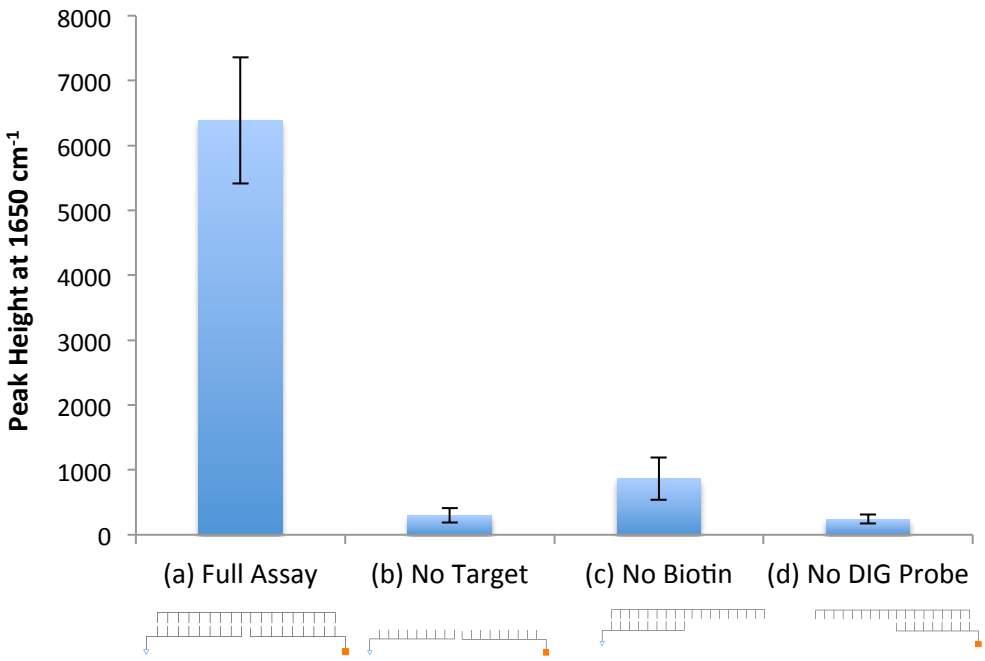

Figure 2.25 - Peak height at 1650 cm^{-1} from assay (a) in the presence of both probes and target DNA, (61.5 nM final concentration) (b) in the presence of both probes and no target DNA, (c) in the presence of the DIG probe and target DNA, (d) in the presence of the biotin capture probe and target DNA. The assay was constructed, washed three times with 0.3 M PBS and analysed in solution at using 532 nm laser excitation, 15 x 1 s accumulation. The error bars represent the standard deviation from replicate samples.

The fully constructed assay containing both labelled probes and the target DNA gave a strong SERRS signal, indicating the successful immobilisation of the TAMRA-labelled nanoparticles on the magnetic beads being analysed. Conversely, the assay constructed containing both probes in the absence of target DNA gave a low signal by comparison. This

is suggestive that when there is no target sequence to tether the biotin-labelled probe and the DIG-labelled probe together, the biotin-labelled probe would be bound to the streptavidin coated magnetic beads whilst the DIG-labelled probe tethered to the SERRS active nanoparticle would be removed in the supernatant during the wash steps. Furthermore, in the absence of the biotin-labelled probe, the level of signal observed is very similar to that seen in the absence of the target strand. This result indicates that while the DIG-labelled probe bound to the SERRS active nanoparticle hybridises with the target strand, there is no mechanism by which the duplex formed can be immobilised on the magnetic bead. Consequently, the nanoparticles are removed in the washing steps. Lastly, without the presence of the DIG-labelled probe, the signal observed is once more similar to that seen in the absence of the target. This is due to the SERRS active nanoparticles having no means by which to bind to the duplex formed between the biotin-labelled probe and the target strand. Consequently, the biotin-labelled probe will bind *via* a biotin-streptavidin interaction to the magnetic beads, however the SERRS active particles that give rise to the signal will be removed during washing.

The results observed correspond well with the data obtained from the UV melting studies discussed previously (Figure 2.4, Figure 2.19, Figure 2.20 & Figure 2.21). It can be concluded that in order for a positive result to be obtained from the assay, the presence of both probes as well as the target sequence is required. The removal of either of the probes results in the diminishment of the SERRS signal to the same level observed in the absence of target DNA. A clear discrimination can be made between the fully constructed assay and one lacking a component. As such, the interactions that are vital for the success of the assay can be easily monitored. If any of the biological interactions required for the complete construction of the assay fails, a minimal SERRS signal will be observed. Consequently, the assay can be considered as highly specific, only giving rise to a positive signal in the presence of all assay components alongside the target DNA.

2.3.5 TARGET VS NONSENSE DISCRIMINATION

In order to assess the specificity of the assay, a second control experiment was introduced whereby the target DNA sequence was replaced by a nonsense DNA sequence. In order to confirm that the nonsense sequence was non-complementary to the probes, a DNA melting

experiment was performed. The melting profile obtained from this experiment can be seen in Figure 2.26. It can be seen that no significant hybridisation occurs between the probes and the nonsense DNA, indicating a lack of complementarity. As such, this nonsense sequence was found to be suitable to test the assay's specificity. We would expect, since the nonsense DNA and the probes are not complementary, that the assay would give no signal. It was therefore expected that the same result would be achieved as was observed in Figure 2.24, in the absence of target DNA.

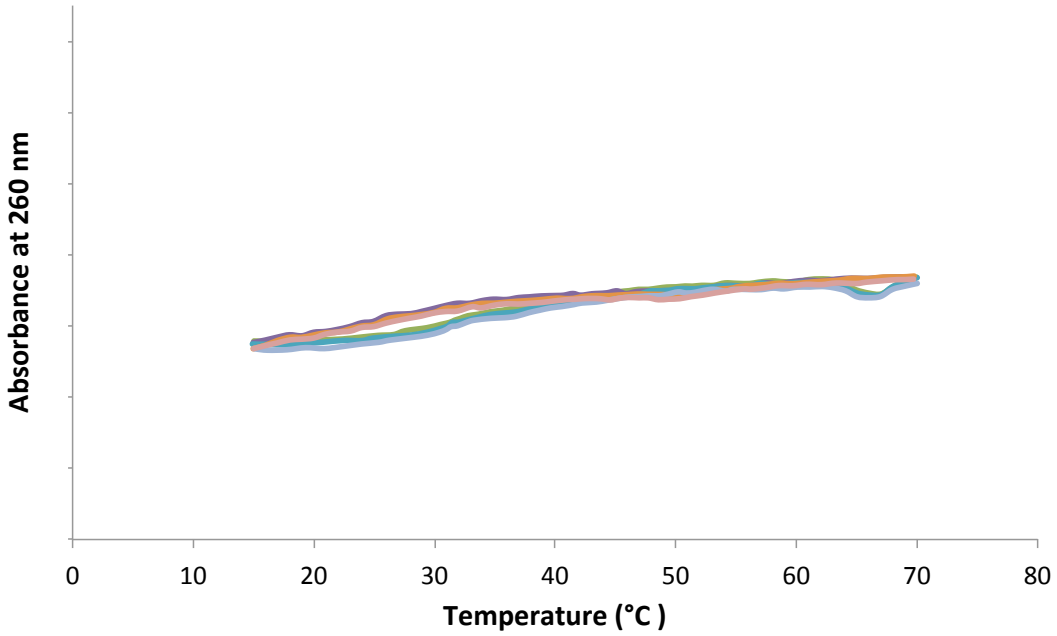

Figure 2.26 - UV melt collected between 15 °C and 70 °C at 260 nm. The sample solution contained the biotin capture probe, the digoxigenin probe and nonsense DNA. 8 cycles are displayed, 4 showing the heating process and 4 showing the cooling.

Three differing versions of the assay were constructed; one containing the probes and target DNA, one containing only the probes and milliQ water in place of DNA, and the last containing the probes and the nonsense DNA. The SERRS intensities for each assay configuration are presented in Figure 2.27. The assay containing the target DNA resulted in a much higher intensity than either of the assays where the target DNA sequence was absent. The discrimination between the assay in the presence of target DNA and the presence of nonsense DNA is profound. In fact, the assay containing the nonsense sequence gave SERRS intensities equivalent to the signal recorded in the absence of any DNA. This indicates that the probes do not form a stable duplex with the nonsense DNA at room temperature.

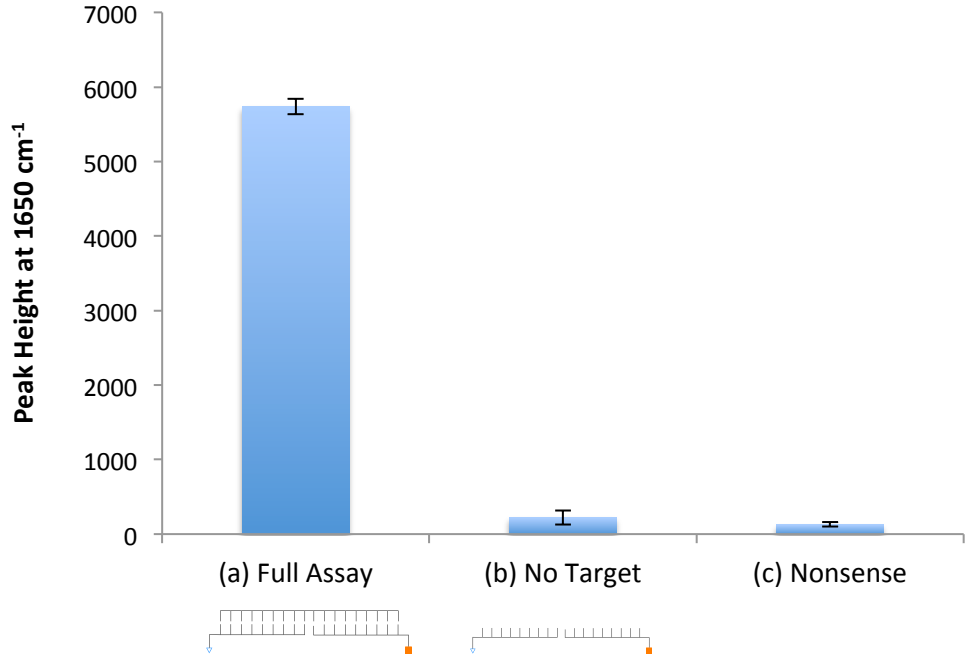

Figure 2.27 - Peak height at 1650 cm^{-1} from assay (a) in the presence of target DNA, (b) in the absence of target DNA, (c) in the presence of nonsense DNA. The assay was constructed, washed three times with 0.3 M PBS and analysed in solution using 532 nm laser excitation, 15 x 1 s accumulation. The error bars represent the standard deviation from replicate samples.

Consequently, it can be concluded that the assay shows excellent specificity, with a clear discrimination between target and nonsense sequences. This is vital for the use of this system for the detection of diseases from clinical samples as these are made up of a complex biological mixture that will contain numerous DNA sequences unrelated to the disease being targeted. As such, it is important that the system can specifically recognise the sequence being targeted in order to avoid false positives.

2.3.6 Detection of Target DNA From PCR Product

This assay was designed for the detection of genomic DNA from clinical samples without the need for PCR or separation steps. As such, PCR product replaced the synthetic target DNA used in the construction of the assay. This was carried out to mimic a clinical sample more closely, since the DNA from a clinical sample would be in the double stranded form and would also be much longer than the synthetic target sequence used. The synthetic target sequence used was 18 bases in length, and each probe designed for use in this assay

is 9 bases long. Therefore, the synthetic sequence used is exactly complementary to the probe sequences, with no overhangs included in the oligonucleotide sequence. However, the PCR product used was 85 bases long with the section that is complementary to the probe sequences located mid-sequence. Consequently, there will be a considerable overhang of unhybridised bases at either side of the probe region. This could prove problematic as the unhybridised sections could result in reduced availability of the hybridised probes.

In order for the PCR product to be incorporated into the assay, it first had to be denatured into its single stranded form. The solution containing the PCR product and the probes was therefore heated to 95 °C to disrupt the base pairing in the duplex. The sample was then rapidly cooled in order to encourage the system to preferentially form the kinetic product, i.e. it would be kinetically favourable for the short probes to bind to the longer single stranded PCR product DNA in comparison with the second strand from the original duplex. The probes were added in an excess to encourage their hybridisation to the single stranded PCR product. The assay was then constructed following the same protocol as previously (Section 2.5.5). The SERRS signal intensity obtained in the presence of synthetic target DNA, in the absence of target DNA and in the presence of PCR product were compared (Figure 2.28).

Whilst the presence of the synthetic target DNA can be easily observed, with excellent discrimination between the target and no target controls, the assay was unsuccessful in detecting the target sequence within the PCR product. This is indicated by the low intensity signal observed, with an intensity measurement almost identical to that seen in the absence of target DNA.

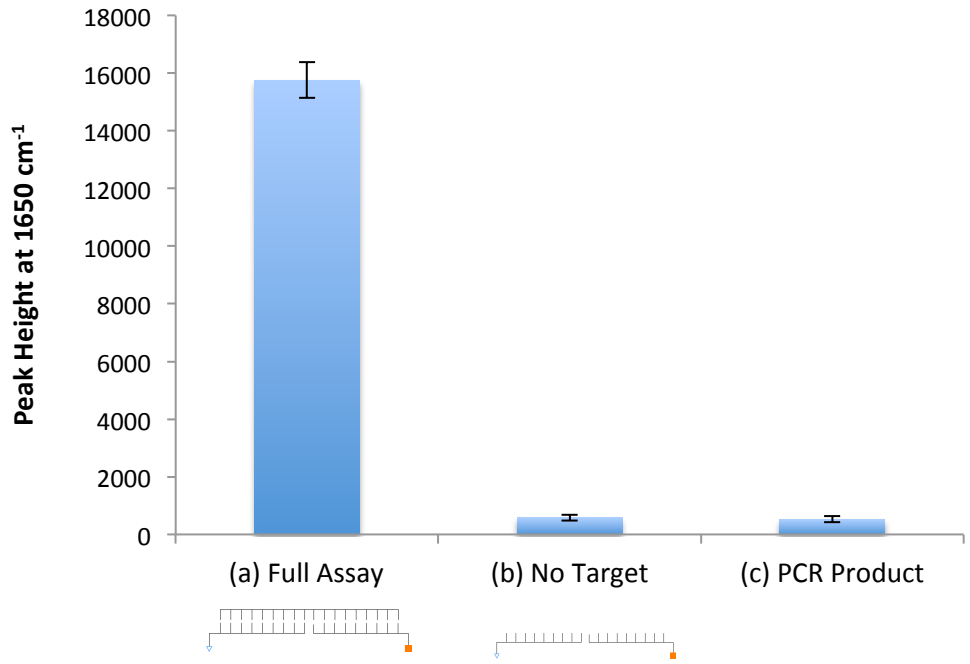

Figure 2.28 - Peak height at 1650 cm^{-1} from assay (a) in the presence of target DNA, (b) in the absence of target DNA, (c) in the presence of PCR product. The assay was constructed, washed three times with 0.3 M PBS and analysed in solution using 532 nm laser excitation, 15 x 1 s accumulation. The error bars represent the standard deviation from replicate samples.

This may be a contribution of a number of factors. Firstly, the PCR product analysed was a 10% dilution of the PCR product (5.75×10^{-12} M). Consequently, the final concentration of the PCR product introduced into the final assay is significantly lower than the concentration of synthetic target previously used. It could be that as a result of this, the DNA concentration was below the detection threshold for the assay. Secondly, careful consideration of the kinetic and thermodynamic influences of the hybridisation process is required in order to maximise the number of oligonucleotide probes successfully bound to the target strand. During the DNA hybridisation step, the mixture was rapidly cooled in order to maximise the amount of kinetic product formed, thereby increasing the number of probes successfully bound to the target DNA. This step in the assay could be optimised further in order to maximise the number of oligonucleotide probes successfully bound to the target strand. Finally, the region of the PCR product that corresponds to the target sequence being detected is mid-strand. This may provide steric hindrance to the nanoparticles and magnetic beads. If the complementary PCR product strand does hybridise with the target strand at either side of the probe region being targeted, it may be

difficult for the antiDIG functionalised nanoparticles to reach the DIG label on the probe after hybridisation has occurred. This is due to the long complementary strand providing an overhang on either side of the targeted region, possibly blocking the hybridised probes. The same problem arises with the streptavidin coated magnetic beads being able to reach the biotin-labelled capture probe. The magnetic bead however is much larger than the nanoparticle, and therefore the steric demands related to this interaction are likely to be higher. This problem could be minimised by either changing the location of the probe sequence in the PCR product region, or by performing an asymmetric PCR reaction instead which would result in more of the target strand being produced compared to its complement. This would reduce the number of complementary strands available to bind to the target strand and may result in more successful DIG-antiDIG and biotin-streptavidin interactions. Consequently, the number of successfully assembled nanoparticle-labelled duplexes bound the magnetic beads in the sample would be increased thereby resulting in an increased signal being observed.

Whilst the assay was unsuccessful in the detection of the target strand from PCR product, the results obtained thus far are positive and suggest that the assay still holds potential for detection in clinical samples. It has been shown that the assay is specific to the DNA sequence being targeted and exhibits a low level of non-specific binding. Consequently, there are a number of parameters that should be investigated further in a bid to make the assay suitable for testing of biological samples. These parameters would include the positioning of the probe sequences within the PCR product, the probe: target ratio and the hybridisation process included in the assay protocol. Careful optimisation of these factors will maximise the number of oligonucleotide probes becoming bound to the target strand. It is anticipated that this would lead to an increase in the signal observed from the assay samples containing PCR product.

2.3.7 LIMIT OF DETECTION STUDY

To evaluate the sensitivity of the assay, a number of samples were prepared containing varying concentrations of target DNA in order to find a limit of detection for the assay. The assay was constructed *via* the protocol described in section 2.5.5. The target DNA was added to a final concentration between 0.65 nM and 25 nM. Previous work indicated that

above this concentration the SERRS intensity had reached a maximum and no longer continues to rise upon increasing the DNA concentration. A calibration graph plotting the peak height of the signal obtained at 1650 cm^{-1} against the final target DNA concentration was constructed (Figure 2.29). The data shown has been background corrected, with the peak height from the corresponding blank assay in the absence of target DNA having been subtracted from the peak height obtained from the sample. This gives a measurement of the "actual" intensity of the SERRS signal observed from the assay due to the presence of the target DNA.

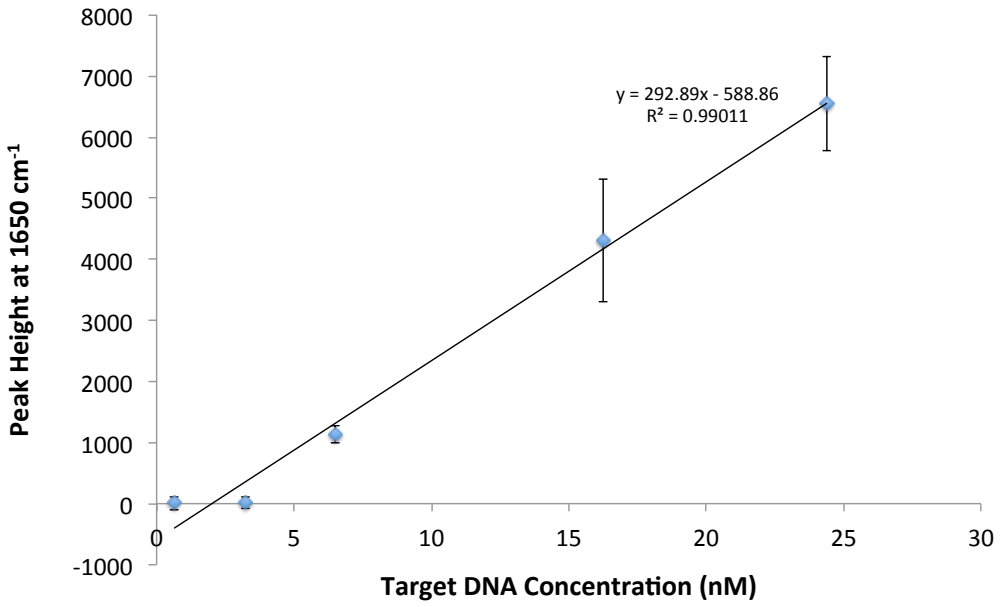

Figure 2.29 - Peak height at 1650 cm^{-1} from assay in the presence of various concentrations of target DNA. The assay was constructed, washed three times with 0.3 M PBS and analysed in solution using 532 nm laser excitation. The values shown have had the peak height of the blank subtracted from them. The error bars represent the combination of standard deviation from replicate samples of each concentration of target DNA and standard deviation from replicate samples of the blank.

It can be seen that within this range the assay exhibited a linear response. The limit of detection was calculated by assigning the limiting signal intensity to be three times the signal collected from the blank. The limit of detection for the assay was calculated from this data to be 4.89 nM. Consequently, it is clear to see that the reason the assay in the presence of PCR product did not give rise to a positive signal was that the concentration of the target strand was below the detection limits for the assay (Section 2.3.6).

2.4 CONCLUSIONS

The main aim for this work was to develop a DNA detection assay capable of selectively detecting DNA with a specific sequence for disease diagnostics. The assay was based on a split-probe configuration, with each probe being complementary to half of the target sequence. The probes were both modified with different biomolecules essential for the construction of the assay. One probe was modified with a digoxigenin molecule, capable of interaction with its corresponding antiDIG antibody. This interaction was utilised in order to provide the assay with a reporter in the form of a SERRS active nanoparticle. The nanoparticle conjugate is SERRS active and functionalised with antiDIG antibodies. Consequently, the DIG-antiDIG interaction was used as a means to tether the SERRS active nanoparticle to the oligonucleotide probe. The second DNA probe was labelled with a biotin molecule, enabling it to become bound to streptavidin coated magnetic beads *via* a biotin-streptavidin interaction. Consequently, upon full construction of the assay, the duplex formed between the probes and the target strand will be labelled with a SERRS active nanoparticle *via* the DIG-antiDIG interaction, allowing for the detection of this duplex upon SERRS analysis. Furthermore, the duplex formed can be immobilised on streptavidin coated magnetic beads, allowing for the entire assay to be gathered onto the side of the sample tube by the introduction of a magnetic field. Consequently, this assay could be developed as a closed tube diagnostic test, where the immobilised magnetic beads, which have the SERRS active nanoparticle tethered to them, can be directly analysed as a pellet in the sample tube by SERRS. However, during the optimisation stages of the assay it was decided to use an open tube format and include a washing step after construction of the assay. Consequently once the assay was constructed, the magnetic beads were pulled to the side of the sample tube and the supernatant containing excess assay components was removed. The assay was then resuspended in buffer and SERRS analysis was performed of the solution.

The development of the assay primarily involved the synthesis of the SERRS active nanoparticles to be used in the assay. It was vital that these nanoparticle conjugates could be easily functionalised with an antibody whilst remaining stable in the assay buffer. Silver nanoparticles were functionalised with a PEG linker that had TAMRA incorporated into its structure. These nanoparticle conjugates then had an antiDIG covalently coupled onto

them. The production of these particles has been developed to maintain their monodispersity and control aggregation within the system. The resulting conjugates are stable in a variety of buffers, including those containing salt. Further to development of the reporter nanoparticles, the optimisation of the conditions used for assay construction was performed. This was important in order for the target-probe duplex formed to maintain its double stranded nature throughout the assay protocol.

From the developed assay, it was shown that there is a clear discrimination between the signal observed in the presence and absence of target DNA. Furthermore, it was also shown that in the absence of any of the probe sequences in the assay, minimal SERRS signal is observed. This series of experiments was performed in order to assess the level of non-specific binding between the SERRS-active nanoparticles and the streptavidin coated magnetic beads. Consequently, it was found that whilst there is a small background signal due to non-specific binding, there is a large discrimination between the intensity of the signal observed in the presence of target DNA and the background signals. Furthermore, the assay can successfully distinguish between target and nonsense DNA with a high degree of discrimination. In the presence of target DNA, a distinctive SERRS spectrum related to the dye on the nanoparticle can be clearly seen. In the absence of the target sequence the signal observed is minimal. This is a vital characteristic of an assay being developed to test biological samples. Biological media is a complex mixture comprising of a variety of components including proteins and DNA. Consequently, it is vital for the assay to be able to successfully detect the target DNA sequence whilst in the presence of numerous other non-targeted sequences. A limit of detection has been calculated at 4.89 nM. Whilst the sensitivity of this area may not be in the femtomolar region, the simplicity of the assay, the minimal sample handling stages, and the ability to discriminate between target and nonsense DNA without the removal of the assay from the magnetic bead are all attributes that make this system appealing. Furthermore, this limit of detection was obtained from the open tube system. In this system, the magnetic particles are analysed in solution. Consequently, the particles are not in close proximity to one another. However, in the proposed closed tube system, the magnetic beads would be pulled into a pellet on the side of the sample tube for direct analysis. Consequently, the beads will be brought into close proximity to one another during the application of the magnetic field. Since the SERRS-active nanoparticles are tethered to the magnetic beads, it is therefore likely that upon

magnetic separation, the nanoparticles on the surface of the beads will also be brought into close proximity, resulting in aggregation. Therefore, it is possible that the SERRS output observed from this assay would increase due to this aggregation. Consequently, upon further optimisation, it is possible that this limit of detection could be improved by direct analysis of the magnetic bead pellet in the closed tube assay system.

2.5 EXPERIMENTAL DETAILS

2.5.1 COLLOID PREPARATION

Two colloidal dispersions of nanoparticles were used throughout the work discussed, 60 nm citrate reduced gold colloid and 35 nm citrate reduced silver colloid. Both were produced in house using the methods detailed below.

2.5.1.1 Aqua Regia Preparation

All glassware was cleaned with aqua regia (HCl, HNO_3 – 3:1 v/v) prior to colloid preparation. Glassware was soaked in aqua regia for 1-2 hours. The glassware was then rinsed with distilled water, and the washings collected. The rinsings were neutralised with sodium carbonate before being washed away with excess water.

2.5.1.2 Preparation of Citrate Reduced Silver Colloid

A 1 litre 3-parallel necked round bottom flask, glass link stirrer, thermometer, 250 mL measuring cylinder and 10 mL measuring cylinder were cleaned with aqua regia as detailed above.

Citrate reduced silver colloid was prepared *via* a modified Lee and Meisel method. [48] 500 mL of distilled water was heated to 45 °C with constant stirring. Silver nitrate (90 mg) was dissolved in 10 mL distilled water and added. Heating was continued until the temperature reached 98 °C, then 100 mL of a 1% aqueous solution of sodium citrate was added. The solution was stirred for 90 minutes, maintaining a temperature of 98 °C throughout. The colloid was then cooled to room temperature.

2.5.1.3 Preparation of Citrate Reduced Gold Colloid

A 1 litre 3-necked round bottom flask and a link stirrer are cleaned with aqua regia as detailed in section 2.5.1.2.

Citrate reduced gold colloid was prepared *via* a modified Turkevich method.[140] Sodium tetrachloroaurate (57.5 mg) was added to 500 mL of distilled water. The solution was heated until boiling, then sodium citrate (60.5 mg) was added in 7.5 mL of distilled water.

The solution was then boiled for 15 minutes with constant stirring. The colloid was then cooled to room temperature.

2.5.1.4 Colloid Analysis

All samples were stored in plastic bottles and analysed by UV-visible spectrophotometry using a Varian Cary 300 Bio UV-Vis spectrophotometer.

The concentration of the colloid was calculated using the Beer-Lambert law as detailed in Equation 2.1.

$$\boldsymbol{A = \varepsilon\, l\, c}$$

Equation 2.1 - Beer Lambert law.

Where c = concentration of sample in mol dm^{-3}

A = absorbance at λ_{max}

ε = extinction coefficient of colloid in $dm^3\ mol^{-1}\ cm^{-1}$

l = path length in cm

The values used for ε vary according to the colloid composition. The following values were used in the calculations contained within this work.

- ε Au (60 nm) = 5.32 x 10^{10} $dm^3\ mol^{-1}\ cm^{-1}$ [141]
- ε Ag (40 nm) = 2.78 x 10^{10} $dm^3\ mol^{-1}\ cm^{-1}$ [141]

The path length remained constant throughout with a value of l = 1 cm.

2.5.2 SYNTHETIC OLIGONUCLEOTIDES

All synthetic oligonucleotide sequences used for the work detailed within this thesis were purchased from external manufacturers. They were purchased either from ATDBio, (Southampton), Eurogentec Ltd., (Belgium) or Eurofins MWG Operon (London) on a micromolar (μmolar) scale with HPLC purification. The base composition of each probe and the complement is given below, complete with modifications.

2.5.2.1 Oligonucleotide Sequences

DIG Labelled Probe

5' – GCT GCG ACA – 3' Modifications: 5' DIG – C_8 diol

Manufacturer Used: Eurogentec & ATDBio

Biotin Labelled Probe

5' – GGG ACT AAG – 3' Modifications: 3' TEG – Biotin

Manufacturer Used: Eurofins MWG Operon

Target

5' – CTT AGT CCC TGT CGC AGC – 3'

Manufacturer Used: Eurofins MWG Operon

2.5.2.2 Oligonucleotide Concentration Calculation

The concentration of all purchased oligonucleotides used was obtained by UV-Vis spectroscopy. The absorbance maximum for DNA is 260 nm, therefore this value was recorded and used to calculate the concentration of the diluted DNA sample by use of the Beer-Lambert law, as given in Equation 2.1.

The four DNA bases each have a distinct extinction coefficient; consequently the base composition is required in order to calculate the concentration. These values are shown in Table 2.3. The value of ε generated is then multiplied by the hypochromicity factor, 0.9. This corrects for the minimal secondary structure of the single stranded DNA compared to the free bases. This allows a final value of ε to be determined which is used in Equation 2.1.

ε Contributor	ε at 260 nm (dm^3 mol^{-1} cm^{-1})
A	15200
G	12010
C	7050
T	8400

Table 2.3 - Extinction coefficient values for DNA bases.

Stock sample solutions were diluted in distilled water until the absorbance at 260 nm was between 0 and 1, and therefore within the linear range of the detector. 100 µl of each sample was analysed and the absorbance at 260 nm obtained. Blanks of distilled water were analysed before each sample.

2.5.3 PREPARATION OF NANOPARTICLE CONJUGATES

2.5.3.1 Preparation of Functionalised Nanoparticles

Gold nanoparticles were prepared by a modified Turkevich method. [140] $HAuCl_4$ was reduced using citrate to afford colloidal gold of approximately 60 nm diameter (as described in section 2.5.1.3).

Silver nanoparticles were prepared by a modified Lee and Meisel method. [48] $AgNO_3$ was reduced using citrate to afford colloidal silver of approximately 45 nm diameter (as described in section 2.5.1.2).

To prepare TAMRA-gold conjugates, PEG_3-TAMRA linker in methanol (20 µl, 1 x 10^{-3} M) was added to citrate stabilised gold colloid (1 mL, 0.36 nM). The linker molecule was added in excess. The samples were incubated for at least 3 hours at room temperature, and then centrifuged (20 min, 6000 rpm). The supernatants was discarded, the pellets washed with H_2O, then centrifuged again (20 min, 6000 rpm). The supernatants were discarded and the pellets resuspended in the desired volume of buffer.

To prepare TAMRA-silver conjugates, PEG_3-TAMRA linker in methanol (20 µl, 1 x 10^{-3} M) was added to citrate stabilised silver colloid (1 mL, 0.67 nM). The linker molecule was added in excess. The samples were incubated for at least 3 hours at room temperature, and then centrifuged (20 min, 6000 rpm). The supernatants was discarded, the pellets washed with H_2O, then centrifuged again (20 min, 6000 rpm). The supernatants were discarded and the pellets resuspended in the desired volume of buffer.

2.5.3.2 Bioconjugation [142]

The TAMRA-linker functionalised nanoparticles (2.5.3.1) were washed and resuspended in phosphate buffer (470 µl, 10 mM, pH 7.6). EDC (10 µl, 2 mg/mL), sulfo-NHS (10 µl, 2 mg/mL) and antiDIG antibody (10 µl, approx. 1 mg/mL) were added.

The reaction mixture was incubated for 16 hours at room temperature. The samples were then centrifuged (20 min, 6000 rpm) and the supernatants discarded. The pellets were washed with phosphate buffer, and then centrifuged again (20 min, 6000 rpm). The supernatants were discarded and the pellets resuspended in 0.3 M PBS (1 mL, 0.3 M NaCl, 10 mM phosphate).

2.5.3.3 UV-Vis Monitoring of Nanoparticle Construction

All UV-Vis spectroscopic analyses were carried out using a Cary 300 UV-Vis spectrophotometer fitted with a Cary temperature control unit. A variety of cuvettes were available, depending on the volume of the sample being analysed. Before collection of the spectra, the instrument was zeroed using a blank solution of the solvent present in the sample.

2.5.3.4 DLS Zeta Potential & Size Measurements

All zeta potential and size measurements were carried out using a Malvern Nanosizer ZS with a dip cell zeta measurement probe. Nanoparticle conjugates were prepared as described in 2.5.3.1 and 2.5.3.2. All prepared conjugates were centrifuged (20 min, 6000 rpm) and the pellets resuspended in distilled water. 1 mL of each sample was used. All measurements were carried out in a disposable polystyrene cuvette. A standard sample consisting of commercially available Nanosphere™ Size Standards (Thermo Scientific Fremont CA.) 40 nm polymer microspheres in water were used as a standard before each set of sizing measurements. The zeta potential measurements were made using a dip cell zeta measurement probe. Before each measurement a standard solution of -68.0 ± 6.8 mV was measured.

2.5.3.5 SEM Imaging of Nanoparticle Conjugates

SEM investigations were carried out by preparing poly(diallyldimethylammonium) (PDDA) coated silicon wafers. Silicon wafers were cleaned with methanol and oxygen plasma

(Diener electronic femto oxygen plasma cleaner, 72 cm^3/min gas flow). They were then coated with a 10 mg/mL PDDA solution in 1 mM NaCl for 30 minutes. After this time the wafers were rinsed with deionised water and dried with N_2. 10 µL of the colloid suspensions were deposited on individual wafers and allowed to rest for 20 minutes, the samples were then removed and the wafer washed. Imaging was carried out on a Sirion 200 Schottky field-emission electron microscope (FEI) operating at an accelerating voltage of 5 kV. The samples did not require additional metallic coating before imaging.

2.5.4 ANTIBODY QUANTIFICATION

2.5.4.1 Standard Calibration Graph

The DIG-labelled probe was diluted with phosphate buffer (10 mM, pH 7.6) to give a dilution series with a final concentration measured between 5 µM and 5 nM. The dye was diluted following the protocol detailed for the Quant-iT OliGreen kit (Invitrogen, Paisley). An aliquot of each DNA concentration (15 µL) had an aliquot of the OliGreen dye added to it (15 µL). The samples were incubated at room temperature for 5 minutes followed by fluorescence analysis using an excitation wavelength of 490 ± 10 nm and an emission wavelength of 520 ± 10 nm.

The measurements were recorded using a Stratagene MX4000.

2.5.4.2 Active Antibody Quantification

Antibody nanoparticle conjugates were prepared as detailed in 2.5.3.1 and 2.5.3.2. An aliquot of the nanoparticle conjugates (15 µL) was added to an aliquot of DIG probe (15 µL, 5 µM) and the samples incubated at room temperature for one hour to allow the DIG probe to become bound to the antiDIG antibody on the nanoparticle surface. An aliquot of the OliGreen dye (15 µL) previously prepared in 2.5.4.1 was added to the samples and the samples incubated for 5 minutes at room temperature. The fluorescence was then measured using an excitation wavelength of 492 nm.

The samples were then centrifuged, the supernatant removed and the pellets resuspended in phosphate buffer. This wash step was repeated and the pellets resuspended in

phosphate buffer (45 µL). The fluorescence analysis was then repeated for the samples and the supernatant.

The samples were then heated to 75 °C and held for 30 minutes, before being cooled to 25 °C. The samples were then centrifuged, the supernatant removed and the pellets resuspended in phosphate buffer (45 µL). Fluorescence analysis was then performed on the samples and the supernatant.

2.5.5 ASSAY CONSTRUCTION & ANALYSIS

Figure 2.1 illustrates the assay that this research is based upon. A target DNA strand corresponding to a specific disease is hybridised to two split probes which, when added together, complete a complement to the target sequence. One of the probes is 3' modified with biotin, whilst the other is 5' modified with digoxigenin.

The silver nanoparticles in the assay are functionalised with a PEG linker with a TAMRA dye incorporated, which is then conjugated to an antiDIG antibody. This antibody will therefore interact with the digoxigenin label on the DNA. Additionally, the biotin on the alternative probe interacts with the streptavidin coating the magnetic beads.

2.5.5.1 Assay Construction Experimental Detail

Functionalised nanoparticles were prepared followed by bioconjugation with the antiDIG antibody, as described in section 2.5.3. The nanoparticles were washed and resuspended in 0.3 M PBS (1 mL, 0.3 M NaCl, 10 mM phosphate).

The target DNA was hybridised to the two strands of single stranded DNA relating to the split probes. Each of these probes is complementary to half of the target strand. DIG-labelled probe (0.1 µl, 100 µM), biotin-labelled capture probe (0.1 µL, 100 µM) and target DNA (0.1 µL, 100 µM) were added to an eppendorf and the solution made up to 100 µL with 0.3 M PBS. The detailed volumes relate to a final target DNA concentration of 61 nM being analysed. The reaction mixture was then incubated at room temperature for 1 hour

to allow the oligonucleotide probes to hybridise to the target strand. In the no target control samples, milliQ water (0.1 µl) was added in place of the target DNA. In the nonsense control samples, nonsense DNA (10 µL, 10 µM) was added in place of the target DNA. In the sample containing the PCR product, PCR product (20 µL, 5.75×10^{-12} M) was added in place of the target DNA. The reaction mixture was heated to 95 °C and held for 2 minutes, followed by rapid cooling at 0 °C for 5 minutes to encourage the probes to bind to the target strand in favour of the complementary strand.

Streptavidin coated magnetic beads (12.5 µL, 4 mg/mL) were washed in 0.3 M PBS. The hybridized DNA solution was added, along with the functionalised nanoparticles (50 µL, 0.1 nM). The mixture was then agitated at room temperature for 1 hour.

The beads were separated from the solution by magnetic separation, the supernatant removed and the beads resuspended in 0.3 M PBS. This washing process was repeated three times. A SERRS spectrum was obtained for the solution using 532 nm laser excitation. Five replicates of each spectrum were taken, with replicate samples constructed for each experiment.

All samples were analysed using an Avalon probe system Ramanstation R3 optical fibre with a 532 nm diode laser excitation. Typical integration times were 1 second and 15 accumulations.

3. DNA DETECTION ASSAY CONTAINING GOLD-MALACHITE GREEN NANOPARTICLE CONJUGATES

3.1 AIMS & CONCEPTS

The work detailed within this chapter is based primarily upon the assay developed in Chapter 2. The assay utilises the split probe system previously detailed to provide an observable signal from the Raman active nanoparticle conjugates in the presence of target DNA. Whilst the results obtained using this system were positive, the linker used for the modification of the nanoparticles is expensive and difficult to synthesise. Furthermore, whilst the nanoparticle conjugates were shown to be stable in ionic conditions once biofunctionalised, the nanoparticles could be quite sensitive until full functionalisation was achieved. Consequently, occasionally the nanoparticles aggregated prior to this stage in the functionalisation process. Therefore a new method of functionalisation was developed where more commercially available reagents could be used to yield stable nanoparticle conjugates. In this chapter, SERRS active nanoparticle conjugates capable of biofunctionalisation were developed to replace the silver-TAMRA nanoparticle conjugates previously used. These conjugates were then incorporated into the split-probe assay previously developed (Figure 2.1).

It was vital for their successful incorporation into the assay that the nanoparticle conjugates developed exhibit an intense SERRS signal, whilst possessing the capability to bind to a biomolecule of choice. Nie *et al*. have developed a class of nanoparticle tags which give rise to intense SERRS signals, and are easily functionalised with ScFv antibody fragments to target tumour cells. [66] These nanoparticle tags were based upon the absorption of isothiocyanate-labelled Raman reporter molecules onto the surface of gold nanoparticles, followed by the introduction of a PEG layer. Since this class of nanoparticle tags meets the criteria for the nanoparticle conjugates required for incorporation into the assay, it was decided to follow this general protocol for the development of the SERRS-active nanoparticle conjugates.

The gold nanoparticles were labelled with malachite green (MG), a non-fluorescent SERRS dye *via* an isothiocyanate anchoring group. Malachite green has a λ_{max} of 629 nm, allowing

the dye to be used in resonance with both the surface plasmon of gold nanoparticles (~520 nm) and a 633 nm laser excitation. Consequently the malachite green labelled gold nanoparticles meet the criteria required for analysis by SERRS. The nanoparticles were then stabilised by the introduction of a PEG bilayer. This bilayer consisted of a short chain, carboxylic acid functionalised PEG linker and a longer chain stabilising linker molecule, both of which were terminated with a thioctic acid group which tethers the linkers to the nanoparticle surface. The carboxylic acid group was introduced to the short linker as a potential site for biofunctionalisation of the nanoparticle. The short chain linker was then coupled *via* the carboxylic acid terminus to an antiDIG antibody. The longer PEG linker was utilised in order to afford extra stability to the nanoparticle, with the long polymer chain available to fold down on top of the surface of the nanoparticle. A similar functionalisation procedure was used by Nie *et al*. [66] The carboxylic acid terminated PEG linker was coupled to a ScFv ligand to allow for the tags to become bound to epidermal growth factor receptor (EGFR).

Initially the assay was based closely upon the assay developed in Chapter 2, with the SERRS-active nanoparticles developed within this chapter replacing the previously used silver-TAMRA nanoparticle conjugates (Figure 3.1). The ability of this probe system incorporating the DIG-antiDIG interaction to selectively detect target DNA has been previously shown (Section 2.3.5), therefore this assay set up will be used as a test system to assess the malachite green labelled, antibody functionalised gold nanoparticle conjugates developed.

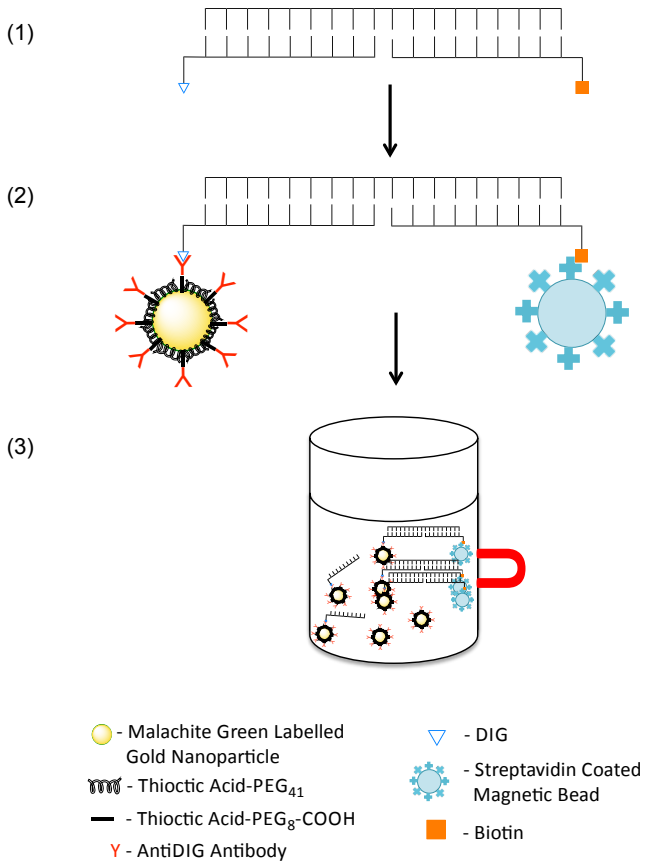

Figure 3.1 - Schematic representation of the fully constructed assay. (1) Target DNA hybridised to digoxigenin and biotin labelled probes. (2) The digoxigenin probe is bound by a hapten-antibody interaction to gold nanoparticles encoded with malachite green and stabilised with a PEG bilayer. The PEG bilayer consists of a shorter and a longer chain PEG molecule. The short PEG molecule is terminated with a carboxylic acid group, through which an antiDIG antibody is conjugated to the nanoparticle. The biotin probe is bound by a biotin-streptavidin interaction to a streptavidin coated magnetic bead. (3) Upon introduction of a magnetic field, the magnetic particles with the SERRS-active particles tethered to them are gathered at the side of the sample vial. Any excess assay components present in the sample will remain in the buffer solution. SERRS analysis is then performed on the magnetic particles either in solution, or directly on the immobilised beads.

The principle of the assay was that in the presence of target DNA, both the DIG-labelled probe and the biotinylated capture probe will become hybridised to the target since they are each made up of probe sequences complementary to half of the target sequence (step 1). The DIG label on the oligonucleotide probe can then interact with the antiDIG antibody on the gold malachite green labelled nanoparticle conjugates, allowing the duplex formed to become labelled with a SERRS active nanoparticle. This labelled duplex can interact *via* the biotin label on the capture probe with the streptavidin coated magnetic beads, resulting in the SERRS active nanoparticle becoming immobilised on the magnetic bead

(step 2). Therefore, a SERRS signal should be seen from the magnetic beads. Ideally, the assay will take the format of a closed tube system. In the idealised assay design, the magnetic beads will be pulled to the side of the sample tube by the introduction of a magnet, forming a pellet (step 3). The pellet can then be directly analysed by SERRS. However during development of the assay, after immobilisation of the target-probe duplex on the magnetic beads, the beads will be pulled to the side of the sample tube and the supernatant containing excess assay components will be removed. This process will be repeated to ensure all unbound SERRS-active nanoparticles are removed from the system, and the beads are resuspended and analysed in solution.

However, if full complementarity is not present, the probe corresponding to the non-complementary region will be unable to bind to the target strand. Consequently the duplex with both the SERRS and magnetic bead labels will be unable to form. If the DIG-labelled probe does not hybridise to the target there is no means by which the SERRS active nanoparticle can interact with the duplex immobilised on the magnetic beads, therefore the conjugates will be removed during washing. Likewise, if the biotin capture probe does not hybridise to the target, the duplex labelled with a SERRS active nanoparticle is unable to be immobilised on the magnetic beads. Therefore the nanoparticle conjugates containing the SERRS reporter will be removed in the supernatant during washing, resulting in an absence of SERRS signal. In the case of the idealised closed tube assay system where the magnetic beads are directly analysed as a pellet, instead of the unbound components being removed from the sample, they will instead remain in the unanalysed supernatant.

After the malachite green labelled, antibody functionalised gold nanoparticle conjugates have been shown to act as a successful replacement for the silver-TAMRA conjugates previously used, these conjugates will be further developed to incorporate the coupling of oligonucleotide probes directly to the carboxylic acid site terminating the short chain PEG molecule. The direct attachment of the oligonucleotide probes to the malachite green labelled, pegylated gold nanoparticle conjugates was suggested in order to remove the need for the DIG-antiDIG interaction in tethering the SERRS-active nanoparticles to the probe/target duplex (Figure 3.2).

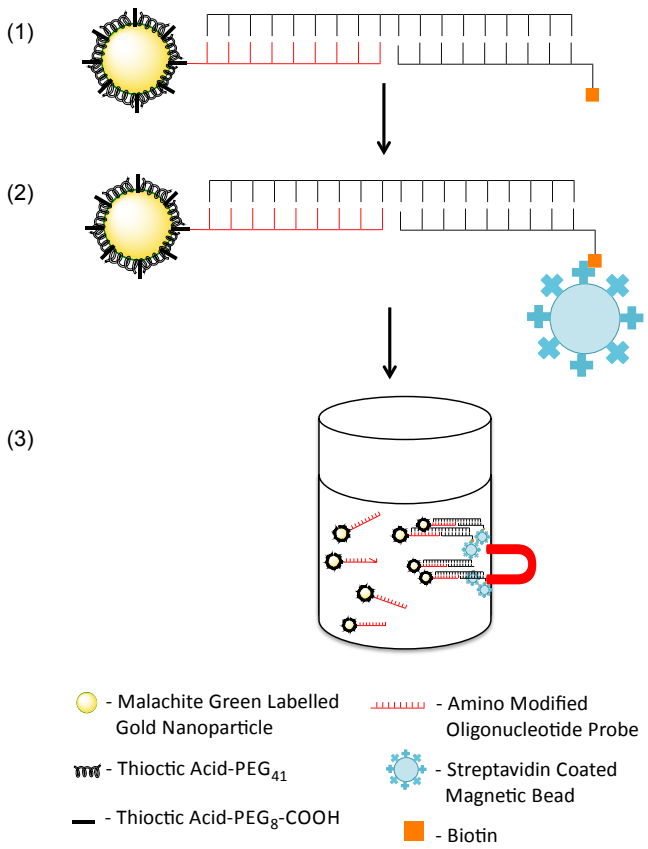

Figure 3.2 - Schematic representation of the fully constructed assay. The gold nanoparticles are encoded with malachite green and stabilised with a PEG bilayer. The PEG bilayer consists of a shorter and a longer chain PEG molecule. The short PEG molecule is terminated with a carboxylic acid group, through which an amino-modified oligonucleotide probe is conjugated to the nanoparticle. (1) The target DNA strand hybridises to the oligonucleotide probe bound to the SERRS active nanoparticle and the biotin probe. (2) The biotin probe is bound by a biotin-streptavidin interaction to a streptavidin coated magnetic bead. (3) Upon introduction of a magnetic field, the magnetic particles with the SERRS-active particles tethered to them are gathered at the side of the sample vial. Any excess assay components present in the sample will remain in the buffer solution. SERRS analysis is then performed on the magnetic particles either in solution, or directly on the immobilised beads.

If this interaction can be successfully removed from the assay construction, the number of biological interactions required for the detection of the target DNA is reduced. Consequently, the number of points for potential failure in the construction of the assay is minimised. Furthermore, for the assay involving the DIG-antiDIG interaction to become multiplexed, a number of different antigen-antibody interactions would have to be used to allow for simultaneous detection of a number of target sequences. However, if the probe can be directly coupled to the dye-labelled nanoparticle conjugates, multiplexing is made much less complex. The sequence of the probe immobilised on the nanoparticle conjugates

could be altered to complement a number of target sequences. Each corresponding oligonucleotide functionalised nanoparticle conjugate could be labelled with a different dye, to produce a series of dye-labelled oligonucleotide-functionalised conjugates which can be used for multiplexed detection of a number of target sequences.

3.2 SYNTHESIS & CHARACTERISATION OF NANOPARTICLE CONJUGATES

3.2.1 REQUIREMENTS

The nanoparticle conjugates designed and synthesised for use in this assay must meet a number of requirements. The three main properties required of these nanoparticle conjugates are:

- The nanoparticle conjugates must give an intense, distinct SERRS signal detectable without the need for additional aggregation of the nanoparticles;
- The conjugates must exhibit high stability in 0.3 M PBS, the buffer of choice for the assay construction and analysis;
- The conjugates must be easily functionalised with a biomolecule of choice.

3.2.2 DYE LABELLING CORE NANOPARTICLES

The first of the requirements for the nanoparticle conjugates to be used in the assay is that they should be SERRS active and should give an intense SERRS signal with distinctive peaks. The introduction of a SERRS dye adsorbed directly onto the surface of a nanoparticle results in intense SERRS signals being produced. One method for tethering a dye molecule directly to the nanoparticle surface in close enough proximity for surface enhancement to occur is *via* an isothiocyanate anchoring group. There are a number of Raman dyes commercially available in the isothiocyanate form, including TAMRA, ROX, fluorescein and malachite green. Malachite green exhibits an advantage over the other dyes listed due to its non-fluorescent nature. It has been previously shown that the introduction of fluorescent molecules close to a metallic surface can result in an enhancement of the fluorescence being observed. [131, 132] As such, use of a non-fluorescent SERRS dye would result in a decreased background signal being observed. Consequently, the peaks in the SERRS spectrum would be more clearly defined and easily discernible.

Malachite green was therefore selected as the dye of choice for introduction onto the nanoparticle surface due to its λ_{max} being at 629 nm. As illustrated in Figure 3.3, this allows for the dye to be in resonance with both the surface plasmon of the gold nanoparticles (~528 nm) and the excitation frequency of the laser at 633 nm.

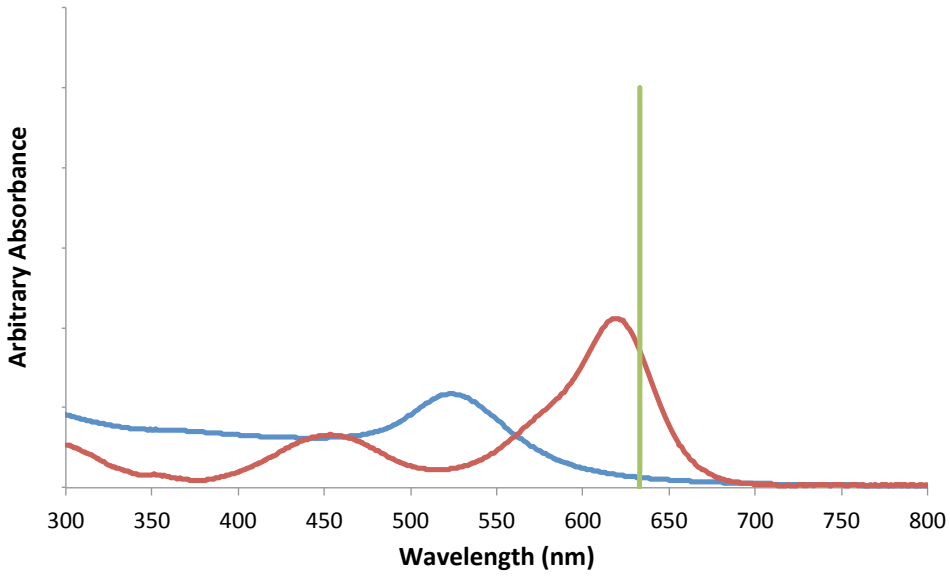

Figure 3.3 - UV-vis spectrum of 60 nm gold colloid (blue) and malachite green (red). The vertical line (green) represents the laser excitation wavelength at 633 nm.

3.2.3 GOLD CORE NANOPARTICLES

Gold nanoparticles (60 nm) were prepared *via* citrate reduction of sodium tetrachloroaurate. The gold salt was reduced from a +3 to 0 oxidation state, forming clusters of gold atoms stabilised by coating of the particles with citrate anions. [143] The size of the particles produced can be controlled by varying the ratio of gold salt and citrate anions used. [144] In order to produce larger particles, the amount of sodium citrate is reduced. This reduction will reduce the amount of citrate anions available for stabilisation of the particles. As such, the small clusters will aggregate into larger particles until the total surface area of the particles in the solution becomes small enough to be stabilised by the citrate ions present. The adsorption of the citrate anions to the nanoparticle surface is vital in the prevention of nanoparticle aggregation. Since the citrate ions are negatively charged, the surface of the nanoparticles will also be rendered negatively charged. Consequently, the nanoparticles will repel each other, overcoming the attractive Van der Waals forces between particles, and minimising nanoparticle aggregation.

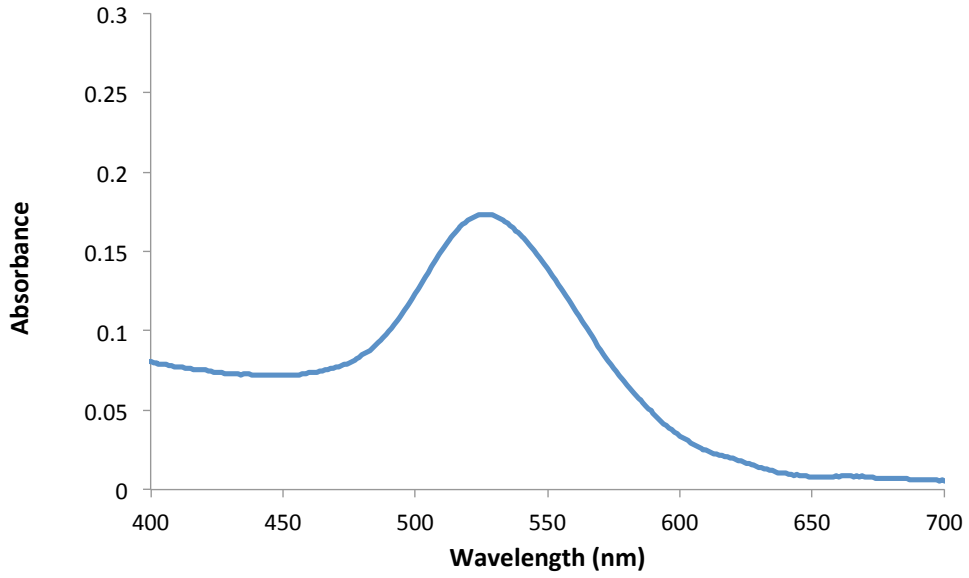

Figure 3.4 - Extinction spectrum of citrate stabilised gold nanoparticles, λ_{max} = 528 nm, FWHM = 50 nm. Dilution factor = 10.

Figure 3.4 shows an extinction spectrum obtained from a batch of citrate stabilised gold nanoparticles prepared for use as nanoparticle cores. The extinction maximum observed due to the surface plasmon of the gold nanoparticles is approximately 528 nm. The extinction profile shows a full width half maximum (FWHM) of approximately 50 nm, indicating the nanoparticles within the suspension could be regarded as relatively discrete with a narrow size distribution. This corresponds well with the SEM images obtained for this gold colloid. A representative example of these images is shown in Figure 3.5.

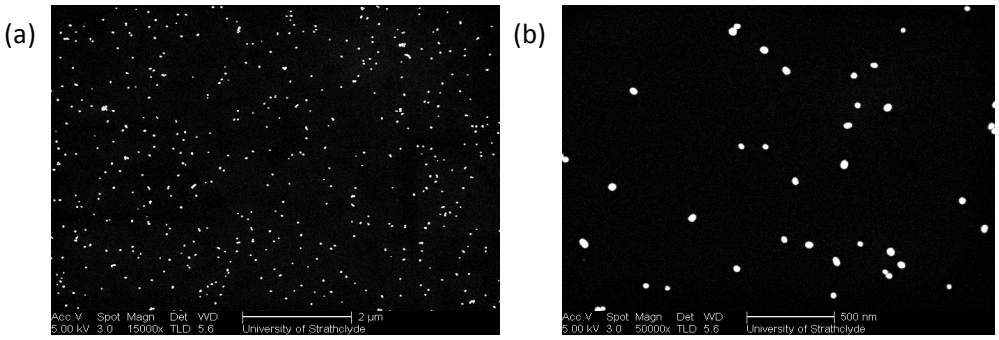

Figure 3.5 - Representative SEM image of gold nanoparticles at (a) 15000 x magnification and (b) 50000 x magnification.

The SEM images show a large number of monomeric gold nanoparticles alongside a small number of dimers and small clusters. The particles appear to have little variation in their diameter, as suggested by the narrow extinction peak observed in Figure 3.4.

3.2.4 DYE LABELLING OF NANOPARTICLES

The dye was held close to the nanoparticle surface *via* an isothiocyanate group attached to the malachite green molecule (Figure 3.6). Nie *et al*. reported that the isothiocyanate group provides an "affinity tag" for binding to gold surfaces resulting in a stable sulphur-gold bond. [80] The same group later reported that upon the addition of thiol-modified PEG, no decrease in SERRS intensity was observed. [66] This indicates that the dye molecules are not displaced by the thiolated PEG molecules, demonstrating the robust nature of the bond between the isothiocyanate group and the gold surface.

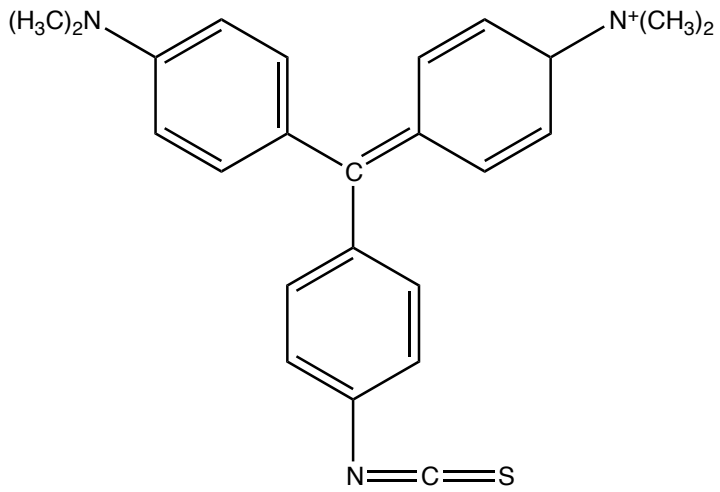

Figure 3.6 - Structure of malachite green isothiocyanate.

In order for the conjugates to be successfully incorporated into the assay, it is vital that aggregation of the nanoparticles during the functionalisation process is kept to a minimum. This is important in order for the SERRS signals collected from the conjugates to be relatively uniform. Introduction of aggregates into the system would create SE(R)RS "hotspots", thereby providing conjugate clusters with heightened SERRS signals, resulting in a dramatically increased signal for the samples containing these clusters. Therefore, in order to reduce sample to sample variation, the nanoparticle conjugates should preferably exist in the monomeric form.

The malachite green dye was tethered to the nanoparticle surface *via* the bonding of the isothiocyanate group present in the dye molecule to the gold surface. Upon addition of the isothiocyanate form of the dye, the citrate ions are displaced from the nanoparticle surface. The addition of the dye to the nanoparticle surface has the potential to cause aggregation between particles due to two effects. Firstly, the displacement of the citrate ions from the surface of the nanoparticle is likely to result in a destabilisation effect. The negatively charged ions act as stabilising ligands on the surface of the nanoparticle, providing electrostatic shielding against permanent aggregation of the particles. With the removal of these ions, the particles are liable to succumb to the attractive inter-particle forces resulting in the formation of clusters. Secondly, due to the positively charged nature of the malachite green dye, shown in Figure 3.6, the probability of nanoparticle aggregation upon introduction of the dye is increased. The introduction of the positive charge to the nanoparticle surface results in the inter-particle repulsive forces, introduced by the adsorption of the citrate ions to the nanoparticle surface, being reduced. Furthermore, the positive charge can readily interact with the negative citrate ions present on neighbouring nanoparticles, increasing the aggregation between particles.

Due to the aggregating nature of the malachite green isothiocyanate dye, it was vital that the addition of the dye to the nanoparticle surface was carried out in such a manner that the level of aggregation was carefully controlled. The concentration at which the dye is added to the colloidal suspension of nanoparticles plays a vital role in the aggregation state of the functionalised sample. Therefore, the concentration of dye solution added to the nanoparticles was investigated in order to provide dye labelled nanoparticles which were still stable and relatively discrete in solution. The aggregation of a nanoparticle suspension can be easily monitored by extinction spectroscopy (Figure 3.7) as well as by eye. Upon initiation of the aggregation process, the particles begin to agglomerate forming small clusters. As the aggregation continues, the clusters grow larger as more particles are destabilised. As such, the clusters formed are much larger in size than the original nanoparticles, resulting in a red-shift of the plasmon peak from the nanoparticle suspension. Consequently, the original peak observed at 528 nm will be decreased, and the peak corresponding to the surface plasmon of the nanoparticles will become much broader as different sized nanoparticle aggregates begin to form. Concomitantly, a peak at approximately 675 nm begins to appear due to the formation of larger aggregates. This

additional peak corresponds to the surface plasmon of these large clusters which is significantly red-shifted in comparison with that of the unaggregated nanoparticle suspension. This red-shift of the surface plasmon results in a visible colour change from red to blue being observed. Therefore, this process can be monitored visually as well as spectroscopically.

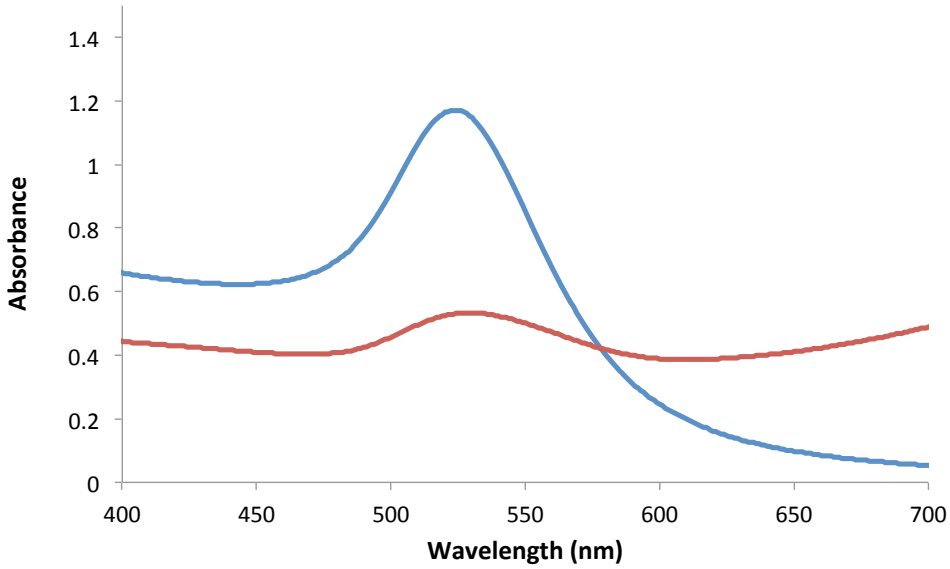

Figure 3.7 - Extinction spectra of gold colloid resuspended in water (blue) and 0.3 M PBS (red). The sample resuspended in water remained unaggregated, whilst the sample resuspended in 0.3 M PBS became visibly aggregated. Samples were analysed undiluted.

An investigation into the concentration of malachite green isothiocyanate that can be added to the gold nanoparticles without aggregation was carried out by monitoring the extinction spectrum of the gold nanoparticles upon addition of aliquots of the dye. Nie *et al*. stated the use of 3 – 4 µM reporter solution, added to rapidly stirring gold colloid in order to successfully synthesise Raman active nanoparticles. [66] Therefore, a malachite green isothiocyanate solution with a concentration of 3 µM was added in 10 µL aliquots to a 1 mL sample of gold colloid (0.08 nM) with rapid stirring and the extinction spectra shown in **Figure 3.8** were obtained. A spectra was recorded after the addition of each 10 µL aliquot of malachite green.

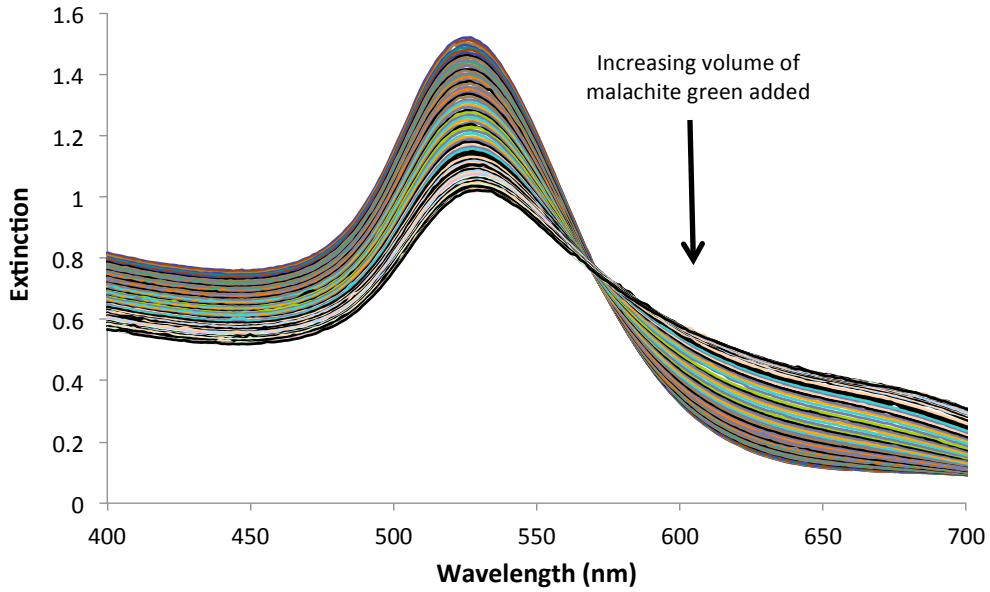

Figure 3.8 - Extinction spectra monitoring the addition of a solution of malachite green isothiocyanate (3 x 10^{-6} M) to citrate stabilised 60 nm gold nanoparticles. A spectra was recorded after the addition of each 10 µL aliquot of malachite green. Samples were analysed undiluted.

It is evident from the absorption profiles collected, that the addition of the dye causes aggregation of the nanoparticles. It can be clearly seen that the peak corresponding to the unfunctionalised nanoparticles at 528 nm has become distinctively smaller and broader as the volume of malachite green added to the sample is increased, with the extinction maximum shifting to 534 nm. This indicates the formation of aggregates of various sizes. The appearance of a second peak is also evident at higher wavelength (650-750 nm), indicating the existence of large aggregates and clusters. A visible colour change could also be noted upon addition of the dye at this concentration, with the sample changing from a red colour to purple. Consequently, it can be suggested that this concentration of malachite green is not suitable for the creation of stable, unaggregated Raman active nanoparticles. This investigation was therefore repeated with a dye concentration of 0.3 µM. It was postulated that, although the addition of a larger volume of dye would be required in order to attain the same level of surface coverage as the more concentrated dye, by lowering the concentration of the reporter solution the aggregating effect of the dye could be minimised. The extinction spectra resulting from the reporter solution being added to rapidly stirring gold colloid at the lowered concentration are displayed in . A spectra was recorded after the addition of each 10 µL aliquot of malachite green.

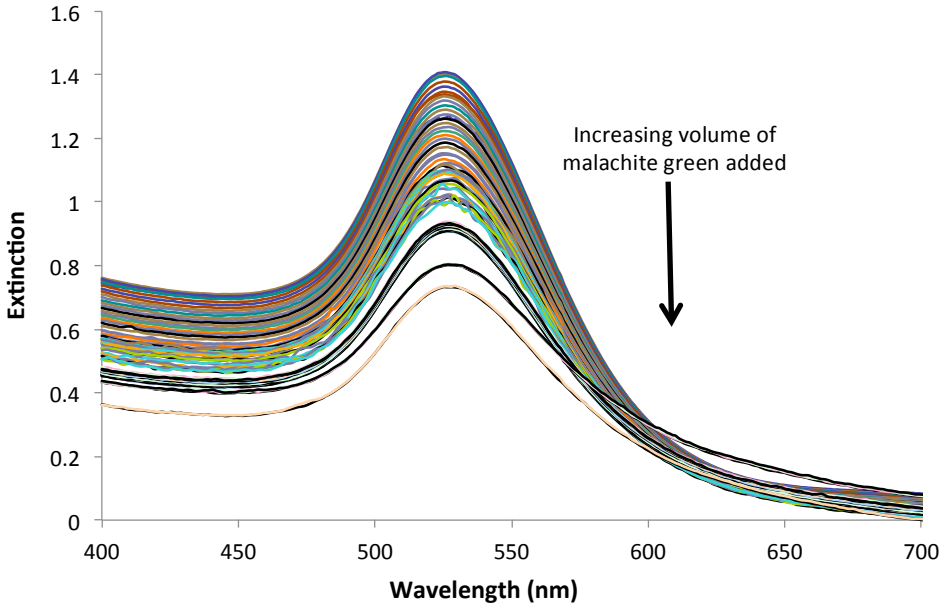

Figure 3.9 - Extinction spectra monitoring the addition of a solution of malachite green isothiocyanate (3 x 10^{-7} M) to citrate stabilised 60 nm gold nanoparticles. A spectra was recorded after the addition of each 10 µL aliquot of malachite green. Samples were analysed undiluted.

For it can be seen that the peak at 528 nm corresponding to the unmodified nanoparticles has become smaller as the volume of malachite green added to the sample is increased, however there is no significant broadening of the peak. This is likely to be due to the dilution of the nanoparticle solution, and was also observed in the control experiment where only water was added. The lack of broadening of the plasmon peak is indicative that upon addition of the dye solution, minimal aggregation has occurred. This theory is supported by the absence of a significant peak at higher wavelengths. This is illustrated in Figure 3.10, where the extinction at 675 nm is monitored upon addition of dye solution for each concentration investigated.

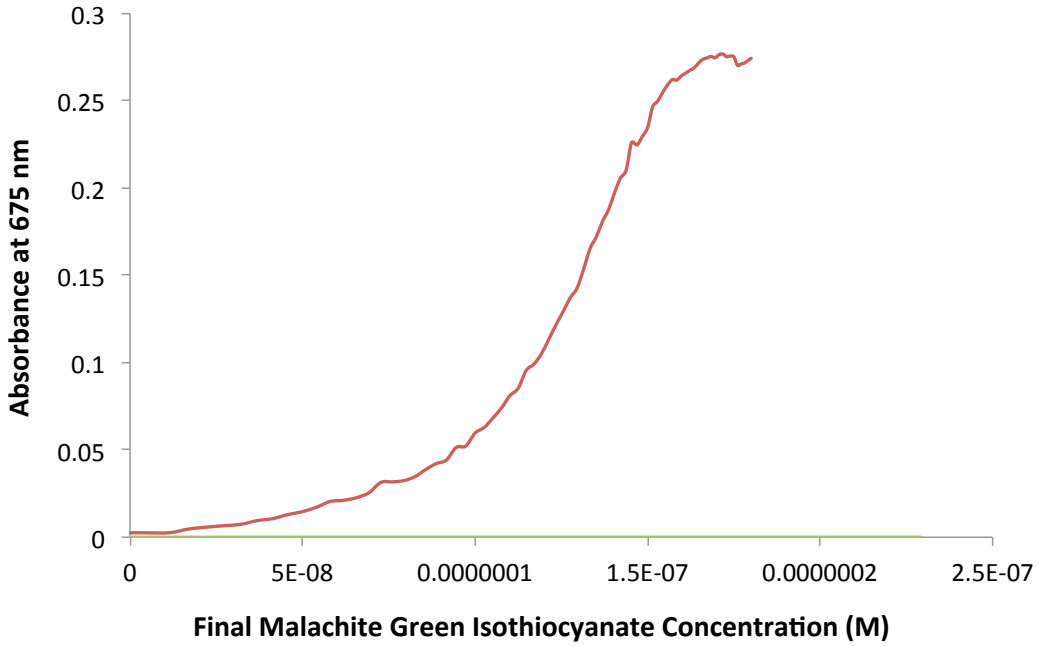

Figure 3.10 - A graph showing the extinction measurement at 675 nm plotted against the volume of malachite green isothiocyanate added for the 3 x 10^{-6} M solution (blue) and the 3 x 10^{-7} M solution (red).

The extinction was monitored at 675 nm since the appearance of a peak at higher wavelengths is implicit with the nanoparticles becoming aggregated and forming clusters. Whilst it is known that a much smaller volume of the 3 µM reporter solution would be required in order to achieve the same level of surface coverage when using the 0.3 µM reporter solution, it can be seen that upon the addition of even small volumes of the more concentrated dye, a peak at 675 nm begins to appear indicating that the nanoparticles are becoming aggregated. It can be noted however that the extinction does not change markedly upon the addition of the more dilute dye, implying that the nanoparticles are more discrete upon addition of this concentration. It can be seen that less reporter solution was added at 3 µM (750 µL) in comparison to that added at 0.3 µM (1500 µL). This is due to the nanoparticles becoming completely aggregated upon the addition of 750 µL of the more concentrated dye. The solution had turned from red to purple and aggregates were beginning to precipitate on to the bottom of the sample when stirring was ceased. However, even after addition of 1500 µL of the more dilute reporter solution had been added, the sample still remained red in colour with no visible signs of aggregation. Therefore, it was decided to proceed with the labelling process using the reporter at an initial concentration of 0.3 µM.

Whilst it was important that the nanoparticles remain stable and relatively unaggregated, it was also vital that they give an intense, distinct SERRS signal. Therefore, the final concentration of malachite green added was optimised to give nanoparticles that retained their stability whilst exhibiting a strong SERRS signal without the need for aggregation. A series of samples were prepared containing gold colloid and varying final concentrations of the reporter molecule. SERRS analysis was performed on these samples, and the resulting spectra were compared (Figure 3.11). The final malachite green concentrations selected for investigation were based upon the range analysed by extinction spectroscopy in Figure 3.10.

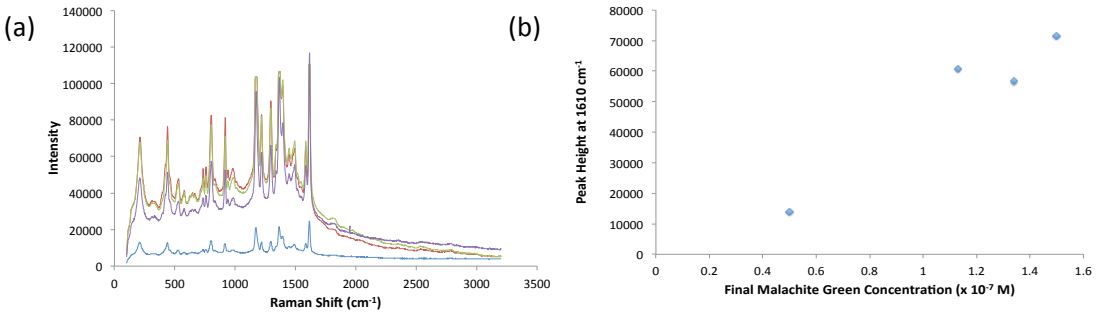

Figure 3.11 - (a) SERRS spectra collected at 633 nm from gold-malachite green nanoparticle conjugates prepared with a final malachite green isothiocyanate concentration of 5.0×10^{-8} M (blue), 1.1×10^{-7} M (purple), 1.3×10^{-7} M (green) and 1.5×10^{-7} M (red). (b) Peak height measured at 1610 cm^{-1} from the SERRS signal obtained upon analysis of the malachite green nanoparticle conjugates. The samples were analysed using 633 nm laser excitation, 1 x 30 s accumulation.

It can be seen that, discounting the sample containing the lowest final concentration of reporter molecule, the samples all gave intense SERRS signals with clear, easily distinguishable peaks. Upon comparison of the signal intensity observed from the samples, there is little difference between the three samples with the highest reporter concentration. Consequently, 1.3×10^{-7} M was selected as the reporter final concentration to be used to prepare the nanoparticle conjugates. This relates to approximately 2.1×10^{4} malachite green molecules *per* nanoparticle. These results are in relatively good agreement with the observations made by Nie *et al*. who found that approximately 1.4×10^{4} reporter molecules were absorbed onto each 60 nm nanoparticle. [66]

3.2.5 STABILISATION OF DYE LABELLED NANOPARTICLES

As shown in Figure 3.7, gold nanoparticles are not stable when resuspended in salt containing buffers. One of the criteria for the production of nanoparticle conjugates was that they must be stable in 0.3 M PBS, the buffer of choice for assay construction and analysis. 0.3 M PBS was used in the construction of the assay in order to allow the probes to hybridise to the target sequence, giving rise to a duplex that is stable at room temperature. In order to afford additional stability to the dye labelled nanoparticle cores, a PEG bilayer was introduced to the nanoparticle surface. It has been claimed that the introduction of thiol-modified PEG linkers do not displace the malachite green when in its isothiocyanate from the nanoparticle surface. [66] The bilayer consisted of two different PEG linkers of differing lengths and functionalities. Both of the linker molecules had a thioctic linker moiety at one terminus. The thioctic acid group acts as a surface complexing group anchoring the linker molecule to the gold surface. Thioctic acid was selected for binding the linker molecule to the nanoparticle surface instead of a thiol group, as it has been shown to impart a heightened stability in comparison with its monothiol counterpart. [115] One of the linker molecules contained a short chain PEG_8 assembly, terminated with a carboxylic acid group. This carboxylic acid group was introduced as a potential site for biofunctionalisation of the nanoparticle. The second linker molecule contained a longer chain PEG_{41} group, and was terminated with a *t*-butyl group. This linker was utilised in order to afford extra stability to the nanoparticle surface, with the long polymer chain available to fold down on top of the surface, as shown in Figure 3.12, blocking the previously unfunctionalised nanoparticle surface. The terminal *t*-butyl group was used to cap the linker, controlling the sites available for coupling to biomolecules.

The quantity of linker molecules added *per* nanoparticle was calculated based on previous work published by Nie *et al.* in which the nanoparticles were stabilised by the addition of at least 30000 PEG molecules *per* nanoparticle. [66] During introduction of the linker molecules, the short chain COOH terminated PEG molecule was introduced to the nanoparticle surface first in order to maximise the number of sites available for biofunctionalisation. The longer chain PEG was then added to stabilise any remaining unpegylated surface.

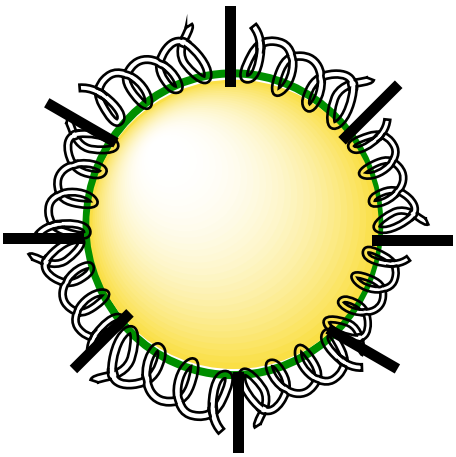

Figure 3.12 - Schematic of 60 nm gold nanoparticle labelled with a monolayer of malachite green isothiocyanate. A long chain PEG linker and a short chain PEG linker terminated with a carboxylic acid group are tethered to the nanoparticle surface *via* a thioctic acid group.

Since it was important to ensure that the nanoparticle conjugates were discrete in solution for the integration into the assay format, it was vital to ensure that the nanoparticles had not aggregated before any further functionalisation procedure was conducted. Therefore, the labelling and stabilisation process was monitored by extinction spectroscopy, assessing the plasmon peak obtained after each stage of the functionalisation protocol, as shown in Figure 3.13. A sample of citrate stabilised gold nanoparticles was analysed before introduction of the malachite green isothiocyanate reporter to the surface. The sample was then analysed again prior to the addition of the stabilising linker molecules. The stabilised nanoparticles were then centrifuged and resuspended in either water or 0.3 M PBS, before extinction spectroscopy was performed.

It can be seen that upon the initial introduction of the reporter molecule to the nanoparticle surface, there is a significant dampening of the surface plasmon observed from the gold nanoparticles at 528 nm. There was however no observation of a second peak at higher wavelengths, which would be indicative of aggregate formation, and no significant broadening of the peak at 528 nm was observed. This suggests that the dampening observed is a dilution effect due to the addition of the reporter solution, and not due to the aggregation of the sample.

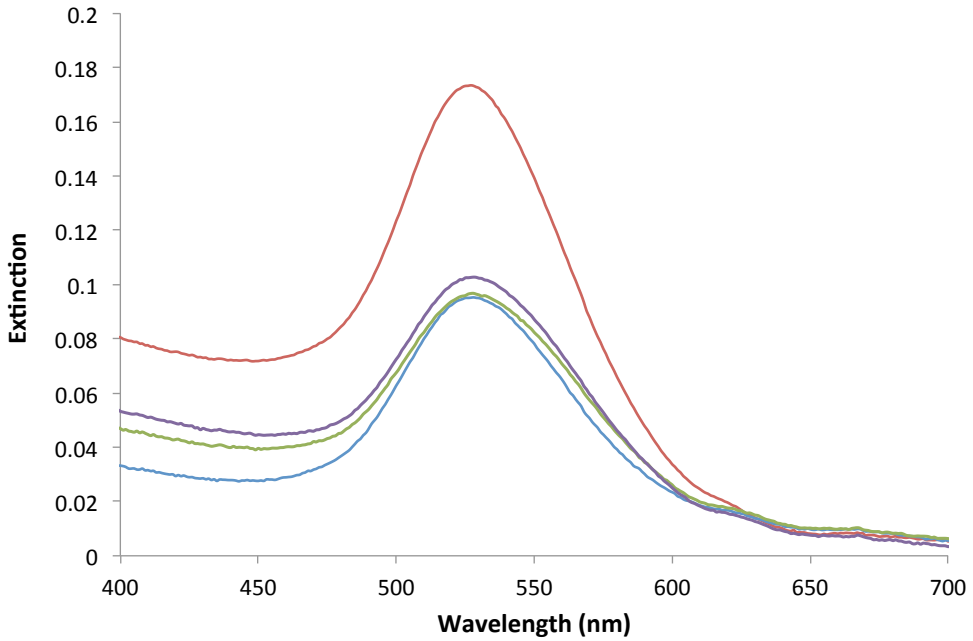

Figure 3.13 - Extinction spectra showing the construction of PEG stabilised Raman active gold nanoparticle conjugates. Gold nanoparticles (red) were labelled with malachite green isothiocyanate (green). A long chain PEG linker and a short chain PEG linker terminated with a carboxylic acid group were tethered to the nanoparticle surface *via* a thioctic acid group. The conjugates were then washed and resuspended in water (blue) or 0.3 M PBS (purple). Dilution factor = 10.

Upon addition of the PEG linker molecules, there was no significant change in the extinction profile when compared to that of the non-pegylated labelled nanoparticles. Furthermore, when resuspended in 0.3 M PBS, a salt-containing buffer, there was little change observed to the peaks. There was no significant broadening of the peak at 528 nm, and no appearance of a secondary peak at higher wavelengths. When compared with the extinction spectrum obtained of unfunctionalised gold nanoparticles in 0.3 M PBS (Figure 3.4) it is clear that the pegylated nanoparticle conjugates are more stable in this buffer. This is vital for the conjugates since this is the buffer that will be used in the final assay.

These findings are also in good agreement with the visual observations made during the preparation of the conjugates. The nanoparticle solution remained red in colour throughout the labelling and stabilisation process. It had previously been observed that upon resuspension in 0.3 M PBS, a solution containing unfunctionalised gold nanoparticles changes colour from red to blue. This is a result of the aggregation induced by the salt within the buffer system. Consequently, if the conjugates constructed were unstable in 0.3 M PBS, a similar colour change of the solution from red to blue would be expected.

However, upon introduction of the conjugates to the salt-containing buffer the solution did not change colour, suggesting that no aggregation had occurred. Therefore, it can be concluded that the addition of the linker molecules has had the desired effect of stabilising the nanoparticles in 0.3 M PBS buffer.

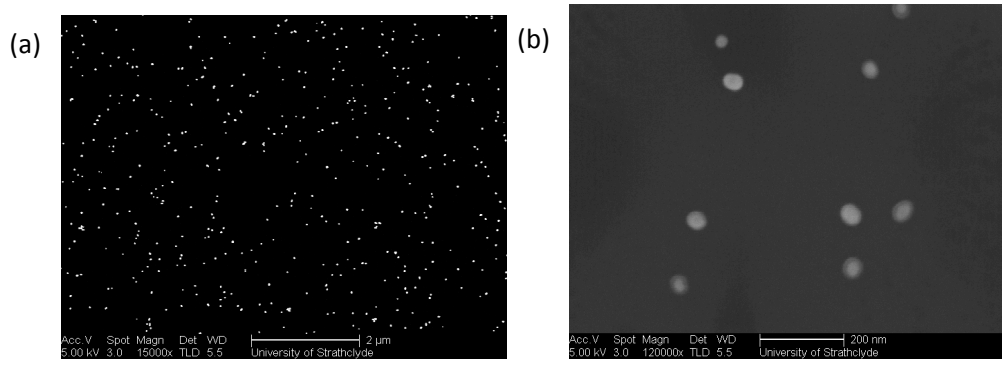

Figure 3.14 - Representative SEM image of gold colloid labelled with malachite green isothiocyanate, stabilised with a bilayer of PEG linker molecules at (a) 15000 x magnification and (b) 120000 x magnification.

This conclusion is further supported by the SEM images obtained for the pegylated particles (Figure 3.14). When compared with the images obtained for unmodified gold colloid (Figure 3.5), the aggregation state of the nanoparticles does not appear to have changed markedly. The images obtained of the dye labelled, pegylated gold (AuMGPEG) nanoparticle conjugates shown a number of dimers and small clusters but no large aggregates can be seen. Upon higher magnification (Figure 3.14(b)), the PEG shell can be seen surrounding the labelled nanoparticles. These shells are believed to aid the stability of the conjugates. The images collected for the unmodified colloid also showed a few small aggregates and dimers (Figure 3.5). This would suggest that the functionalisation protocol carried out has not induced any further aggregation of the nanoparticles. As such, the conjugates prepared can be considered to have retained the monodispersity of the original colloidal suspension.

The long term stability of the nanoparticle conjugates was also assessed since it is important that the conjugates can be prepared and stored in their non-biofunctionalised state ready for use and subsequent biofunctionalisation when required. A batch of AuMGPEG conjugates was prepared in phosphate buffer and the extinction spectrum recorded. The sample was then stored at room temperature for three months, and the extinction spectrum repeated. The extinction profiles obtained were compared (Figure 3.15).

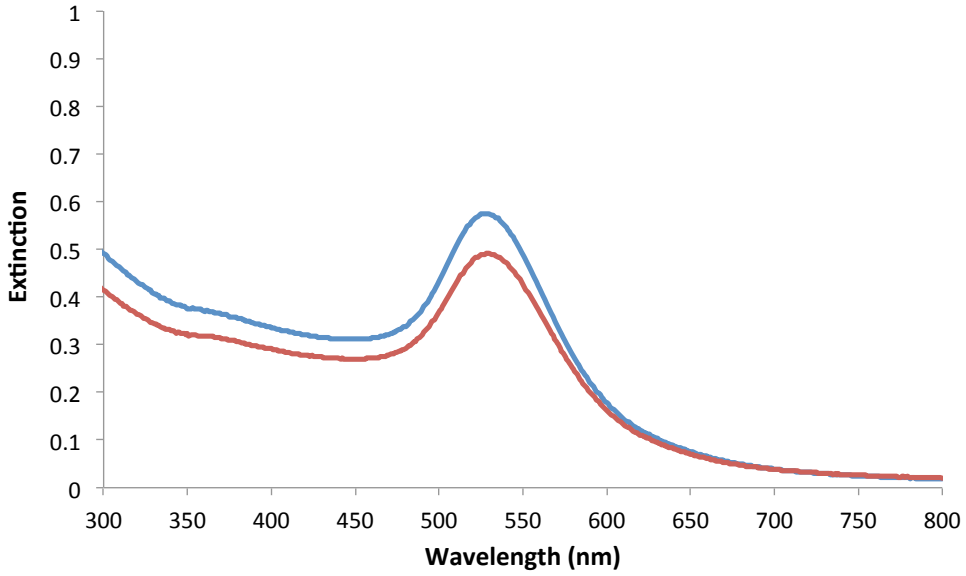

Figure 3.15 - Extinction spectrum of gold nanoparticles labelled with malachite green isothiocyanate, then functionalised with a bilayer of long and short chain PEG molecules *via* a thioctic acid anchoring group. The spectra were collected upon preparation (blue), and repeated 3 months later (red). Samples were analysed undiluted.

After storage of the conjugates, the peak corresponding to the surface plasmon at 528 nm has decreased slightly. This peak however appeared to have retained its original shape, with no significant broadening observed. There is also no appearance of a peak at higher wavelengths, indicating minimal aggregation has occurred. In light of these results, it can be concluded that the labelled, polymer stabilised nanoparticles can be considered as stable for at least three months in aqueous conditions at room temperature.

3.2.6 Antibody Functionalisation of Core Nanoparticles

Since the TAMRA labelled, antibody functionalised silver nanoparticle conjugates used in Chapter 2 had yielded positive results when used in the assay system (Figure 2.27), it was vital that the AuMGPEG nanoparticle conjugates, developed as a replacement, could yield comparable results when incorporated into the same assay (Figure 3.1). This comparison was performed in order to confirm the ability of the developed antibody functionalised, malachite green labelled gold nanoparticle conjugates (AuMGPEGAb) to bind specifically to the DIG-labelled oligonucleotide probe *via* the coupled antiDIG antibody, and also to

identify whether the SERRS signal obtained from the conjugates was measureable in an assay format. In order for this comparison to be made, the AuMGPEG nanoparticles must be further functionalised with antiDIG antibodies to allow the rest of the components of the assay set up to remain unchanged (Figure 3.1).

Gold nanoparticles were labelled with malachite green isothiocyanate, followed by stabilisation by the introduction of a PEG linker bilayer. The nanoparticles were then centrifuged and resuspended in phosphate buffer (pH 7.6). AntiDIG antibodies were conjugated to the carboxylic acid group at the end of the short chain linker molecules *via* an EDC/ sulfo-NHS coupling (Figure 3.16). [142] This coupling procedure had been used previously to successfully couple this antibody onto the carboxylic acid group at the terminus of a PEG linker (Section 2.5.3.2).

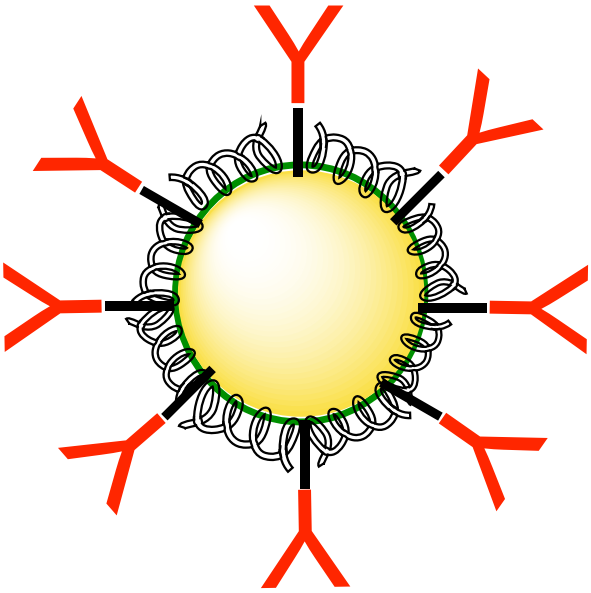

Figure 3.16 - Schematic of a 45 nm gold nanoparticle labelled with a monolayer of malachite green isothiocyanate. A long chain PEG linker and a short chain PEG linker terminated with a carboxylic acid group were tethered to the nanoparticle surface *via* a thioctic acid group. An antiDIG antibody was then conjugated to the carboxylic acid group *via* an EDC/sulfo-NHS coupling process.

In order to confirm the unaggregated nature of these fully functionalised nanoparticle conjugates, SEM images of the conjugates (**Figure 3.17**) were compared with those obtained of the unmodified gold colloid (**Figure 3.5**), and the AuMGPEG nanoparticles (**Figure 3.14**).

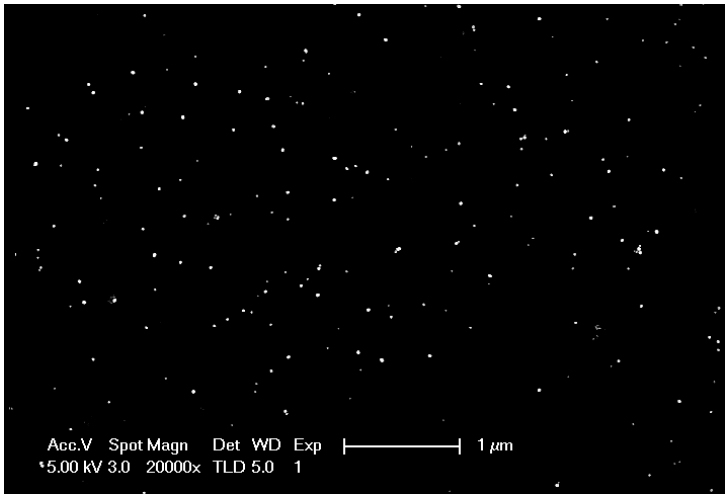

Figure 3.17 - Representative SEM image of gold colloid labelled with malachite green isothiocyanate, stabilised with a bilayer of PEG linker molecules. The short chain PEG linker then has an antiDIG antibody coupled to the carboxylic acid group at its terminus.

In these SEM images, the particles appear to be in a relatively unaggregated state, with a few dimers and small clusters visible. When compared to the images obtained earlier in the functionalisation process, the aggregation state of the conjugates does not appear to have altered noticeably. This is in agreement with the visual observations made where, after washing and resuspension of the antibody functionalised conjugates in either phosphate buffer or 0.3 M PBS, the solution remained red in colour with no significant colour change observed. These results would indicate that a protocol has been successfully developed for the preparation of these stable dye-labelled, biofunctionalised conjugates that does not induce nanoparticle aggregation, with the synthesised conjugates retaining their monodispersity.

3.3 ASSAY CONSTRUCTION

There are a series of steps involved in the construction of the final assay (Figure 3.1). The DIG-labelled oligonucleotide probe and the biotin-labelled probe must hybridise to the target DNA (step 1), followed by introduction of the AuMGPEGAb nanoparticles and the magnetic beads (step 2). Following incubation of the sample, the magnetic beads are washed with 0.3 M PBS after the introduction of a magnetic field to allow collection of the magnetic beads at the side of the sample tube (step 3). The supernatant is removed and

the beads resuspended in 0.3 M PBS. This wash step is repeated three times in order to remove all unbound DNA and dye labelled nanoparticles. The solution containing the magnetic beads is then analysed by SERRS using an excitation wavelength of 633 nm.

3.3.1 TURBOBEADS

It was shown in Section 2.3.2 that the introduction of the streptavidin coated magnetic beads to the assay solution has a marked effect on the SERRS signal obtained from the sample. This was due to the micron-sized magnetic beads affecting the scattering of light from the SERRS-active nanoparticles, preventing the light from reaching the detector, and thereby resulting in a reduced SERRS signal being observed. With a view to minimising the dampening effect observed upon the introduction of the magnetic beads to the assay solution, streptavidin coated TurboBeads® were investigated as an alternative to the conventional streptavidin coated magnetic beads used previously.

TurboBeads® are magnetic particles with a metallic core and a graphene coating which are approximately 30 nm in diameter. It was conjectured that due to their decreased size in comparison with the conventional magnetic beads used previously, the beads would have less effect on the scattered light from the nanoparticles and would therefore reduce the signal reduction observed.

In order to compare the dampening of the SERRS signal observed from the TurboBeads® with the reduced signal observed previously from to the streptavidin coated magnetic beads, a comparable experiment was conducted using the TAMRA functionalised silver nanoparticles previously used in Section 2.3.2. An aliquot of silver nanoparticles was functionalised with PEG_3-TAMRA linker, bringing the Raman active dye into close proximity with the metal surface. A SERRS spectrum was collected of this sample using 532 nm laser excitation. An aliquot of streptavidin coated TurboBeads® were then added to the sample, and a second spectrum collected. The intensity of the SERRS signal obtained from each of the samples was then compared, as seen in Figure 3.18.

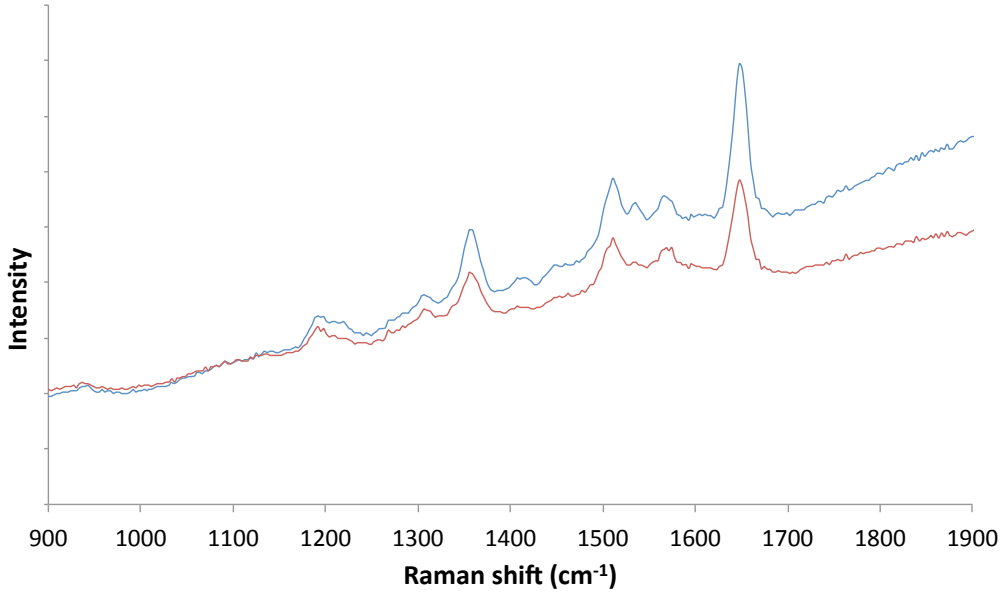

Figure 3.18 - SERRS spectrum obtained at 532 nm before the addition of streptavidin coated TurboBeads®. (blue), and after the addition of streptavidin coated TurboBeads® (red), investigating the effect of addition of magnetic beads on the SERRS response collected.

The SERRS signal collected from the SERRS active nanoparticles is reduced slightly upon the addition of the streptavidin coated TurboBeads®. However, when compared with the reduction observed upon the addition of the conventional streptavidin coated magnetic beads used previously (Section 2.3.2), the TurboBeads® have a much lesser effect. Consequently, it was ascertained that the use of the streptavidin coated TurboBeads® in place of the streptavidin coated magnetic beads previously used could result in increased sensitivity from the assay.

3.3.2 TARGET VS NONSENSE

It had been shown in Section 2.3.5 that the nonsense DNA sequence selected as a control to test the selectivity of the assay does not hybridise to the probe sequences. Therefore, this sequence was introduced in place of the target sequence in order to test the success of the assay after the replacement of the TAMRA labelled nanoparticle core with the AuMGPEGAb nanoparticle conjugates. It has been shown previously (Section 2.3.5) that the assay has potential for good discrimination between target and nonsense DNA sequences. Before further development of the conjugates and the assay, it was important to establish

whether the introduction of the newly developed conjugates would have any adverse effect on the function of the assay.

The assay was constructed as detailed in Section 3.7.5.1. Two differing versions of the assay were set up; one containing the probes and target DNA, and a control containing the probes and nonsense DNA. The sample was agitated for one hour after the addition of the nanoparticle conjugates and streptavidin coated magnetic beads. The magnetic beads were then separated on a magnetic separation rack, and the supernatant removed. The beads were resuspended, and the wash step repeated three times. The SERRS spectra were recorded for each sample using 633 nm laser excitation (Figure 3.19).

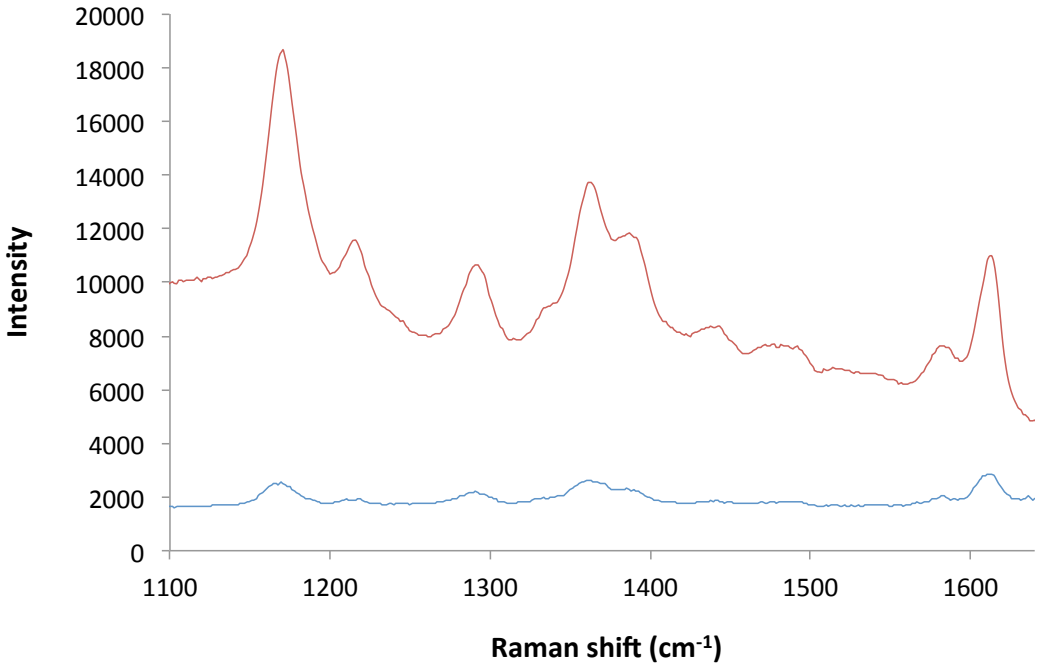

Figure 3.19 - SERRS spectrum obtained of the assay in the presence of target DNA (red), and the assay in the presence of nonsense DNA (blue). The assay was constructed, washed three times with 0.3 M PBS and analysed in solution using 633 nm laser excitation, 1 x 30 s accumulation.

The assay containing both labelled probes and the target DNA gave a prominent SERRS signal, indicating the successful immobilisation of the malachite green encoded nanoparticles on the magnetic beads. Conversely, the control assay containing both probes in the presence of a nonsense DNA sequence gave a low signal by comparison. This indicates that when there is no target sequence to tether the biotin probe and the DIG probe together, the biotin probe would be bound to the streptavidin coated magnetic

beads whilst the DIG probe tethered to the SERRS active nanoparticle would remain in solution and be removed in the supernatant during the wash steps. From Figure 3.19 it can be observed that there is clear discrimination between the signal collected in the presence of target DNA and that obtained in the presence of nonsense DNA. Consequently, it can be concluded that this assay can successfully distinguish between a target sequence and a control with a non-complementary sequence. These results indicate that the nanoparticle conjugates developed can be successfully implemented as a replacement for the silver-TAMRA nanoparticle conjugates used previously.

3.4 DNA FUNCTIONALISATION OF CORE NANOPARTICLES

3.4.1 SYNTHESIS OF OLIGONUCLEOTIDE FUNCTIONALISED NANOPARTICLE CONJUGATES

DNA-nanoparticle conjugates have found much success in recent years, being used in wide variety of DNA detection assays. [70, 83, 85, 88, 90, 92, 95-98] The functionalisation of the nanoparticle varies between research groups depending upon their function within the final assay developed. However, the one detail that they all have in common is the immobilisation of oligonucleotides on the nanoparticle surface. One popular approach for the anchoring of these sequences to the nanoparticle surface is *via* the modification of the oligonucleotide with a thiol group. [70, 85] This thiol group allows for the attachment of the DNA strand to the nanoparticle surface *via* the interaction of the sulphur with the metal surface. The conjugates then undergo a salt aging process to facilitate the packing of the oligonucleotides onto the surface, affording stable conjugates. One disadvantage of this technique however is that its success has been found to be dependent upon the sequence of DNA being immobilised. Whilst some sequences can be easily used to functionalise the nanoparticle to produce a densely packed surface resulting in robust conjugates, other sequences produce a less densely packed surface, with the conjugates produced being less stable and often aggregating before the functionalisation procedure is complete. [145, 146]

In order to circumvent this sequence dependency issue, a new method for functionalising nanoparticles with oligonucleotides was proposed based upon the work detailed in Section 3.2. The gold nanoparticle conjugates labelled with malachite green isothiocyanate, and stabilised with a PEG bilayer, were used as the core for the DNA functionalised nanoparticle

conjugates. Instead of functionalisation with an antibody, as described in Section 3.2.6, it was proposed that these conjugates could be functionalised with oligonucleotides (Figure 3.20). In order for this functionalisation to be possible, it was necessary for the oligonucleotide probes to be modified with an amino group, allowing for conjugation to the carboxylic acid moiety at the terminus of the PEG linker *via* an EDC/ sulfo-NHS coupling mechanism.

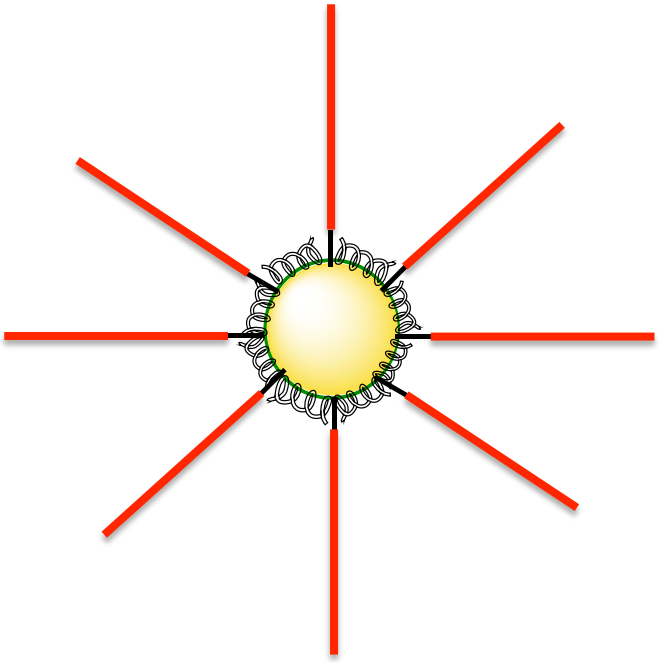

Figure 3.20 - Schematic of 60 nm gold nanoparticle labelled with a monolayer of malachite green isothiocyanate. A long chain PEG linker and a short chain PEG linker terminated with a carboxylic acid group are tethered to the nanoparticle surface *via* a thioctic acid group. An amino-modified oligonucleotide is then conjugated to the carboxylic acid group *via* an EDC/sulfo-NHS coupling process.

Due to the method of functionalisation, and the distance the oligonucleotide will be held from the surface, the only prerequisite for the DNA sequence selected is that is should have an amine modification at the 5' end selected for tethering to the nanoparticle. No special considerations have to be made regarding the sequence of the bases that compose the strand, other than their complementarity to the target sequence. This may deliver a significant advantage over the method detailed by Mirkin *et al*., [70] allowing a large library of DNA sequences to be available for immobilisation on the nanoparticle for the production of stable DNA-nanoparticle conjugates.

Graham *et al.* previously published work detailing the coupling of Raman active PEG linkers to amino-modified oligonucleotides. [82] It was reported that whilst the coupling of the oligonucleotides to the nanoparticles functionalised with the PEG linkers was possible, the process appeared to have a low efficiency with only a small number of oligonucleotides bound *per* nanoparticle to the finalised conjugates. In the method previously described by Mirkin *et al.* [70] the oligonucleotides were required in order to stabilise the nanoparticle, therefore it is important that the nanoparticles have a relatively large number of oligonucleotide strands immobilised on the surface. It is this dense packing of the DNA on the surface that enhances the stability of the nanoparticles, making the conjugates stable in salt containing solutions. Conversely, in the method proposed here, the conjugates are already stable in salt containing buffers before their functionalisation with oligonucleotides due to the stabilisation imparted by the PEG molecules tethered to the metal surface. Furthermore, the sparsely modified nanoparticle may provide a further advantage over the more densely packed oligonucleotide-conjugates in terms of steric hindrance. In order for the conjugates prepared *via* the immobilisation of thiolated oligonucleotides to be stable, the DNA strands have to form one of two arrangements. Either, they have to be very densely packed together in order to fully protect the particle surface, or the strands would have to lie flat upon the surface of the particle, shielding it from destabilising components, such as NaCl. When considering the incorporation of these conjugates into an assay involving a DNA hybridisation event, where the immobilised oligonucleotide on the nanoparticle has to hybridise with a complementary strand, neither of these arrangements are optimal for hybridisation efficiency.

If the densely packed surface is considered, there are two main issues that may affect the hybridisation efficiency of the nanoparticle conjugate to a target strand. Firstly, the oligonucleotides are tethered directly to the nanoparticle surface *via* a thiol group at the terminus. Therefore, the sequence will be held in close proximity to the nanoparticle. This positioning of the nanoparticle in relation to the oligonucleotide probe may result in significant steric hindrance during the hybridisation process. Due to the significantly large size of the nanoparticle in relation to that of the oligonucleotide probe, the availability of the probe to the complementary sequence may be impaired, preventing the target strand from aligning with the probe sequence to allow hybridisation. Secondly, the packing of the oligonucleotides on the surface may induce further issues for the hybridisation process.

Whilst the dense packing of the DNA strands is required in order to stabilise the nanoparticles, it may also hinder the ability of the target strand to access the oligonucleotide strands immobilised on the particle surface. Furthermore, the negatively charged phosphate backbone in the packed oligonucleotide strands may also offer electrostatic repulsion towards the backbone of the target strand upon its approach to the nanoparticle conjugate. The summed contribution of each of these factors results in the hybridisation of the target strand to the immobilised oligonucleotide probes being both sterically and electrostatically hindered, thereby resulting in the hybridisation efficiency being lowered as the surface packing increases. [146] If the oligonucleotide conjugates with the DNA strands lying flat on the particle surface are considered, there is one primary issue that will affect the hybridisation efficiency. In this conformation, the availability of this probe for hybridisation to the target strand is greatly reduced by its close proximity to the nanoparticle surface. Consequently, the likelihood of the target hybridising with the probe sequence is significantly minimised.

Conversely, if the oligonucleotide conjugates developed within this chapter are considered, there is scope for significant improvement upon the steric issues detailed for the conjugates prepared with thiolated oligonucleotides. Firstly, the distance between the oligonucleotide coupled to the PEG molecule and the nanoparticle surface is taken into consideration. The PEG molecule is tethered to the metallic surface via a thioctic acid group at one terminus. At the opposite end of the linker molecule, the amino-modified DNA is coupled to the terminal carboxylic acid group. Therefore, rather than the oligonucleotide being held directly on the nanoparticle surface, it is held at a distance by the linker molecule. This increased distance between the nanoparticle surface and the DNA strand decreases the steric hindrance, making the oligonucleotide probes more available for hybridisation with the complementary sequence. Secondly, the packing of the oligonucleotides on the particle surface can be considered. It has been shown in work involving the coupling of amino-modified DNA to PEG linkers that the number of oligonucleotides immobilised *per* nanoparticle is relatively low. [82] Consequently, the oligonucleotide probes are likely to adopt a more sparse arrangement on the nanoparticle surface, improving the accessibility of the probes to the target strand, and increasing he likelihood of hybridisation. [146] Therefore, the low coupling efficiency of the amino modified

DNA to the PEG linker could be advantageous in terms of the hybridisation of the conjugates to target DNA.

Due to the advantages that the conjugates developed by pegylation followed by coupling of the oligonucleotide probes may offer over those developed by the immobilisation of thiolated oligonucleotides directly on the nanoparticle surface, these conjugates were developed for integration into the assay shown in Figure 3.2. A solution of gold nanoparticles were labelled with malachite green isothiocyanate. After encoding of the nanoparticles, they were stabilised by the introduction of a PEG bilayer. The nanoparticles were then centrifuged and resuspended in phosphate buffer (pH 7.6). Amino-modified DNA probes were conjugated to the carboxylic acid group on the terminus of the shorter chain linker molecules; the nanoparticles were then washed and resuspended in two different buffers. The buffers considered were phosphate buffer (pH 7.6) and 0.3 M PBS. An extinction spectrum was collected for each sample, as shown in Figure 3.21.

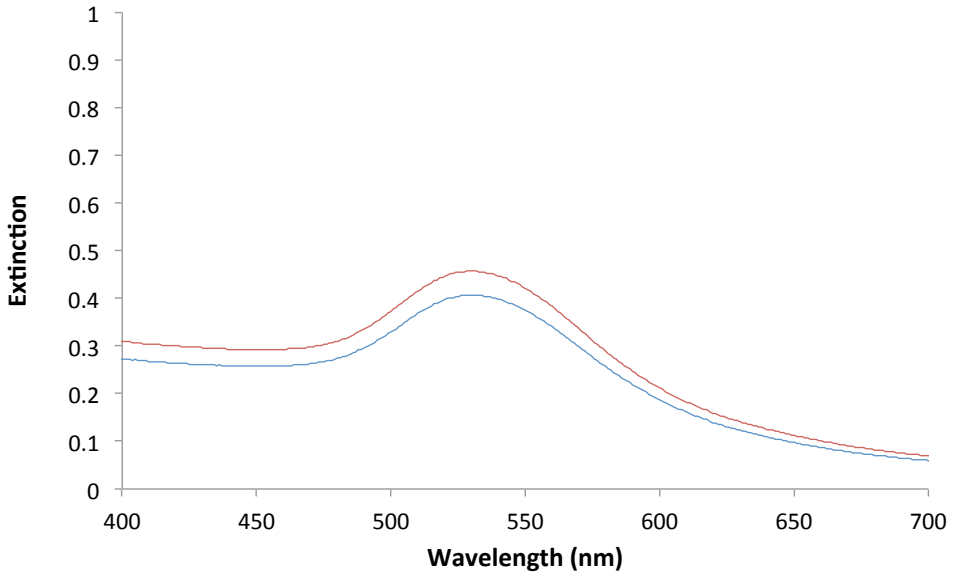

Figure 3.21 - Extinction spectra of malachite green labelled gold nanoparticles, functionalised with a short and long chain PEG bilayer. The short chain PEG is terminated with a carboxylic acid group that has an amino-modified DNA sequence coupled to it. The spectra were collected from the sample resuspended in phosphate buffer (pH 7.6) (red) and 0.3 M PBS (blue). Samples were analysed undiluted.

This experiment was performed in order to ascertain two key points. The first reason was to discover whether the functionalisation of the AuMGPEG nanoparticle conjugates with

the oligonucleotide probes induced aggregation of the nanoparticles in the sample. A distinct peak corresponding to the surface plasmon of the gold nanoparticles can still be clearly observed at approximately 533 nm. This peak appears slightly red shifted in comparison with the peak observed for the AuMGPEG conjugates that had an extinction maximum at 528 nm. This shift in the surface plasmon peak could be indicative of an increase in the size of the nanoparticle conjugates [147] and/or a change in the refractive index near the nanoparticle surface, [148, 149] suggesting the oligonucleotide probes have been successfully coupled to the PEG linker on the surface of the nanoparticle. There is also an absence of any peak at higher wavelengths that would indicate the formation of clusters of particles upon aggregation of the sample. Consequently, it could be concluded that there is no significant aggregation induced upon biofunctionalisation of the nanoparticle conjugates. This is confirmed by the SEM images collected of the conjugates, which showed no significant change in the aggregation state of the conjugates upon addition of the oligonucleotide probes (Figure 3.22).

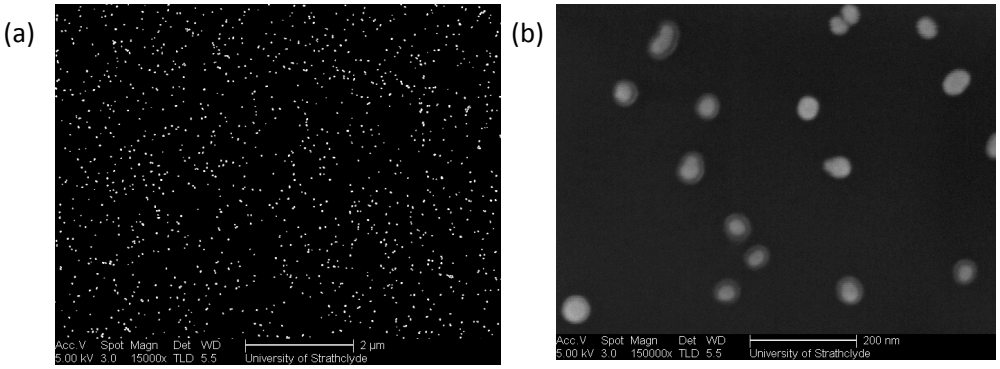

Figure 3.22 - Representative SEM images of gold colloid labelled with malachite green isothiocyanate, stabilised with a bilayer of PEG linker molecules. The short chain PEG linkers have amino-modified oligonucleotides coupled to the carboxylic acid moiety at their terminus. The images were obtained at (a) 15000 x magnification and (b) 150000 x magnification.

Upon higher magnification an opaque shell, possibly the polymer coating, can still be seen surrounding the nanoparticle conjugates (Figure 3.22(b)). It is clear from these images that the particles remain mostly discrete with a small number of dimers and small clusters present. This is similar to the aggregation state observed for the initial unfunctionalised colloid (Figure 3.5) implying that the biofunctionalisation with oligonucleotides did not induce significant aggregation of the particles.

Secondly, it was vital to ascertain whether the functionalised nanoparticles remained stable in 0.3 M PBS, the salt containing buffer in which the assay would be carried out (Figure 3.21). Whilst it had been shown previously that the AuMGPEG conjugates were stable in 0.3 M PBS (Figure 3.13), it had to be ensured that the DNA-functionalised malachite green labelled gold (AuMGPEGDNA) nanoparticle conjugates were also stable in this buffer. It can clearly be seen that upon resuspension in 0.3 M PBS, there is a slight decrease in the surface plasmon peak at 533 nm (Figure 3.21), however there is no appearance of a second peak at higher wavelengths. Therefore, it can be concluded that the conjugates remain in an unaggregated state, and that these can be considered stable in 0.3 M PBS, making them suitable for use in the assay conditions previously utilised.

Whilst the extinction spectra obtained confirm that the nanoparticles are stable in salt containing buffers, and that the coupling protocol for the addition of DNA to the PEG linker does not induce aggregation, it does not give any definitive information on whether the conjugates have been successfully functionalised with the oligonucleotides. However, the construction of the nanoparticle conjugates can also be monitored by measuring the particle size at each stage of functionalisation. If the oligonucleotides have been successfully tethered to the linker molecules, an increase in the size of the conjugates would be expected. DLS measurements do not give information on the precise physical size of the nanoparticles; instead they measure the hydrodynamic diameter of the particle. However, a change in the size of the conjugates will be obvious upon comparison of the measurements taken at each stage in the functionalisation process.

Table 3.1 shows the DLS size measurements obtained for unmodified gold nanoparticles, malachite green labelled nanoparticles (AuMG), malachite green labelled, pegylated nanoparticles and DNA functionalised nanoparticle conjugates. The unmodified gold nanoparticles were sized to be 65.1 nm, whilst the particles after dye labelling were sized at 64.9 nm. These results agree with the predicted outcome, with the introduction of the malachite green isothiocyanate not resulting in any great difference in size. This is due to the small size of the malachite green molecule which displaces the citrate formerly on the nanoparticle surface, and the 55 ° inclined orientation adsorption geometry which malachite green adopts. [150]

Sample	Particle Diameter (nm)	Standard Deviation
Au colloid	65.056	9.018
AuMG	64.585	6.750
AuMGPEG	79.615	8.487
AuMGPEGDNA	90.007	5.778

Table 3.1 - DLS size measurements of constructed nanoparticle conjugates.

The conjugates prepared by addition of the malachite green isothiocyanate followed by introduction of a PEG bilayer were measured to be 79.6 nm, indicating an increase in diameter of approximately 15 nm. This corresponds well with the measurements observed by Nie *et al.* who saw an increase in hydrodynamic diameter of approximately 20 nm upon addition of PEG to gold nanoparticles. [66] This also indicates that the polymer chain has folded down on the nanoparticle surface, as the increase in particle diameter is less than the approximate distance of two of the long PEG chains. Consequently, it can be assumed that the long chain PEG is draped on the particle surface rather than assuming a perpendicular arrangement to the nanoparticle face. This corresponds well with the theory that the addition of a long chain PEG linker would aid stabilisation of the conjugates by protection of the nanoparticle surface previously unmodified by the short chain linker. This increasing particle size is also reflected by comparison of the SEM images obtained of the gold nanoparticles (Figure 3.5) and the AuMGPEG nanoparticles (Figure 3.14). It can be seen upon addition of the PEG bilayer, that a shell measuring approximately 10 nm in thickness was introduced to the surface of the nanoparticle.

Upon coupling the amino-modified DNA to the carboxylic acid group of the short PEG linker, an increase in hydrodynamic diameter of approximately 11 nm was observed, with the DNA modified conjugates being sized at 90.0 nm. The oligonucleotides conjugated to the linker molecules are nine bases in length and contain a C6-NH_2 modification. It is known that each base in a DNA strand measures 0.34 nm, [15] implying the length of the oligonucleotide chain introduced to be approximately 3.06 nm. Considering the length of the spacer introduced in the amino-modification, the overall length of the oligonucleotide probes can be approximated at 4.36 nm. Theoretically, if the probes were successfully tethered to the linker molecules, a maximum increase in diameter of approximately 8.7 nm would be expected, twice the length of the probe sequence. This hypothesis is in good

agreement with the data collected for the DLS particle sizing of the fully functionalised conjugates which saw a particle diameter increase of approximately 11 nm, implying that the conjugates have been successfully labelled with the oligonucleotide probes.

3.4.2 QUANTIFICATION OF IMMOBILISED OLIGONUCLEOTIDE PROBES

In order to ascertain whether the assumptions made regarding the sparse arrangement of the oligonucleotide probes on the surface were correct, it was vital to quantify the number of oligonucleotide probes present on the nanoparticle surface. This will allow for a more though understanding of the issues affecting the hybridisation of the target strand to the conjugates.

Demers *et al.* detailed a method by which the number of single stranded DNA molecules bound to a gold nanoparticle could be quantified. [146] However this method was dependent upon the competition between the DNA and the displacing ligand and it was suggested that in the case whether both ligands exhibit similar affinities for the nanoparticle surface, the quantification of the immobilised oligonucleotides might be inaccurate. Recently, Graham *et al.* published details of a method for quantification of fluorescently labelled biomolecules attached to metallic nanoparticles that eradicates the problems associated with the surface competition between ligands. [151] The protocol was developed based upon hydrolysis of the phosphodiester linkages in the DNA backbone by the endonuclease, DNase I, releasing a fluorescent label from the terminus of the oligonucleotide probe (Figure 3.23). This method of quantification was selected for the quantification of the oligonucleotide probes on the nanoparticle conjugates developed here.

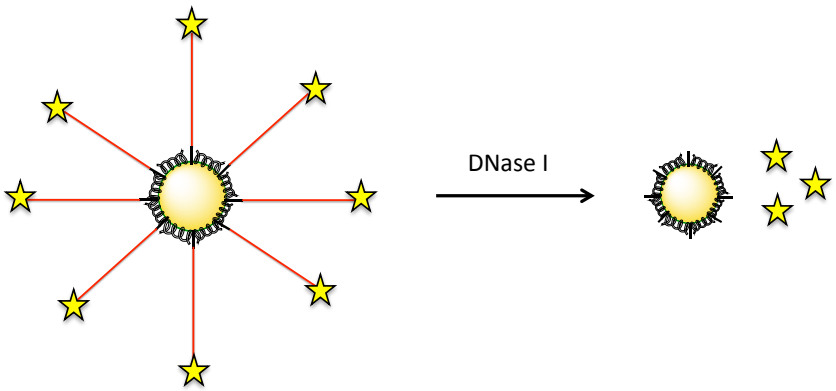

Figure 3.23 - Schematic representing the DNase I activity on the oligonucleotide-functionalised nanoparticle conjugates. The DNase I will hydrolyse the DNA, releasing the fluorescent FAM labels.

A sample of dye labelled, pegylated nanoparticle conjugates were functionalised by coupling FAM labelled oligonucleotides to the PEG linker molecules *via* a sulfo-NHS/EDC coupling protocol. The nanoparticle conjugates were washed by centrifugation three times with phosphate buffer (pH 7.6) to remove any unbound DNA that would emit a fluorescent signal, therefore the only fluorescently labelled DNA now present in the sample should be bound to the nanoparticles. It has been shown that metal nanoparticles are able to quench [116-119] or enhance [131, 132] fluorescence; therefore it was necessary to remove the fluorescently labelled oligonucleotide probes from the vicinity of the metallic surface prior to analysis. A control sample was also prepared where no fluorescently labelled oligonucleotides were immobilised on the nanoparticle surface. This was vital to ensure that the dye labelled, pegylated conjugates did not give rise to any background fluorescent signal upon undergoing treatment with the DNase I. The samples were resuspended in DNase I reaction buffer and an aliquot of DNase I was added to each sample. The samples were incubated at 37 °C for 16 hours before centrifugation. The supernatant was then removed and analysed by fluorescence spectroscopy using an excitation wavelength of 495 nm. The supernatant should contain the FAM labels previously attached to the oligonucleotide terminus farthest from the particle surface.

Whilst it is unknown which phosphodiester bonds are hydrolysed in the presence of the DNase I, due to the terminal positioning of the FAM label, the breaking of any of the bonds along the DNA backbone will result in the fluorescent label being removed from the metallic surface. The concentration of the FAM label present in the supernatant was determined by correlation with a standard calibration graph prepared from various

dilutions of the FAM-labelled oligonucleotide probe (Figure 3.24). The number of fluorescently labelled oligonucleotides *per* nanoparticle was then calculated based upon the FAM fluorescence signal from the supernatant evaluated against the original nanoparticle conjugate concentration.

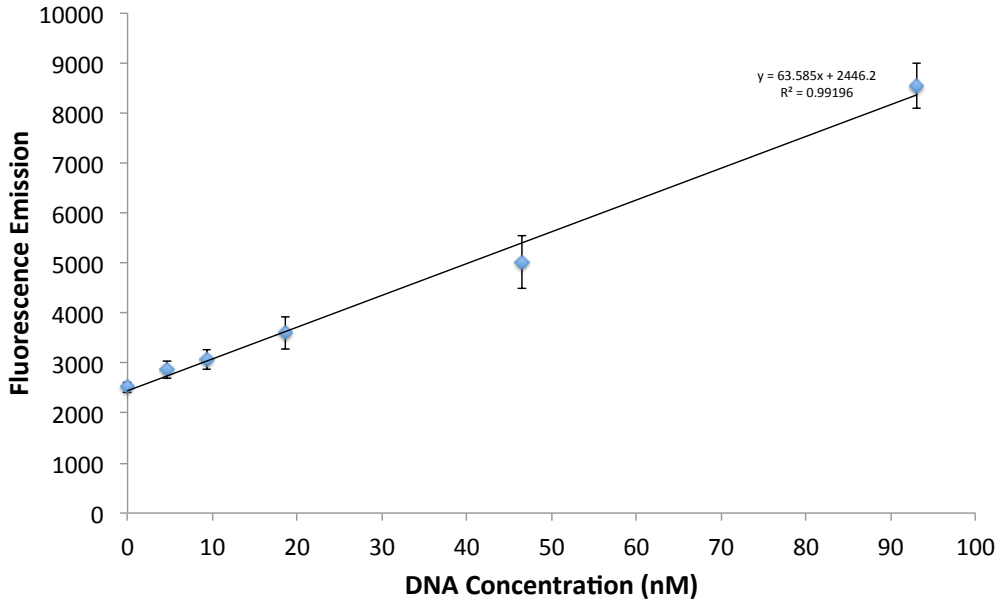

Figure 3.24 - Calibration graph of the FAM labelled DNA sequence subsequently coupled onto the nanoparticle conjugates. The error bars represent one standard deviation between 5 replicate samples.

Using this method, the number of fluorescently labelled probe sequences *per* dye-labelled, pegylated nanoparticle conjugate was estimated to be 230.0 ± 36.9. Although there is a large difference in the number of carboxylic acid functionalised PEG molecules added to stabilise the nanoparticles, estimated at approximately 30000 PEG molecules *per* nanoparticle, and the number of fluorescently labelled oligonucleotides calculated to be bound to the particle, there are a number of considerations to be made. Firstly, whilst Nie *et al.* state that at least 30000 PEG molecules are required in order to stabilise the nanoparticle conjugates, it may be the case that not all of these molecules are immobilised on the particle surface. Furthermore if all of these linker molecules are indeed immobilised on the nanoparticle in order to stabilise it, there is no information given on the availability of these molecules on the nanoparticle. It is possible that whilst all of the molecules are present on the metallic surface, not all of them are accessible to the oligonucleotide probes added. Indeed, the longer linker molecules are added in order to stabilise any previously

unpegylated particle surface providing additional stabilisation. These long PEG chains fold on top of the nanoparticle surface, potentially creating a barrier between the particle surface and its environment. [66] As a result of this folding, it is possible that a number of the terminal carboxylic acid groups on the shorter PEG molecules are rendered inaccessible. This would result in a lower number of available conjugation sites for the oligonucleotide probes to the nanoparticle conjugates. Secondly, Graham *et al.* previously showed that the coupling of amino modified oligonucleotides onto carboxylic acid functionalised PEG molecules, whilst possible, does not occur with a high efficiency. [82] Whilst the linker molecules used in the work reported here are different from those shown in the literature, they contain the same functionalities at either terminus of the molecule. The literature showed that the coupling efficiency of the oligonucleotide probes to the linker molecules was low, with the number of immobilised oligonucleotides being low in comparison with the number of immobilised linker molecules. Since similar coupling methods are used in the literature as is used in this work, a similar coupling efficiency can be expected. [82]

3.5 ASSAY CONSTRUCTION

The required assay involved a number of steps to be completed before SERRS analysis could be performed (Figure 3.2). Firstly, the biotin labelled probe and the DNA-nanoparticle conjugates are hybridised to the target DNA (step 1), followed by the introduction of the magnetic beads (step 2). Following incubation, the magnetic beads are washed with 0.3 M PBS by magnetic separation of the beads on the side of the tube (step 3). The supernatant containing any excess probes and nanoparticle conjugates is removed, and the beads are resuspended in 0.3 M PBS. This washing procedure is repeated in order to ensure all unbound DNA and SERRS active nanoparticles have been removed from the samples. The magnetic beads are then resuspended and analysed in solution by SERRS with an excitation wavelength of 633 nm. Once the assay has been fully optimised, the final concept is for it to be performed in a closed tube, with the SERRS analysis performed directly on the immobilised pellet and the excess assay components remaining unanalysed in solution.

It was shown in Section 3.3.1, that the use of streptavidin coated TurboBeads® in place of conventional streptavidin coated magnetic beads results in a decrease in the reduction of the SERRS signal observed due to the presence of these particles. Whilst this is an

advantage in terms of sensitivity, it is also important that the results obtained using these particles are comparable in terms of reproducibility with the conventional magnetic beads. Whilst carrying out the work described in Section 3.3.2, the latter batches of TurboBeads® supplied did not give results consistent with what had been seen previously. Upon investigation, it was found that the TurboBeads® appeared to be aggregating uncontrollably before addition to the sample, resulting in them precipitating out of solution. It was thought that sonication might help to break up the aggregates and improve the particles' monodispersity in solution. However, after sonication the particles still settled out of solution onto the bottom of the sample vial over time.

During analysis the laser beam was focussed on the surface of the liquid in a microtitre plate, therefore only particles remaining in solution would be within the interrogation volume of the laser beam. Consequently, this settling of the particles was clearly problematic when analysing of the samples. Particles settled at the bottom of the well would be excluded from the sampling volume, and therefore would not contribute to the observed signal. This resulted in the SERRS signals observed varying greatly as the number of particles remaining in solution upon analysis varies from sample to sample, resulting in irreproducibility between samples. Furthermore, as a result of this settling of the particles from the solution, it is possible that positive samples could give a false negative. As a direct consequence of this variation previously observed whilst using the TurboBeads® it was decided that, whilst the TurboBeads® may offer an advantage in terms of sensitivity, conventional streptavidin coated magnetic beads would be used in the future development of the assay.

3.5.1 TARGET VS NO TARGET

In order to assess the specificity of the assay, the assay was carried out in the presence and absence of target DNA, with milliQ water replacing the target strand in the control assay. This comparison was made in order to confirm that the binding of the SERRS active nanoparticles to the magnetic beads in the absence of the target sequence is minimal.

The assay was constructed as detailed in Section 3.7.5.2. The sample was agitated for one hour after the addition of the streptavidin coated magnetic beads to allow for the

immobilisation of the nanoparticle-labelled duplex onto the beads. The magnetic beads were then washed with 0.3 M PBS on a magnetic separation rack by the separation of the magnetic beads and removal of the supernatant, followed by resuspension of the beads in 0.3 M PBS. The samples were analysed in a 384 well microtitre plate and the SERRS spectra were recorded for each sample using 633 nm laser excitation (Figure 3.25).

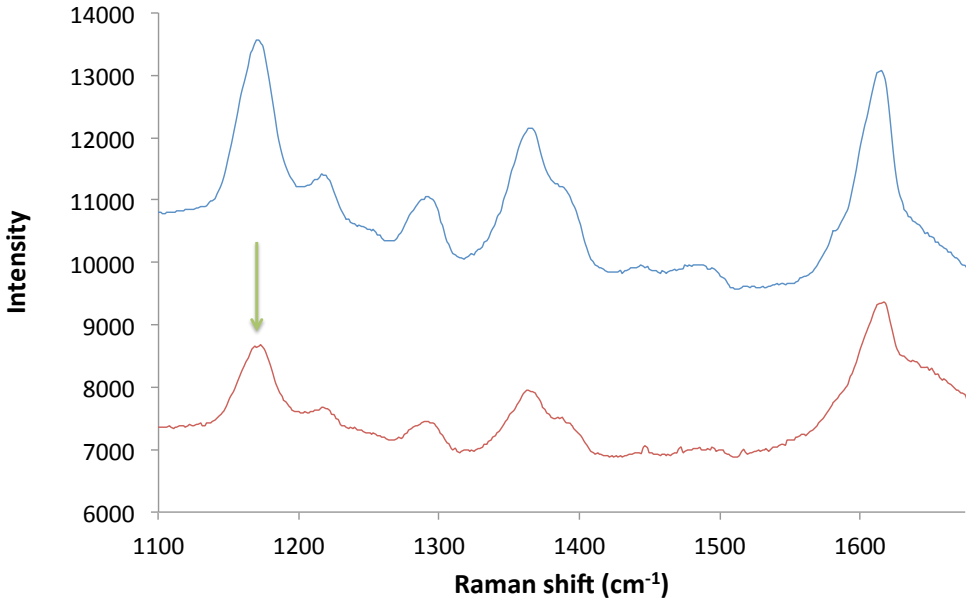

Figure 3.25 - SERRS spectrum obtained of the assay in the presence of target DNA (blue), and the assay in the absence of target DNA (red). The assay was constructed, washed three times with 0.3 M PBS and analysed in solution using 633 nm laser excitation, 1 x 30 s accumulation. The green arrow indicates the peak at ~1169 cm^{-1} selected to monitor the peak height from each sample.

When comparing the SERRS spectra collected in the presence of target DNA with that observed in the absence of the target sequence it was observed that the peaks in the presence of target DNA are higher. Although it can be seen that there is a difference in the intensities of the SERRS signals collected, it is also apparent that there is a significant background signal observed from the assay in the absence of the target sequence. Consequently, it was thought that monitoring the height of one of the principal peaks from the malachite green spectrum would aid in viewing the discrimination between the signals. The peak at ~1169 cm^{-1} indicated in Figure 3.25 was selected for this purpose.

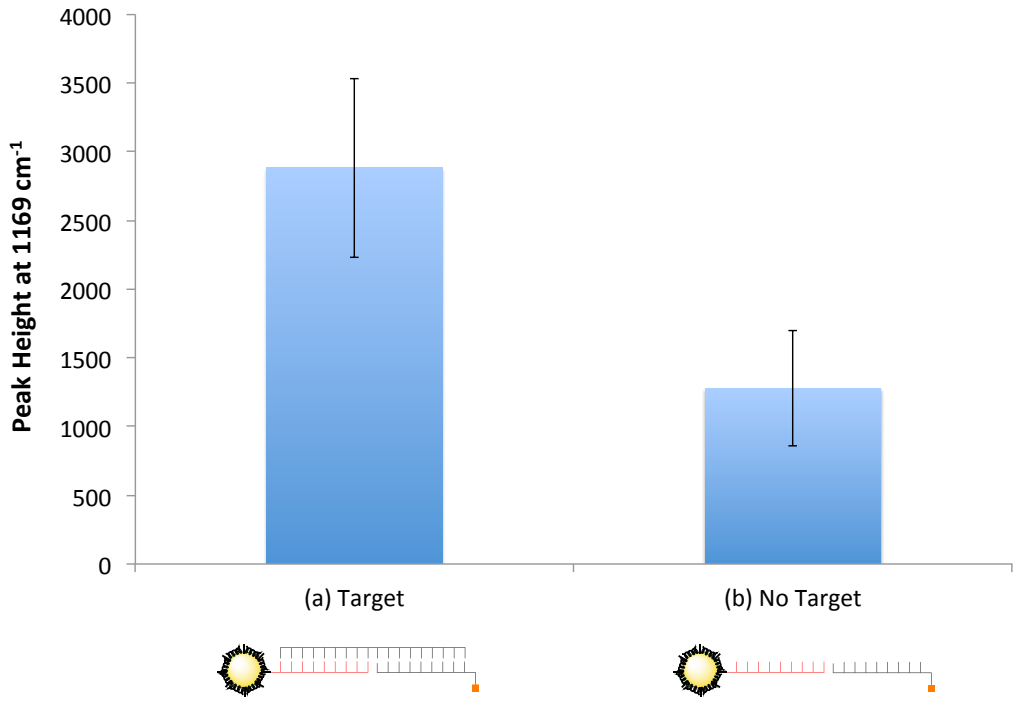

Figure 3.26 - Peak height at 1169 cm^{-1} from assay (a) in the presence of target DNA, (b) in the absence of target DNA. The assay was constructed, washed three times with 0.3 M PBS and analysed in solution using 633 nm laser excitation, 1 x 30 s accumulation. The error bars represent one standard deviation from 5 replicate samples.

The peak height of the SERRS signal obtained in the presence of the target DNA can be seen to be significantly higher than that of the signal observed from the assay in the absence of the target sequence, where the probes alone were present (Figure 3.26). This outcome is in good agreement with results observed from the UV melting experiments of samples containing the target DNA sequence compared with those containing the probes alone, where a distinctive melting curve was only observed from the sample containing the target sequence (Figure 2.4 & Figure 2.21).

It is important to note that the assay in the absence of target DNA does however yield a significant SERRS signal. It would be ideal to minimise the signal collected from the control sample, since although there is clear discrimination between the positive and control samples shown in Figure 3.26, it is likely that this discrimination will be highly dependent on the concentration of target DNA being detected. It is expected that as the concentration of target DNA is decreased, the number of bound SERRS active nanoparticles, and consequently the intensity of the SERRS signal will also decrease. Therefore at low target

DNA concentrations, it is likely that the discrimination between the positive and negative control samples will be minimised, or lost altogether. There are a number of potential reasons for the SERRS background observed from the control sample. It is likely that the SERRS active nanoparticles, which give rise to the signal from the assay, are becoming non-specifically bound to the magnetic beads. If this were the case there are a number of solutions to this problem. These could include changing the washing protocol used after assay construction to minimise this non-specific binding, or pre-coating the magnetic beads with the biotin capture probe before their introduction to the samples to reduce the availability of the surface of the beads to the AuMGPEGDNA conjugates. A second potential reason for the SERRS background observed is non-specific binding of the malachite green label used to functionalise the AuMGPEGDNA nanoparticle conjugates onto the magnetic beads. This however is considered unlikely, as the robust nature of this labelling procedure has been demonstrated by Nie *et al.* under a variety of conditions. [66]

3.5.2 TARGET VS NONSENSE

Whilst the assay exhibits discrimination between a sample containing target DNA and one containing no target, only the probes alone, this is not a realistic scenario for diagnostic testing. In order for an assay to be successfully incorporated into a diagnostic assay it must be able to successfully detect the targeted DNA sequence in a clinical sample, e.g. urine, blood etc. These samples contain a complex biological matrix containing a variety of biomolecules including proteins and DNA with an assortment of sequences. Consequently, it is vital for the assay to be able to distinguish successfully between a DNA sequence relating to the targeted disease state and a sequence not related to the disease in question.

The specificity of the assay was therefore investigated by the incorporation of a nonsense sequence in place of the target strand into the assay system. The assay was constructed as detailed in Section 3.7.5.2. Two differing versions of the assay were therefore constructed; one containing the probes and target DNA and a control containing the probes and nonsense DNA. The results obtained upon analysis of the samples are presented in Figure 3.27.

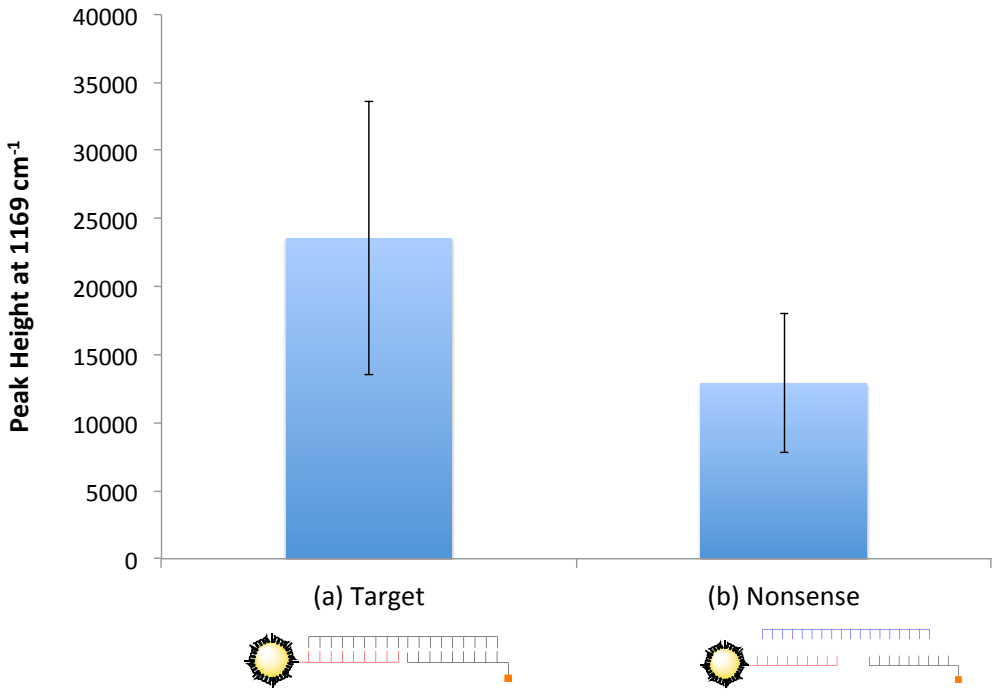

Figure 3.27 - Peak height at 1169 cm^{-1} from assay (a) in the presence of target DNA, (b) in the presence of nonsense DNA. The assay was constructed, washed three times with 0.3 M PBS and analysed in solution using 633 nm laser excitation, 1 x 30 s accumulation. The error bars represent one standard deviation from 5 replicate samples.

The intensity of the SERRS signal observed in the presence of the target DNA sequence was distinguishably higher than that observed in the presence of the nonsense sequence. The discrimination between average peak height of the signal from the assay in the presence of the target DNA and the presence of nonsense DNA is clear. In fact the discrimination between the target and nonsense sequences is almost equal to that observed between the target sequence and the probes alone. This is in agreement with the UV-vis melting data previously collected, indicating that at room temperature the probes do not form a duplex with the nonsense DNA. Consequently, the signal observed from these samples is lower than that seen upon the successful formation of a duplex between the probes and the target sequence. These results lead to the conclusion that the assay is able to specifically detect DNA with a sequence corresponding to the disease targeted. This is vital for the development of the assay into a successful technique for disease detection in clinical samples. The ability of the system to specifically recognise the sequence being targeted is vital in order to avoid false positive results and improve the reliability of the assay.

However, whilst there is a distinction between the signal observed in the presence of the target sequence and the signal observed in the presence of a nonsense sequence, it is also important to note that a significant signal can be observed from the nonsense control. This background signal is likely to prove detrimental to the sensitivity of the assay, since at low target DNA concentrations it is likely that the discrimination between positive and negative samples will be lost. Consequently it is vital to locate the source of this background signal, and minimise the observed signal.

3.5.3 Source of Non Specific Binding

It was shown previously that the assay, in the presence of target DNA, exhibits a clear SERRS signal corresponding to the malachite green dye used to label the nanoparticle conjugates. This is to be expected as the hybridisation of the oligonucleotide functionalised dye encoded nanoparticles to the target strand is followed by the immobilisation of the duplex formed *via* the biotin capture probe also hybridised to the target sequence. However, when considering the results shown in Section 3.5.1 and Section 3.5.2, it was seen that the assay in the absence of target DNA does in fact exhibit a visible SERRS signal. Decreasing the signal observed from the no target control will lead to an increase in the discrimination of the assay.

In order to make this improvement, it is necessary to identify the reason for this background signal. It has been shown in Figure 2.21 that the probes designed for use in the assay do not offer any great degree of complementarity to each other, therefore it is unlikely that the signal observed is due to the probes forming a duplex labelled with the dye labelled nanoparticles and becoming immobilised on the magnetic bead. A potential reason for the background signals observed is the non-specific binding of malachite green dye onto the surface of the magnetic beads, producing a SERRS signal. This is thought to be less likely however since Nie *et al.* demonstrated the robust nature of the Raman reporter molecule binding to the surface of the gold nanoparticle in a variety of harsh environments. Furthermore, whilst the composition of the magnetic beads is unknown, it is unlikely that they are composed of a metal that would give rise to SERRS. Therefore, it was postulated that the signal observed was likely to be a result of non-specific binding of the SERRS-active nanoparticle conjugates to the magnetic particles.

In order to test this hypothesis and identify the reason behind the signals observed, two different samples were prepared. A sample of the magnetic beads was incubated with an aliquot of either the dye-labelled, pegylated conjugates or the fully functionalised oligonucleotide-labelled conjugates. These experiments were designed in order to identify the component of the nanoparticle conjugates responsible for the non-specific binding. Malachite green is a charged dye, and it was hypothesised that the binding observed may be an electrostatic interaction due to this charge. DNA is a complex molecule capable of many different interactions and binding processes. Therefore it was considered that the oligonucleotide probes immobilised on the nanoparticle conjugates might be the reason for the non-specific binding observed. Furthermore, if the signal is a result of the malachite green label becoming non-specifically bound to the magnetic beads, a signal will be observed from both samples. After incubation, the samples were subjected to the same washing protocol used for the assay, and the beads resuspended in buffer. SERRS analysis was then performed using 633 nm laser excitation on the sample solutions.

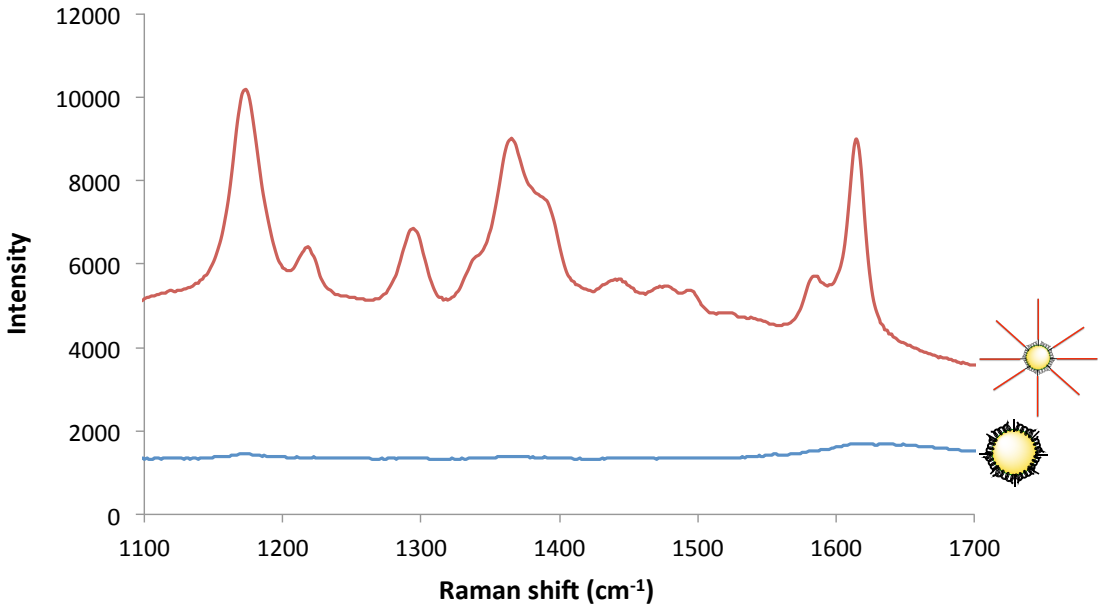

Figure 3.28 - SERRS spectrum obtained of the streptavidin coated magnetic beads after incubation with pegylated nanoparticle conjugates (blue) or DNA functionalised pegylated nanoparticle conjugates (red). The beads were washed three times with phosphate buffer prior to SERRS analysis using 633 nm laser excitation, 1 x 30 s accumulation.

Figure 3.28 shows the resultant SERRS spectra observed upon analysis of the samples prepared. It would appear that the sample incubated with the dye-labelled, pegylated

nanoparticles gave rise to very little signal after the washing protocol had been complete. This suggests that these conjugates do not non-specifically bind to the streptavidin coated magnetic beads, and that the washing protocol successfully removes the unbound conjugates from the sample solution. Consequently, it can be deduced that the non-specific binding seen is not due to the malachite green label on the nanoparticle surface. Conversely, the sample incubated with the fully functionalised oligonucleotide-labelled conjugates displayed a distinct SERRS signal upon analysis. Since the conjugates pegylated and labelled with the dye did not give rise to any significant signal, it can be deducted that the conjugation of the oligonucleotide probes to the nanoparticle conjugates must have given rise to the source of the non-specific binding previously observed in the negative control samples. Further investigation was then conducted to both deduce the nature of this binding, and minimise it.

3.5.3.1 Investigation of Wash Buffer

One area that was investigated with a view to reduce the non-specific binding was the buffer used in the washing protocol of the assay. 0.3 M PBS had previously been used as the buffer during the washing protocol with great success (Chapter 2), however it was thought that the inclusion of some additional components to the buffer might improve the issue of non-specific binding. Urea is often included in concentrations of up to 8 M in buffers due to its capability to act as a denaturant. [152-155] Urea belongs to a class of compounds known as chaotropic denaturants that unravel the tertiary structure of proteins by destabilising internal, non covalent bonds between atoms. Tween is also commonly incorporated into biological buffer systems as a washing agent to prevent non-specific binding. It is commonly dissolved in tris-buffered saline or phosphate buffered saline with a final dilution of between 0.05 and 0.5%. Whilst a pH corresponding to a physiological pH of approximately 7 is commonly adopted for the buffers within a biological assay, it was thought that adjusting this pH could aid in the prevention of non-specific binding. At pH 9 the DNA strands begin to ionize, causing double stranded DNA to denature in alkaline conditions. However, care must be taken to ensure that whilst minimising the non-specific binding, it was vital to maintain the double stranded nature of the probe-target duplex formed while executing the assay.

A series of experiments were designed in order to assess the effect that washing using a variety of different buffers has on the non-specific binding within the system. Nanoparticle conjugates were prepared and functionalised with oligonucleotides, then resuspended in 0.3 M PBS as normal. The streptavidin coated magnetic beads were washed and resuspended in the buffer being investigated. MilliQ water was also added to the assay sample in place of the biotin probe and target DNA usually added in order to maintain the final volume of the full assay. The samples were then incubated for one hour, followed by completion of the washing protocol with the buffer being investigated. SERRS analysis of the various samples was then performed using 633 nm laser excitation. The results obtained can be observed in Figure 3.29.

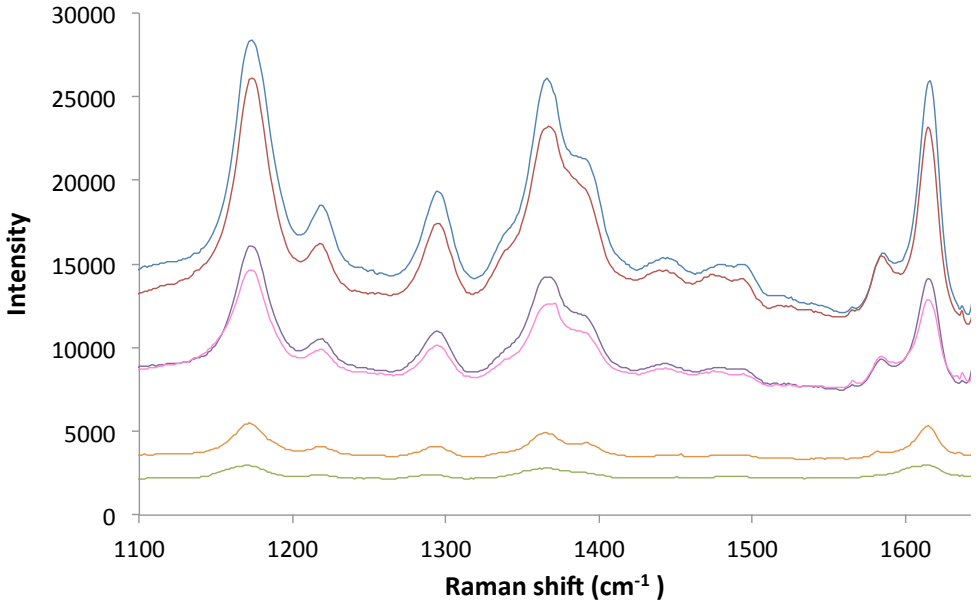

Figure 3.29 - SERRS spectrum obtained of the streptavidin coated magnetic beads after incubation with DNA functionalised pegylated nanoparticle conjugates. The beads were washed three times with 0.3 M PBS (pH 7) (blue); 0.3 M PBS (pH 7) and 2 M Urea (red); 0.3 M PBS (pH 7) and 0.1% Tween 20 (green); 0.3 M PBS (pH 9) (purple); 0.3 M PBS (pH 9) and 2 M Urea (pink); 0.3 M PBS (pH 9) and 0.1% Tween 20 (orange). The samples were then analysed by SERRS using 633 nm laser excitation, 1 x 30 s accumulation.

The non-specific binding previously observed from the assay can be clearly observed by the sample after washing in 0.3 M PBS (pH 7), which is to be expected as this is the buffer previously used in the washing protocol. It can also be observed that the addition of urea with a final concentration of 2 M to this buffer has little effect on the signals observed from the magnetic beads. However, upon altering the pH from 7 to 9, a decrease in the SERRS

signal from the magnetic beads was observed. Biomolecules are naturally found within a living being, e.g. an animal or a human, and as such they are at their most stable in a pH range that mimics the conditions in which they would be found naturally. Most physiological conditions have a pH of approximately 7; therefore it can be considered that biomolecules would be stable at this pH. Upon altering the pH of the environment to which the biomolecule is exposed, the molecule is likely to become less stable and begin to denature. Although the interaction responsible for the non-specific binding of the oligonucleotide-conjugates to the streptavidin-coated magnetic beads is unknown, it has been shown that this interaction only occurs when the conjugates have been functionalised with oligonucleotides. Consequently it can be suggested that at least one biomolecule takes part in the interaction in question. It is known that at pH 9 DNA begins to ionise causing the duplex to become unstable therefore it is possible that the alteration of the buffer pH is disrupting DNA-DNA interactions. Furthermore, if a second biomolecule which is not DNA is interacting with the oligonucleotide probes on the nanoparticle conjugates, it is likely that this molecule will be at least partly denatured at this heightened pH. It is thought that this hypothesis is unlikely however since urea is very effective at denaturing proteins and antibodies and no effect was observed upon the addition of urea to the wash buffer. However, if we consider that the pI of streptavidin is ~5-6, increasing the pH of the buffer solution would lead to an increase in the negative charge on the streptavidin. Consequently, it is possible that this would lead to an increase in the repulsion between the negatively charged protein and the phosphate backbone of the DNA. Conversely, if the oligonucleotide probes are not interacting with a second biomolecule and are instead interacting electrostatically with a component on the surface of the magnetic beads, the induction of the ionisation of the DNA by alteration of the pH may disrupt this interaction.

Addition of Tween 20 to the wash buffer appears to have had a drastic effect on the non-specific binding observed. Although Tween 20 and other surfactants are often used in order to prevent non-specific binding events, there is a further consideration to be made with regards to the results observed. Whilst Tween 20 is a surfactant that is often used to reduce non-specific binding in biotechnical applications, it is also used as a foaming agent. Due to the ability of this surfactant to aid in the formation of foam, it is possible that the results observed are a factor of this. The analysis of the samples prepared during the assay was performed in a microtitre plate, where the laser is focussed on the surface of the sample to

avoid signals from the plastic plate. Upon addition of the sample to the plate, it is important that the sample is analysed in a timely manner to ensure that the magnetic beads are still suspended in solution, as they will begin to settle to the bottom over time. However, this is problematic in the analysis of samples washed using the buffers containing Tween as they were found to foam upon addition to the wells, resulting in the surface that would normally be focussed on by the laser being covered in bubbles. This causes issues when focussing the laser for sample analysis, as it is important that the laser is focussed to the same degree for each sample in order to minimise sample-to-sample variation. Therefore, the best way to minimise this variation is to allow the bubbles to dissipate before analysis is performed. However, this also contributes a source of error to the results obtained since the time taken for the bubbles to disperse varies from sample to sample, therefore the number of magnetic beads remaining in solution will also vary. Therefore, when analysing the samples prepared the laser was focussed just below the surface of the sample in an attempt to circumvent both the foaming and the settling issues. The results obtained were very promising as seen in Figure 3.29, where minimal background SERRS signal was observed. However, it is also possible that this result is in fact due to the laser not being focussed adequately due to the foaming from the samples.

Consequently, it would appear from the results observed that the optimal buffer to be used in the washing step of the assay was 0.3 M PBS (pH 7) containing Tween 20 (0.1%). The signal observed from the magnetic beads washed in this assay were minimal when compared with that observed from magnetic beads washed in 0.3 M PBS (pH 7). However further investigation into the effect that the foaming from the Tween 20 has on the focussing of the laser onto the sample would have to be performed in order to verify these results.

3.5.3.2 Immobilisation of Biotin Capture Probe on Magnetic Beads

It is clear that the oligonucleotide-functionalised nanoparticle conjugates become non-specifically bound to the surface of the streptavidin coated magnetic beads resulting in a SERRS signal being observed from the magnetic beads in the absence of target DNA. It was postulated that if the streptavidin coated magnetic beads were introduced to the biotinylated capture probe before their addition to the samples, this might reduce this non-specific binding event. The magnetic beads were incubated in an excess of biotinylated

capture probes, resulting in the formation of magnetic beads which have been pre-coated with the capture probe. It was shown in Figure 3.28 that the nanoparticle conjugates only bind to the magnetic beads once functionalised with the oligonucleotide probes, indicating that this binding is a consequence of an interaction between the probes and a second component on the surface of the magnetic beads. The pre-coating of the magnetic beads with the capture probes might reduce the oligonucleotide probes availability to the surface of the magnetic beads *via* repulsion of the negatively charged sugar-phosphate backbone of the probes on the nanoparticle with that of the capture probes. Furthermore, the immobilisation of the biotinylated probes on the bead surface may sterically inhibit the approach of the nanoparticle conjugates, thereby reducing their accessibility to the surface of the beads.

To test this hypothesis, an experiment was designed in order to compare the non-specific binding observed from a sample where the oligonucleotide-labelled nanoparticle conjugates were incubated with streptavidin coated magnetic beads, compared with when the conjugates were incubated with the streptavidin coated magnetic beads which have been pre-coated with the biotin capture probe. After incubation the samples were washed and analysed by SERRS using 633 nm laser excitation (Figure 3.30).

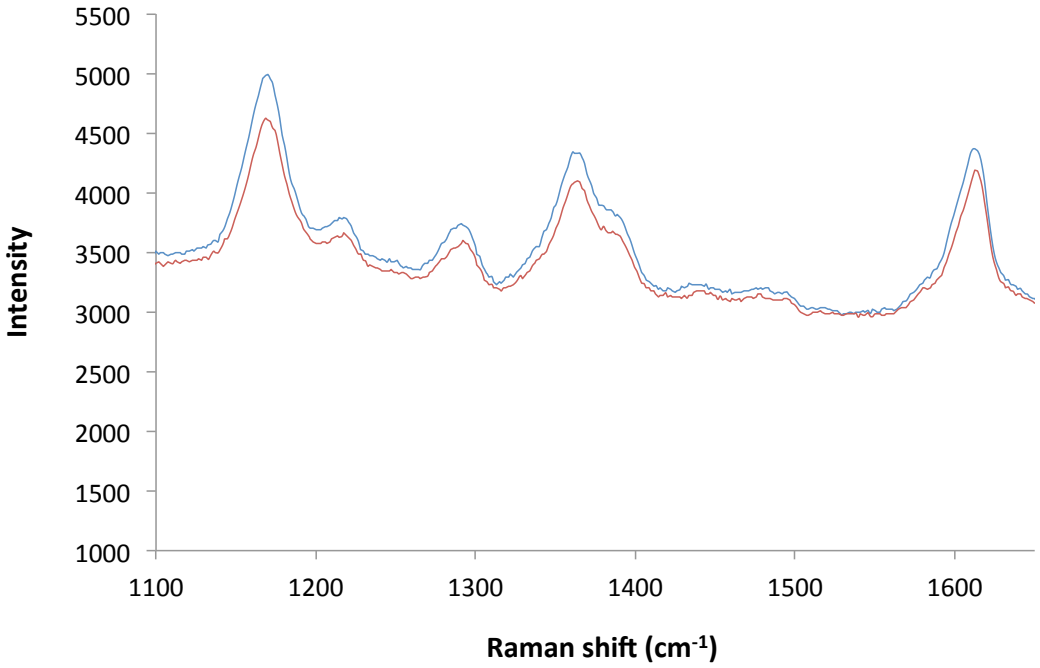

Figure 3.30 - SERRS spectrum after the oligonucleotide-functionalised nanoparticle conjugates were incubated with (a) streptavidin coated magnetic beads, (b) streptavidin coated magnetic beads pre-coated with biotin capture probes. The samples were washed three times with 0.3 M PBS and analysed in solution using 633 nm laser excitation, 1 x 30 s accumulation.

This comparison shows that there is little difference in the signal intensity observed from the sample prepared with magnetic beads pre-coated with the biotin capture probe in comparison to the streptavidin coated beads used previously. These results suggest that the non-specific binding is unaltered by modification of the magnetic beads and that in turn, the modification offers no distinct advantage in the prevention of non-specific binding.

3.5.4 Investigation of Sampling Methods

One distinct characteristic observed from the results obtained over the course of the assay development is the relatively large variation between replicate samples. This variation leads to large errors, as can be seen by the error bars in the bar charts illustrating the signal intensity of the SERRS spectra collected (Figure 3.26 & Figure 3.27). It was therefore decided that a potential source of error that could be improved upon in order to reduce this variation was the sampling method used when analysing the samples. In order to investigate this, a variety of sampling methods were trialled.

3.5.4.1 Microtitre Plate

During the development of the assay, the samples were analysed in a 384 well microtitre plate. The laser was focussed on the surface of the sample solution allowing for analysis of the solution within the laser interrogation volume. The focussing of the laser beam on the surface of the sample possesses both advantages and disadvantages with regards to signal collection. Firstly, if the laser is focussed on the surface of the sample the likelihood of collecting a signal from the plastic well plate is reduced. Secondly, when analysing the samples in a microtitre plate a 180 ° backscattering system is utilised, with the scattered light being collected by the objective. When the laser is focussed on the surface of the sample, the scattered light only has to travel through air, not through the sample solution, in order to reach the objective. Consequently the scattered light is less likely to be absorbed by the surroundings, resulting in a truer measurement of the actual intensity of the Raman scattering from the sample being made. Finally, in order to minimise sample-to-sample variation, it was important that the microscope was focussed on the same position within the samples each time. The simplest way to do this was by focussing the laser on the surface of the solution. However, this method does also yield disadvantages, giving rise to a number of challenges.

The main disadvantage is observed when the samples are being analysed over an extended period of time. Due to the laser beam being focussed on the sample, the buffer solution will become heated and evaporation begins to take place. This evaporation process results in a reduction in the depth of the sample. Therefore before each scan is recorded it is vital to ensure that the laser remains focussed on the surface of the solution. This can be a time-consuming process and can add a significant period of time onto the analysis of the assay. Furthermore, the signals observed are sensitive to changes on the surface of the sample being analysed, e.g. the foaming effect previously observed from the addition of Tween 20 or the settlement of dust or other small particulates onto the surface of the solution.

Regardless of the positioning of the laser focus, the use of microtitre plates also yields a further problem for the analysis of the developed assay. The SERRS-active particles are immobilised on streptavidin coated magnetic beads, which are suspended in a buffer solution. Analysis of the sample is then performed on this suspension by SERRS. In order for accurate results to be obtained it is vital for the magnetic beads to remain in solution

during analysis. However the magnetic beads have a tendency to precipitate out of solution over time, settling on the bottom of the sample tube. This settling of the magnetic beads can make analysis in a microtitre plate challenging. Firstly, it can be visually difficult to monitor the dispersity of the beads in the sample solution once it has been added to the well. Furthermore, after the laser has been focussed on the sample within the well it is difficult to agitate the solution to redisperse the beads without affecting the focus of the laser on the sample. Consequently, the laser would have to be refocused each time the sample required agitation. This leads to a greatly increased analysis time, making the overall time required for the assay much longer.

3.5.4.2 Cuvette

The analysis of the samples using a macrosampler assembly to focus into a cuvette may prove beneficial over the microtitre plate for the reduction of signal variation. The macrosampler assembly is used to convert the microscope system into a macroscopic system through the use of mirror/lens assembly. The assembly fits into one of the apertures in the microscope objective turret. It is fitted with a reflector, which turns the optics axis from vertical to horizontal, allowing for the analysis of a cuvette held in the accompanying cuvette holder attached to the microscope stage. The main advantage of this sampling set up is that the laser and cuvette holder are held in a fixed position. This allows for each sample to be analysed then replaced with another cuvette without affecting the positioning of the laser on the cuvette. Furthermore, the laser is introduced perpendicular to the cuvette, through the plastic sides and is focussed in the centre of the sample solution during analysis. Therefore, the evaporation of the buffer due to the heating of the solution by the laser should prove much less problematic.

To enable the spectrometer previously used to analyse samples in a cuvette, a macrosampler assembly was fitted to the microscope. Before sample analysis is performed, a standard sample is analysed and the intensity of the signal collected recorded. The signal intensity of the standard after the macrosampler was fitted was significantly lower than that of the standard set up. As such, it is likely that the signal observed from the assay would be much lower than is normally observed upon analysis in the microtitre plate. There are two principal reasons for this reduction in signal. Since the laser is focussed within the cuvette, the scattered light has to travel back through the sample before reaching the

objective. This can result in scattered light being absorbed by particles within the sample, therefore decreasing the intensity of the signal collected. Furthermore, when using the macrosampler assembly, a mirror is used to bend the light at a 90 ° angle, resulting in a further loss of light.

Whilst the aim of this investigation was to minimise the variation within the analysis, it was vital that this was not achieved to the detriment of the sensitivity of the analysis. Consequently, whilst the use of the macrosampler for sample analysis may decrease the variation, it is not an ideal method of analysis as it is likely to prove limiting in terms of the sensitivity offered in comparison to analysis in the microtitre plate.

3.5.4.3 Micro Cuvette Flow Cell

A potential method for analysis of the samples involved the utilisation of a micro-cuvette made for use as a continuous flow cell. The cuvette has a total sample volume of 50 µL and consists of a UV-transparent sample window and two hose barb connections for the connection of the inlet and outlet of the device to a pump. The introduction of this device offers a number of advantages over the previously discussed sampling methods. The assay washing protocol involves the repeated gathering of the magnetic beads, removal of supernatant and resuspension of the sample. A small number of magnetic beads will be lost upon each removal of the supernatant, resulting in the introduction of a considerable source of error between samples since the number of magnetic beads lost during the washing protocol will vary from one sample to another. Since the SERRS active nanoparticles responsible for the response monitored during analysis are tethered to the magnetic beads, this variable loss of magnetic beads will directly result in the variation of the signal intensity recorded from like samples. However, if a method of sample washing could be developed where the beads are held stationary and the wash buffer is flowed through the immobilised beads, the uncontrollable loss of magnetic beads during washing may be reduced.

The second major advantage of the use of this device is the possibility of increased signal intensity along with a decrease in the variability of the signals. If the magnetic beads are collected into a pellet before analysis, it was thought that this could hold a two-fold advantage for the development of the assay. The analysis has previously taken place in a

solution containing dispersed magnetic beads, where the signal observed is dependent upon the aliquot of the sample solution present in the laser beam at the time of analysis. This introduces a source of variability between repeat measurements, even within the same sample. However, if the magnetic beads can be collected into a pellet and analysed directly, it was hoped that this would reduce the variability. Furthermore, It has been shown that bringing nanoparticles into close proximity with one another creates an area of intense electromagnetic fields between the nanoparticles. [64] These areas, known as "hotspots", result in a heightened level of SERS enhancement. [64, 156, 157] Consequently, by bringing the SERRS active nanoparticle conjugates immobilised on the magnetic beads into close proximity with each other, it could possibly increase the sensitivity of the assay.

It was hypothesised that the use of the micro cuvette flow cell may offer an advantage in relation to each of these issues. If the cuvette was mounted on the microscope stage in such a way as to allow for SERRS analysis to take place *in situ* it may be possible to introduce a magnetic field beneath the optical window of the flow cell, immobilising the magnetic beads. The beads can then be washed by the introduction of a flow of wash buffer through the cuvette. Furthermore, if the magnetic beads are immobilised in the optical window, it was thought possible for the beads to be analysed whilst collected in a pellet rather than in solution.

Initial experiments were performed in order to assess the feasibility of this set up for sample analysis. The micro-cuvettes were positioned on the microscope stage with the optical window aligned under the microscope objective (Figure 3.31). The inlet and outlet of the flow cell was connected to tubing to allow for the introduction and removal of buffer *via* a peristaltic pump. The stage was positioned to allow a magnet to be introduced directly beneath the optical window of the cuvette.

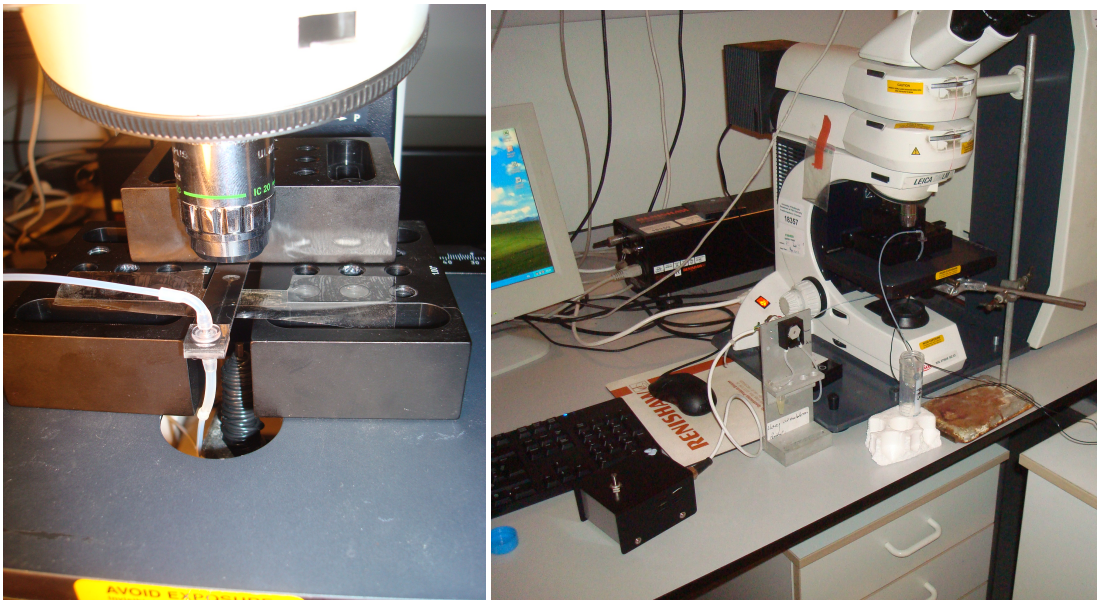

Figure 3.31 –Photographs of flow cell construction. The micro-cuvette flow cell is positioned with the optical window directly below the microscope objective, and the inlet of the cell is attached to tubing from a peristaltic pump for sample delivery and removal. The magnet is positioned introduced through the void in the microscope stage, directly beneath the flow cell.

A series of experiments were then performed to assess the suitability of the flow cell for *in situ* SERRS analysis of the assay samples. Initially, the ability to perform SERRS analysis of the samples through the optical window was assessed. A sample of dye-labelled PEG stabilised nanoparticle conjugates was introduced to the cuvette and the sample window filled with the solution. The laser was focussed on the optical window, and SERRS spectra were recorded from the sample solution contained within the window (Figure 3.32). Peaks corresponding to the malachite green anchored to the surface of the gold nanoparticles can clearly be observed. No significant addition peaks were observed in the spectrum collected corresponding to the materials used to construct the optical window. It can be seen however that the spectrum observed does have a poor signal to noise ratio. This is likely to be due to the high background signal collected from the optical window during analysis.

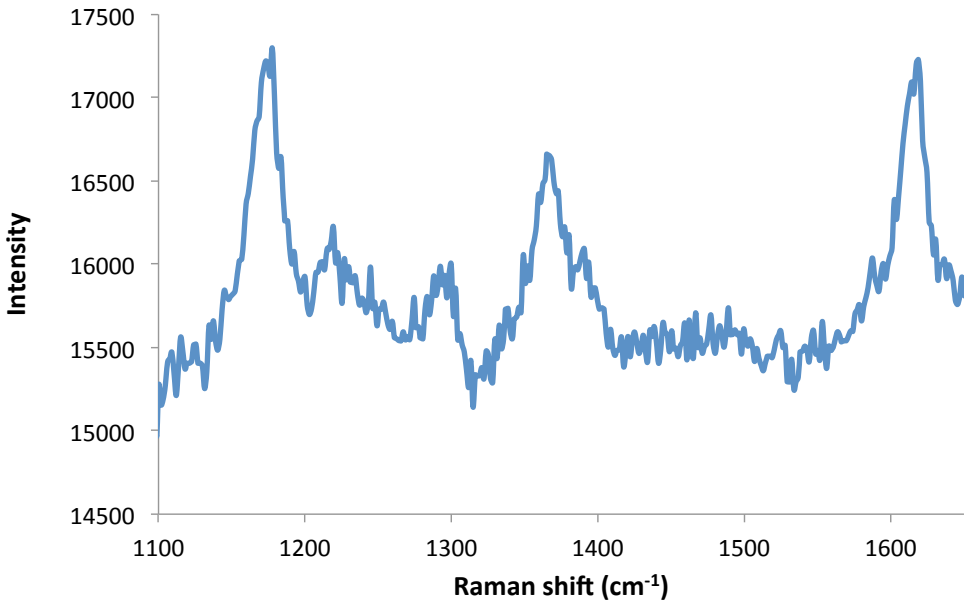

Figure 3.32 – SERRS spectra of malachite green-labelled, pegylated nanoparticle conjugates introduced into micro-cuvette flow cell. SERRS analysis was performed using 633 nm laser excitation through the optical window of the cuvette, 1 x 30 s accumulation.

Once the possibility of analysis of the sample within the micro-cuvette flow cell had been confirmed, it was vital to assess the ability to wash the magnetic beads within the cuvette. It was important to ascertain that the nanoparticle conjugates could be washed from the cell and did not remain bound to the film on the sample window. In order to assess this the nanoparticle conjugates previously analysed were eluted and the sample window washed through with water and analysed by SERRS (Figure 3.33). There are no significant SERRS peaks discernible from the signal collected. This is a positive result towards the introduction of an *in situ* washing protocol for the assay as it shows that the nanoparticle conjugates could be successfully removed from the sample window by a simple washing step. It is important to note that a relatively high background signal is observed, as was previously seen in Figure 3.32.

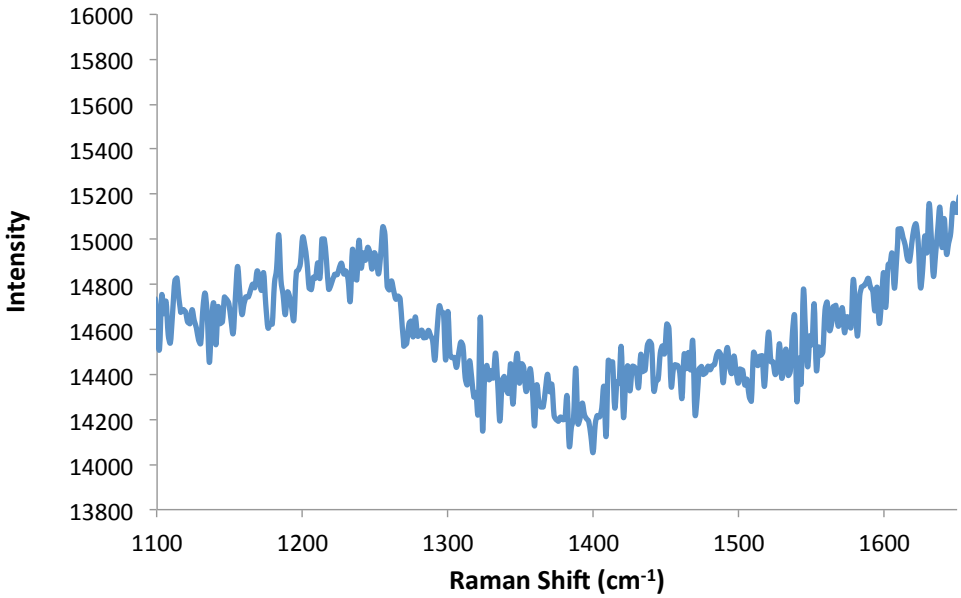

Figure 3.33 - The malachite green labelled, pegylated nanoparticle conjugates were eluted from the device and the sample window was washed with water. The solution was then analysed using 633 nm laser excitation through the optical window of the cuvette, 1 x 30 s accumulation.

The third vital component that had to be assessed was the ability to immobilise the magnetic beads in the optical window to allow analysis and remove the beads post-analysis. An aliquot of the magnetic beads used in the construction of the assay was suspended in water and introduced into the micro-cuvette flow cell. The sample was viewed through the microscope, and the magnetic beads were seen to be regularly dispersed throughout the sample solution, as shown in Figure 3.34.

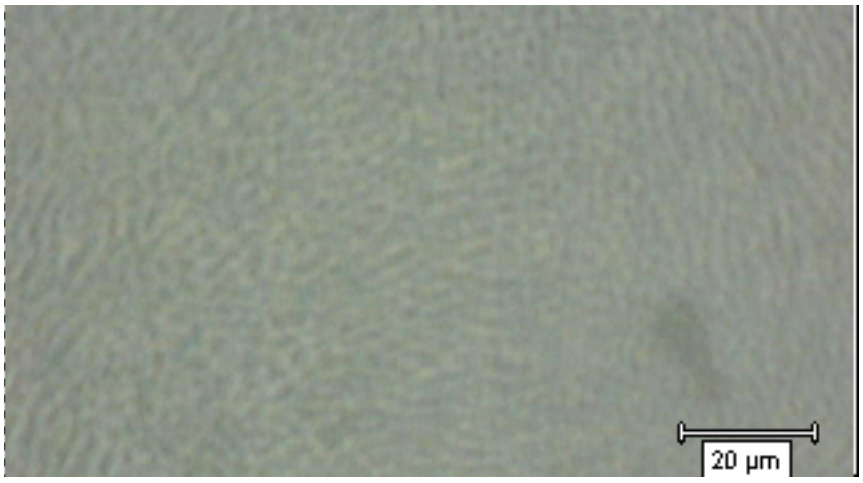

Figure 3.34 - White light image of the magnetic beads dispersed in buffer solution viewed through optical window of micro-cuvette flow cell.

As a magnet was introduced below the optical window the magnetic beads were seen to move towards this point, with the particles going from being randomly dispersed in solution (Figure 3.34) to forming areas with high densities of magnetic beads (Figure 3.35). These observations positively supported the possibility of immobilising the magnetic beads in the optical window, allowing for SERRS analysis of the beads to be performed directly.

Figure 3.35 - White light image of magnetic beads dispersed in buffer solution subjected to magnetic field. Sample is viewed through optical window of micro-cuvette flow cell.

The magnet was then removed and water was flowed through the cell to observe whether the magnetic beads could be removed from the micro-cuvette post-analysis. It was seen that with gentle agitation the magnetic beads were successfully removed from the device.

A final experiment was performed in order to assess the suitability of this assembly for assay analysis. A sample containing target DNA, which had been previously incorporated into the assay and tested, was introduced into the flow cell. The sample was pumped into the flow cell and circulated in a loop until the magnetic beads had been visibly removed from the sample solution and immobilised by the magnet beneath the optical window. The laser was then focussed on a densely populated area of these beads and a SERRS spectrum was recorded (Figure 3.36).

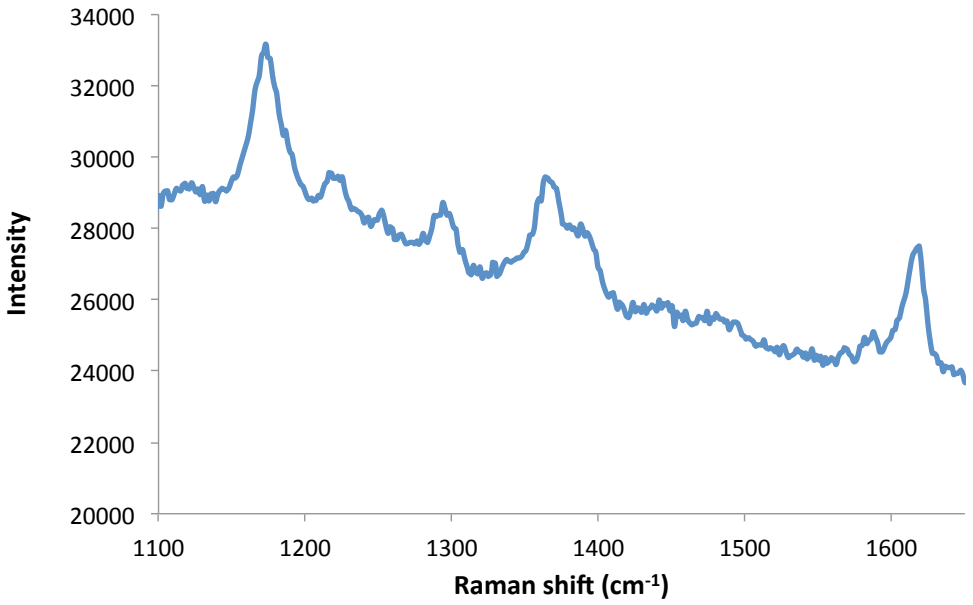

Figure 3.36 - SERRS spectra from the immobilised magnetic beads in a positive sample introduced to the micro-cuvette. Analysis was performed using 633 nm laser excitation through the optical window of the cuvette, 1 x 30 s accumulation.

A clear SERRS signal corresponding to the malachite green dye was observed, and the signal intensity was found to be comparable to that observed from the sample analysed in a microtitre plate. Whilst this suggests that the analysis of the magnetic beads as a pellet does not result in an increase in SERRS signal, it does indicate that the analysis of the assay would be possible in the flow cell set up described. The next stage was to perform the full assay incorporating the *in situ* washing of the magnetic beads.

The assay was constructed as detailed in Section 3.7.5.2 and the sample introduced into the flow cell. The AuMGPEGDNA nanoparticle conjugates and biotin capture probe were hybridised to the target DNA. The streptavidin coated magnetic beads were then added and the mixture agitated for one hour. The sample was circulated in a loop through the cell to allow for all of the magnetic beads to be captured. 0.3 M PBS was flowed through the cell in order to remove any unbound oligonucleotides and nanoparticle conjugates. This process was monitored using the optical microscope to ensure the magnetic beads remained positioned within the optical window during this washing process. The buffer was seen to visibly flow through the beads whilst the magnetic beads remained stationary. The magnetic beads appeared to form a fine layer on the surface of the optical window. This was likely due to the fact that the magnet was approximately the same dimensions as the

window itself. It was thought that because of the fine dispersion of the magnetic beads it would be difficult to focus directly on them, making it difficult to obtain a signal from the sample. This was found to be the case with little signal being observed upon analysis. There were a large number of the beads clustering around the edge of the optical window which it was thought would give a stronger signal, however due to their close proximity to the edge of the sample window it was difficult to focus on these clusters. In order to improve upon these initial results, a smaller diameter electromagnet was introduced to the assembly to decrease the dispersity of the magnetic beads.

The assay was constructed and the sample introduced to the flow cell and washed. The position of the particles after washing was viewed in order to assess the effect of the introduction of the smaller diameter electromagnet. Since the magnet was positioned beneath the centre of the optical window, it was expected that the magnetic beads would be collected as a pellet directly above this position, as shown in Figure 3.37.

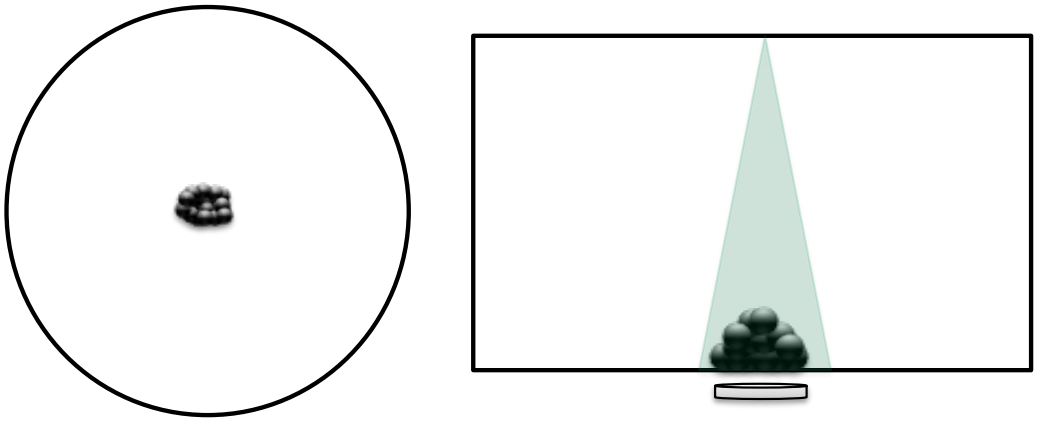

Figure 3.37 - Schematic representation of sample orientation upon introduction of magnet beneath the optical window.

However, it was found that the magnetic beads appeared to be dispersed as small clusters or single particles throughout the optical window, as shown in Figure 3.38. There were also a number of densely packed beads still clustered around the edge of the optical window. Upon further investigation it was found that the single particles were in fact columns of particles stacked upon one another (Figure 3.38). This could be seen by moving the cell slightly in relation to the magnet beneath it causing these columns to tilt as the beads moved.

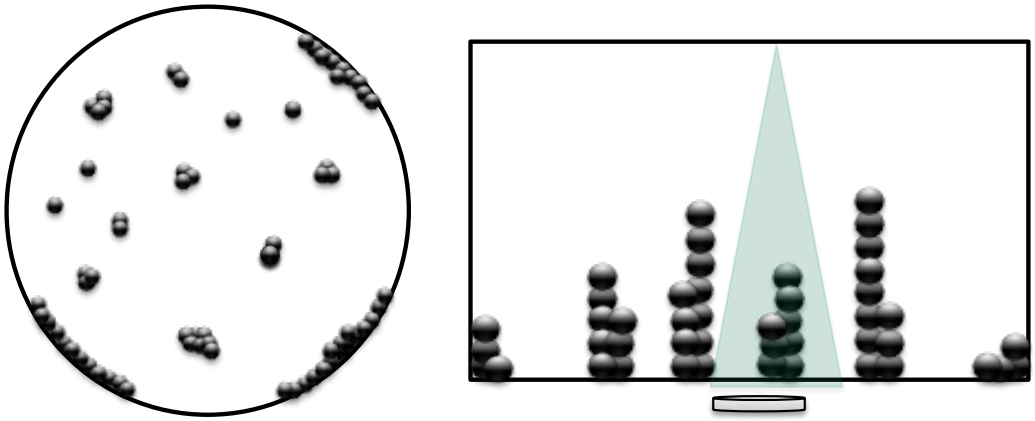

Figure 3.38 - Schematic representation of observations made upon introduction of magnet beneath the optical window.

The sample was analysed by SERRS with the laser focussed on the small clusters, however only background signal was observed (Figure 3.39). This was likely to be due to only a small area of the magnetic particles being exposed to the beam. It was postulated that if these columns could be tilted slightly to expose more of the magnetic beads present in the column, a greater response would be observed. The SERRS signal was recorded using a number of short accumulations. It appeared that for the first accumulation a clear response was observed, albeit with a low intensity, however the proceeding accumulations gave rise to a blank signal.

Upon observation of the sample at this point through the microscope it was seen that the beads that had previously been focussed on had moved due to the tilting of the column. It was found that although tilting the columns of magnetic particles made it possible for more beads to be analysed, it was not possible to maintain this tilted positioning whilst holding the beads stationary.

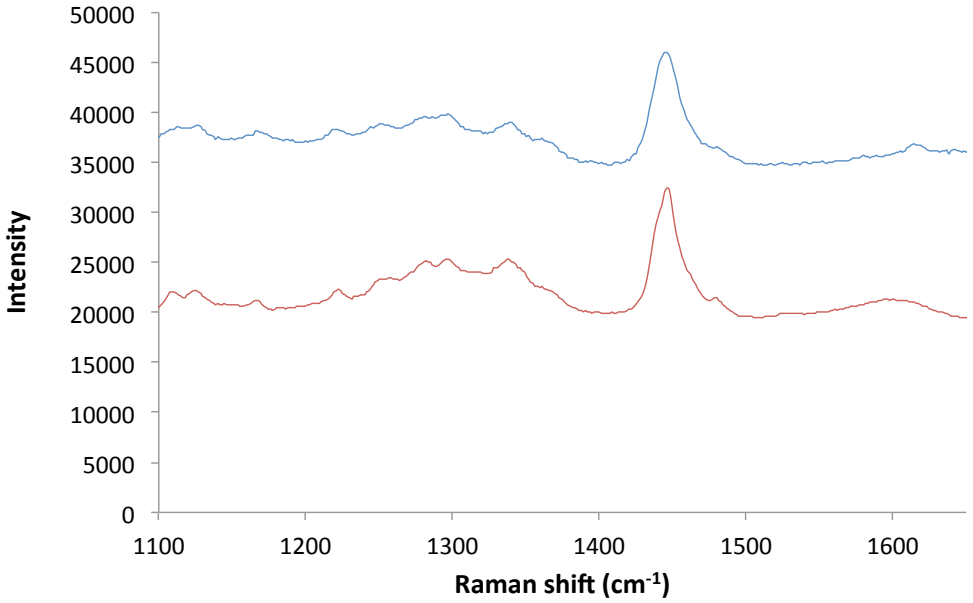

Figure 3.39 - SERRS spectra from the immobilised magnetic beads in a positive sample (red) or negative control sample (blue) constructed then introduced to the micro-cuvette and washed. Analysis was performed using 633 nm laser excitation through the optical window of the cuvette, 10 x 2 s accumulation.

It would appear from the results observed that the incorporation of the micro-cuvette flow cell into the assembly for sample analysis holds promise. It has been shown that the nanoparticle conjugates used in the construction of the assay can be successfully detected in the optical window of the cell. It has also been observed that the magnetic beads can be immobilised by the introduction of a magnet beneath the optical window and that buffer can be flowed through the beads to wash the sample without removing the beads. Furthermore, it has been shown that a previously constructed and analysed sample could be successfully immobilised and analysed in the optical window. It is thought that the clustering seen in this sample that allowed for the successful analysis may due to the sample being previously prepared, analysed and stored. It is possible that during storage the functionalised magnetic beads had aggregated slightly, causing them to cluster together. Consequently if the magnetic particles had become aggregated prior to their introduction to the flow cell, this would explain the observation of clustered magnetic beads in the previous sample, whilst the freshly prepared sample yields a dispersion of columns of magnetic beads.

These results are all indicative that this set up could be successfully implemented for analysis of the developed assay. However, further work is required on the immobilisation

step in order for the beads to be arranged in such a way as to allow for their analysis within the window. It was hypothesised that the magnetic beads would gather in a pellet above the magnet, however it was found that they instead formed columns, which are thought to be positioned along the magnetic field lines. These columns were difficult to obtain SERRS signals from due to their small cross-sectional area. In order to improve this immobilisation process, a smaller magnet could be used. The electromagnet previously utilised had a diameter that, although smaller than the optical window, still inhabited a large proportion of it. Therefore the magnetic beads have a fairly large area over which to be positioned. If a smaller diameter magnet were introduced to the system even if the magnetic beads still formed columns, there would be a smaller area over which these could be distributed. Therefore the beads would be brought into closer proximity with each other. In this case, more beads would be present within the laser beam for analysis, resulting in a higher signal being observed. Consequently the requirement to tilt the columns of magnetic beads in order to achieve a detectable signal would be removed, allowing for the laser to be focussed on them without difficulty.

3.6 CONCLUSIONS

The primary aim for this work was to develop nanoparticle conjugates that are stable in salt-containing buffer conditions, exhibit a clear SERRS signal and are easily functionalised with a variety of biomolecules. The development of these conjugates would allow for their use as tags in DNA detection systems for disease diagnostics. The subsequent aim was to develop an assay for the detection of DNA with a specific sequence using SERRS, which will incorporate these nanoparticle conjugates as a reporter system. The initial assay was designed to use a DIG-antiDIG interaction to immobilise the nanoparticle conjugates to the constructed assay, however the final aim was to produce oligonucleotide labelled nanoparticle conjugates for the direct labelling of the duplex produced with the SERRS active conjugates.

A protocol has been developed for the construction of stable SERRS active nanoparticle conjugates which are easily bio-functionalised. Gold nanoparticles were labelled with malachite green isothiocyanate to produce a core shell with an intense SERRS signature at 633 nm. These nanoparticle cores were stabilised by the introduction of a PEG bilayer to

the nanoparticle surface. This bilayer consisted of two different lengths of PEG, one short chain linker which was terminated with a carboxylic acid group which acted as a site for functionalisation, and one longer chain linker which acted as a stabilising ligand. These conjugates then had an antiDIG antibody, or an amino-modified oligonucleotide probe covalently coupled to them *via* the carboxylic acid moiety on the PEG linker. The production of these particles has been developed in such a way as to minimise aggregation. Due to the stability afforded by the polymer bilayer, the conjugates were stable in a number of buffers, including those containing salt. They were also stable in their pegylated form at ambient conditions for a number of months. The assay developed as proof of concept, using the DIG-antiDIG interaction was shown to be able to distinguish between target and nonsense DNA with a relatively high degree of discrimination. In the presence of target DNA, a distinctive SERRS signal corresponding to the malachite green dye tethered to the nanoparticle surface could be clearly observed. In the absence of the target sequence however, the signal observed was much lower in intensity.

Further work was then done to incorporate the oligonucleotide functionalised nanoparticles into the assay system. In the presence of target DNA, a higher intensity SERRS signal was observed than in the absence of target DNA. Upon the introduction of nonsense DNA, discrimination could be seen between the signal observed in the presence of the target sequence and from a control assay containing a nonsense sequence. Whilst these results were positive, it was noted that the signals observed from the assays varied greatly, causing significant error in the results obtained. There were a number of aspects of both the assay construction and the analysis protocol that were investigated in order to reduce this variation. Further work was also done in order to improve the discrimination between the assay output in the presence of target DNA and in the absence of the target strand.

It was found that the DNA functionalised nanoparticle conjugates bind non-specifically with the streptavidin coated magnetic beads. It was thought that if this non-specific binding could be reduced the negative control samples would exhibit a lower SERRS response, thereby improving the discrimination of the assay. One of the vital assay components which was thought could effect this was the wash buffer used to remove the excess nanoparticles and oligonucleotide probes from the assay prior to analysis. The addition of different additives as well as the pH of the wash buffer was therefore investigated. Furthermore, it

was shown that the nanoparticle conjugates only bind to the magnetic beads when they have been functionalised with oligonucleotide probes. The non-functionalised pegylated conjugates do not appear to bind and are successfully removed during washing. Therefore it was thought that the oligonucleotide probes must interact with a component on the surface of the streptavidin coated beads. Consequently, it was investigated whether the pre-coating of the streptavidin coated magnetic beads with the biotin capture probes before the addition of the beads to the assay samples would prevent this interaction.

The sampling method adopted for the analysis of the assay samples was investigated in order to minimise the signal variation both between replicate scans and between samples, with the aim of producing a more robust analysis procedure. During the development of the assay the samples had been analysed in a microtitre plate, however it was thought that there were a number of issues arising from this analysis protocol that may give rise to signal variation. It was suggested that the introduction of a macrosampler in the setup previously used to allow for the analysis of a cuvette might improve the sampling error. Furthermore, the development of a sampling assembly that utilised a micro-cuvette flow cell was undertaken as this offered a number of advantages over the previously adopted assemblies.

In summary, stable SERRS active nanoparticle conjugates were constructed which could be modified with a biomolecule of choice. It is thought that the protocol developed provides a method whereby stable SERRS active oligonucleotide-nanoparticle conjugates could be produced. These conjugates were incorporated into an assay that could successfully distinguish between target and nonsense DNA. Whilst a marked difference can be seen between the signal produced in the presence and absence of target DNA, further optimisation of the assay was required to improve the discrimination. Also, further work has to be done into the improvement of the signal variation observed. The results seen to date are promising and with further optimisation it is believed that this assay system holds potential to both sensitively and selectively detect targeted DNA.

3.7 EXPERIMENTAL DETAILS

3.7.1 OLIGONUCLEOTIDES

All synthetic oligonucleotide sequences used for this work were purchased from external manufacturers. They were purchased either from ATDBio, (Southampton), Eurogentec Ltd., (Belgium) or Eurofins MWG Operon (London) on a micromolar (µmolar) scale with HPLC purification. The base composition of each probe and the complement is given below, complete with modifications.

3.7.1.1 Oligonucleotide Sequences

DIG Labelled Probe

5' – GCT GCG ACA – 3'	Modifications:	5'	DIG – C_8 diol
Manufacturer Used: Eurogentec & ATDBio			

Biotin Labelled Probe

5' – GGG ACT AAG – 3'	Modifications:	3'	TEG – Biotin
Manufacturer Used: Eurofins MWG Operon			

Amino Modified Probe

5' – GCT GCG ACA – 3'	Modifications:	5'	NH_2-C_6
Manufacturer Used: Eurofins MWG Operon			

FAM Labelled Amino Modified Probe

5' – TCTCAACTCGTA – 3'	Modifications:	5'	NH_2-C_6 – $(HEG)_3$
Manufacturer Used: ATDBio		3'	FAM C_7

Target

5' – CTT AGT CCC TGT CGC AGC – 3'

Manufacturer Used: Eurofins MWG Operon

3.7.2 SYNTHESIS OF PEG LINKER MOLECULES

3.7.2.1 Preparation of thioctic acid functionalised PEG_8-COOH.

-COOH Functionalised Resin (**1**)

Wang resin (1.00 g, 1.0 mmol) was suspended in dichloromethane (DCM) (50 mL). Succinic anhydride (0.5 g, 5.0 mmol) and 4-dimethylaminopyridine (DMAP) (0.6 g, 5.0 mmol) were added. The mixture was heated at 60 °C for 6 hours. The resin was separated from the reaction mixture by filtration, and washed several times with DCM (20 mL) and methanol (20 mL). A pale brown solid product was isolated. Acid functionalisation of the resin was checked by performing a malachite green test.

A few of the beads were suspended in 0.25% malachite green oxalate in ethanol. 100 µL of triethylamine (TEA) was added and the mixture was left to stand for 2 minutes. The beads were isolated and washed with ethanol.

PEG_8 - COOH Functionalised Resin (**2**)

The acid functionalised resin (**1**) was suspended in DCM (50 mL). N,N'-diisopropylcarbodiimide (DIC) (775 µL, 5.0 mmol) and O, O, -Bis (2-aminopropyl) polypropylene glycol-block-polyethylene glycol-polypropylene glycol 500 (2.64 mL, 5 mmol) were added and agitated for 16 hours at room temperature. The resin was separated from the reaction mixture by filtration and washed several times with methanol (20 mL) and DCM (20 mL) to afford a light brown crystalline product.

Thioctic acid – PEG_8 – COOH (**3**)

The functionalised resin (**2**) was suspended in DCM (50 mL). Thioctic acid (516 mg, 2.5 mmol) and DIC (387 µL, 2.5 mmol) were added. The reaction was agitated for 16 hours at room temperature. The resin was separated by filtration and washed several times with DCM (20 uL) and methanol (20 uL). The linker was cleaved from the resin by treatment with 10% trifluoroacetic acid (TFA) in DCM, shaken at room temperature for 3 hours. The resin was removed by filtration and the filtrate was concentrated under reduced pressure and dried *in vacuo*. The product was rinsed with diethyl ether and dried *in vacuo*. A solution of the final product in methanol was made to a final concentration of 1×10^{-3} M.

^{1}H NMR (400 MHz, $CDCl_3$) δ 1.15 – 1.40 (m, thioctic acid), 3.66 (s, CH_2 -PEG backbone)

^{13}C NMR (100.62 MHz, $CDCl_3$) δ 69.89, 41.77, 22.93.

HRMS: 846.3 [$(M-H)^-$] ($C_{38}H_{74}N_2O_{14}S_2$ requires 847.27).

3.7.2.2 Preparation of thioctic acid functionalised PEG_{41}

-COOH Functionalised Resin (**4**)

Wang resin (1.00 g, 1.0 mmol) was suspended in DCM (50 mL). Succinic anhydride (0.5 g, 5.0 mmol) and DMAP (0.6 g, 5.0 mmol) were added. The mixture was heated at 60 °C for 6 hours. The resin was separated from the reaction mixture by filtration, and washed several times with DCM (20 mL) and methanol (20 mL). A pale brown solid product was isolated. Acid functionalisation of the resin was checked by performing a malachite green test (Section 3.7.2.1).

PEG_{41} - COOH Functionalised Resin (**5**)

The acid functionalised resin (**4**) was suspended in DCM (50 mL). DIC (775 µL, 5.0 mmol) and O, O, -Bis (2-aminopropyl) polypropylene glycol-block-polyethylene glycol-polypropylene glycol 1900 (9.5 g, 5 mmol) were added and agitated for 16 hours at room temperature. The resin was separated from the reaction mixture by filtration and washed several times with methanol (20 mL) and DCM (20 mL) to afford a white crystalline product.

Thioctic acid – PEG_{41} – COOH (**6**)

The functionalised resin (**5**) was suspended in DCM (50 mL). Thioctic acid (516 mg, 2.5 mmol) and DIC (387 µL, 2.5 mmol) were added. The reaction was agitated for 16 hours at room temperature. The resin was separated by filtration and washed several times with DCM (20 mL) and methanol (20 mL). The linker was cleaved from the resin by treatment with 10% TFA in DCM, shaken at room temperature for 3 hours. The resin was removed by filtration and the filtrate was concentrated under reduced pressure and dried *in vacuo*. The product was rinsed with diethyl ether and dried *in vacuo*.

Thioctic acid – PEG_{41} – ^{t}Bu (**7**)

The –COOH terminated PEG_{41} linker (**6**) was suspended in DCM. ^{t}Bu-amine (0.095 mL, 0.905 mmol) and DIC (139 µL, 0.905 mmol) were added. The reaction was agitated for 16 hours at

room temperature. The product was dried *in vacuo*, and a solution of the final product in methanol was made to a final concentration of 1 x 10^{-3} M.

^{1}H NMR (400 MHz, $CDCl_3$) δ 1.10 – 1.36 (m, thioctic acid), 3.61 (s, CH_2 -PEG backbone)
^{13}C NMR (100.62 MHz, $CDCl_3$) δ 69.94, 41.55, 28.21, 27.10, 22.96.
HRMS: 2379.3 [$(M+Na)^+$] ($C_{108}H_{215}N_3O_{46}S_2$ requires 2379.3).

3.7.3 PREPARATION OF NANOPARTICLE CONJUGATES

3.7.3.1 Preparation of Functionalised Nanoparticles

Gold colloid with a diameter of 60 nm was prepared *via* citrate reduction of $HAuCl_4$ (Section 2.5.1).[140] Malachite green isothiocyanate in water (600 µL, 3 × 10^{-7} M) was added drop wise to rapidly stirring gold colloid (1 mL, 0.08 nM) to afford a final reporter concentration of 1.125 × 10^{-7} M. After one hour, a thioctic acid-PEG_8-COOH solution in methanol (14 µL , 1x10^{-3} M) was added to the Raman-encoded nanoparticles. A minimum ratio of 30000 PEG molecules per 60 nm gold nanoparticle was used.[66] This was incubated for a minimum of 3 hours at 25 °C before an equivalent amount of thioctic acid-PEG_{41} in methanol (14 µL, 1x10^{-3} M) was added and incubated for at least 3 hours.

3.7.3.2 Bioconjugation

The Raman-encoded nanoparticles (1 mL) were washed by centrifugation (6000 rpm, 15 mins) with triple distilled water and resuspended in phosphate buffer (Na_2HPO_4/NaH_2PO_4) (470 µL, 10 mM, pH 7.6). To activate the –COOH group on the nanoparticle surface for covalent conjugation, freshly prepared ethyl dimethylaminopropyl carbodiimide (EDC) solution (10 µL, 2 mg/mL) and sulfo-NHS (10 µL, 2 mg/mL) were added.

To prepare antibody labelled conjugates, antiDIG antibody (10 µL, 1 mg/mL) was then added and the solution incubated for 16 hours at 25 °C. [142] The antibody labelled SERRS-active nanoparticles (500 µL) were washed by centrifugation (6000 rpm, 15 mins) and resuspended in 0.3 M PBS (10 mM phosphate, 0.3 M NaCl, 500 µL).

To prepare DNA labelled conjugates, amino-modified DNA (10 µL, 100 µM) was then added and the solution incubated for 16 hours at 25 °C. The DNA labelled SERRS-active nanoparticles (500 µL) were washed by centrifugation (6000 rpm, 15 mins) and resuspended in 0.3 M PBS (10 mM phosphate, 0.3 M NaCl, 500 µL).

3.7.3.3 UV-Vis Monitoring of Nanoparticle Construction

All UV-Vis spectroscopic analyses were carried out using a Cary 300 UV-Vis spectrophotometer fitted with a Cary temperature control unit. A variety of cuvettes were available, depending on the volume of the sample being analysed. Before collection of the spectra, the instrument was zeroed using a blank solution of the solvent present in the sample.

3.7.3.4 DLS Size Measurements

All size measurements were carried out using a Malvern Nanosizer ZS. Nanoparticle conjugates were prepared as described in Section 3.7.3.1**.** All prepared conjugates were centrifuged (20 min, 6000 rpm) and the pellets resuspended in distilled water. 1 mL of each sample was used. All measurements were carried out in a disposable 1 cm polystyrene cuvette. A standard sample consisting of commercially available Nanosphere™ Size Standards (Thermo Scientific Fremont CA.) 40 nm polymer microspheres in water were used as a standard before each set of sizing measurements.

3.7.3.5 SEM Imaging of Nanoparticle Conjugates

SEM investigations were carried out by preparing poly(diallyldimethylammonium) (PDDA) coated silicon wafers. Silicon wafers were cleaned with methanol and oxygen plasma (Diener electronic femto oxygen plasma cleaner, 72 cm^3/min gas flow). They were then coated with a 10 mg/mL PDDA solution in 1 mM NaCl for 30 minutes. After this time the wafers were rinsed with deionised water and dried with N_2. 10 µL of the nanoparticle solutions were deposited on individual wafers and allowed to rest for 20 minutes, the samples were then removed and the wafer washed. Imaging was carried out using a Sirion 200 Schottky field-emission electron microscope (FEI) operating at an accelerating voltage of 5 kV. The samples did not require additional metallic coating before imaging.

3.7.4 OLIGONUCLEOTIDE PROBE QUANTIFICATION [151]

3.7.4.1 Standard Calibration Graph

All fluorescence measurements were carried out using a Stratagene MX3005P. The FAM labelled oligonucleotide was diluted to give a series with a final concentration between 4 nM and 100 nM. The samples were analysed by fluorescence using an excitation wavelength of 492 nm.

3.7.4.2 Oligonucleotide Probe Quantification

Pegylated nanoparticle conjugates were prepared as detailed in Section 3.7.3.1. FAM-labelled oligonucleotides were then coupled to the conjugates *via* the method described in Section 3.7.3.2. The nanoparticle conjugates were washed by centrifugation (6000 rpm, 15 mins) and resuspended in DNAse I buffer. An aliquot of the nanoparticle conjugates (100 µL) was added to an aliquot of the DNAse I enzyme (final concentration 125 units mL^{-1}) and the samples incubated at 37 °C for 16 hours. The sample was then centrifuged and the supernatant removed and analysed by fluorescence spectroscopy using an excitation wavelength at 492 nm. The concentration of the FAM label in the supernatant was determined using a calibration graph of standard solutions. The number of biomolecules *per* nanoparticle was determined from the fluorescence emission by evaluating the FAM concentration against the nanoparticle concentration.

3.7.5 ASSAY CONSTRUCTION & ANALYSIS

3.7.5.1 Assay Construction Experimental Detail – Antibody Conjugates

Functionalised nanoparticles were prepared followed by bioconjugation with antiDIG antibodies, as described in Section 3.7.3.2. The nanoparticles were washed by centrifugation (6000 rpm, 15 mins) and resuspended in 0.3 M PBS (10 mM phosphate, 0.3 M NaCl, 500 µL).

The target DNA was hybridised to the two oligonucleotide probes, each of which is complementary to half of the target strand. DIG labelled probe (1 µL, 100 µM), biotin capture probe (1 µL, 100 µM) and target DNA (1 µL, 100 µM) were added to an eppendorf and the solution made up to 1 mL with 0.3 M PBS. The reaction mixture was then incubated

at room temperature for 1 hour to allow the oligonucleotide probes to hybridise to the target strand. In the nonsense control samples, nonsense DNA (10 µL, 10 µM) was added in place of the target DNA.

Streptavidin coated TurboBeads® (2.5 mg) were washed in 0.3 M PBS. The hybridised DNA solution was added along with the functionalised nanoparticles (619 µL, 0.1 nM). The mixture was then agitated at room temperature for 1 hour.

The beads were separated from the reaction solution by the introduction of a magnetic field, the supernatant removed and the beads resuspended in 0.3 M PBS. This washing protocol was repeated three times before SERRS analysis. A SERRS spectrum was obtained for the solution using 633 nm laser excitation. Replicate samples were prepared, with replicate measurements recorded from each sample.

SERRS spectra were collected using a 632.8 nm HeNe laser coupled to a Renishaw inVia microscope system. The samples were analysed in microtitre plates using a 20× long-working distance objective. Spectra were obtained using 180 ° backscattering from 96-well microtitre plates. The samples were analysed using a single 30 s accumulation, and the spectrometer grating was centred at 1400 cm^{-1}.

A calibration spectrum was recorded prior to analysis using a silica standard, which was used to calibrate the wavenumber position.

3.7.5.2 Assay Construction Experimental Detail – Oligonucleotide Conjugates

Functionalised nanoparticles were prepared followed by bioconjugation with the amino modified oligonucleotide probe, as described in Section 3.7.3.2. The nanoparticles were washed by centrifugation (6000 rpm, 15 mins) and resuspended in 0.3 M PBS (10 mM phosphate, 0.3 M NaCl, 500 µL).

The target DNA was hybridised to the two strands of single stranded DNA, each of which is complementary to half of the target strand. Biotin capture probe (1 µL, 1 µM) and target DNA (1 µL, 1 µM) were added to an eppendorf along with the oligonucleotide functionalised nanoparticles (10 µL, 0.1 nM). The reaction mixture was heated to 70 °C then

cooled to room temperature to allow the oligonucleotide probes to hybridise to the target strand. In the nonsense control samples, nonsense DNA (1 µL, 1 µM) was added in place of the target DNA.

Streptavidin coated magnetic beads (5 µL, 4 mg/mL) were washed in 0.3 M PBS then added to the DNA solution. The mixture was then agitated at room temperature for 1 hour.

The beads were separated from the reaction solution by the introduction of a magnetic field, the supernatant removed and the beads resuspended in 0.3 M PBS. This washing protocol was repeated three times before SERRS analysis. A SERRS spectrum was obtained for the solution using 633 nm laser excitation. Replicate samples were prepared, with replicate measurements recorded from each sample.

3.7.5.3 SERRS Analysis – Microtitre Plate

SERRS spectra were collected using a 632.8 nm HeNe laser coupled to a Renishaw inVia microscope system. The samples were analysed in microtitre plates using a 20× long-working distance objective. Spectra were obtained using 180 ° backscattering from 384-well microtitre plates. The samples were analysed using a single 30 s accumulation, and the spectrometer grating was centred at 1400 cm^{-1}.

A calibration spectrum was recorded prior to analysis using a silica standard, which was used to calibrate the wavenumber position.

3.7.5.4 SERRS Analysis – Cuvette

A Ventacon macrosampler was used to focus the laser beam into the centre of a 1 cm plastic cuvette for analysis of the samples.

A calibration spectrum was recorded prior to analysis using a cyclohexane standard, which was used to calibrate the wavenumber position.

3.7.5.5 SERRS Analysis – Micro-Cuvette Flow Cell

The input and output of a Fluorovette micro-cuvette flow cell (ALine Inc, California, USA) was attached to PTFE tubing (o.d. 1/16”, i.d. 0.023”). The device was attached to a

peristaltic pump equipped with a variable direction/speed function. The flow cell was held in place on the microscope stage ensuring the optical window was over the void in the centre of the stage. The magnet was positioned beneath the optical window when required. The samples were analysed using a 20x long-working distance objective. Spectra were obtained using 180° backscattering. The samples were analysed using a single 30 s accumulation, and the spectrometer grating was centred at 1400 cm^{-1}.

4. SYNTHESIS OF GOLD SHELLED-MAGNETIC NANOPARTICLES

The work presented in this chapter was performed alongside Andrea MacDonald, a final year undergraduate student, as part of a final year research project.

4.1 INTRODUCTION

Over the past few decades, the development of magnetic nanoparticles has become the centre of a mass of research. Due to the huge amount of attention this field has received, magnetic nanoparticles have been incorporated into a large number of applications in fields such as drug delivery, [158, 159] magnetic resonance imaging (MRI) [160, 161] and biosensing. [162-164] In particular iron oxide nanoparticles have attracted a vast amount of attention. Magnetite nanoparticles are commonly researched due to their chemical stability and low toxicity in comparison with iron nanoparticles.

Magnetite (Fe_3O_4) is a common magnetic iron oxide, which is abundant in nature and has a cubic crystalline structure. Magnetite has an inverse spinel structure with the oxygen ions closely packed in a cubic structure, and the Fe cations filling the interstitial tetrahedral and octahedral sites. Bulk magnetite is ferrimagnetic at room temperature, however below a critical diameter of 128 nm magnetite nanoparticles can be considered as superparamagnetic. [165] This is a desirable characteristic as it means that the particles are magnetic under the application of a magnetic field, however upon removal of the magnetic field, the particles no longer act magnetic. Therefore, the likelihood of the particles becoming attracted to one another and aggregating is reduced.

Whilst the magnetism of the particles is a vital property in the development of the magnetic particles, it is also important that the particles can be modified in such a way as to allow for targeting of specific molecules. Furthermore the introduction of a surface coating preserves the magnetic core, which is often highly susceptible to oxidation from the air. A number of coatings have been utilised including polymers, silica and precious metals. [165]

Gold coating of magnetic nanoparticles in particular has become the centre of a large amount of attention. [166-173] A key advantage offered by the introduction of a gold shell to the magnetic particle is the ability to adopt the diverse surface chemistry of gold without affecting the magnetic properties of the particles. Furthermore, since gold nanoparticles are a popular SERRS substrate, the addition of the gold shell to the magnetic nanoparticles provides a potential new analysis technique for biosensing assays developed utilising these particles. Previously, magnetic nanoparticle have been used in a variety of biosensing formats with the conventional readout systems being based upon the measurement of the relaxation time of the particles, or the measurement of a change in the electric current within the sensor. [163, 174] However, recently research has been focussed on the incorporation of gold-coated magnetic nanoparticles into SERRS assays for the detection of a number of target biomolecules.

Gu *et al*. recently demonstrated the ability to selectively detect a specific antigen by using antibody-functionalised gold-shelled magnetic nanoparticles. [175, 176] A method was developed whereby a direct immunoassay could be performed utilising the magnetic nanoparticles without the requirement of assembly of a sandwich structure on a solid surface. Gold coated magnetic nanoparticles were synthesised and labelled with goat anti-rabbit IgG antibodies. In conjunction with the formation of these conjugates, a second batch of functionalised nanoparticles were prepared. Gold nanoparticles were synthesised and labelled with mercaptobenzioc acid (MBA), a Raman reporter molecule, followed by their functionalisation with goat anti-rabbit antibodies. A solution containing both of these nanoparticles was mixed with the corresponding antigen and the particles were sedimented by the application of a magnetic field. Upon SERS analysis, peaks corresponding to the MBA label could be observed, indicating that the magnetic immuno-labelled particles and the SERS active nanoparticles have successfully bound to the target antigen. Upon further investigation, a limit of detection of 0.1 – 1 fg/ mL was reported. The assay was then further tested to assess the ability to specifically detect the target antigen. Gold coated magnetic nanoparticles and MBA-labelled gold nanoparticles were capped with goat anti-rabbit IgG and added to a solution containing either rabbit IgG or mouse IgG. In the presence of rabbit IgG, an intense SERS signal corresponding to the MBA label is observed from the sedimented particles. However, in the presence of mouse IgG no obvious SERS

peaks were observed. Furthermore, it was found that the system is capable of successfully separating a mixture of the two antigens with a concentration as low as 0.1 pg/mL.

Similar work has also been demonstrated by Zhong *et al*., where gold shelled magnetic nanoparticles were functionalised with antibodies. [173, 177] The group showed that in the presence of a Raman active gold nanoparticle functionalised with the corresponding antigen, a distinct SERS signal can be observed. However, when the antigen present on the gold nanoparticle surface does not correspond with the antibody tethered to the magnetic nanoparticles surface, no signal is seen. This system was also monitored using UV-vis spectroscopy, indicating that in the presence of the target antigen on the gold nanoparticle surface, the nanoparticles become aggregated. This is shown by a dampening of the surface plasmon resonance peak and the appearance of a peak at higher wavelengths. In the presence of a non-complementary antigen, no change in the surface plasmon peak is observed.

Whilst it has been demonstrated that gold-coated magnetic nanoparticles have been successfully used to detect antigens corresponding to antibodies immobilised on the nanoparticles surface, work has also been done towards the detection of DNA. Johnson *et al.* have recently developed a method utilising gold-coated paramagnetic nanoparticles and Raman-dye labelled oligonucleotide probes to detect target DNA. [178] Two DNA targets were selected based upon the RNA genomes of West Nile Virus (WNV) and Rift Valley Fever Virus (RVFV). A capture probe and a detection probe were designed for each sequence. The capture probe was functionalised with a thiol group and immobilised on the surface of the gold-coated magnetic nanoparticles. The capture probe was modified with a Raman reporter molecule, the WNV probe with erythrocin and the RVFV probe with malachite green, to indicate the presence of each target. In the presence of the target DNA, the detection probe hybridises with the target strand, which in turn also hybridises to the capture probe, thereby tethering the Raman dye to the nanoparticle surface, producing a SERS response. Initial experiments indicated that in the presence of the target sequence, both detection systems prove successful in the detection of the DNA with both showing a linear response when comparing the SERS intensity with the concentration of target DNA within the system. The ability of this system to be used for the multiplexed detection of target sequences was then tested by the introduction of both sets of probes and both

targets simultaneously to the system. Upon examination of the SERRS signals collected, peaks corresponding to both Raman reporters could be elucidated, indicating the successful detection of both targets. Control experiments were also carried out showing that the probes developed are specific for their corresponding target sequence, with no SERRS response being observed from either system in the presence of the non-complementary target sequence.

4.2 AIMS & CONCEPTS

In this chapter a method for the synthesis of magnetite nanoparticles, and their encapsulation in a gold shell is demonstrated. These magnetic nanoparticles were designed to be integrated into the assay developed in Chapter 2. It has been previously shown in Section 3.3.1 that the introduction of streptavidin coated TurboBeads in place of the conventional streptavidin coated magnetic beads yields an advantage in terms of the reduced SERRS signal induced by the presence of the beads. It was thought that the reduction in the decrease in SERRS signal by the replacement of the streptavidin coated magnetic beads with TurboBeads was a consequence of the substantially smaller diameter (30 nm) of the TurboBeads. Due to this difference in size, the TurboBeads interfere less with the scattered light during SERRS analysis than the larger beads; therefore the signal observed was less affected. However, the TurboBeads yielded problems in the assay system due to their reduced stability in solution compared with the conventional magnetic beads, and as a result they rapidly precipitated from solution. This was problematic for the analysis of the samples since the analysis protocol involved analysing the magnetic beads in solution. Therefore, the aim of this work was to synthesise magnetic nanoparticles that would be of a similar size to the TurboBeads, but would be more stable in solution allowing them to remain dispersed in the sample medium for a reasonable period of time. Furthermore, in order for the magnetic particles produced to be implemented as a suitable replacement for the TurboBeads, it was vital that they are easily functionalised with a biomolecule of choice.

Magnetite core nanoparticles were synthesised *via* a co-precipitation method. [179] The co-precipitation method is a popular approach for the synthesis of magnetite nanoparticles as it is relatively quick and sample, and can be performed at ambient conditions. It involved the co-precipitation of a solution of Fe^{2+} and Fe^{3+} salt in the presence of a base, and is usually performed at temperatures below 100 °C. These magnetite nanoparticles produced were to be used as core nanoparticles for the production of gold-shelled magnetic nanoparticles. The introduction of the gold shell was implemented for two main reasons. Firstly, it is vital that the magnetic nanoparticles produced for incorporation into the assay systems are stable in solution, and it has been shown that the introduction of a noble metal shell to the magnetite nanoparticles provides an increased stability. Secondly, the

introduction of the gold shell allows for the surface of the nanoparticles to be easily modified with a wide variety of thiolated molecules, thereby improving the functionalisation prospects for the nanoparticles.

The core nanoparticles were then subjected to a shelling protocol in order to afford a gold shell on the magnetic particle's surface. [180] The shelling method adopted involved the reduction of aqueous gold ions by glucose in the presence of the magnetite nanoparticles, in order to facilitate the growth of a gold shell on the surface of the magnetic nanoparticles. A number of parameters in the shelling protocol required investigation including; shelling time, shelling temperature and Fe_3O_4:$HAuCl_4$ ratio. Furthermore, a method for the assessment of the success of the shelling protocol was required.

Upon the synthesis of the gold-shelled magnetite nanoparticles, the assay systems previously developed were modified to allow for the incorporation of these particles (Figure 4.1). The gold coated magnetic nanoparticles were functionalised with a PEG bilayer, similar to the functionalisation method used in Chapter 3. An amino-modified oligonucleotide was then coupled to them to afford oligonucleotide-functionalised magnetic nanoparticles. These particles were then incorporated into the modified assay system to assess their compatibility for replacement of the streptavidin coated magnetic beads previously used.

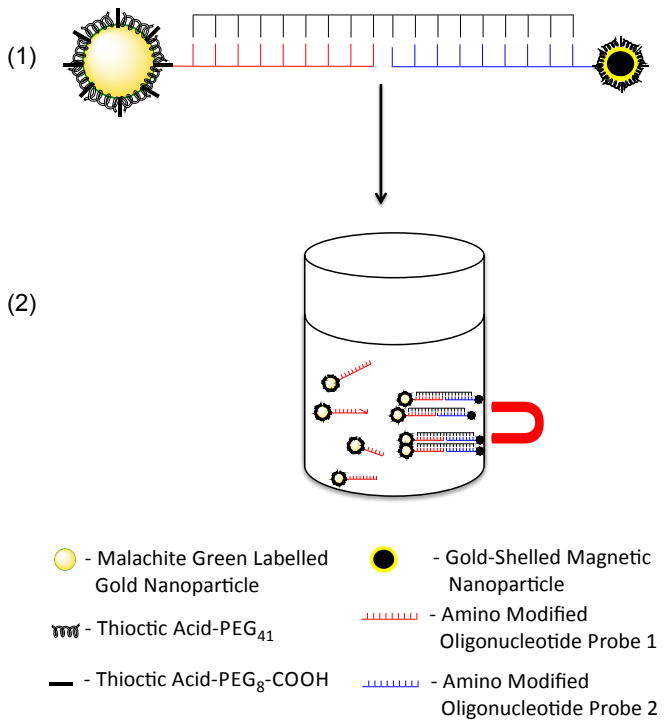

Figure 4.1 – Schematic representation of the fully constructed assay. The gold nanoparticles are encoded with malachite green and stabilised with a PEG bilayer. The PEG bilayer consists of a shorter and a longer chain PEG molecule. The short PEG molecule is terminated with a carboxylic acid group, through which an amino-modified oligonucleotide probe is conjugated to the nanoparticle. The gold-shelled nanoparticles are functionalised with the same PEG bilayer and a second amino modified oligonucleotide probe is conjugates to the magnetic nanoparticles. (1) The target DNA strand hybridises to the oligonucleotide probe bound to the SERRS active nanoparticle and the oligonucleotide-functionalised magnetic nanoparticle. (2) Upon introduction of a magnetic field, the magnetic nanoparticles with the SERRS-active particles tethered to them are gathered at the side of the sample vial. Any excess assay components present in the sample will remain in the buffer solution. SERRS analysis is then performed on the magnetic particles either in solution, or directly on the immobilised beads.

4.3 Synthesis & Characterisation of Magnetic Core Nanoparticles

4.3.1 Specifications

A number of specifications were established for the magnetic nanoparticles designed and synthesised. The three principle requirements for these nanoparticles were:

- The particles produced must have a diameter measureable in nanometres, preferably less than 100 nm;

- These nanoparticles must be magnetic in nature and be easily manipulated in solution by the introduction of a magnetic field;
- The nanoparticles must remain disperse in solution.

Furthermore, to allow for the nanoparticles to be incorporated into the assay system developed in Chapter 2, the particles must be easily functionalised with a biomolecule.

4.3.2 SYNTHESIS OF MAGNETITE NANOPARTICLES

There have been a number of protocols developed to yield high quality magnetite nanoparticles with a variety of size distributions. [181] These include co-precipitation, [182-186] thermal decomposition, [187-189] micelle synthesis [190] and laser pyrolysis. [191-193] The preparation of magnetite nanoparticles in the liquid phase is generally less expensive and higher yielding when compared to gas phase synthesis. [181] A large amount of publications have focussed on the synthesis of magnetite nanoparticles using co-precipitation from aqueous solutions.

Co-precipitation is an easy and convenient method for the production of iron oxide nanoparticles from aqueous ferrous and ferric salts in an alkaline environment (Equation 4.1).

$$FeCl_2 + 2\,FeCl_3 + 8\,OH^- \rightarrow Fe_3O_4 + 4\,H_2O + 8\,Cl^-$$

Equation 4.1 - Formation of magnetite *via* co-precipitation of ferrous and ferric salts in an alkaline environment.

With this method alteration of a number of factors such as the temperature, pH and Fe^{2+}/Fe^{3+} ratio can control the size, shape and composition of the magnetic particles produced. [165, 194-196] However, once the reaction conditions are fixed, the nanoparticles can be made reproducibly to give nanoparticles of the same morphology.

Magnetite nanoparticles were prepared *via* the co-precipitation of iron (II) and iron (III) salts in the presence of ammonia. It had been reported previously that the particles produced could be oxidised to yield maghemite nanoparticles with a diameter of approximately 8 nm. [179] It was therefore expected that the magnetite nanoparticles used in

this process would be of approximately similar dimensions. This procedure was therefore thought to be a good starting point since the protocol was quick and fairly simple and was expected to produce particles in the target size range. The protocol yielded a solution of black nanoparticles that upon placement in a magnetic separation rack were shown to be magnetic (Figure 4.2).

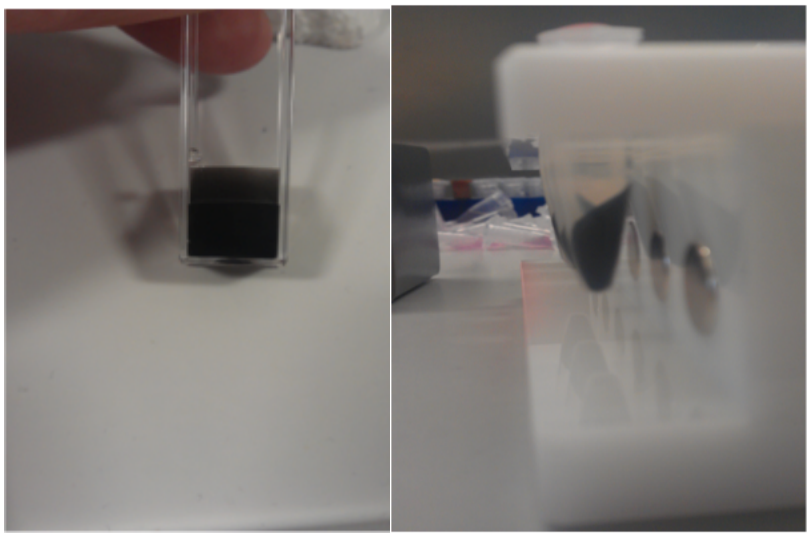

Figure 4.2 – (Left) Photograph of unshelled magnetite nanoparticles. (Right) Photograph of magnetite nanoparticles on a magnetic separation rack, illustrating the magnetic nature of the nanoparticles.

Upon introduction of the sample to a magnet, the nanoparticles responded instantly and were separated out of solution promptly. This was a promising result since the nanoparticles were designed with the ultimate aim of being incorporated into the assay. Since the nanoparticles would be introduced to the assay system in order to provide a means of immobilisation, it was vital that the magnetic particles could be immobilised on a magnet effectively in a timely manner.

One noted undesirable characteristic of the nanoparticles produced was that they did not remain suspended in solution over time. Over a few minutes, the nanoparticles could be seen to precipitate out of solution and collect at the bottom of the sample vial. The samples were sonicated in a bid to improve upon the particles dispersibility, however this had no effect. However, it has been stated in the literature that the introduction of a noble metal shell improves upon the stability of the unmodified magnetite nanoparticles. [180] Therefore,

it was decided to continue with the modification protocol and assess the dispersibility after the shelling process with gold had been completed.

4.3.3 Extinction Spectroscopy of Magnetite Nanoparticles

Since the magnetite nanoparticles were going to be used as a core to grow a gold shell, it was important to characterise the nanoparticles to allow monitoring of the shelling process. Therefore, the extinction spectrum of the magnetite nanoparticle solution was recorded (Figure 4.3). It was hoped that the appearance of a peak corresponding to the introduction of a gold shell (~520 nm) could be monitored as long as the spectrum obtained for the magnetite nanoparticles did not have any peaks present in this region of the extinction spectrum.

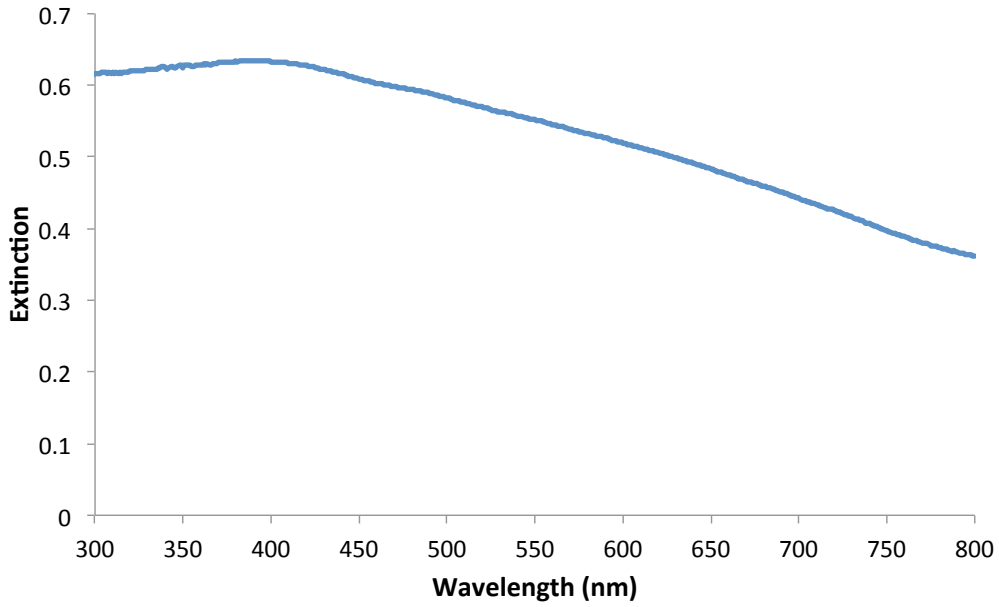

Figure 4.3 - Extinction spectrum of magnetite nanoparticles. Dilution factor = 1000.

It is clear that there are no peaks visible in the region where the surface plasmon of gold nanoparticles would normally appear (~520 nm). This is a positive result as it may allow for the monitoring of the appearance of a peak in this region after the magnetite core nanoparticles have undergone the shelling protocol. However, unfortunately the background signal observed from the magnetite nanoparticles was high, which could potentially make visualisation of the additional peak due to the presence of the gold shell

difficult. Further characterisation of the nanoparticles was therefore required in order to develop a method for confirming the presence of the gold shell.

4.3.4 MAGNETITE NANOPARTICLES ZETA POTENTIAL MEASUREMENTS

Since the introduction of a gold shell on the magnetite nanoparticles results in an alteration of the surface chemistry of the particles, consequently increases their stability, it was hypothesised that this modification could be monitored by measuring the zeta potential of the particles. It was expected that the surface of the particles would be negatively charged due to the O^- groups from the Fe_3O_4. It was further anticipated that the zeta potential of the particles would be relatively low, as it has been visually observed that the particles are not stable in solution and quickly settle on the bottom of the sample tube. Nanoparticle solutions with a zeta potential measurement greater than +25 mV or less then -25 mV can be considered to be highly stable. [137] The average zeta potential of the unshelled magnetite nanoparticles was measured to be -11.1 mV which is significantly higher than -25 mV, therefore the nanoparticles would not be expected to be stable. This is in good agreement with the observed instability of the particles in solution.

4.3.5 MAGNETITE NANOPARTICLES SIZE MEASUREMENTS

Since the introduction of the gold shell onto the magnetite nanoparticle would result in an increase in the overall diameter of the particle, it was postulated that measuring the size of the nanoparticles before and after the shelling protocol might allow for the introduction of the gold shell to be observed.

The literature had previously shown that magnetite nanoparticles synthesised by the same method could be oxidised to produce maghemite nanoparticles with a diameter of 8 nm. [179] Therefore it was anticipated that the magnetite nanoparticles produced by this method would be approximately the same size. DLS measurements of the magnetite nanoparticle solution were made (Table 4.1). It was noted however that upon removal of the samples from the instrument, the magnetite nanoparticles had all precipitated out of solution. It is not known at which stage of the sample measurement the particles had precipitated out of solution; therefore it was unknown whether the measurements obtained were from the

nanoparticles dispersed in solution. In an attempt to rectify this, a series of dilutions of the magnetite solution were prepared. It was postulated that the dilution of the magnetic nanoparticles might improve the dispersity of the colloid since the concentration of the particles would be lowered and the distance between particles would be increased. This would therefore reduce the attractive forces between the particles, allowing them to stay in suspension longer. However, even at low concentrations the particles could still be seen to quickly precipitate out of solution.

Sample	Z-average Diameter (nm)	Peak 1 Diameter (nm)	Peak 1 %
10% magnetite	3190	3340	100
1% magnetite	2190	2370	100
0.1% magnetite	3010	1270	100
0.01% magnetite	1800	455	100

Table 4.1 - DLS measurements of magnetite nanoparticles. The samples were diluted to varying degrees. 15 measurements was performed and the average of these measurements shown as the z-average measurement.

It was theorised that this lack of dispersity of the nanoparticles in the solution is the reason behind the unusual results obtained from the DLS size measurements (Table 4.1). Since the nanoparticles fall rapidly to the bottom of the cuvette, it is likely that there are very few if any particles still present in the sample solution upon analysis of the sample. Therefore, the large diameters observed are likely “noise” observed from the instrument due to a lack of particles dispersed in the sample solution. A second possibility is that these results could be due to the formation of large aggregates prior to precipitation of the nanoparticles.

It was clear that these results do not accurately represent the size of the magnetite particles produced. Therefore another approach had to be taken in order to establish the size of the nanoparticles, and monitor their growth upon introduction of the metal shell.

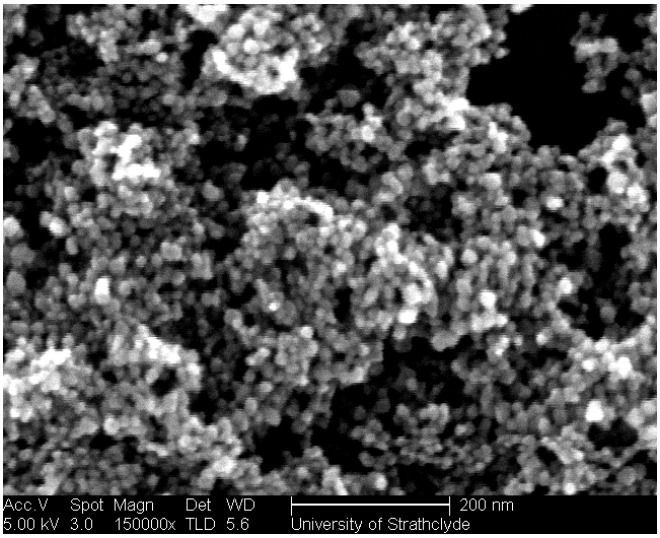

Figure 4.4 - Representative SEM image of magnetite nanoparticles.

Consequently, SEM images were obtained from the unshelled magnetite nanoparticles (Figure 4.4). Image processing software, ImageJ64, could then be used to estimate the diameter of the nanoparticles therefore allowing for the growth of the particles to be monitored. It is important to note however that the samples were dried onto silicon wafers prior to SEM analysis. Therefore, whilst the images can be processed to give information on the size of the particles, no conclusions can be drawn on the aggregation state of the nanoparticles.

A series of images were recorded from the magnetite nanoparticles, and each image was processed in order to ascertain a size distribution for the particles analysed (Figure 4.5). A number of particles from each image were measured using the scale bar as a reference and the measurements recorded. For each sample a number of images were taken and at least 250 particles from each image were measured, resulting in a minimum of 2000 particles being measured for each sample. These results were then combined to give information on the frequency of each nanoparticle diameter within the sample.

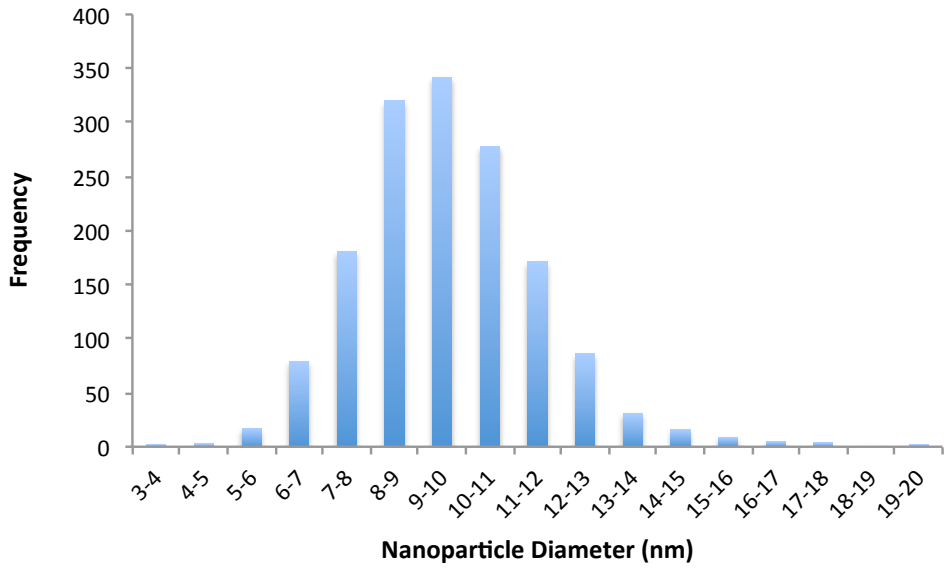

Figure 4.5 – Distribution graph showing the diameter of magnetite nanoparticles measured from SEM images.

It can be seen that the magnetite synthesis yields nanoparticles with a relatively narrow size distribution between 5-15 nm, with the majority of nanoparticles measuring between 8-10 nm. This is in good agreement with the previously published results shown from this analysis method. [179] Therefore, the use of SEM imaging alongside Image J 64 image processing software was considered to be a useful tool in the sizing of the magnetite nanoparticles and consequently in monitoring the success of shelling the core shells.

These results indicate that the particles synthesised have met two of the three designated specifications. The nanoparticles produced have been shown to be magnetic in nature and are easily separated from solution by the introduction of a magnetic field. The processing of the images obtained of the particles has also shown that the particles have an average diameter of approximately 9 nm. This particle size is within the targeted size range for the magnetite core particles. However the third specification, the stability, has not been met since the particles have been shown to not remain dispersed in suspension for any length of time.

4.4 SYNTHESIS & CHARACTERISATION OF GOLD COATED MAGNETIC NANOPARTICLES

It was proposed that the introduction of a noble metal shell to the magnetite nanoparticles would result in a two-fold advantage. First, it had been shown that the addition of a metallic shell improves the stability of the magnetite nanoparticles preventing further oxidation by the air and minimising aggregation. Secondly, the strong interaction between thiolated compounds and gold can be exploited to provide a method by which a number of molecules can be immobilised on the nanoparticle surface. [197, 198] Consequently the magnetic nanoparticles produced could be easily functionalised with oligonucleotide probes, as has been previously shown with metallic nanoparticles, allowing for their inclusion in DNA detection assays. This is of particular interest for the assays developed in Chapters 1 & 2, where the capture probe was previously bound to the magnetic bead *via* a streptavidin-biotin interaction. Therefore, the need for an additional biological interaction in the assay construction would be removed.

Therefore, it was decided to attempt to encapsulate the magnetite nanoparticles in a gold shell with the view to produce stable, easily functionalised magnetic nanoparticles. A co-precipitation method was adopted for the synthesis of the magnetite nanoparticles. The co-precipitation method is a convenient way to synthesis magnetite nanoparticles at ambient temperature from an aqueous iron salt solution in alkaline conditions. The protocol selected for the gold-shelling of the particles involved reducing a solution containing gold ions in the presence of the magnetic nanoparticle cores to induce the growth of a gold shell on the core nanoparticles as the gold ions are reduced. [180]

Glucose was added to the solution to serve two functions. The glucose is first utilised as a mild reducing agent, resulting in the gold ions from the metal salt being reduced to metallic gold on the nanoparticle surface. [199] The addition of this mild reducing agent, as opposed to stronger agents such as sodium citrate, was chosen since it was hoped it would induce the formation of gold shells on the magnetite core particles instead of the synthesis of gold nanoparticles in solution. Secondly, upon the shelling of the nanoparticles the gluconate ions, produced by the oxidation of the glucose, are adsorbed onto the metal surface, acting

as a capping agent. The gluconate anions afford a negative charge onto the nanoparticles, thereby providing them with electrostatic protection. [200]

A sample of the magnetite nanoparticles synthesised as detailed in 4.7.1.1 was sonicated for 15 minutes prior to the commencement of the shelling in order to break up any aggregates present within the colloidal solution. A solution containing sodium tetrachloroaurate and glucose was then added, and the solution stirred and heated in a water bath in order to facilitate the encapsulation of the magnetite nanoparticles in a gold shell.

4.4.1 Optimisation of Shelling Parameters

Whilst the shelling protocol implemented has been shown to successfully introduce a gold shell to magnetite nanoparticles, it was previously discussed that the variation in the ratio of the gold salt and iron oxide can provide gold shells of various thicknesses. [180] Furthermore, the protocol did not give details on the optimum temperature for the shelling procedure and did not discuss whether the procedure had undergone any optimisation. Therefore, a number of parameters were selected for investigation in the shelling protocol: Fe_3O_4:$HAuCl_4$ ratio, shelling temperature and shelling time.

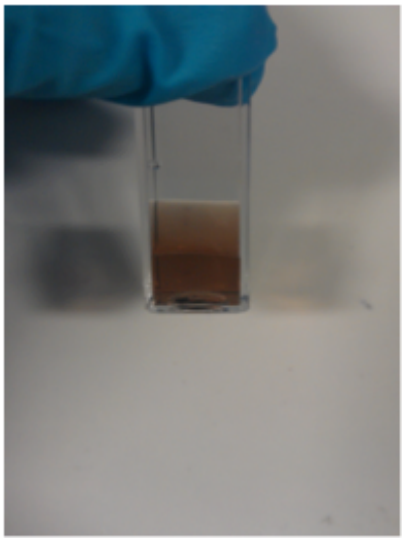

Figure 4.6 – Photograph of magnetite nanoparticles after undergoing the gold shelling protocol.

Prior to the shelling protocol, the magnetite nanoparticle synthesis method used was shown to afford a solution of black nanoparticles (Figure 4.2). It was detailed in the

literature that upon the gold shelling of the core magnetite nanoparticles, the black Fe_3O_4 nanoparticles could be seen turning reddish-brown. [180] This colour change would be an easy visual method for the initial detection of the gold shell on the magnetite particles. The nanoparticle solution afforded after the shelling protocol was indeed brown in colour (Figure 4.6), indicating that the nanoparticles had been successfully encapsulated in a gold shell. However, this colour change could not be used as conclusive proof of the success of the shelling protocol and further characterisation would have to be performed. Furthermore, the shelled nanoparticles remained in suspension significantly longer than the unshelled particles, which had previously been shown to quickly precipitate out of suspension. This can be regarded as a further indication that there has been an alteration of the surface of the magnetite nanoparticles, leading to their improved dispersibility.

4.4.2 Extinction Spectroscopy of Shelled Magnetite Nanoparticles

It had been shown previously that the magnetite nanoparticles exhibit a high extinction background (Figure 4.3). It had been hypothesised that this high background signal would make the appearance of the gold shell on the magnetite nanoparticles difficult to monitor by extinction spectroscopy, as the peak corresponding to the gold shell would be masked by the background signals. This was shown to be the case upon collection of an extinction spectrum from a sample of the shelled magnetite nanoparticles (Figure 4.7). The extinction profile observed is similar in shape to that observed from the unshelled sample, with no additional peaks corresponding to the gold shell observed.

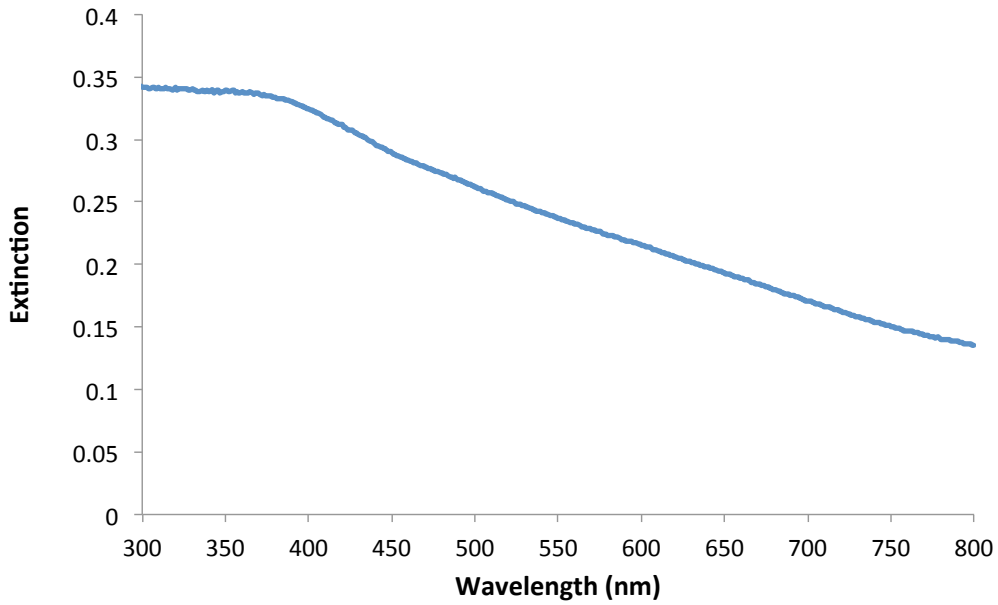

Figure 4.7 - Extinction spectrum of gold shelled magnetite nanoparticles. Background correction against water was performed. Dilution factor = 1000.

Although it is clear that the extinction profile corresponding to the magnetic nanoparticles dominates the extinction spectra collected, there may be a small contribution from the gold shell that is difficult to see by eye. Therefore, the collection of the absorption spectra was repeated using a reference standard of unshelled magnetite instead of water. However, no addition peak was observed from this spectrum. Consequently it can be concluded that, as expected, extinction spectroscopy cannot be used in order to detect the presence of the gold shell on the magnetite nanoparticles.

4.4.3 Zeta Potential Measurements

Since the introduction of a gold shell to the magnetite nanoparticles results in an alteration of the nanoparticle surface, it was decided that the success of the gold shelling protocol might be able to be monitored by a change in the zeta potential values of the nanoparticle solutions. It had been detailed previously that altering the ratio of Fe_3O_4:$HAuCl_4$ could result in a variation of the thickness of the gold shells observed. From these results, it is clear that the ratio of these components is vital for the successful shelling of the nanoparticles to be achieved. Therefore, a series of samples were prepared with varying Fe_3O_4:$HAuCl_4$,, and the zeta potential for each ratio was recorded (Table 4.2).

Ratio Fe_3O_4:$HAuCl_4$	Temperature of water bath (°C)	Time in water bath (mins)	Average Zeta Potential (mV)
1:1	70	60	-22.4
2:1	70	60	-29.6
5:1	70	60	-25.2

Table 4.2 - Zeta potential values from samples shelled with varying Fe:Au ion ratios.

The zeta potential values from this series of samples are more negative than that obtained from the unshelled sample, indicating that a negative charge has been introduced onto the nanoparticle surface. The larger value is also indicative of an increase in nanoparticle stability and is in good agreement with the visual observations made, with the shelled particles remaining in solution much longer than the core shell magnetite nanoparticles. It can be seen that whilst a range of zeta potential values are observed from the shelled particles, they are all significantly different from the value obtained from the magnetite nanoparticle (-11.1 mV), suggesting that the samples have all undergone shelling. Whilst these results suggest that the shelling protocol has been successful in developing a gold metallic shell on the nanoparticles, they do not give any information on the thickness of this core. In order for an assessment of the effect the variation of the Fe_3O_4:$HAuCl_4$ ratio has on the thickness of the gold shell produced, further investigation was required.

Whilst the literature detailed the need for the shelling to be performed in a water bath, no information was given on the optimum temperature at which the shelling should be performed at. [180] Therefore a series of shelling experiments were performed, altering the temperature of the water bath. It was shown that upon shelling of the particles in a water bath of various temperatures (60 °C, 70 °C, 80 °C) a distinct change in the zeta potential of the nanoparticle solution could be observed (Table 4.3). This alteration in zeta potential indicates that each sample has had the surface of the nanoparticles altered over the course of the shelling protocol. Although there appears to be a small difference between the zeta potential observed between samples, they all have zeta potential values significantly lower than that of the unshelled particles. This alteration in zeta potential indicates that the nanoparticles surface has become more negatively charged, and that in turn the nanoparticles would be more stable in solution. This is in good agreement with the observations made upon completion of the shelling protocol, where it was observed that

the shelled particles remained in solution much longer than their unshelled counterparts. Furthermore, it would appear that increasing the temperature of the water bath from 60 °C to 80 °C yields no significant advantage as there is no significant difference between the values obtained from samples prepared at either temperature. Therefore, 60 °C was selected as the optimum water bath temperature for the shelling protocol.

Ratio Fe_3O_4:$HAuCl_4$	Temperature of water bath (°C)	Time in water bath (mins)	Average Zeta Potential (mV)
1:1	60	60	-31.8
1:1	70	60	-22.4
1:1	80	60	-29.9

Table 4.3 - Zeta potential values from samples shelled at varying temperatures.

An investigation was performed into the shelling time required to successfully shell the particles. A series of samples were prepared and the length of time the samples were stirred in the water bath was varied in order to investigate the effect of the shelling time (Table 4.4). It can be seen that for each of the samples prepared, the zeta potential measurement has become more negative indicating the introduction of a gold shell to the core particle. It had been reported previously when investigating the need for glucose in the shelling protocol, that increased heating times lead to larger particles with a non-uniform coating. [180] Therefore, the minimum shelling time required in order to observe a significant change in zeta potential was selected in order to prevent non-uniformity of the shell grown. Consequently, a shelling time of 60 minutes was chosen.

Ratio Fe_3O_4:$HAuCl_4$	Temperature of water bath (°C)	Time in water bath (mins)	Average Zeta Potential (mV)
1:1	70	60	-22.4
1:1	70	120	-28.5
1:1	70	300	-30.7
1:1	70	420	-31.5

Table 4.4 - Zeta potential values for samples shelled over varying lengths of time.

4.4.4 SHELLED NANOPARTICLE SIZE MEASUREMENTS

SEM imaging was employed alongside Image J 64 image processing software to approximate the size of the nanoparticles after completion of the shelling protocol. It was anticipated that since the magnetite nanoparticles are so small, directly viewing the gold shell on the particles would not be possible. This was shown to be the case upon examination of the SEM images obtained from the shelled magnetite nanoparticles (Figure 4.8).

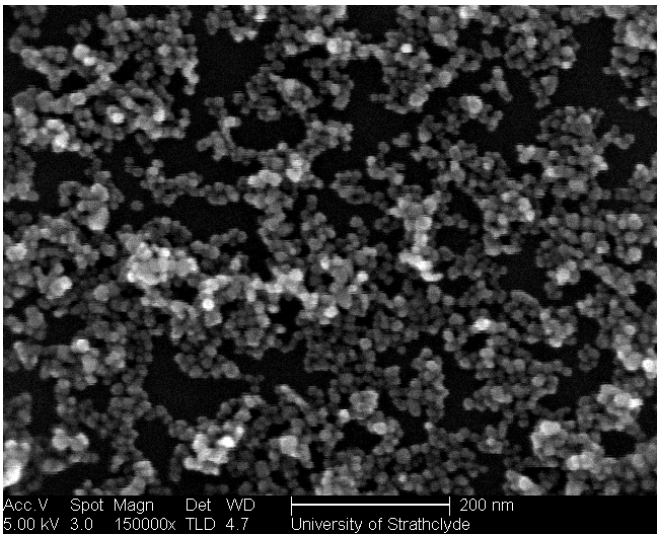

Figure 4.8 - Representative SEM image of magnetite nanoparticles after undergoing gold shelling protocol.

In comparison with the images obtained for the magnetite nanoparticles (Figure 4.4), no observable difference can be seen between the particles before and after shelling has occurred. Therefore, the images were processed in the same way as was used for the particle sizing of the magnetite nanoparticles in order to obtain the size of the particles post-shelling.

By comparing the distribution curve observed from the nanoparticles post-shelling with that of the curve obtained from the magnetite core nanoparticles, it can be seen that there is a distinct shift in the nanoparticle size distribution (Figure 4.9). Upon examination of the distribution obtained from the unshelled nanoparticles, it would appear that the size is centred on nanoparticles measuring between 9-10 nm in diameter. In comparison, when examining the distribution curve obtained from the nanoparticles after the gold-shelling protocol has been carried out, it would appear that the centre of the distribution curve has

shifted to approximately 12-13 nm. Consequently, it can be assumed that this shift in distribution is likely to be due to the introduction of a gold shell onto the surface of the magnetite nanoparticles, resulting in an increased nanoparticle diameter.

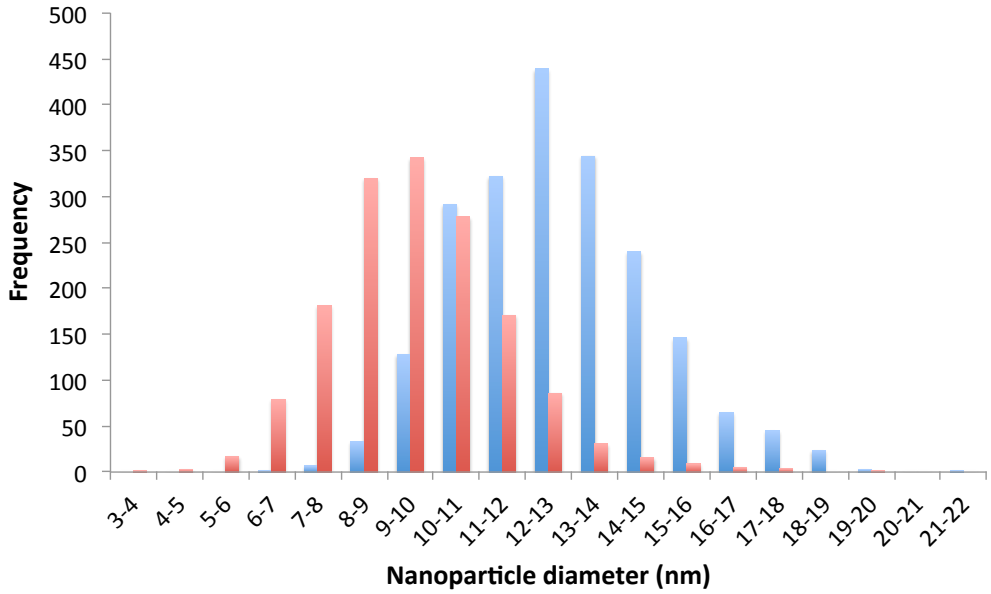

Figure 4.9 – Comparison of size distribution of unshelled magnetite core nanoparticles (red) and gold-shelled magnetite nanoparticles (blue). A minimum of 2000 particles were counted from each sample.

This size comparison was repeated on a number of samples investigating a variety of synthetic parameters. The results, shown in Table 4.5, indicate that the nanoparticle diameter has increased upon each shelling protocol. When comparing the results obtained from the samples where shelling temperature was varied, a similar nanoparticle size was obtained. Furthermore, by comparison of the principal peak on the distribution graph, it is also shown that varying the shelling time has little influence on the diameter of the nanoparticles obtained. It had previously been stated that by altering the Fe_3O_4:$HAuCl_4$ ratio, the thickness of the gold shell could be altered. [180] By comparison of the principal nanoparticle diameter for the samples obtained with various concentrations of sodium tetrachloroaurate, it does not appear that there is a distinct difference in the overall diameter of the nanoparticles after the shelling protocol has been completed. However, since these measurements were done in order to observe the introduction of the gold shell by monitoring the shift in the distribution of the nanoparticle, and do not give definitive size values for the nanoparticles it is not possible to definitively make this conclusion without further analysis. Due to the small size of the nanoparticles produced, the resolution

of the SEM images obtained are not as high as would be ideal. The use of TEM would therefore yield higher resolution images that could be used for a more accurate comparison of the thickness of the gold shell introduced. However, from the results obtained it can be suggested that the nanoparticles have increased in diameter during the shelling process due to the introduction of a gold shell.

Ratio Fe_3O_4:$HAuCl_4$	Temperature of water bath (°C)	Time in water bath (mins)	Principal nanoparticle diameter (nm)
1:1	60	60	12-13
1:1	70	60	11-13
1:1	80	60	12-13
2:1	70	60	12-13
5:1	70	60	13-14
1:1	70	120	12-13
1:1	70	420	10-11

Table 4.5 – Principal nanoparticle diameters obtained from the size distribution graphs of the gold-shelled nanoparticles for samples shelled varying a selection of parameters.

These measurements are in good agreement with the zeta potential values from the series of samples. The increase in the negative zeta potential of the nanoparticles upon shelling obtained also suggested that all of the samples had been successfully shelled whilst varying a number of parameters in the shelling protocol. Consequently, since it was shown that the alteration of the shelling time and temperature did not greatly effect the results obtained, and that the variation of the sodium tetrachloroaurate concentration did not yield any distinct variation in results, it was concluded that the ideal conditions under which the nanoparticle shelling procedure would be conducted was using a 1:1 Fe_3O_4:$HAuCl_4$ ratio at 60 °C for 60 minutes.

4.4.5 SERRS Assessment of Shelling Protocol

It has been shown previously that malachite green isothiocyanate is capable of binding to gold metallic nanoparticles *via* a bond between the gold surface and the sulphur containing

isothiocyanate group (Section 3.2.4). After the dye is tethered to the nanoparticle surface, SERRS analysis gives rise to a clear signal corresponding to the malachite green. This interaction between the dye and the gold surface could therefore be exploited to assess the success of the shelling protocol.

It was anticipated that upon introduction of the malachite green isothiocyanate to the magnetite core shell nanoparticles, no binding between the dye and the nanoparticle surface would occur. Therefore washing the nanoparticles would remove the malachite green from the sample solution. Furthermore, even if the malachite green dye did bind to the unshelled nanoparticles, the SERRS activity of iron would be extremely low when compared with that of gold since iron is not a strongly enhancing surface. [45] Consequently, upon SERRS analysis no peaks corresponding to the malachite green dye would be observed. Conversely, upon the introduction of the malachite green isothiocyanate to the successfully gold-shelled magnetite nanoparticles, the dye would become tethered to the nanoparticle surface. Upon washing, excess malachite green would be removed from the sample, however the bound dye molecules would remain present on the surface of the nanoparticles. Therefore upon SERRS analysis, peaks corresponding to the malachite green molecule present on the nanoparticle surface would be observed.

A solution of malachite green isothiocyanate was added to shelled magnetite nanoparticles and incubated at room temperature for 1 hour to allow for binding to occur. The sample was then washed by centrifugation and resuspended in water. The same protocol was followed for a control sample using unshelled magnetite nanoparticles instead. The samples were analysed using 633 nm laser excitation and the spectra compared (Figure 4.10).

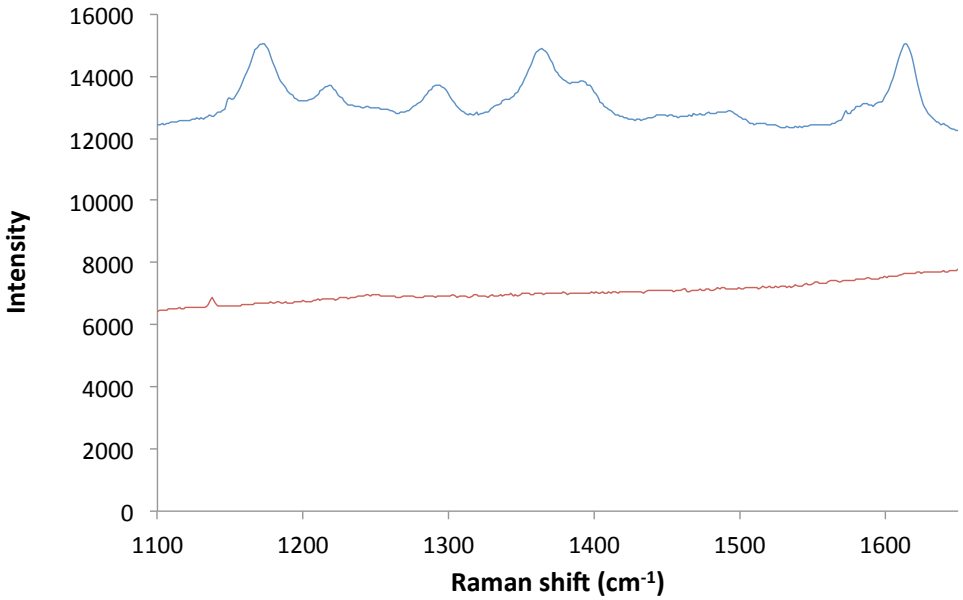

Figure 4.10 – SERRS spectrum obtained from unshelled magnetite (red) and shelled magnetite (blue) incubated with a solution of malachite green isothiocyanate. The samples were washed prior to SERRS analysis using 633 nm laser excitation, 1 x 30 s accumulation.

It can be seen that the unshelled magnetite nanoparticles that had been incubated with the malachite green isothiocyanate gives rise to minimal SERRS signal upon analysis. Conversely, the shelled magnetite nanoparticles result in clear SERRS peaks corresponding to the malachite green. Consequently, it can be concluded that the malachite green molecules were bound to the gold-shelled magnetite particles whereas in the case of the unshelled particles, the malachite green has been removed during washing. These results therefore indicate that a gold layer was present on the surface of the magnetic nanoparticles.

Further to analysis of the results shown in Figure 4.10 it was postulated that there might be an alternative explanation for the presence of SERRS peaks from the shelled nanoparticles. In order to achieve a gold shell on the surface of the magnetite nanoparticles a solution containing gold ions was introduced to the magnetic nanoparticles along with glucose. The glucose was added as a reducing agent to reduce the gold ions to metallic gold on the magnetite nanoparticle surface. Glucose was selected as the reducing agent due to its mild nature in a bid to produce only gold shells on the pre-existing magnetite nanoparticles. However it is possible that this reduction process also yields gold nanoparticles. If this were the case, the sample may contain a mixture of unshelled or shelled magnetite nanoparticles

and gold nanoparticles. Therefore it is possible that the SERRS signal observed is from malachite green isothiocyanate bound to the surface of the by-product gold nanoparticles.

In order to ascertain the source of the SERRS signal observed a sample of the shelled magnetite nanoparticles was incubated with a solution of malachite green isothiocyanate. The sample was washed by centrifugation to remove any excess malachite green, and resuspended in water. Further to centrifugal washing, the sample was then placed in a magnetic separation rack and the magnetic nanoparticles gathered in a pellet on the side of the sample tube. The supernatant was then removed in order to remove any gold nanoparticles produced during the shelling procedure. Whilst these nanoparticles would be gathered alongside the magnetic particles during centrifugation, upon the application of a magnetic field only the magnetic particles would be collected. The particles were then resuspended in water and analysed by SERRS using 633 nm excitation wavelength (Figure 4.11).

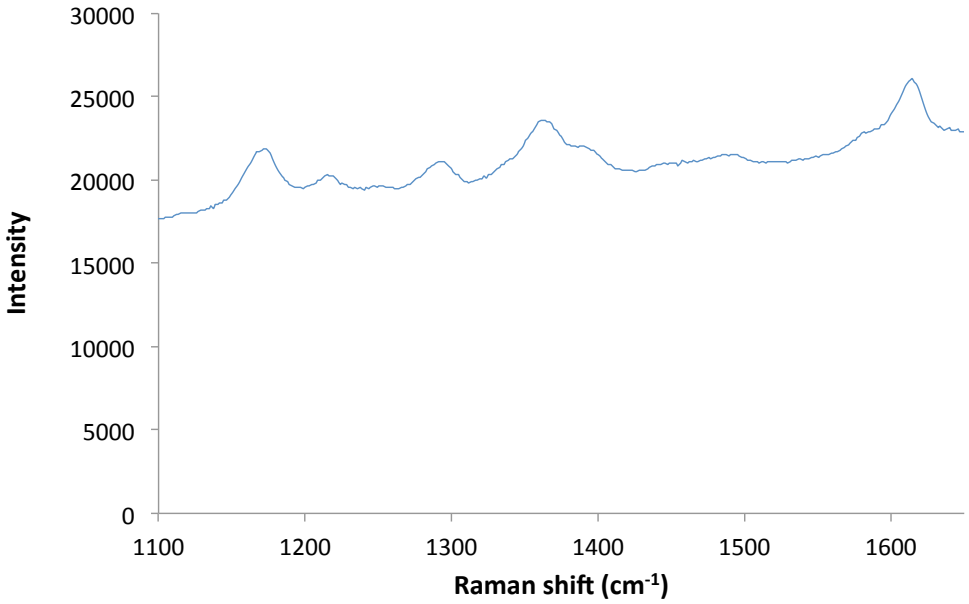

Figure 4.11 - SERRS spectrum obtained from shelled magnetite incubated with a solution of malachite green isothiocyanate. The samples were washed using centrifugation and magnetic separation prior to SERRS analysis using 633 nm excitation wavelength, 1 x 30 s accumulation.

It can be clearly seen that upon washing the nanoparticle solution with magnetic separation a clear SERRS signal with peaks corresponding to the malachite green dye can be seen. This would suggest that the spectrum observed is due to the malachite green dye becoming

bound to the gold-shelled magnetic nanoparticles. Therefore it can be concluded that the magnetite nanoparticles in the sample have been successfully encapsulated with a gold shell.

4.4.6 STABILITY OF SHELLED NANOPARTICLES

It has been shown that upon completion of the shelling protocol the nanoparticles exhibit improved stability, as indicated by their enhanced dispersity and relatively high negative zeta potential values. Since the dispersibility of the nanoparticles is a key issue and is directly related to their stability, it is important to understand how the stability of the shelled magnetic particles varies over time. Whilst the nanoparticles are dispersed in water post-shelling, it was hypothesised that the addition of a stabilising ligand to the solution may further improve the stability of the nanoparticles. Sodium citrate is often used as a reducing agent and capping molecule in the synthesis of gold nanoparticles as it effectively reduces gold ions into metallic gold, giving rise to stable colloidal solutions. In this case, citrate was not used as the reducing/capping agent during gold shelling in order to avoid the synthesis of gold nanoparticles and encourage the shelling of the magnetite cores. However, the introduction of sodium citrate post-shelling may impart improved stability on the shelled nanoparticles synthesised. Consequently, a comparison was conducted of the gold shelled magnetite nanoparticles resuspended in both water and citrate solutions over a period of time (Figure 4.12).

It can be seen that the nanoparticles resuspended in a sodium citrate solution have a higher initial zeta potential value that those resuspended in water. This is due to the presence of the citrate anions on the surface of the nanoparticle, increasing the exposed negative charge on the nanoparticle surface. It has been proposed that when the citrate anion tethers to a silver surface, one of the COO^- groups is left exposed. [63] It is likely that when adsorbed onto a gold nanoparticle, the citrate anion adopts a similar orientation, resulting in a negatively charged surface. When glucose reduces gold ions to metallic gold, the gluconate anion produced is absorbed onto the particles surface. Whilst this would give rise to a negative charge, glucose (pKa ~12) is also associated with the surface through hydrogen bonding. Consequently, the surface will have a mixture of charged and uncharged

molecules associated with it. This will result in the nanoparticle produced by glucose reduction having a lower zeta potential than those produced by citrate reduction.

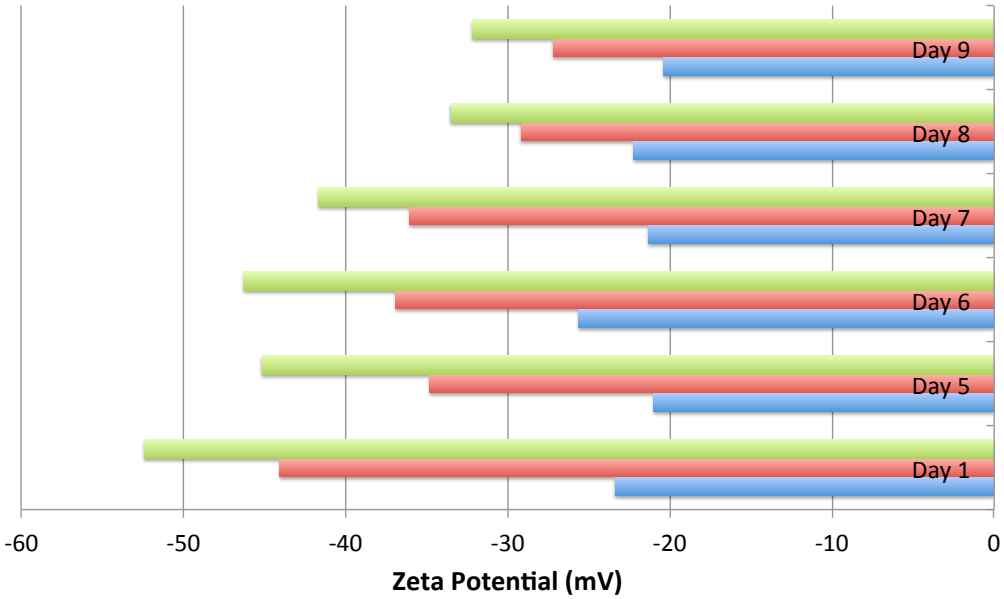

Figure 4.12 – Comparison of the average zeta potential measurements of the gold shelled magnetite nanoparticles resuspended in water (blue), 0.6 mM sodium citrate (red) and 1 mM sodium citrate (green) over time. A number of sample replicates were prepared and analysed, and the average zeta potential plotted.

Over time, the zeta potential values for the shelled nanoparticles resuspended in different concentrations of citrate have both steadily decreased. However, although the values have decreased over time, both samples still have a final zeta potential value greater than that of the sample resuspended in water. Nevertheless, upon monitoring the zeta potential of the shelled nanoparticles in water the variation in the zeta potential values is significantly less than the variation observed from the samples resuspended in a citrate solution. Therefore, whilst it appears that resuspension of the nanoparticles in a citrate solution improves the stability of the particles, it is unknown whether this effect would be observed over a longer period of time. It was shown that the solutions resuspended in various concentrations of sodium citrate solution exhibit a gradual decrease in their zeta potential values. Therefore, it is unknown whether these values would continue to decrease over a longer period of time to give an end value comparable with that of the particles resuspended in water. Consequently in order to give a thorough explanation of the results obtained, it is suggested that the experiment should be repeated over a longer period of time.

Whilst it has been shown that it may be possible to improve upon the stability of the nanoparticles, it should be noted that the nanoparticles resuspended in water maintain a relatively high zeta potential value. This result alone is positive, indicating that the particle surface is stable for short-term storage at room temperature.

4.5 Introduction of Shelled Magnetic Nanoparticles in an Assay Format

In order to test the viability of the inclusion of the shelled magnetite nanoparticles into the assay shown in Chapter 2, a proof of concept experiment was designed (Figure 4.1). One of the main issues that requires to be resolved in the work shown previously was the issue of non-specific binding of the oligonucleotide-functionalised nanoparticle conjugates. If this non-specific binding interaction could be minimised, the sensitivity of the assay could be improved. An experiment was therefore designed based upon the assay set up previously developed to ascertain whether the gold shelled nanoparticles could be incorporated into this assay in order to eliminate this issue.

The gold-coated nanoparticles were functionalised in order to allow them to act as a substitute for the streptavidin coated magnetic beads previously used for immobilisation. Whilst the beads previously used were coated with streptavidin, and the biotin-streptavidin interaction was utilised for the immobilisation of the biotinylated capture probe on the magnetic beads, a different method for immobilisation of the oligonucleotide probe was proposed. Instead of the sequence being immobilised *via* an interaction between the modification on its terminus and the streptavidin coating the magnetic beads, it was suggested that the oligonucleotide could be directly bound to the nanoparticle surface. This immobilisation was suggested by the method previously developed for the functionalisation of the SERRS active nanoparticle conjugates (Section 3.4.1). Due to the gold shell on the magnetic nanoparticles, sulphur containing molecules were able to bind to the solid surface, as shown in Figure 4.11. Consequently it was hypothesised that the nanoparticles could be functionalised with the PEG bilayer previously used, yielding two advantages. First, the addition of the polymer to the nanoparticle surface may aid the stability of the nanoparticles in solution. Whilst this has not been shown to be an issue over

the short time period monitored, the addition of the PEG shell will prevent the nanoparticles from aggregating in longer-term storage, consequently aiding their dispersibility in solution. Secondly, the addition of this PEG layer allows for the nanoparticles to be easily functionalised utilising the carboxylic acid functionality at the terminus of the short chain PEG molecule. Due to this functionality, an amino-modified oligonucleotide probe with the same sequence as the biotin capture probe could be coupled to the short chain PEG molecule tethered to the magnetic nanoparticles. Consequently the magnetite nanoparticles will have the probe sequence directly tethered to them, eliminating the need for the biotin-streptavidin interaction.

As shown in Figure 4.1, this assay involves a number of preparation steps to be completed before SERRS analysis can be performed. The oligonucleotide-functionalised nanoparticle conjugates previously developed were produced with a probe sequence, complementary to one half of the target sequence, immobilised on them. A sample of gold-shelled magnetite nanoparticles were modified by the introduction of a PEG bilayer. The nanoparticles were then centrifuged and resuspended in phosphate buffer (pH 7.6). Amino-modified DNA probes, complementary to the other half of the target sequence, were conjugated to the carboxylic acid moiety on the short chain PEG molecules, the nanoparticles washed and resuspended in 0.3 M PBS. Whilst the assay had previously included a DNA hybridisation step prior to the addition of the magnetic beads, this is no longer required as the probes are now both bound to nanoparticle conjugates. Consequently, the SERRS-active nanoparticle conjugates and functionalised magnetic nanoparticles were mixed together with a solution of the target DNA and incubated at room temperature in order to allow for the oligonucleotide probes to become bound to the target strand (step 1). In order to assess the specificity of the binding of the nanoparticle conjugates, a control sample was also prepared containing no target sequence. The magnetic nanoparticles were then washed by the introduction of a magnetic field, allowing the beads to be collected at the side of the sample tube (step 2). The supernatant containing any excess SERRS-active nanoparticles was removed, and the sample resuspended in 0.3 M PBS. This washing protocol was repeated three times before analysis of the sample to ensure all of the unbound nanoparticle conjugates which could give rise to a SERRS signal were removed. The sample was then analysed using an excitation wavelength of 633 nm (Figure 4.13).

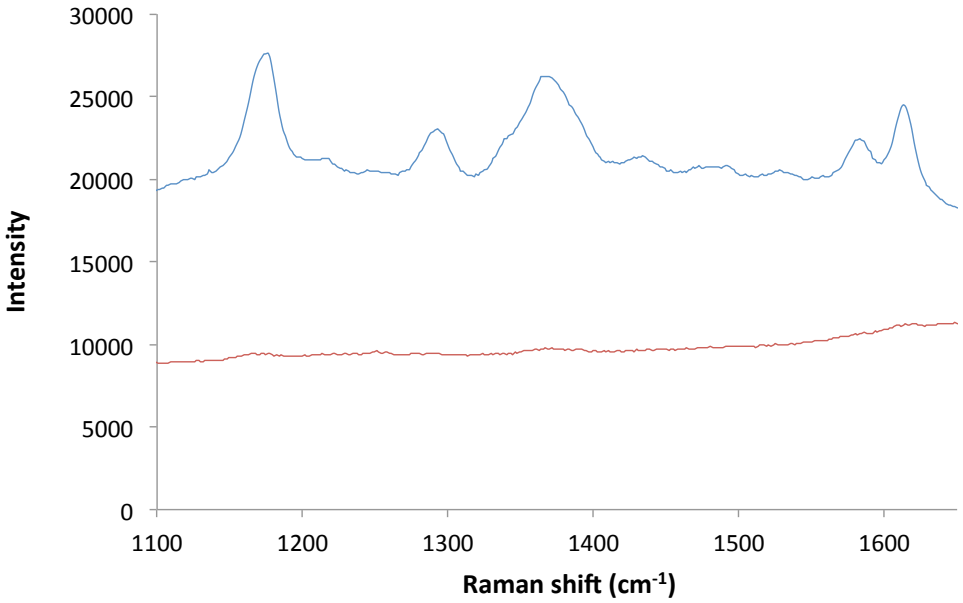

Figure 4.13 - SERRS spectrum obtained of the assay in the presence of target DNA (blue), and the assay in the absence of target DNA (red). The assay was constructed, washed three times with 0.3 M PBS and analysed in solution using 633 nm laser excitation, 1x 30 s accumulation.

It is clear that the sample containing target DNA yields a clear SERRS signal, corresponding to malachite green. However, in the absence of the target strand, the assay produced minimal SERRS output. These results are encouraging for two reasons. First, it would appear that the oligonucleotide functionalised magnetite nanoparticles are able to successfully hybridise to the target sequence along with the dye-labelled nanoparticle conjugates giving rise to the probe-target duplex hypothesised. Consequently, the magnetic nanoparticles have shown the possibility for their incorporation into the previously developed assay in place of the streptavidin coated magnetic beads. Secondly, by assessing the signal collected in the absence of target DNA it can be seen that there is little background SERRS response exhibited. It has been shown previously that the probes immobilised on the nanoparticles are non-complementary and are therefore unable to hybridise to each other (Figure 2.21). Consequently, since the SERRS-active nanoparticles are unable to bind to the magnetic nanoparticles they are removed from the sample during washing. Whilst it was thought that this would be the case for the assay developed in Chapter 2, it was shown that the assay in the absence of target DNA gave rise to a SERRS signal corresponding to the malachite green labelled nanoparticles. This was investigated and was shown to be an artefact of non-specific binding of the oligonucleotide-functionalised SERRS-active nanoparticles and the streptavidin coated magnetic beads.

However, when considering the results obtained from the assay utilising the gold-shelled magnetite nanoparticles, it can be seen that the assay in the absence of target DNA shows minimal SERRS response. Consequently, it can be concluded that the oligonucleotide functionalised SERRS-active nanoparticles remain unbound from the magnetic nanoparticles and can be successfully removed from the samples during washing. This elimination of the non-specific binding previously observed may prove to be a significant advantage in terms of the sensitivity of the assay.

Upon consideration of these initial results, it is postulated that the introduction of these nanoparticles could lead to a significant improvement to the assay previously developed. It has been shown that the nanoparticles can be successfully functionalised and incorporated into the assay. The incorporation of these particles may lead to an improvement in the sensitivity of the assay due to a number of advantages offered over the streptavidin coated magnetic beads previously used. It has been previously shown that the use of TurboBeads in place of the conventional magnetic beads leads to a decrease in the dampening of the SERRS signal observed from the nanoparticle conjugates (Section 3.3.1). This decrease in the dampening observed was ascribed to the smaller size of the TurboBeads in comparison with the magnetic beads. Since the TurboBeads are smaller they offer less interference to the Raman scattered light from the beads upon analysis. Consequently, less reduction is SERRS signal is observed from the samples with these particles present. Using this understanding of the dampening process previously seen, it can be concluded that the magnetic particles synthesised which are similar in size to the TurboBeads would result in the same improvement upon the signal dampening. Since the sensitivity of the assay is dependent upon the detection of a low concentration of the SERRS-active nanoparticles, the lesser the dampening caused by the magnetic beads, the lower the concentration of these nanoparticles, and consequently DNA, is able to be detected. Additionally, since it has been shown that the assay containing the magnetic nanoparticles gives rise to minimal SERRS signal, indicating negligible non-specific binding between the dye-labelled nanoparticles and the magnetic nanoparticles, the discrimination between target and non-target DNA is likely to be improved. This improvement upon the discrimination of the assay is likely to lead to a lowered detection limit for the system.

4.6 CONCLUSIONS

The initial aim of the work detailed within this chapter was to successfully synthesise particles that were nano-sized and magnetic in nature allowing them to be easily manipulated by the introduction of a magnetic field, as well as being stable in solution. These nanoparticles were developed for incorporation into the assay previously detailed in Chapter 3. Upon carrying out the work previously detailed using TurboBeads (Section 3.3.1), it had been shown that the introduction of nano-sized magnetic particles to this assay could yield a significant advantage to the sensitivity of the system. However, the TurboBeads appeared to be instable in solution resulting in the nanoparticles settling to the bottom of the sample vial. Therefore the aim was to synthesise nanoparticles that would offer the same advantages as the TurboBeads, whilst also remaining dispersed within the solution. The subsequent aim was to introduce a gold metal shell to the synthesised nanoparticles, allowing for the surface of the particles to be easily modified by any thiol-containing molecule. This was designed for the introduction of the PEG bilayer, followed by coupling of an oligonucleotide probe. This would allow for the oligonucleotide capture probe previously bound to the magnetic particle *via* a streptavidin-biotin interaction to be directly bound to the magnetic nanoparticle.

A protocol has been developed for the synthesis of magnetite nanoparticles approximately 8-10 nm in diameter *via* a coprecipitation approach. These particles were also shown to be easily manipulated by the introduction of a magnetic field. Therefore 2 out of the 3 previously designated specifications have been met. A shelling protocol was developed for the successful encapsulation of the magnetite core nanoparticles in a gold metallic shell. A number of parameters were investigated in the development of this process. Furthermore, a method for the assessment of the success of the shelling protocol was developed using zeta potential measurements and monitoring the particle size distribution of the particles. The ability of the surface to bind with thiolated molecules, a property characteristic of a gold surface, was also tested by the addition of malachite green isothiocyanate. A spectrum corresponding to the dye was seen upon SERRS analysis, indicating the gold encapsulation of the magnetic nanoparticle cores, and the ability of the isothiocyanate containing dye to bind to the particle surface. It was subsequently demonstrated that the SERRS signal

observed was not due to the labelling of gold nanoparticles produced as a by-product during the shelling process.

A proof of concept experiment was designed in order to assess two key points (Figure 4.1). First, the ability of the nanoparticles to be functionalised with oligonucleotide probes allowing for them to be incorporated into the previously developed assay (Chapter 3) without the need for the biotin-streptavidin interaction previously exploited to tether the capture probe to the magnetic bead. Secondly, the degree of non-specific binding between the oligonucleotide functionalised SERRS-active nanoparticle conjugates and the magnetic nanoparticle conjugates produced had to be evaluated. It had been shown previously that the assay in the absence of target DNA still gave rise to a significant SERRS signal. It was shown that this was due to the non-specific binding of the nanoparticle conjugates to the magnetic beads. It was therefore anticipated that the reduction of this non-specific binding would prove to be advantageous to the development of the assay.

The magnetic nanoparticles were functionalised with a PEG bilayer in order to add extra stability and functionality. The PEG layer consists of a short chain linker terminated with a carboxylic acid group, which affords additional functionality to the nanoparticles, and a longer chain linker that acts as a stabilising ligand. These nanoparticles then had an amino-modified oligonucleotide probe covalently coupled to them *via* the carboxylic acid group on the short-chain linker molecule. These particles were then incorporated into the assay developed in Chapter 3 in place of the streptavidin coated magnetic beads and biotinylated capture probe. In the presence of target DNA, a distinctive SERRS signal corresponding to the malachite-green isothiocyanate tethered to the gold nanoparticle conjugates was observed. In the absence of the target sequence however, only a minimal SERRS output it observed. These results indicate that these functionalised magnetic nanoparticles were not subject to the non-specificity binding previously observed in the presence of the streptavidin coated magnetic beads. Consequently, their advancement for inclusion in the assay previously developed could prove advantageous in terms of the sensitivity observed from the system.

4.7 EXPERIMENTAL DETAIL

4.7.1 SYNTHESIS OF MAGNETITE NANOPARTICLES

4.7.1.1 Preparation of Magnetite Nanoparticles

Iron (II) chloride tetrahydrate (3.26 g) and Iron (III) chloride hexahydrate (8.70 g) were dissolved in triple distilled water (380 mL). Ammonia (20 mL, 25%) was added while rapidly stirring the solution. After sedimentation the precipitate was removed by decantation and resuspended in distilled water.

4.7.2 CHARACTERISATION OF MAGNETITE NANOPARTICLES

4.7.2.1 DLS Size Measurements of Magnetite Nanoparticles

Analysis was performed using a Malvern Zetasizer Nano ZS. Analysis was performed at 25 °C with an equilibration time of 120 s, and 15 replicate scans were recorded.

Magnetite nanoparticles were prepared as described in Section 4.7.1.1. The prepared nanoparticles were washed after magnetic separation with water (1 mL), and then centrifuged for 20 minutes at 8000 rpm. The supernatants were discarded and the pellets resuspended in water (1 mL). To determine the hydrodynamic diameter of the particles in the solution, samples (1 mL) were measured in a four-sided disposable polystyrene cuvette.

4.7.2.2 Zeta Potential Analysis of Magnetite Nanoparticles

Analysis was performed using a Malvern Zetasizer Nano ZS. Analysis was performed at 25 °C with an equilibration time of 0 s, and between 10 and 100 repeat scans being recorded.

Magnetite nanoparticles were prepared as described in Section 4.7.1.1. The prepared nanoparticles were washed after magnetic separation with water (1 mL), and then centrifuged for 20 minutes at 8000 rpm. The supernatants were discarded and the pellets resuspended in water (1 mL). To determine the zeta potential of the solution, samples (1 mL) were measured in a four-sided disposable polystyrene cuvette, into which a zeta potential dip cell was inserted.

4.7.2.3 Scanning Electron Microscope (SEM) Imaging of Magnetite Nanoparticles

SEM investigations were carried out by preparing poly(diallylmethylammonium) (PDDA) coated silicon wafers. Silicon wafers were cleaned with methanol and oxygen plasma (Diener electronic femoto oxygen plasma cleaner, 72 cm^3/ min gas flow). The wafers were then coated with a PDDA (10 mg/ mL) solution in NaCl (1 mM) for 30 minutes. After this time, the wafers were rinsed with distilled water and dried with N_2. Magnetite nanoparticle solutions (10 μL) were deposited on individual wafers and allowed to rest for 20 minutes, the samples were then removed and the wafer washed with distilled water. A small amount of magnetite nanoparticle solution (approximately 2 μL) were deposited on one side of the wafer and dried. Imaging was carried out on a Sirion 200 Schottky field-emission electron microscope (FEI) operating at an accelerating voltage of 5 kV. The samples did not require additional metallic coating before imaging. Samples analysed were unshelled magnetite particles and replicates of each were taken.

Image analysis was performed using Image J 64, v. 1.45s in order to more accurately determine the diameter of the nanoparticles. When nanoparticle sizing was performed, more than 2000 particles were sized.

4.7.3 GOLD SHELLING OF MAGNETITE NANOPARTICLES

4.7.3.1 Preparation of Gold-Shelled Magnetite Nanoparticles

The magnetite nanoparticles prepared in Section 4.7.1.1 were shelled using the method described by Mandal *et al*. [180] The magnetite nanoparticles (1 mL) were mixed with a solution of sodium tetrachloroaurate (1 mL) and glucose (0.5 g). The mixture was sonicated for 30 minutes before it was agitated in a water bath. The prepared nanoparticles were washed after magnetic separation with water (1 mL), and then centrifuged for 20 minutes at 8000 rpm.

Various experimental parameters were investigated, including; $HAuCl_4$:Fe_3O_4 ratio (1:1, 2:1 and 5:1), temperature of the water bath (60 °C, 70 °C and 80 °C) and time spent in water bath (1, 2, 5 and 7 hours).

For the investigation of the effect of the Fe:Au ratio on the shelling process, sodium tetrachloroaurate solutions of various concentrations were prepared.

4.7.3.2 SERRS Analysis of Shelled Magnetite Nanoparticles

Gold-shelled magnetite nanoparticles were prepared as detailed in Section 4.7.3.1. The shelled magnetite nanoparticles (100 µL) were stirred and the malachite green isothiocyanate (60 µL, 3 x10^{-7} M) added. The mixture was then stirred for an hour. The resulting solution was then magnetically separated, and the supernatant discarded. The magnetic particles were then resuspended in distilled water (100 µL). This wash process was repeated three times.

SERRS spectra were collected using a Renishaw inVia microscope system (Renishaw, Wolten-under-edge, UK). Excitation was 632.8 nm by a ~30 mW HeNe laser attenuated using neutral density filters. The samples were analysed using a 20x long-working distance objective. Spectra were obtained using 180 ° backscattering from 96-well microtitre plates. The samples were analysed using a single 30 s accumulation, and the spectrometer grating was centred at 1400 cm^{-1} Raman shift.

A calibration spectrum was recorded prior to analysis using a silica standard, which was used to calibrate the wavenumber position.

4.7.3.3 Stability Analysis of Shelled Magnetite Nanoparticles

Magnetite nanoparticles (1 mL) were centrifuged at 8000 rpm for 20 minutes. The supernatant was discarded and the pellet resuspended in buffer (1 mL). One set of samples was resuspended in distilled water, and the remaining two in a citrate solution (0.6 mM and 1.0 mM). The samples were stored at room temperature and zeta potential measurements recorded over a period of 9 days.

4.7.4 ASSAY CONSTRUCTION

4.7.4.1 Preparation of Functionalised Nanoparticles

Gold colloid with a diameter of 60 nm was prepared *via* citrate reduction of $HAuCl_4$ (Section 2.5.1).[140] Malachite green isothiocyanate in water (600 µL, 3 × 10^{-7} M) was added drop wise

to rapidly stirring gold colloid (1 mL, 0.08 nM) to afford a final reporter concentration of 1.125×10^{-7} M. After one hour, a thioctic acid-PEG_8-COOH solution in methanol (14 µL , $1x10^{-3}$ M) was added to the Raman-encoded nanoparticles. A minimum ratio of 30000 PEG molecules per 60 nm gold nanoparticle was used.[66] This was incubated for a minimum of 3 hours at 25 °C before an equivalent amount of thioctic acid-PEG_{41} in methanol (14 µL, $1x10^{-3}$ M) was added and incubated for at least 3 hours.

Gold-shelled magnetite nanoparticles were prepared as detailed in Section 4.7.3.1. Thioctic acid-PEG_8-COOH solution in methanol ($1x10^{-3}$ M, 40 µL) was added and the solution incubated for a minimum of 3 hours at 25 °C. An equivalent amount of thioctic acid-PEG_{41} in methanol ($1x10^{-3}$ M) was then added, and the sample incubated for at least 3 hours.

4.7.4.2 DNA Sequences

The DNA sequences used were purchased from MWG Eurofins Operon, London.

Gold Nanoparticle Probe

5' – GCT GCG ACA – 3' Modifications: 5' NH_2-C_6

Magnetite Nanoparticle Probe

5' – GGG ACT AAG – 3' Modifications: 3' NH_2-C_6

Target

5' – CTT AGT CCC TGT CGC AGC – 3'

4.7.4.3 Bioconjugation with Amino-Modified DNA

The Raman-encoded nanoparticles, and magnetite nanoparticles were washed with triple distilled water and resuspended in phosphate buffer (Na_2HPO_4/NaH_2PO_4) (470 µL, 10 mM, pH 7.6). To activate the –COOH group on the nanoparticle surface for covalent conjugation, freshly prepared ethyl dimethylaminopropyl carbodiimide (EDC) solution (10 µL, 2 mg/mL) and sulfo-NHS (10 µL, 2 mg/mL) were added. The amino-modified DNA (10 µL, 100 µM) was then added and the solution incubated for 16 hours at 25 °C. The DNA labelled SERRS-active nanoparticles (500 µL) and DNA-labelled magnetite nanoparticles (500 µL) were washed and resuspended in 0.3 M PBS (10 mM phosphate, 0.3 M NaCl, 500 µL).

4.7.4.4 Assay Construction

DNA-functionalised Raman reporter nanoparticles (50 µL) and DNA-functionalised magnetite nanoparticles (50 µL), prepared as described previously, were mixed and target DNA solution added (100 µL, 0.1 µM). The samples were incubated for one hour at room temperature. The samples were then washed three times by magnetic separation, and resuspended in 0.3 M PBS. A SERRS spectrum was obtained for the solution using 633 nm laser excitation. Replicate measurements were recorded for each sample. A control experiment was also performed in which distilled water was added in place of target DNA.

4.7.4.5 SERRS Analysis of Assay

SERRS spectra were collected using a Renishaw inVia microscope system (Renishaw, Wolten-under-edge, UK). Excitation was at 632.8 nm by a ~30 mW HeNe laser attenuated using neutral density filters. The samples were analysed in microtitre plates using a 20× long-working distance objective. Spectra were centred around 1400 cm^{-1}, and were obtained using 180° backscattering from 96-well microtitre plates.

5. CONCLUSIONS

Several advances have been made towards the development of two DNA detection assays for diagnostic purposes. SERRS is an attractive analysis technique for the field of disease detection due to its sensitive nature, and its ability to be multiplexed. A DNA detection assay using SERRS as the analysis technique was developed incorporating functionalised silver nanoparticles as the source of the signal for the system. The nanoparticles were functionalised with a customised PEG linker in order to afford stable, SERRS active nanoparticle conjugates. These linker molecules incorporated a disulphide anchor for nanoparticle surface attachment, a carboxylic acid moiety for conjugation to a biomolecule of choice, and a TAMRA molecule to confer SERRS activity to the nanoparticle conjugates. The functionalised nanoparticles were demonstrated to possess stability in ionic buffers, and exhibit a distinct SERRS signal. Further to their synthesis, these conjugates were incorporated into a split-probe DNA detection assay. It was shown that the assay developed could successfully detect target DNA, with little signal observed from the no target controls. Furthermore, it was shown that the assay could selectively detect this target sequence with no signal observed from the assay in the presence of a nonsense control sequence. A limit of detection has been calculated at 4.89 nM. The assay was tested by the introduction of PCR product in place of the synthetic target, however it was not successful in the detection of the target strand. However, after obtaining a limit of detection for the assay, this is thought to be due to the concentration of the target strand being below the detection limit of the assay.

In order to make this assay more suitable for the multiplexed detection of DNA, a new series of SERRS active nanoparticle conjugates were developed. The previously developed assay system had utilised a DIG-antiDIG interaction to tether the SERRS active nanoparticles to one of the oligonucleotide probes in the system. These conjugates were developed with aim to exhibit excellent stability whilst being able to directly couple an oligonucleotide probe to them. Gold nanoparticles were functionalised with malachite green isothiocyanate to provide the conjugates with a SERRS active group close to the surface of the nanoparticle, giving rise to a SERRS signal. The nanoparticles were then stabilised with a PEG bilayer consisting of a short chain PEG molecule terminated with a carboxylic acid group to provide a site for biofunctionalisation, and a long chain PEG molecule to enhance

the stability of the conjugates. It was shown that these conjugates were stable in ionic buffers without the need for further functionalisation. These conjugates were then initially functionalised with the antiDIG antibody and incorporated into the previous assay set up. It was shown that the replacement of the silver nanoparticle conjugates with the newly developed gold conjugates was not detrimental to the assay system, with a clear distinction observed between the signals observed from the assay in the presence of target DNA and the signals observed in the presence of a nonsense DNA sequence.

Subsequently, the pegylated nanoparticle conjugates were then functionalised with amino-modified DNA, and the assay set up was modified slightly to incorporate them. Upon inclusion of the newly developed oligonucleotide functionalised nanoparticles, the selectivity of the assay was assessed. It was found that whilst there is discrimination between the assay in the presence of the target sequence and the assay containing the probes alone, there is a high background observed from the control sample. This was also observed upon comparison of the target-containing sample with a nonsense control sample. It was suggested that this background signal was arising due to non-specific binding of the oligonucleotide-functionalised SERRS active nanoparticles to the magnetic beads. Further investigation demonstrated that this non-specific interaction only arose once the nanoparticle conjugates had been functionalised with the oligonucleotide probes, and that the dye-labelled, pegylated nanoparticles bound significantly less to the magnetic nanoparticle. A number of parameters were investigated in order to reduce this background signal in a bid to improve the assay discrimination. An investigation of various sampling techniques was also carried out in order to improve the analysis protocol, giving rise to less variable results.

Both DNA detection assays developed incorporated streptavidin coated magnetic beads into the system as a means to immobilise the probe-target duplex labelled with the SERRS-active nanoparticles. It had been noted whilst developing these assays that the incorporation of a smaller diameter magnetic beads capable of binding to this duplex could prove to be beneficial to the sensitivity of the assay. Consequently, iron oxide nanoparticles were synthesised to provide a magnetic core for the development of gold-shelled magnetic nanoparticles. A shelling protocol was developed to encapsulate the magnetic nanoparticles in a gold shell, allowing for the widely utilised gold-sulphur bond to be used

in the modification of the nanoparticles. The shelled nanoparticles were analysed by using SEM, zeta potential measurements and SERRS to verify the presence of the gold shell on the surface of the magnetic particles.

Upon verification, a proof of concept assay was designed to assess the suitability of the synthesised conjugates for incorporation into the previously developed assays. A similar functionalisation method to that which yielded the stable SERRS-active gold nanoparticle conjugates was utilised, with the introduction of a PEG bilayer to the shelled magnetic nanoparticles. An amino-modified oligonucleotide probe was coupled to this layer, giving rise to oligonucleotide-functionalised magnetic particles. The incorporation of these into the assay system would allow for the streptavidin-biotin interaction to be removed from the assay, resulting in the magnetic beads being directly attached to the probe-target duplex. The assay incorporating the newly developed magnetic nanoparticles yielded positive results, with a distinct discrimination observed between samples containing target DNA and negative control samples.

6. FURTHER WORK

Silver nanoparticles were functionalised with a TAMRA-labelled PEG linker to give rise to SERRS active nanoparticle tags, which could be easily functionalised with a biomolecule of choice. These tags were incorporated into a DNA detection assay that has shown the ability to selectively detect target DNA. Initial work was performed for the detection of a target strand from PCR product, with little success. However, after calculating the limit of detection for the assay, it is thought that this is likely to be due to the low concentration of PCR product introduced to the assay. To investigate this further, a higher final concentration of PCR product could be included. If after the inclusion of a higher concentration of target strand no improvement is observed, the probe region of the PCR product could be altered so as to reduce competition between the approach of the SERRS active nanoparticles and magnetic beads with the hybridisation of the complementary product strand. Furthermore, Johnson *et al*. demonstrated significantly lower limits of detection from a similar system by analysing the magnetic particles as a pellet.[96] The introduction of this concept to the analysis of the developed assay may lead to a significantly lower limit of detection, and therefore should be investigated further.

Oligonucleotide-functionalised malachite green labelled gold nanoparticles were developed as a replacement for the previously used TAMRA-labelled silver nanoparticles and incorporated into an assay system for the detection of a target DNA sequence. Initial work on this assay system has shown promising results, however there are a number of parameters that require further optimisation. It had been shown that in the absence of the target sequence, the assay exhibits a relatively high background signal. It is believed that this signal is an artefact of non-specific bind of the SERRS-active nanoparticles onto the magnetic beads. Further investigation into the minimisation of this non-specific binding is required in order to improve the discrimination of the assay. Preliminary investigations showed that the introduction of Tween 20 into the wash buffer could prove advantageous. Therefore, a full investigation into the effect of this should be performed. Furthermore, it is postulated that increasing the temperature that the assay is washed at could reduce the background signals by disrupting the non-specific binding of the nanoparticles to the magnetic beads, and this should be investigated.

Preliminary work was performed into the development of a new sample technique for the assay system, using a micro-cuvette flow cell. The initial results obtained from this work are promising, and indicate that the analysis of the assay may be possible within the system. It is thought that further investigation into the mode of immobilisation of the magnetic beads is required, investigating the use of a smaller magnet in order to obtain clusters of the magnetic beads. It is thought that if the magnetic particles can be held in close enough proximity to one another, the sample could be successfully analysed in the device.

It is suggested that the development of silver nanoparticle conjugates akin to the malachite green labelled gold nanoparticles developed could lead to an improvement in the sensitivity of the assay, since silver tends to give larger SERRS enhancements than gold. Consequently, it is desirable for stable SERRS-active silver nanoparticles to be produced using a similar functionalisation protocol to that used for the gold nanoparticles. Furthermore, it would be interesting to explore the incorporation of a variety of Raman reporter molecules into the SERRS-active nanoparticles developed. If a series of conjugates could be developed containing different reporters, and labelled with different oligonucleotide probes, the assay developed may provide a basis for the development of a multiplexed DNA detection assay.

The work involving the synthesis of magnetic nanoparticles required further characterisation work to be performed in order to give detailed information on the particles produced. Characterisation of the magnetic core nanoparticle is required in order to identify the composition of the iron oxide present. This can be done using X-ray diffraction and comparing the nanoparticles produced with reference patterns for magnetite, as well as other common iron oxides. In order to obtain a more thorough understanding of the gold shell, TEM images should be obtained of the nanoparticles. These would give more definitive information on the success of the shelling protocol and the thickness of the gold shell produced.

Optimisation and characterisation of the oligonucleotide-functionalised magnetic nanoparticles is also required. This work should include the optimisation of the stabilisation process by the introduction of PEG, assessing the stability of the nanoparticles in a number of conditions, and over a period of time. Characterisation of the bio-functionalised

nanoparticles should also be performed to give information on the number of oligonucleotides bound to the nanoparticles, and consequently estimate the binding capability of the nanoparticles.

The results obtained using the oligonucleotide-labelled conjugates in the previously developed assay systems were promising. Further work should be performed using these particles in the assay system, and comparing the results to those obtained using the streptavidin coated magnetic beads.

7. REFERENCES

1. S. Yang and R. E. Rothman, *The Lancet Infectious Diseases*, 2004, **4**, 337-348.
2. A. Linacre and D. Graham, *Expert Review of Molecular Diagnostics*, 2002, **2**, 346-353.
3. R. Higuchi, G. Dollinger, P. S. Walsh and R. Griffith, *Bio-Technology*, 1992, **10**, 413-417.
4. H. Li, L. Ying, J. J. Green, S. Balasubramanian and D. Klenerman, *Analytical Chemistry*, 2003, **75**, 1664-1670.
5. R. A. Keller, W. P. Ambrose, P. M. Goodwin, J. H. Jett, J. C. Martin and M. Wu, *Applied Spectroscopy*, 1996, **50**, 12A - 32A.
6. W. E. Moerner and D. P. Fromm, *Review of Scientific Instruments*, 2003, **74**, 3597-3619.
7. K. Kneipp, Y. Wang, H. Kneipp, L. T. Perelman, I. Itzkan, R. Dasari and M. S. Feld, *Physical Review Letters*, 1997, **78**, 1667-1670.
8. S. Nie and S. R. Emory, *Science*, 1997, **275**, 1102-1106.
9. H. X. Xu, E. J. Bjerneld, M. Kall and L. Borjesson, *Physical Review Letters*, 1999, **83**, 4357-4360.
10. J. A. Dieringer, R. B. Lettan, K. A. Scheidt and R. P. Van Duyne, *Journal of the American Chemical Society*, 2007, **129**, 16249-16256.
11. E. C. Le Ru, M. Meyer and P. G. Etchegoin, *Journal of Physical Chemistry B*, 2006, **110**, 1944-1948.
12. K. Faulds, R. P. Barbagallo, J. T. Keer, W. E. Smith and D. Graham, *Analyst*, 2004, **129**, 567-568.
13. J. A. Dougan and K. Faulds, *Analyst*, 2012, **137**, 545-554.
14. G. M. Blackburn and M. J. Gait, *Nucleic Acids in Chemistry and Biology*, Oxford University Press, New York, 1996.
15. J. D. Watson and F. H. C. Crick, *Nature*, 1953, **171**, 737-738.
16. J. M. Gulland, D. O. Jordan and C. J. Threlfall, *Journal of the Chemical Society*, 1947, **25**, 1129-1129.
17. J. M. Gulland, D. O. Jordan and H. F. W. Taylor, *Journal of the Chemical Society*, 1947, **25**, 1131-1141.
18. J. M. Creeth, J. M. Gulland and D. O. Jordan, *Journal of the Chemical Society*, 1947, **25**, 1141-1145.
19. E. Chargaff, *Experientia*, 1950, **6**, 201-209.
20. M. H. F. Wilkins, W. E. Seeds, A. R. Stokes and H. R. Wilson, *Nature*, 1953, **172**, 759-762.
21. J. W. Strutt, *Phil. Mag.*, 1871, **41**, 107-120.
22. A. Compton, *Phys. Rev.*, 1923, **21**, 483-502.
23. A. Smekal, *Naturwissenschaften*, 1923, **43**.
24. C. V. Raman and K. S. Krishnan, *Nature*, 1928, **121**, 501-502.
25. F. T. Docherty, P. B. Monaghan, C. J. McHugh, D. Graham, W. E. Smith and J. M. Cooper, *Ieee Sensors Journal*, 2005, **5**, 632-640.
26. W. Kiefer and H. J. Bernstein, *Appl. Spectrosc.*, 1971, **25**, 500-501.
27. J. Koster, J. Popp and S. Schlücker, *Journal of Raman Spectroscopy*, 2006, **37**, 384-391.
28. F. C. Thorley, K. J. Baldwin, D. C. Lee and D. N. Batchelder, *Journal of Raman Spectroscopy*, 2006, **37**, 335-341.

29. H. S. Sands, I. P. Hayward, T. E. Kirkbride, R. Bennett, R. J. Lacey and D. N. Batchelder, *Journal of Forensic Sciences*, 1998, **43**, 509-513.
30. E. Smith and G. Dent, *Modern Raman Spectroscopy: A Practical Approach*, John Wiley & Sons, Inc., West Sussex, England, 2005.
31. M. Fleischman, P. J. Hendra and A. McQuilla, *Chemical Physics Letters*, 1974, **26**, 163-166.
32. D. L. Jeanmaire and R. P. Van Duyne, *Journal of Electroanalytical Chemistry*, 1977, **84**, 1-20.
33. G. M. Albrecht and A. J. Creighton, *J. Am. Chem. Soc.*, 1977, **99**, 5215-5217.
34. W. E. Smith, *Chemical Society Reviews*, 2008, **37**, 955-964.
35. A. R. Tao and P. D. Yang, *Journal of Physical Chemistry B*, 2005, **109**, 15687-15690.
36. K. Kneipp, H. Kneipp, I. Itzkan, R. R. Dasari and M. S. Feld, *Chemical Reviews*, 1999, **99**, 2957-2975.
37. B. N. J. Persson, *Chemical Physics Letters*, 1981, **82**, 561-565.
38. L. Brus, *Accounts of Chemical Research*, 2008, **41**, 1742-1749.
39. L. X. Chen and J. B. Choo, *Electrophoresis*, 2008, **29**, 1815-1828.
40. P. Kambhampati, O. K. Song and A. Campion, *Physica Status Solidi a-Applied Research*, 1999, **175**, 233-239.
41. P. Hildebrandt, S. Keller, A. Hoffmann, F. Vanhecke and B. Schrader, *Journal of Raman Spectroscopy*, 1993, **24**, 791-796.
42. A. Kudelski and J. Bukowska, *Chemical Physics Letters*, 1996, **253**, 246-250.
43. P. Hildebrandt, A. Epding, F. Vanhecke, S. Keller and B. Schrader, *Journal of Molecular Structure*, 1995, **349**, 137-140.
44. I. T. Shadi, B. Z. Chowdhry, M. J. Snowden and R. Withnall, *Spectrochimica Acta Part a-Molecular and Biomolecular Spectroscopy*, 2003, **59**, 2213-2220.
45. Z.-Q. Tian, B. Ren and D.-Y. Wu, *The Journal of Physical Chemistry B*, 2002, **106**, 9463-9483.
46. M. Moskovits, *Reviews of Modern Physics*, 1985, **57**, 783-826.
47. E. J. Zeman and G. C. Schatz, *The Journal of Physical Chemistry*, 1987, **91**, 634-643.
48. P. C. Lee and D. Meisel, *Journal of Physical Chemistry*, 1982, **86**, 3391-3395.
49. P. Hildebrandt and M. Stockburger, *The Journal of Physical Chemistry*, 1984, **88**, 5935-5944.
50. K. Kneipp, R. R. Dasari and Y. Wang, *Applied Spectroscopy*, 1994, **48**, 951-955.
51. B. Ren, X.-F. Lin, Z.-L. Yang, G.-K. Liu, R. F. Aroca, B.-W. Mao and Z.-Q. Tian, *Journal of the American Chemical Society*, 2003, **125**, 9598-9599.
52. J. A. Creighton, C. G. Blatchford and M. G. Albrecht, *Journal of the Chemical Society, Faraday Transactions 2: Molecular and Chemical Physics*, 1979, **75**, 790-798.
53. J. A. Creighton, C. G. Blatchford and M. G. Albrecht, *Journal of the Chemical Society-Faraday Transactions Ii*, 1979, **75**, 790-798.
54. R. J. Stokes, A. Macaskill, P. J. Lundahl, W. E. Smith, K. Faulds and D. Graham, *Small*, 2007, **3**, 1593-1601.
55. M. Faraday, *Phil. Trans. R. Soc. Lond.*, 1857, **147**, 145-181.
56. S. M. Heard, F. Grieser, C. G. Barraclough and J. V. Sanders, *Journal of Colloid and Interface Science*, 1983, **93**, 545-555.
57. G. C. Weaver and K. Norrod, *Journal of Chemical Education*, 1998, **75**, 621-624.
58. D. Graham, K. Faulds and W. E. Smith, *Chemical Communications*, 2006, 4363-4371.
59. J. C. Jones, C. McLaughlin, D. Littlejohn, D. A. Sadler, D. Graham and W. E. Smith, *Analytical Chemistry*, 1998, **71**, 596-601.
60. K. Faulds, W. E. Smith and D. Graham, *Analyst*, 2005, **130**, 1125-1131.

61. I. Khan, E. Polwart, D. W. McComb and W. E. Smith, *The Analyst*, 2004, **129**, 950-955.
62. C.-Y. Wu, W.-Y. Lo, C.-R. Chiu and T.-S. Yang, *Journal of Raman Spectroscopy*, 2006, **37**, 799-807.
63. C. H. Munro, W. E. Smith, M. Garner, J. Clarkson and P. C. White, *Langmuir*, 1995, **11**, 3712-3720.
64. M. Moskovits, *Journal of Raman Spectroscopy*, 2005, **36**, 485-496.
65. H. S. Basu and L. J. Marton, *Biochemical Journal*, 1987, **244**, 243-246.
66. X. M. Qian, X. H. Peng, D. O. Ansari, Q. Yin-Goen, G. Z. Chen, D. M. Shin, L. Yang, A. N. Young, M. D. Wang and S. M. Nie, *Nature Biotechnology*, 2008, **26**, 83-90.
67. D. S. Grubisha, R. J. Lipert, H. Y. Park, J. Driskell and M. D. Porter, *Analytical Chemistry*, 2003, **75**, 5936-5943.
68. C.-H. Yeh, C.-Y. Hung, T. C. Chang, H.-P. Lin and Y.-C. Lin, *Microfluidics and Nanofluidics*, 2009, **6**, 85-91.
69. S. P. Xu, X. H. Ji, W. Q. Xu, X. L. Li, L. Y. Wang, Y. B. Bai, B. Zhao and Y. Ozaki, *Analyst*, 2004, **129**, 63-68.
70. C. A. Mirkin, R. L. Letsinger, R. C. Mucic and J. J. Storhoff, *Nature*, 1996, **382**, 607-609.
71. R. Elghanian, J. J. Storhoff, R. C. Mucic, R. L. Letsinger and C. A. Mirkin, *Science*, 1997, **277**, 1078-1081.
72. J. J. Storhoff, R. Elghanian, R. C. Mucic, C. A. Mirkin and R. L. Letsinger, *Journal of the American Chemical Society*, 1998, **120**, 1959-1964.
73. H. Ko, S. Singamaneni and V. V. Tsukruk, *Small*, 2008, **4**, 1576-1599.
74. G. J. Kovacs, R. O. Loutfy, P. S. Vincett, C. Jennings and R. Aroca, *Langmuir*, 1986, **2**, 689-694.
75. B. J. Kennedy, S. Spaeth, M. Dickey and K. T. Carron, *The Journal of Physical Chemistry B*, 1999, **103**, 3640-3646.
76. M. Tsen and L. Sun, *Analytica Chimica Acta*, 1995, **307**, 333-340.
77. Q. Ye, J. Fang and L. Sun, *The Journal of Physical Chemistry B*, 1997, **101**, 8221-8224.
78. S. Schlücker, *ChemPhysChem*, 2009, **10**, 1344-1354.
79. S. P. Mulvaney, M. D. Musick, C. D. Keating and M. J. Natan, *Langmuir*, 2003, **19**, 4784-4790.
80. W. E. Doering and S. M. Nie, *Analytical Chemistry*, 2003, **75**, 6171-6176.
81. M. Gellner, K. Kömpe and S. Schlücker, *Analytical and Bioanalytical Chemistry*, 2009, **394**, 1839-1844.
82. J. Wrzesien and D. Graham, *Tetrahedron*, 2012, **68**, 1230-1240.
83. T. A. Taton, G. Lu and C. A. Mirkin, *Journal of the American Chemical Society*, 2001, **123**, 5164-5165.
84. T. A. Taton, C. A. Mirkin and R. L. Letsinger, *Science*, 2000, **289**, 1757-1760.
85. D. G. Thompson, A. Enright, K. Faulds, W. E. Smith and D. Graham, *Analytical Chemistry*, 2008, **80**, 2805-2810.
86. F. McKenzie, K. Faulds and D. Graham, *Small*, 2007, **3**, 1866-1868.
87. L. Sun, C. Yu and J. Irudayaraj, *Analytical Chemistry*, 2007, **79**, 3981-3988.
88. M. B. Wabuyele and T. Vo-Dinh, *Analytical Chemistry*, 2005, **77**, 7810-7815.
89. H. N. Wang and T. Vo-Dinh, *Nanotechnology*, 2009, **20**, 065101
90. K. Faulds, L. Fruk, D. C. Robson, D. G. Thompson, A. Enright, W. Ewen Smith and D. Graham, *Faraday Discussions*, 2006, **132**, 261-268.
91. S. Tyagi and F. R. Kramer, *Nature Biotechnology*, 1996, **14**, 303-308.
92. D. Graham, D. G. Thompson, W. E. Smith and K. Faulds, *Nature Nanotechnology*, 2008, **3**, 548-551.

93. D. G. Thompson, K. Faulds, W. E. Smith and D. Graham, *The Journal of Physical Chemistry C*, 2010, **114**, 7384-7389.
94. F. McKenzie, K. Faulds and D. Graham, *Nanoscale*, 2010, **2**, 78-80.
95. F. McKenzie and D. Graham, *Chemical Communications*, 2009, 5757-5759.
96. H. Zhang, M. H. Harpster, H. J. Park, P. A. Johnson and W. C. Wilson, *Analytical Chemistry*, 2011, **83**, 254-260.
97. Y. W. C. Cao, R. C. Jin and C. A. Mirkin, *Science*, 2002, **297**, 1536-1540.
98. G. Braun, S. J. Lee, M. Dante, T.-Q. Nguyen, M. Moskovits and N. Reich, *Journal of the American Chemical Society*, 2007, **129**, 6378-6379.
99. K. Faulds, R. Jarvis, W. E. Smith, D. Graham and R. Goodacre, *Analyst*, 2008, **133**, 1505-1512.
100. N. M. Green, *Methods in Enzymology*, 1990, **184**, 51-67.
101. X. C. Tong and L. M. Smith, *Analytical Chemistry*, 1992, **64**, 2672-2677.
102. E. P. Diamandis and T. K. Christopoulos, *Clinical Chemistry*, 1991, **37**, 625-636.
103. J. Chevalier, J. Yi, O. Michel and X.-M. Tang, *Journal of Histochemistry & Cytochemistry*, 1997, **45**, 481-491.
104. U. Abshagen and N. Rietbrock, *Naunyn-Schmiedeberg's Archives of Pharmacology*, 1973, **276**, 157-166.
105. P. H. Hinderling, *Journal of Pharmaceutical Sciences*, 1984, **73**, 1042-1053.
106. L. Salphati, *Xenobiotica*, 1999, **29**, 171-185.
107. D. K. H. Tan and D. Schlosshan, *International Journal of Cardiology*, 2012, **158**, 154-155.
108. M. Gheorghiade, K. F. Adams and W. S. Colucci, *Circulation*, 2004, **109**, 2959-2964.
109. P. J. Hauptman and R. A. Kelly, *Circulation*, 1999, **99**, 1265-1270.
110. S. Schlehuber, G. Beste and A. Skerra, *Journal of Molecular Biology*, 2000, **297**, 1105-1120.
111. G. Neuert, C. Albrecht, E. Pamir and H. E. Gaub, *Febs Letters*, 2006, **580**, 505-509.
112. H. J. Holtke and C. Kessler, *Nucleic Acids Research*, 1990, **18**, 5843-5851.
113. Avert, STD Statistics & STDs in the UK, http://www.avert.org/std-statistics-uk.htm, Accessed 23/08/2012, 2012.
114. BASHH, ed. B. A. f. S. H. a. HIV, 2010.
115. B. C. Mei, E. Oh, K. Susumu, D. Farrell, T. J. Mountziaris and H. Mattoussi, *Langmuir*, 2009, **25**, 10604-10611.
116. C. S. Yun, A. Javier, T. Jennings, M. Fisher, S. Hira, S. Peterson, B. Hopkins, N. O. Reich and G. F. Strouse, *Journal of the American Chemical Society*, 2005, **127**, 3115-3119.
117. B. N. J. Persson and N. D. Lang, *Physical Review B*, 1982, **26**, 5409-5415.
118. K. Aslan and V. Pérez-Luna, *Journal of Fluorescence*, 2004, **14**, 401-405.
119. B. N. J. Persson and S. Andersson, *Physical Review B*, 1984, **29**, 4382-4394.
120. E. Morag, E. A. Bayer and M. Wilchek, *Biochemical Journal*, 1996, **316**, 193-199.
121. A. Holmberg, A. Blomstergren, O. Nord, M. Lukacs, J. Lundeberg and M. Uhlén, *Electrophoresis*, 2005, **26**, 501-510.
122. A. Roos, L. H. Bouwman, D. J. van Gijlswijk-Janssen, M. C. Faber-Krol, G. L. Stahl and M. R. Daha, *Journal of Immunology*, 2001, **167**, 2861-2868.
123. Z. J. Qiu, Y. Ying, M. Fox, K. Peng, S.-C. Lewin-Koh, D. Coleman, J. Good, J. Lowe, A. Rahman, J. Yang, J. Jiang, V. Quarmby and A. Song, *Journal of Immunological Methods*, 2010, **362**, 101-111.
124. D. Xu, K. O. Evans and T. M. Nordlund, *Biochemistry*, 1994, **33**, 9592-9599.
125. C. Burns, W. U. Spendel, S. Puckett and G. E. Pacey, *Talanta*, 2006, **69**, 873-876.
126. M. Neviere and R. Reinisch, *Physical Review B*, 1982, **26**, 5403-5408.

127. L. L. Jensen and L. Jensen, *The Journal of Physical Chemistry C*, 2008, **112**, 15697-15703.
128. L. Mulfinger, S. D. Solomon, M. Bahadory, A. V. Jeyarajasingam, S. A. Rutkowsky and C. Boritz, *Journal of Chemical Education*, 2007, **84**, 322-325.
129. P. Lundahl, R. Stokes, E. Smith, R. Martin and D. Graham, *Micro & Nano Letters, IET*, 2008, **3**, 62-65.
130. S. E. J. Bell and N. M. S. Sirimuthu, *The Journal of Physical Chemistry A*, 2005, **109**, 7405-7410.
131. J. R. Lakowicz, B. Shen, Z. Gryczynski, S. D'Auria and I. Gryczynski, *Biochemical and Biophysical Research Communications*, 2001, **286**, 875-879.
132. J. Lukomska, J. Malicka, I. Gryczynski and J. Lakowicz, *Journal of Fluorescence*, 2004, **14**, 417-423.
133. A. W. P. Vermeer and W. Norde, *Biophysical journal*, 2000, **78**, 394-404.
134. L. J. Harris, E. Skaletsky and A. McPherson, *Journal of Molecular Biology*, 1998, **275**, 861-872.
135. K.-B. Lee, S.-J. Park, C. A. Mirkin, J. C. Smith and M. Mrksich, *Science*, 2002, **295**, 1702-1705.
136. M. K. Boehm, J. M. Woof, M. A. Kerr and S. J. Perkins, *Journal of Molecular Biology*, 1999, **286**, 1421-1447.
137. nanoComposix, in *nanoComposix*, nanoComposix, San Diego, CA, 2012.
138. G. Li, R. Stewart, B. Conlan, A. Gilbert, P. Roeth and H. Nair, *Vox Sanguinis*, 2002, **83**, 332-338.
139. R. G. Hamilton, *The Human IgG Subclasses*, Calbiochem-Novabiochem Corporation, 1987.
140. J. Turkevich and P. C. S. a. J. Hillier, Discuss. Faraday Soc., 1951, vol. 11, pp. 55-74.
141. J. Yguerabide and E. E. Yguerabide, *Analytical Biochemistry*, 1998, **262**, 137-156.
142. F. McKenzie, A. Ingram, R. Stokes and D. Graham, *Analyst*, 2009, **134**, 549-556.
143. C. A. Mirkin, *Inorganic Chemistry*, 2000, **39**, 2258-2272.
144. G. Frens, *Nature Physical Science*, 1973, **241**, 20-22.
145. J. J. Storhoff, R. Elghanian, C. A. Mirkin and R. L. Letsinger, *Langmuir*, 2002, **18**, 6666-6670.
146. L. M. Demers, C. A. Mirkin, R. C. Mucic, R. A. Reynolds, R. L. Letsinger, R. Elghanian and G. Viswanadham, *Analytical Chemistry*, 2000, **72**, 5535-5541.
147. S. Link and M. A. El-Sayed, *Journal of Physical Chemistry B*, 1999, **103**, 4212-4217.
148. P. K. Jain, X. Huang, I. H. El-Sayed and M. A. El-Sayed, *Accounts of Chemical Research*, 2008, **41**, 1578-1586.
149. K. L. Kelly, E. Coronado, L. L. Zhao and G. C. Schatz, *The Journal of Physical Chemistry B*, 2002, **107**, 668-677.
150. D. Fischer, W. R. Caseri and G. Hähner, *Journal of Colloid and Interface Science*, 1998, **198**, 337-346.
151. F. McKenzie, V. Steven, A. Ingram and D. Graham, *Chemical Communications*, 2009, 2872-2874.
152. S. M. West, A. D. Guise and J. B. Chaudhuri, *Food and Bioproducts Processing*, 1997, **75**, 50-56.
153. A. Das and C. Mukhopadhyay, *The Journal of Physical Chemistry B*, 2009, **113**, 12816-12824.
154. T. T. Herskovits, H. Jaillet and B. Gadegbeku, *Journal of Biological Chemistry*, 1970, **245**, 4544-4550.
155. D. R. Canchi, D. Paschek and A. E. Garcia, *Journal of the American Chemical Society*, 2010, **132**, 2338-2344.

156. M. Futamata, Y. Maruyama and M. Ishikawa, *The Journal of Physical Chemistry B*, 2003, **107**, 7607-7617.
157. H. Xu, J. Aizpurua, M. Käll and P. Apell, *Physical Review E*, 2000, **62**, 4318-4324.
158. T. Neuberger, B. Schöpf, H. Hofmann, M. Hofmann and B. von Rechenberg, *Journal of Magnetism and Magnetic Materials*, 2005, **293**, 483-496.
159. O. Veiseh, J. W. Gunn and M. Zhang, *Advanced Drug Delivery Reviews*, 2010, **62**, 284-304.
160. V. I. Shubayev, T. R. Pisanic Ii and S. Jin, *Advanced Drug Delivery Reviews*, 2009, **61**, 467-477.
161. C. Sun, J. S. H. Lee and M. Zhang, *Advanced Drug Delivery Reviews*, 2008, **60**, 1252-1265.
162. Z. Liu, Y. Liu, H. Yang, Y. Yang, G. Shen and R. Yu, *Analytica Chimica Acta*, 2005, **533**, 3-9.
163. J. B. Haun, T.-J. Yoon, H. Lee and R. Weissleder, *Wiley Interdisciplinary Reviews: Nanomedicine and Nanobiotechnology*, 2010, **2**, 291-304.
164. J. M. Perez, L. Josephson and R. Weissleder, *ChemBioChem*, 2004, **5**, 261-264.
165. A.-H. Lu, E. L. Salabas and F. Schüth, *Angewandte Chemie International Edition*, 2007, **46**, 1222-1244.
166. L. Wang, H.-Y. Park, S. I. I. Lim, M. J. Schadt, D. Mott, J. Luo, X. Wang and C.-J. Zhong, *Journal of Materials Chemistry*, 2008, **18**, 2629-2635.
167. U. Tamer, Y. Gundogdu, I. H. Boyaci and K. Pekmez, *Journal of Nanoparticle Research*, 2010, **12**, 1187-1196.
168. C. Leostean, O. Pana, R. Turcu, M. L. Soran, S. Macavei, O. Chauvet and C. Payen, *Journal of Nanoparticle Research*, 2011, **13**, 6181-6192.
169. Z. Fan, M. Shelton, A. K. Singh, D. Senapati, S. A. Khan and P. C. Ray, *Acs Nano*, 2012, **6**, 1065-1073.
170. T. T. Hien Pham, C. Cao and S. J. Sim, *Journal of Magnetism and Magnetic Materials*, 2008, **320**, 2049-2055.
171. G. K. Kouassi and J. Irudayaraj, *Analytical Chemistry*, 2006, **78**, 3234-3241.
172. C.-H. Liang, C.-C. Wang, Y.-C. Lin, C.-H. Chen, C.-H. Wong and C.-Y. Wu, *Analytical Chemistry*, 2009, **81**, 7750-7756.
173. I.-I. S. Lim, P. N. Njoki, H.-Y. Park, X. Wang, L. Wang, D. Mott and C.-J. Zhong, *Nanotechnology*, 2008, **19**, 305102.
174. I. Koh and L. Josephson, *Sensors*, 2009, **9**, 8130-8145.
175. S. Chen, Y. Yuan, J. Yao, S. Han and R. Gu, *Chemical Communications*, 2011, **47**, 4225-4227.
176. F. Bao, J.-L. Yao and R.-A. Gu, *Langmuir*, 2009, **25**, 10782-10787.
177. H.-Y. Park, M. J. Schadt, Wang, I. I. S. Lim, P. N. Njoki, S. H. Kim, M.-Y. Jang, J. Luo and C.-J. Zhong, *Langmuir*, 2007, **23**, 9050-9056.
178. H. Zhang, M. H. Harpster, W. C. Wilson and P. A. Johnson, *Langmuir*, 2012, **28**, 4030-4037.
179. A. Bee, R. Massart and S. Neveu, *Journal of Magnetism and Magnetic Materials*, 1995, **149**, 6-9.
180. M. Mandal, S. Kundu, S. K. Ghosh, S. Panigrahi, T. K. Sau, S. M. Yusuf and T. Pal, *Journal of Colloid and Interface Science*, 2005, **286**, 187-194.
181. A. S. Teja and P.-Y. Koh, *Progress in Crystal Growth and Characterization of Materials*, 2009, **55**, 22-45.
182. K. Petcharoen and A. Sirivat, *Materials Science and Engineering B-Advanced Functional Solid-State Materials*, 2012, **177**, 421-427.

183. T. Perez-Gonzalez, A. Rodriguez-Navarro and C. Jimenez-Lopez, *Journal of Superconductivity and Novel Magnetism*, 2011, **24**, 549-557.
184. H. El Ghandoor, H. M. Zidan, M. M. H. Khalil and M. I. M. Ismail, *International Journal of Electrochemical Science*, 2012, **7**, 5734-5745.
185. Y. Sahoo, H. Pizem, T. Fried, D. Golodnitsky, L. Burstein, C. N. Sukenik and G. Markovich, *Langmuir*, 2001, **17**, 7907-7911.
186. J. Lee, T. Isobe and M. Senna, *Journal of Colloid and Interface Science*, 1996, **177**, 490-494.
187. L. F. Cotica, V. F. Freitas, G. S. Dias, I. A. Santos, S. C. Vendrame, N. M. Khalil, R. M. Mainardes, M. Staruch and M. Jain, *Journal of Magnetism and Magnetic Materials*, 2012, **324**, 559-563.
188. D. Maity, S. N. Kale, R. Kaul-Ghanekar, J.-M. Xue and J. Ding, *Journal of Magnetism and Magnetic Materials*, 2009, **321**, 3093-3098.
189. A. Angermann and J. Toepfer, *Journal of Materials Science*, 2008, **43**, 5123-5130.
190. Y. Lee, J. Lee, C. J. Bae, J. G. Park, H. J. Noh, J. H. Park and T. Hyeon, *Advanced Functional Materials*, 2005, **15**, 503-509.
191. F. Dumitrache, I. Morjan, R. Alexandrescu, V. Ciupina, G. Prodan, I. Voicu, C. Fleaca, L. Albu, M. Savoiu, I. Sandu, E. Popovici and I. Soare, *Applied Surface Science*, 2005, **247**, 25-31.
192. H. Hofmeister, F. Huisken, B. Kohn, R. Alexandrescu, S. Cojocaru, A. Crunteanu, I. Morjan and L. Diamandescu, *Applied Physics a-Materials Science & Processing*, 2001, **72**, 7-11.
193. S. Martelli, A. Mancini, R. Giorgi, R. Alexandrescu, S. Cojocaru, A. Crunteanu, I. Voicu, M. Balu and I. Morjan, *Applied Surface Science*, 2000, **154-155**, 353-359.
194. A. A. Khaleel, *Chemistry-a European Journal*, 2004, **10**, 925-932.
195. E. Tronc, P. Belleville, J. P. Jolivet and J. Livage, *Langmuir*, 1992, **8**, 313-319.
196. Â. L. Andrade, D. M. Souza, M. C. Pereira, J. D. Fabris and R. Z. Domingues, *Química Nova*, 2010, **33**, 524-527.
197. J. C. Love, L. A. Estroff, J. K. Kriebel, R. G. Nuzzo and G. M. Whitesides, *Chemical Reviews*, 2005, **105**, 1103-1170.
198. C. Vericat, M. E. Vela, G. Benitez, P. Carro and R. C. Salvarezza, *Chemical Society Reviews*, 2010, **39**, 1805-1834.
199. J. Liu, G. Qin, P. Raveendran and Y. Ikushima, *Chemistry – A European Journal*, 2006, **12**, 2131-2138.
200. K. M. Mayya, N. Jain, A. Gole, D. Langevin and M. Sastry, *Journal of Colloid and Interface Science*, 2004, **270**, 133-139.